Dissertazione presentata per il conseguimento del titolo

di Dottore di Ricerca in Ingegneria delle Strutture

Innovative technologies for the vibration control of equipment in critical facilities

Anna Reggio

Roma, novembre 2011

Ciclo XXIII

Il Coordinatore del Dottorato

Prof. Giuseppe Rega

Abstract

La ricerca proposta nella presente tesi si inquadra nelle tematiche della modellazione dinamica, della progettazione antisismica e del monitoraggio permanente di apparecchiature in costruzioni strategiche. L'obiettivo primario perseguito consiste nella valutazione della fattibilità e dell'efficacia di tecnologie innovative di controllo delle vibrazioni applicate alla protezione sismica delle apparecchiature. Le tecnologie studiate comprendono: l'isolamento sismico di una singola apparecchiatura (*equipment isolation systems*); l'isolamento sismico di un intero piano di una struttura portante (*isolated raised floor systems*), sul quale ancorare un insieme eventualmente complesso di apparecchiature; l'assorbitore a massa accordata (*Tuned Mass Damper*) in una nuova configurazione di tipo non convenzionale, nella quale una massa significativa già presente su di una struttura portante, nella fattispecie un'apparecchiatura, è utilizzata quale massa ausiliaria accordata allo scopo di ridurre la risposta sismica della struttura.

Si ritiene, in primo luogo, che l'argomento rivesta una valenza applicativa innovativa, dato il numero ancora esiguo di lavori scientifici e le conseguenti lacune normative esistenti al riguardo. In secondo luogo, la ricerca proposta trova aspetti di maggiore interesse scientifico ed originalità nei seguenti temi, a cui è dato adeguato rilievo: lo studio dell'interazione dinamica tra gli apparati isolati, dotati di massa significativa, e la struttura portante di sostegno; l'elaborazione di criteri e metodologie di progettazione ottimale dei sistemi di isolamento che prendano in considerazione la suddetta interazione; la definizione, ai fini progettuali, di modelli strutturali di ordine ridotto dinamicamente equivalenti; la modellazione costitutiva di un sistema di isolamento innovativo avente comportamento non lineare isteretico; l'analisi dinamica di sistemi non classicamente smorzati e non lineari isteretici; la definizione di indici energetici per la valutazione dell'efficacia delle tecnologie proposte. Un elemento distintivo del lavoro è rappresentato, infine, dal carattere sperimentale: i risultati delle analisi condotte sui modelli numerici sono stati validati mediante sperimentazione dinamica su tavola vibrante.

L'obiettivo ultimo che la tesi si propone è quello di definire criteri e metodi che consentano di armonizzare la progettazione antisismica delle apparecchiature con quella dei sistemi strutturali, nel perseguimento congiunto dei livelli prestazionali di operatività richiesti alle costruzioni strategiche dalle attuali normative internazionali.

Abstract

The present thesis settles in the framework of the dynamic modelling, seismic mitigation and permanent health monitoring of equipment in critical facilities. The main objective is to assess the feasibility and the effectiveness of innovative mitigation technologies including: the passive isolation of a single equipment (*equipment isolation systems*); the passive isolation of a raised floor, on which a group of several equipment is anchored (*isolated raised-floor systems*); a *non-conventional Tuned Mass Damper* (TMD), realized by converting a large mass already present on the structure, *e.g.* the mass of an equipment, into a tuned mass, in order to reduce the structural response.

The area of research is believed to have the potential for a wide application, since a still limited number of authors has addressed the theoretical and technical issues associated with the seismic design and protection of equipment. As a result, international seismic codes and standards also appear to be inadequate in this regard. Furthermore, the proposed technologies give the opportunity of addressing topics of significant scientific interest: the analysis of the dynamic interaction between an equipment and its supporting structure, generally neglected in current Literature and seismic codes; the definition of reduced-order generalized models, introduced for design purposes; the constitutive modelling of nonlinear hysteretic isolation systems; the dynamic analysis of non-proportionally damped systems and nonlinear hysteretic systems; the stochastic analysis of the dynamic response, given the probabilistic nature of the earthquake excitation; the proper definition of energy indices to assess, in a synthetic and effective way, the performance of the proposed mitigation technologies. A distinctive aspect of the work is eventually given by the use of shaking table tests on reduced scale models, for the sake of dynamic identification and seismic analysis.

In the end, the thesis aims at defining criteria and methodologies to harmonize the seismic design of equipment with the one of the structure, in a joint and coordinated effort to achieve the operational performance objectives prescribed to critical facilities by international seismic codes.

Ai miei genitori,
con gratitudine.

Contents

List of Figures

List of Tables

Introduction

Motivation

The present thesis settles in the framework of the dynamic modelling, seismic mitigation and health monitoring of equipment in critical facilities.

Designated as *critical facilities* are the constructions that host essential public and economic functions or particularly hazardous activities, typically including: buildings with post-earthquake emergency functions (hospitals, government buildings, ...); industrial facilities whose failure poses catastrophic risk to the environment or a large number of people (petrochemical plants, nuclear plants, ...); high-technologies facilities with high-precision and high-value equipment (electronic factories, internet collocation facilities, ...); industrial plants strongly affecting the economic system on a national or a regional scale. Owing to their crucial purposes, international seismic codes prescribe them to meet enhanced performance objectives than ordinary buildings: whilst the latter can incur, under a major earthquake, in extensive damage as long as life safety is protected (*Life Safe* performance level), critical facilities are required to suffer only minor damage, remaining functional and in operation during and after the seismic event (*Operational* performance level).

Operational continuity of critical facilities primarily depends on the integrity and functionality of the engineering systems and their mechanical, electrical and electronic equipment: even in the absence of structural failure, the equipment damage might cause the post-earthquake downtime and result in indirect life and economic losses. Furthermore, in most types of critical facilities, equipment represents also a major portion of the total construction investment and, as such, its damage might be the biggest contributor to the direct property losses resulting from earthquakes.

Despite these considerations, equipment has long been treated as secondary elements in importance, since the theory driving seismic codes has been to protect the structure, substantially neglecting the nonstructural components. Recent severe earthquakes (Tohoku, Japan, 2011; L'Aquila, Italy, 2009; Nisqually, USA, 2001; Kocaeli, Turkey, 1999; Northridge, USA, 1994), however, have led to recognize that a correct analysis of the seismic risk posed to critical facilities should consider structural failure as well as nonstructural damage and, in particular, damage to equipment. As a consequence, an urgent need of developing knowledge, vulnerability studies, analysis

methodologies, design procedures and mitigation strategies for equipment is nowadays widely recognized.

Mainly relying on the observation of data field collected during earthquakes, authors have established a taxonomy of equipment based on its functionality, vulnerability and the consequences of its failure (Filiatrault *et al.*, 2001; Taghavi and Miranda, 2003). Although each type of equipment responds in a different manner when subjected to seismic excitation and exhibits its own failure mode, they are generally classified as *acceleration-sensitive* components since subjected to damage from inertial loading. Correlated failure modes might be of two sorts, depending either on the internal damage to vibration sensitive apparatus or on the excessive sliding or rocking (overturning) of the equipment and the possible consequent rupture of service lines.

Conversely, a still limited number of research works has addressed the theoretical and technical issues associated with the seismic design and protection of equipment. As a result, international seismic codes and standards also appear to be inadequate in this regard, making it difficult to harmonize structural and nonstructural design criteria in order to jointly achieve the performance objective of operational continuity. In view of the safety and economic significance of nonstructural damage, however, high seismicity countries (*e.g.* United States, New Zealand and Italy) have recently devoted an increasing attention to the development of seismic design requirements for nonstructural components. Intended to provide, in a form as simple as possible, conservative estimates of the seismic forces, these provisions are easy to implement and sufficiently accurate when designing light ordinary components in ordinary building. In the presence of either particularly vulnerable equipment or an increased seismic hazard level, as in critical facilities, they result to be oversimplified and inaccurate, while more sophisticated design procedures are required due to the importance of the application.

A number of research issues clearly emerges and needs to be investigated in order to improve the seismic design requirement for critical facilities. The weight of equipment represent a first, significant shortcoming of current codes, which indeed exclude from their scope and application heavy nonstructural components. In such cases, the dynamic interaction between the equipment and the whole structure cannot be neglected unless gross errors, but accurate methodologies that take account of it for the analysis and the verification/design are missing and left, in case, to the responsibility of the designer. Furthermore, due to the enhanced performance objectives required to critical facilities, standard protective measures are not workable means to effectively insure the continuing functioning of equipment. The development of innovative strategies and technologies for the vibration control appears to be feasible and appropriate and then deserves to be fully exploited. A substantial improvement of the seismic risk mitigation and the permanent health monitoring of critical facilities is the broad objective to achieve. The emerging research needs identified in the field are believed to have a great potential for a wide application and will be considered as a constant guide throughout the development of the present thesis.

Objectives and outline

The present thesis aims at assessing the feasibility and the effectiveness of innovative technologies for the seismic protection of equipment in critical facilities.

An effective way to mitigate the seismic risk posed to acceleration-sensitive equipment consists in implementing an isolation system between the apparatus to be protected and its supporting structure, if floor-mounted, or the ground, if ground-mounted. As a result, the absolute accelerations transmitted to the equipment are considerably reduced and damages due to excessive inertial loads are prevented. Among the various strategies hereafter investigated, it is included: the passive isolation of a single equipment (*equipment isolation systems*) (Gavin and Zaicenco, 2007; Lu and Lin, 2008); the passive isolation of a raised floor, on which a group of several equipment is anchored (*isolated raised-floor systems*) (Alhan and Gavin, 2005; Ismail *et al.*, 2009); a *non-conventional Tuned Mass Damper* (TMD) realized by converting a large mass already present on the structure, *e.g.* the mass of an equipment, into a tuned mass, in order to reduce the responses of the structure and of all of the equipment anchored to it. Regarding the implementation of these strategies in real applications, two different kinds of passive bearings are proposed and studied: High-Damping Rubber Bearings (HDRB), whose mechanical behaviour is described by means of a linear Kelvin-Voigt visco-elastic model; a novel isolator showing nonlinear hysteretic behaviour, composed of a rolling pendulum plus hysteretic elements to provide supplemental energy dissipation.

The proposed technologies stand out for their innovative and original character and compete with other vibration control techniques (*e.g.* base isolation, dissipative bracings) already in use in current engineering practice. Hence, optimal design criteria and methodologies have to be specifically developed. This gives the opportunity of addressing aspects of significant scientific interest: the analysis of the dynamic interaction between the isolated equipment and its supporting structure, generally neglected in current Literature and building codes; the definition of reduced-order generalized models, introduced for design purposes and representative of the dynamic interaction; the constitutive modelling of nonlinear hysteretic systems; the dynamic analysis of non-proportionally damped systems and nonlinear hysteretic systems; the stochastic analysis of the dynamic response, given the probabilistic nature of the earthquake excitation; the proper definition of energy indices to assess, in a synthetic and effective way, the performance of the proposed mitigation technologies.

The thesis is structured in three parts, described in detail in the following.

The first part (Chapters 1, 2 and 3) discusses the research framework as set by current seismic codes and Literature. Chapter 1 describes the State of the Art in the field of seismic design of nonstructural components, this general category covering equipment, architectural components and building contents. Major findings of the Literature about the seismic vulnerability of nonstructural components and their dynamic behaviour are reported, with particular reference to the analysis of the dynamic

interaction in combined primary-secondary systems. A comparative study of current building codes in high seismicity countries (in USA, FEMA 450/2003 and FEMA P-750/2009; in New Zealand, NZS 4219:2009; in Europe, EN 1998-1:2004; in Italy, D.M. 14/01/2008) is then carried out. The seismic design requirements provided by the codes are critically assesses and compared in order to identify their shortcomings and the emerging research needs. Chapter 2 is focused on a single class of nonstructural components, the equipment, and on a special type of constructions, the critical facilities. The significance of seismic risk mitigation in critical facilities is shown with evidence and a literature review about the innovative technologies for the seismic protection of equipment is presented. A case study is eventually set in Chapter 3. A combined primary-secondary system is considered which consists of a supporting structure housing a single equipment. The equipment is modelled as a rigid body having a single attachment point to the supporting structure (*floor-mounted block-type equipment*). In the uncontrolled configuration, the equipment is non-isolated and rigidly fixed to the attachment floor of the supporting structure; in the controlled configuration, the equipment is isolated from the attachment floor *via* a passive isolation system. Reduced order single-degree-of-freedom (SDOF) and two-degree-of-freedom (2-DOF) models are derived for design purposes, in the case of a decoupled and a coupled analysis approach, respectively.

The second part (Chapters 4, 5 and 6) deals with the equipment and raised-floor isolation technologies. In Chapter 4, a passive equipment isolation system composed of HDRB is introduced and the optimal design problem is set and solved. Unlike previous studies, that generally decouple and analyze the isolated equipment individually, the proposed design methodology is specifically developed to adopt a coupled approach and to account for the dynamic interaction phenomena. A multi-objective optimization procedure is developed to consider both the responses of interest: the absolute acceleration of the isolated equipment and the displacement across the isolation system. Distinctive of the procedure is the consideration of the peculiar damping properties of HDRB in the context of a non-proportionally damped system. In Chapter 5 a passive isolation system with nonlinear hysteretic behaviour is proposed and studied. The novel isolators are suited to the seismic protection of equipment under horizontal motion by virtue of their attractive mechanical properties, summarized as follows: the decoupling between an elastic restoring force, to provide a re-centering mechanism, and a hysteretic restoring force, to provide rate-independent damping; a nonlinear geometric stiffness suitable to achieve multiple performance objectives throughout the course of motion; a high energy dissipation capability to limit the horizontal displacements induced by severe earthquake. The study first addresses the problem of formulating a constitutive relationship for the isolation system and an integrable hysteresis model, derived from the mathematical Duhem operator, is adopted owing to its versatility and analytical tractability. The developed constitutive model is then used in Chapter 6 for the optimal design of the equipment isolation system. Two optimization criteria

are defined, involving both the reduction of the equipment absolute acceleration to a threshold value allowable for full operation and the maximization of a properly defined energy performance index. The methodology is proved to account, in a synthetic and effective way, for both the different response quantities of the equipment (absolute acceleration and relative displacement) and the energy dissipation in the isolation system. Furthermore, it is prone to be extended to achieve multiple performance objectives at different input levels by separately optimize the parameters of the nonlinear isolation system, in accordance to the principles of multi-objective performance-based seismic design.

The third part (Chapter 7) deals with the dynamic response and the optimal design of a non-conventional large mass ratio TMD. Like for the equipment isolation systems previously discussed, the implementation of a non-conventional TMD is based on the decoupling between a mass and its supporting structure. As a consequence of this analogy, the two technologies can be studied by means of the same structural models, but the design criteria are essentially different: on the one hand, in the case of an equipment isolation system, the primary objective is to reduce the absolute acceleration transmitted to the isolated equipment; on the other hand, in the case of a non-conventional TMD, the objective is pursued of minimizing the dynamic response of the supporting structure and, then, of the whole equipment the structure houses.

A distinctive aspect of the thesis is finally given by the use of dynamic tests. The effectiveness and the robustness of two of the proposed technologies, the equipment isolation system by means of HDRB and the non-conventional large mass ratio TMD, are discussed in the light of the extensive experimental results obtained by shaking table tests in the MAT-Qual Laboratory of ENEA (Italian National Agency for the New Technologies, Energy and Environment), "Casaccia" Research Center in Rome. The tests have been carried out on a 1:5 scale model consisting of a two-storey steel frame, having the role of a supporting structure, and a large mass, representing a block-type equipment, mounted on the second floor. The tests consisted of both dynamic identification tests and seismic tests, the latter performed under a wide selection of natural and artificial seismic inputs.

Part I

Research framework

Chapter 1

Seismic design of nonstructural components: state of the art

1.1 Preliminaries

Nonstructural components[1] in buildings and industrial facilities are all the elements attached to floors, roof and walls that are not part of the load-bearing structural system. Figure 1.1, taken from the guideline "Reducing the risks of nonstructural damage - A practical guide" issued by the Federal Emergency Management Agency (FEMA 74, 1994 [35]), identifies the structural and nonstructural components of a typical building. Accordingly, nonstructural components may be classified into three broad categories:

- equipment and systems required for the normal or a particular operation of the construction;
- architectural components;
- building contents.

[1]Some results in this chapter have been published in the following papers:

♢ Parise, G., Reggio, A., De Angelis, M. Criteria for the Definition of the Equipment Seismic Levels (ESL): Comparisons between USA and European Codes. *IEEE Transactions on Industry Applications*, DOI: 10.1109/TIA.2013.2289947, 2014.

♢ Parise, G., De Angelis, M., Reggio, A., A Darwinian Evolution Of Electrical Power Systems Design For Preventing Seismic Risks In Sensitive Buildings. *Proceedings of 2011 IEEE/IAS Industrial & Commercial Power Systems Technical Conference (I&CPS 2011)*, Newport Beach, CA (USA), May 1-5, 2011.

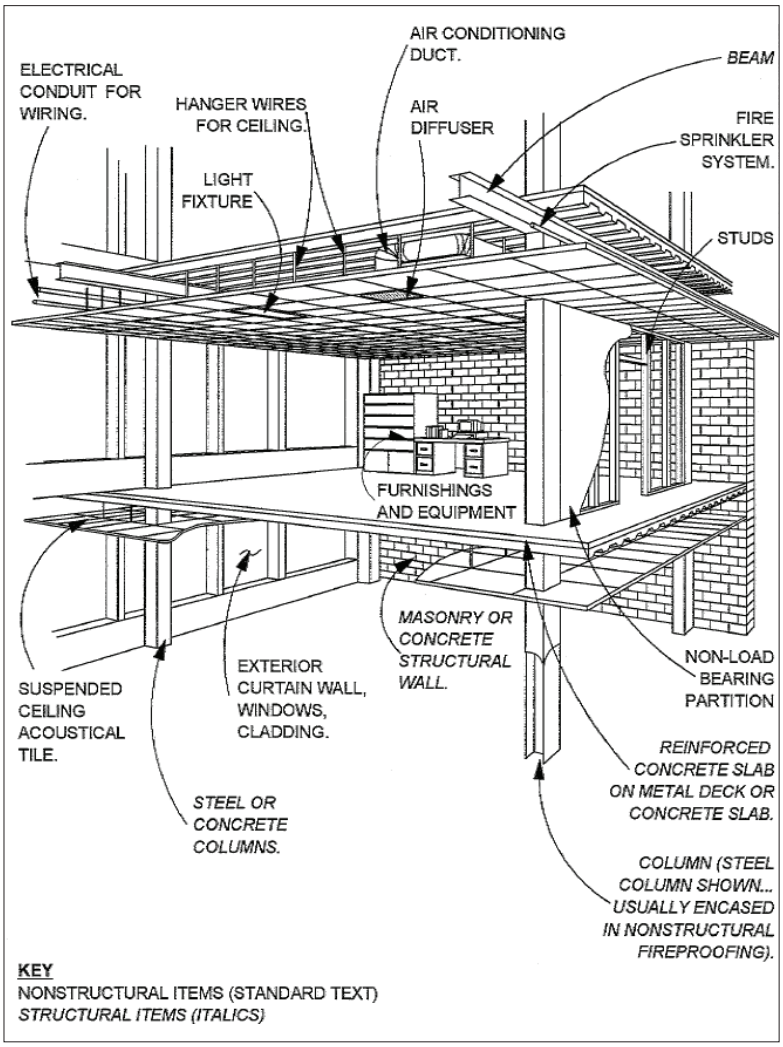

Figure 1.1. Structural and nonstructural components of a typical building. After FEMA 74, 1994 [35].

Examples in the first category include mechanical, electrical and electronic equipment such as manufacturing and processing machinery, engines, turbines, pumps, generators, transformers, switchgears, battery racks, emergency power systems, control panels, computer-and-data-acquisition systems, fuel storage tanks, pressure vessels, boilers and water heaters, chillers, Heating Ventilation and Air Conditioning (HVAC) units. Some examples in the second category are interior partitions, suspended ceilings, lighting fixtures, cladding panels, parapets, windows and glazing. The third category includes all the nonstructural components belonging to building occupants, like furniture, bookshelves and storage racks.

Alternative names by which nonstructural components are known are "building attachment" and "secondary elements". In spite of these names, however, nonstructural components are far from being secondary in importance. Recent severe earthquakes (Northridge, USA, 1994 [108]; Nisqually, USA, 2001 [46]; Kocaeli, Turkey, 1999 [113];

L'Aquila, Italy, 2009 [7], [27]) led to recognize that nonstructural damage may result in serious threats to life safety and in major direct and indirect economic losses. In the worst case of critical facilities (hospitals, government buildings, power plants, large industrial facilities, ...), the failure of nonstructural components strongly impacts also on the post-earthquake functionality, causing the loss of essential services or businesses. This highlights that a target seismic resilience for a building can be achieved only by optimizing and harmonizing performance levels between structural and nonstructural components. Even if the structural components achieve the desired performance level during and after an earthquake, the failure of nonstructural components can lower the performance level of the entire building system.

Research in the field of the seismic design of nonstructural components is a major effort but it is needed to a great extent, as the increasing attention devoted by the latest seismic standards testifies: in USA, FEMA 450/2003 [39], FEMA P-750/2009 [42] and a revision of FEMA 74 expected in 2010; in New Zealand, NZS 4219:2009 [126]; in Europe, EN 1998-1:2004 (Eurocode 8) [30]; in Italy, "Nuove Norme Tecniche per le Costruzioni – D.M. 14/01/2008" [90]. At present, there is a limited information on the seismic performance of nonstructural components in comparison with structural components since basic work has been sparse and empirical, based on field surveys and engineering intuition rather than on experimental and analytical findings. As a result, current seismic provisions for nonstructural components are still oversimplified, likely to be either overconservative, when designing ordinary nonstructural components in ordinary buildings, or inaccurate, when more sophisticated design procedures are required due to the importance of the application.

Last but not least, it is worthy to note that developments in this research field cannot set aside the integration of the various specialities and disciplines. The seismic design of nonstructural components involves a number of various professional figures: architects, structural engineers, mechanical engineers, electrical engineers, ... Each discipline has responsibilities for the design of different systems with respect to regulatory requirements, client demands and contractual negotiations, but no one of them has the overall responsibility for the performance of nonstructural components. The effort for coordination is thus strongly needed, in particular when designing equipment in complex critical facilities, as it will be widely shown afterwards.

The present chapter describes the State of the Art in the field of seismic design of nonstructural components. Major findings of the Literature about the seismic vulnerability of nonstructural components and their dynamic behaviour are reported, with particular reference to the analysis of the dynamic interaction in combined primary-secondary systems. A comparative study of the current building codes in high seismicity countries (USA, New Zealand, Italy) is then carried out. The seismic design requirements provided by the codes are critically assessed and compared in order to identify their shortcomings. The chapter closes with a summary of the emerging research needs to improve the seismic design of nonstructural components.

1.2 Seismic vulnerability of nonstructural components

A first crucial need is to investigate the seismic behaviour of nonstructural components in order to assess their vulnerability under seismic events and the consequences of their failure. Mainly relying on the observation of data field collected during recent earthquakes, authors have established a taxonomy of nonstructural components based on their functionality, vulnerability and damage-related issues [46, 130].

Each type of nonstructural component responds in a different manner when subjected to seismic excitation and exhibits its own failure modes. In particular, each nonstructural component shows sensitivity to one or more response parameters of the structure and the damage of the component is correlated to these response parameters. According to the standard FEMA 356/2000 [38], seismic vulnerable nonstructural components are classified into three categories depending on their sensitive response parameter:

- acceleration-sensitive components;
- deformation-sensitive components;
- acceleration- and deformation-sensitive components.

Nonstructural components that are sensitive to and subjected to damage from inertial loading are classified as *acceleration-sensitive* components. Correlated failure modes might be of two sorts depending on the degree of restraint between the component and the structure. In the presence of a rigidly anchored component, failure occurs when the accelerations transmitted to it become intense enough to cause internal damage, as suffered by equipment like computers, communications systems and medical equipment. In the presence of an unanchored or inadequatly anchored component, failure is caused by the excessive sliding or rocking (overturning) of the component, involving the possible rupture of service lines between the component and the structure and the release of toxic or hazardous substances.

Nonstructural components that are sensitive to and subjected to damage from the deformation of the structure are classified as *deformation-sensitive* components. While acceleration-sensitive components have usually a single attachment point, these are typically attached to multiple points in the construction. As a consequence, failure is caused by an excessive deformation imposed by the structure to the component, for example due to inter-storey displacements or drifts. Most architectural components such as glass panes, partitions and veneer are damaged because of this distortion and not because they themselves are shaken or damaged by inertial forces.

A component that is sensitive to both the deformation of the structure and the inertial loading is classified as *acceleration- and deformation-sensitive* component.

Fig. 1.2 gives a non-exhaustive list of nonstructural components classified according to their sensitive response parameter. In Figs. 1.3 and 1.4, some of the possible damages are illustrated.

COMPONENT		Sensitivity Acc.	Def.
A. ARCHITECTURAL			
1.	**Exterior Skin**		
	Adhered Veneer	S	P
	Anchored Veneer	S	P
	Glass Blocks	S	P
	Prefabricated Panels	S	P
	Glazing Systems	S	P
2.	**Partitions**		
	Heavy	S	P
	Light	S	P
3.	**Interior Veneers**		
	Stone, Including Marble	S	P
	Ceramic Tile	S	P
4.	**Ceilings**		
	a. Directly Applied to Structure	P	
	b. Dropped, Furred, Gypsum Board	P	
	c. Suspended Lath and Plaster	S	P
	d. Suspended Integrated Ceiling	S	P
5.	**Parapets and Appendages**	P	
6.	**Canopies and Marquees**	P	
7.	**Chimneys and Stacks**	P	
8.	**Stairs**	P	S

COMPONENT		Sensitivity Acc.	Def.
B. MECHANICAL EQUIPMENT			
1.	**Mechanical Equipment**		
	Boilers and Furnaces	P	
	General Mfg. and Process Machinery	P	
	HVAC Equipment, Vibration Isolated	P	
	HVAC Equipment. Nonvibration Isolated	P	
	HVAC Equipment, Mounted In-line with Ductwork	P	
2.	**Storage Vessels and Water Heaters**		
	Structurally Supported Vessels (Category 1)	P	
	Flat Bottom Vessels (Category 2)	P	
3.	**Pressure Piping**	P	S
4.	**Fire Suppression Piping**	P	S
5.	**Fluid Piping, not Fire Suppression**		
	Hazardous Materials	P	S
	Nonhazardous Materials	P	S
6.	**Ductwork**	P	S

Acc.=Acceleration-Sensitive
Def.=Deformation-Sensitive
P = Primary Response
S = Secondary Response

Figure 1.2. Seismic vulnerable nonstructural components: response sensitivity. After FEMA 356/2000 [38].

Nonstructural damage is of great concern for the seismic risk mitigation since it might have direct and indirect consequences in all of the three risk categories associated to earthquake [35]:

- *loss of life*, that is the risk that people could be injured or killed by damaged or falling nonstructural components. Life safety threats might also be the secondary effect of nonstructural damage, for example when dislodged and fallen fallen items extensively block the escape routes in a building;
- *loss of property*, that is the risk associated to the initial investment in nonstructural components. For example, in the case of commercial buildings, such a cost is typically estimated between the 65% and 85% of the total cost of the building, hence far greater than the cost of structural components. Nevertheless, nonstructural components has been treated as secondary elements till recently, since the theory driving seismic codes has been to protect the structure and not the nonstructural components;
- *loss of function*, that is the risk of incurring in disrupted operation of essential systems like emergency power generation, power distribution, communications, ventilation, air conditioning. In such cases, nonstructural damage might cause the post-earthquake downtime of critical facilities (*i.e.* hospitals, fire stations, major industrial plants, ...) even in the absence of relevant structural damage.

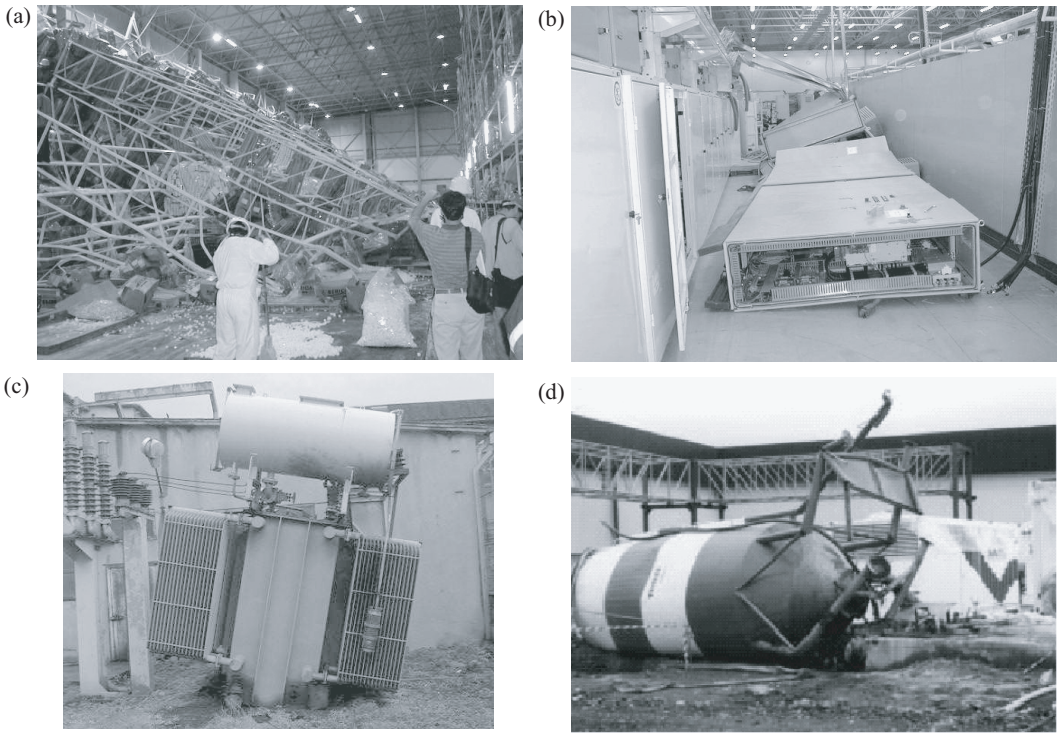

Figure 1.3. Examples of acceleration-sensitive nonstructural components and their damage. (a) Storage rack in pharmaceutical plant. (b) Data cabinets. (c) Transformer. (d) Water tank. After Scawthorn [70].

Figure 1.4. Examples of deformation-sensitive nonstructural components and their damage. (a) External cladding panels. (b) Glazing. (c) Interior partitions. (d) Suspended ceiling. After Dipartimento della Protezione Civile [27].

1.3 Seismic analysis of nonstructural components

In view of the safety and economic importance of nonstructural damage, increasing research efforts have been devoted in the last three decades to the development of rational methods for the seismic analysis of nonstructural components. Excellent state-of-the-art reviews on this subject have been presented by Chen and Soong [11], Soong [119] and Villaverde [141, 143].

The dynamic response of a system composed by a supporting structure and one or more nonstructural components exhibits a number of complex aspects that pose some difficulties to the seismic analysis. They can be are summarized as follows:

- *Filtering effect of the structure.* The dynamic response of a nonstructural component depends not only on its dynamic properties but also on the dynamic properties of the structure to which it is attached. Ground motion, filtered through the supporting structure, shows amplifications and changes in frequency content when it is experienced as base motion by the nonstructural component.

- *Dynamic interaction.* Under some circumstances, there may be a significant dynamic interaction between a nonstructural component and its supporting structure. That is, the component presence may modify the structural response and vice versa.

- *Location.* The dynamic response of a nonstructural component depends on its location within the supporting structure. For instance, in case of a frame structure, the component response depends on the height of the floor on which it is installed.

- *Attachment configuration.* Attachment detailing has a strong influence on the performance of nonstructural components during earthquakes. However, attachment configurations vary and result to be quite complex to be modelled.

- *Non-classical damping.* In general, the system composed by a supporting structure and a nonstructural component is not classically damped because of the different damping characteristics of the structure and the component. Hence, complex valued eigenvalues and eigenvectors have to be determined through a complex modal analysis.

- *Tuning.* Natural frequencies of a nonstructural component may be close to or coincide with the natural frequencies of the supporting structure. In such cases, the system composed by the structure and the component has closely spaced natural frequencies and resonance effects may occur.

- *Nonlinearities.* The dynamic response of a nonstructural component is affected by its own inelastic behaviour as well as that of its supporting structure.

Different degrees of accuracy are achieved depending on how these aspects are taken into account in the seismic analysis of nonstructural components. Two basic approaches exist in current literature:

i. *The coupled or combined primary – secondary system approach.* The supporting structure, or primary subsystem, and the nonstructural component, or secondary subsystem, are considered as coupled parts of a combined primary – secondary system and analysed together.

ii. *The decoupled or systems-in-cascade approach.* The supporting structure and the nonstructural component are decoupled and analysed individually, neglecting their dynamic interaction. This approach leads to two alternative methods of analysis, the former being dynamic, the latter static:

   a. the floor response spectrum method;

   b. the equivalent static lateral force method.

Features and limits of these methods are described in the following.

1.3.1 Combined primary – secondary system approach

In the most general approach, nonstructural secondary components are included along with the primary supporting structure in the analytical model to evaluate their time history response to earthquake ground motions. Both modal and time history analyses have been used for this purpose.

In general, modal analysis requires the calculation of complex eigenvalues and eigenvectors of the damped system. In fact, a combined primary – secondary system is usually non-classically damped, even though each subsystem has proportional damping characteristics, hence its damping matrix cannot be diagonalized by the eigenvectors of the undamped system. Such a complex modal analysis is unavoidable since the use of approximate classically damped solution, by neglecting the off-diagonal terms of the damping matrix, has been proven to give non-conservative results. According to parametric studies on the nonstructural response [11], the effect of non-classical damping becomes especially significant when the following conditions occur: i. a nonstructural component frequency is tuned to a supporting structure frequency; ii. damping properties of the nonstructural component are much smaller than those of the supporting structure.

Until a few years ago, the combined primary – secondary system approach ran into serious computational difficulties due to the large number of degrees of freedom and the large differences existing between properties (masses, stiffnesses, damping constants) of primary and secondary subsystems. In order to improve the numerical accuracy and efficiency of combined analyses, perturbation methods were first introduced by Sackmann and Kelly [111] under the assumption that mass, stiffness and

damping properties of the secondary subsystem could be considered small (perturbed parameters) as compared to those of the primary subsystem. These techniques were successfully applied to calculate the combined modal properties [110, 128] and dynamic response [26, 59]. Computational capacities nowadays available enable to overcome the aforementioned difficulties and carry out accurate and efficient combined analyses even in presence of large mass equipment.

1.3.2 Floor response spectrum method

Numerical difficulties associated with the combined primary – secondary system approach have led authors to develop simplified, yet rational methods for the seismic analysis of nonstructural components. These methods are based upon a *decoupled* or *systems-in-cascade* approach [141] that neglects the dynamic interaction between the nonstructural component and its supporting structure. The nonstructural component is assumed to be in cascade with the supporting structure, such that it receives the input from the supporting structure but it is not able to modify this input. This assumption has been proven accurate for nonstructural components whose masses are much smaller than the mass of the supporting structure and whose natural frequencies are not tuned to a natural frequency of the structure. Design criteria are currently employed in engineering practice in deciding whether a decoupled or a coupled approach is required. A typical criterion is shown in Fig. 1.5, which is given for a two-degree-of-freedom system, *i.e.* a single-degree-of-freedom nonstructural component mounted on a single-degree-of-freedom supporting structure [11].

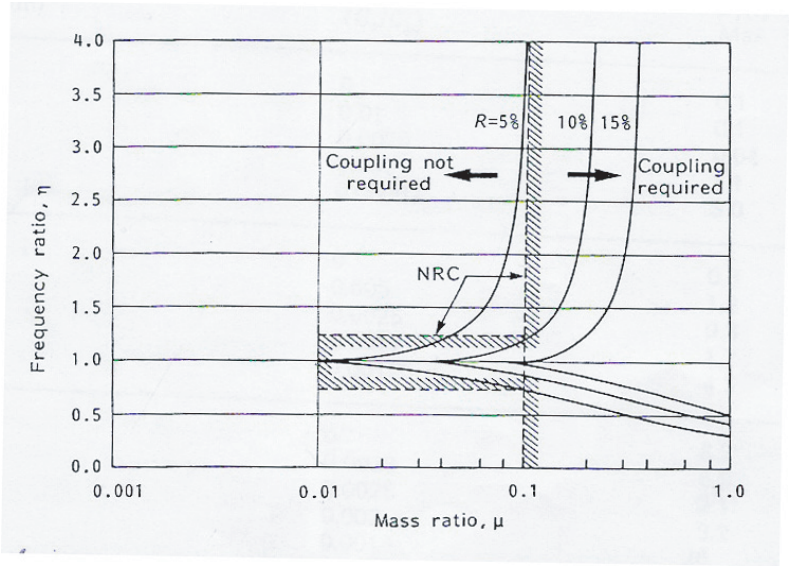

Figure 1.5. Decoupling criterion. After Chen and Soong [11].

Variable R is defined as

$$R = \frac{|\omega - \omega_s|}{\omega_s} \tag{1.1}$$

where ω is the fundamental frequency of the combined system and ω_s is the fundamental frequency of the structure. R is shown *versus* the mass ratio μ and the frequency ratio η, letting the former be defined by

$$\mu = \frac{m_c}{m_s} \tag{1.2}$$

and the latter be defined by

$$\eta = \frac{\omega_c}{\omega_s} \tag{1.3}$$

where subscripts c and s refer to the component and the structure, respectively. As the mass ratio increases or when the frequency ratio approaches one, a greater primary – secondary systems interaction is expected and a coupled approach is required; otherwise, a decoupled approach is allowed.

In the spirit of a decoupled approach, the floor response spectrum method has been developed for the seismic analysis of nonstructural components. According to this method, the dynamic response of the supporting structure is first determined while neglecting the presence of the nonstructural component. By means of a time domain analysis with recorded or synthetic ground accelerograms, the acceleration time history is determined at the point – or floor – of the structure to which the component is attached. This acceleration time history is then used to generate the required floor response spectrum, which in turn is employed for the dynamic analysis of the nonstructural component. Stochastic methods have been developed also to generate floor response spectra by using the floor power spectral density [50].

On the one hand, the floor response spectrum method is easy to implement and it does not pose numerical difficulties, which is why it has been widely used in engineering practice, specially in the nuclear industry [137]. On the other hand, however, its original formulation meets some shortcomings: since a decoupled approach is adopted, no account is taken of non-classical damping and closely spaced modes of the combined system; furthermore, the effects associated with the inelastic behaviour of the supporting structure and of the nonstructural components are neglected or improperly considered. For these reasons, attempts have been made to improve the method.

To incorporate the dynamic interaction between the nonstructural component and the supporting structure, authors have proposed a mode synthesis method. Such a method consists in obtaining the modal properties of the combined system in terms of the individual modal properties of the primary and secondary subsystem. These combined eigenproperties can then be used to calculate the response of the subsystems, in both deterministic and stochastic analyses [31, 32], and particularly to generate floor response spectra [129]. Recently, floor response spectra have been developed also for inelastic [89] and seismically base-isolated structures [56].

1.3.3 Equivalent static lateral force method

In the spirit of a decoupled approach, an equivalent static lateral force method has been developed for the seismic analysis of nonstructural components. Seismic action effects are determined by applying at the component's centre of mass a horizontal force, whose general format is given by

$$F_c = \frac{W_c \, a_g \, A}{q_c} \tag{1.4}$$

where

- W_c is the component weight under normal operating condition, including the weight of any contents (such as fuel) likely to be present;
- a_g is the peak ground acceleration, expressed in terms of gravity acceleration;
- A is the dynamic amplification factor of the peak ground acceleration to the component acceleration;
- q_c is the behaviour factor, which accounts for the ductility capacity of the component to reduce the lateral force.

Since a decoupled approach is adopted, the dynamic amplification factor A in Eq. (1.4) can be expressed as the product of two independent factors

$$F_c = \frac{W_c \, a_g \, A_f \, A_c}{q_c} \tag{1.5}$$

The former, A_f, is the floor amplification factor, which accounts for the ground motion amplification due to the structure at the location where the component is; the latter, A_c, is the component amplification factor, which accounts for the floor motion amplification due to the component. In general, A_f and A_c are affected in a complex manner by several parameters: the dynamic characteristics of both the supporting structure and the component; the dynamic interaction between the structure and the component; the component location within the structure; the attachment detailing; the effect of nonlinearities in both the structural and the component behaviour. Notwithstanding, for the sake of design applicability, current seismic codes have implemented Eq. (1.5) by introducing simplifying assumptions on A_f and A_c, even at the cost of a reduced accuracy. Only recently, authors have attempted to improve the estimates given by the codes. Villaverde [144] pointed out that the response of a nonstructural component is significantly affected by the nonlinear behaviour of the supporting structure, mainly in the form of a reduction over the corresponding linear response, but also, in some cases, in the form of an amplification. Singh *et al.* [115, 116] carried out numerical studies on irregular buildings and demonstrated that a first-mode based approximation of the structural response may lead to a non-conservative estimate of the nonstructural response because of higher modes resonances.

1.4 Comparative assessment of code provisions

This section focuses on the assessment of current building codes and guidelines for the seismic design of nonstructural components in high seismicity countries: United States of America, New Zealand, Europe and Italy in particular. Due to the still relatively limited analytical and experimental studies on the seismic performance of nonstructural components, current provisions were formulated on observation data from past earthquakes and have mainly an empirical nature. Oriented for the most to the practical design of ordinary nonstructural components in ordinary buildings, they provide different degrees of simplicity and conservatism depending on how many parameters are taken into account as regards the dynamic behaviour of the main structure and the nonstructural component.

In the present inventory, current provisions are critically assessed and compared in order to identify their shortcomings. The evolution of seismic codes over the years is also reported when the understanding of these changes may clarify the simplifying assumptions introduced in code provisions.

1.4.1 United States of America

In the United States of America, reference building codes for the seismic design of nonstructural components are of four sorts:

- the *Uniform Building Code* (UBC), updated every three years since 1927 to 1997 by the International Conference of Building Officials (ICBO). The UBC is a key regulation in the mitigation of the seismic hazard since it has long provided the basis for the seismic provisions for new buildings in local jurisdictions of California and other seismically active states, particularly in the western United States;
- the *International Building Code* (IBC), updated every three years since 2000 by the International Code Council (ICC). The IBC has superseded the UBC with the intent of standardizing a single buiding code for use in the entire United States;
- the *NEHRP Guidelines for the Seismic Rehabilitation of Buildings* and the *NEHRP Recommended Provisions for the Development of Seismic Regulations for New Buildings*, first published in 1985, funded by the Federal Emergency Management Agency (FEMA) as part of the National Hazard Reduction Program (NEHRP) and developed by the Building Seismic Safety Council (BSSC);
- other FEMA-funded guidelines specifically relating to the seismic performance of nonstructural components.

The UBC and the IBC are model codes that become law when officially adopted by a local or state jurisdiction. States generally mandate that local jurisdictions adopt

a specific edition of a building code by a given date. The local jurisdictions may add specific provisions and create a local building code. FEMA-funded NEHRP Guidelines are used by designers on a voluntary basis, but their use is widespread since they represent a state-of-the-art consensus resource document. According to this, the UBC and the IBC often assimilate the latest seismic provisions of NEHRP Guidelines. Several guidelines and recommendations [70] has been also developed by a number of professional associations (American Society of Civil Engineers (ASCE), American Society of Mechanical Engineers (ASME), Structural Engineers Association of California (SEAOC), Institute of Electrical and Electronic Engineers (IEEE), ...). These documents refer to specific installations and do not provide general design methods, therefore they are not of great interest to the purpose of the present inventory and they are not taken into account.

Before the 1960s, building codes in United States did not contain any specific seismic design requirements for nonstructural components, which were designed for gravity loads only. The 1961 edition of the UBC first introduced a seismic force analysis procedure applicable to nonstructural building components. Shortly after, the 1971 San Fernando earthquake demonstrated that nonstructural damage was a primary cause of injuries and economic losses and it became even more evident the importance of nonstructural component issues in seimic design. During the 1980s and early 1990s, some research work was done on the dynamic behaviour and the seismic protection of critical equipment, such as piping systems and control panels, in nuclear power plants and other special-purpose facilities [4, 131, 78]. Rigorous methods were formulated for the dynamic analysis and the design of these components, but they were not included into building codes because too sophisticated. The intent of building codes at that time was limited to prescribe design-oriented simplified methods suitable for the seismic design of ordinary nonstructural components in ordinary buildings.

A notable advance of seismic code provisions for nonstructural components was driven by the work by Soong *et al.* [120]. Aiming at critically assessing and updating previous NEHRP Provisions, this work clearly identified the parameters affecting the nonstructural response and prescribed an equivalent static lateral force method, oriented to the design of ordinary nonstructural components in ordinary buildings. Every simplifying assumption in the method was justified on the basis of dynamic analyses, experimental results and observation data from historical earthquakes and this meant an improvement on the past. Recommendations proposed by Soong *et al.* were rapidly included into the 1994 edition of *NEHRP Recommended Provisions for the Development of Seismic Regulations for New Buildings*(FEMA 222A) [34] and into the 1997 edition of *NEHRP Guidelines for the Seismic Rehabilitation of Buildings* (FEMA 273 and FEMA 274) [37, 36]. Since then, the design criteria for nonstructural components have remain essentially unchanged up to the current NEHRP Provisions, *i.e.* the 2003 edition (FEMA 450) [39] and the 2009 edition (FEMA P-750) [42]. The same recommendations have been included also in the UBC 1997 Edition [63] and in the IBC,

2000 to 2009 Editions [62].

Examined below are the seismic design requirements prescribed by FEMA 450/2003 for nonstructural components that are permanently attached to structures and for their supports and attachments. A static procedure is defined which requires the nonstructural component to be designed for a seismic force determined as follows

$$F_p = \frac{0.4\, a_p\, S_{DS}\, W_p}{R_p/I_p} \left(1 + 2\,\frac{z}{h}\right) \tag{1.6}$$

with the lower and upper limit values

$$0.3\, S_{DS} I_p W_p \leq F_p \leq 1.6\, S_{DS} I_p W_p \tag{1.7}$$

where the following notation has been introduced:

a_p	the component amplification factor
S_{DS}	the short period spectral acceleration parameter for 5% damping and for the design hazard level
W_p	the operating weight of the component
R_p	the component response modification factor
I_p	the component importance factor
h	the average roof height of the supporting structure above the base
z	the height above the base of the attachment point of the component, varying from 0 to h

The seismic design force F_p must be centered at the component's centre of gravity and distributed relative to the component's mass distribution. It is independently applied in each of two orthogonal horizontal directions in combination with service loads. In addition, a concurrent force $\pm 0.2\, S_{DS} W_p$ is applied in the vertical direction.

The formulation of Eq. (1.6) is discussed in detail in order to discern which are the assumptions and the limits it is founded on. As stated in Sec. 1.3, the decoupled approach, upon which the method is based, has been proven sufficiently accurate only when the ratio between the mass of the nonstructural component and the mass of the supporting structure is small. Eq. (1.6) is thus intended only for light nonstructural components and this limit is expressly indicated by FEMA 450/2003: "*where the individual weight of supported components and nonbuilding structures with period greater than 0.06 seconds exceeds 25 percent of the total seismic weight W, the structure shall be designed considering interaction effects between the structure and the supported components*".

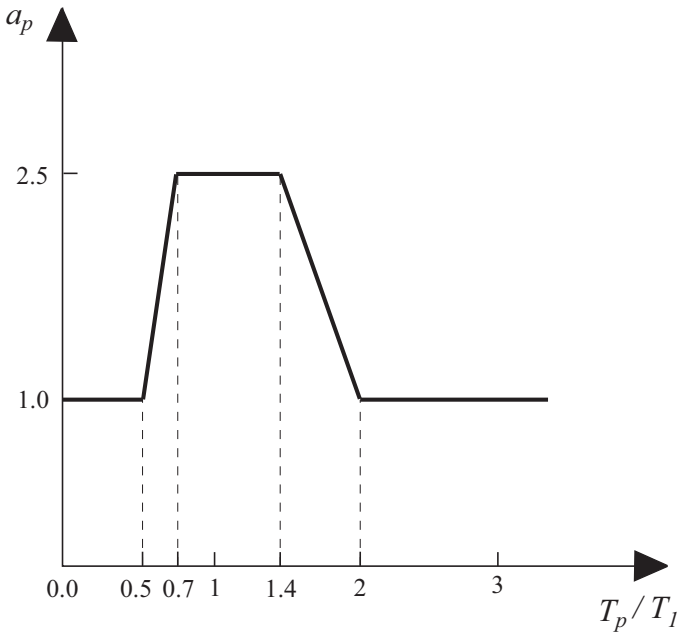

Figure 1.6. Variation of the component amplification factor a_p with the ratio between the component period T_p and the fundamental period T_1 of the structure. After Soong *et al.* [120].

As a consequence of neglecting the dynamic interaction, the floor amplification effect and the component amplification effect are separately considered by means of two independent factors. In Eq. (1.6), the quantity $0.4\,S_{DS}$ represents the spectral acceleration at 0 second period, that is the peak ground acceleration, and includes site effects. It is multiplied by the floor amplification factor, given by $\left(1 + 2\,z/h\right)$, and by the component amplification factor a_p. The latter can assume only two discrete values depending on the component flexibility: 1.0 is for rigid components and rigidly attached components, whose natural period T_p is taken as not greater than 0.06 s; 2.5 is for flexible components and flexibly attached components, whose natural period T_p is taken as greater than 0.06 s. These values were proposed by Soong *et al.* [120] by means of the simplified amplification curve shown in Fig. 1.6, based on experimental results, but lacking a theoretical basis. The component amplification factor a_p varies linearly with the ratio between the component period T_p and the fundamental period T_1 of the structure: when the ratio is close to 1.0, a_p reaches the maximum value 2.5; when the ratio is sufficiently distant from 1.0, a_p is equal to the value 1.0, which represents no amplification.

The last two parameters that come into Eq. (1.6) are the component importance factor I_p and the component response modification factor R_p. Parameter I_p operates to increase the magnitude of the seismic design force F_p when required by the significance of the nonstructural component, its function or the structure it is housed in. It is taken as 1.5 if any of the prescribed conditions apply: i. the component is required to function after an earthquake; ii. the component contains hazardous material; iii.

the failure of the component could impair the continued operation of essential services for post-earthquake recovery. These conditions occur in critical facilities, in all other cases I_p is taken as 1.0. Parameter R_p accounts for the ductility capacity of the component and its attachment to reduce the magnitude of the seismic design force F_p. Energy absorption capabilities in the inelastic range have been estimated for a variety of nonstructural components, both architectural ones and equipment, whose response modification factors R_p are tabulated in FEMA 450/2003. These values, ranging from 1.0 to 3.5, are reported in Tab. 1.1 and Tab. 1.2 together with the values of the component amplification factor a_p.

Mechanical or Electrical Component	a_p	R_p
General Mechanical		
Boilers and Furnaces	1.0	2.5
Pressure vessels on skirts and free-standing	2.5	2.5
Stacks	2.5	2.5
Cantilevered chimneys	2.5	2.5
Other	1.0	2.5
Manufacturing and Process Machinery		
General	1.0	2.5
Conveyors (non-personnel)	2.5	2.5
Piping Systems		
High deformability elements and attachments	1.0	3.5
Limited deformability elements and attachments	1.0	2.5
Low deformability elements and attachments	1.0	1.5
HVAC System Component		
Vibration isolated	2.5	2.5
Non-vibration isolated	1.0	2.5
Mounted in-line with ductwork	1.0	2.5
Other	1.0	2.5
Elevator Components	1.0	2.5
Escalator Components	1.0	2.5
Trussed Towers (free-standing or guyed)	2.5	2.5
General Electrical		
Distribution systems (ducts, conduit, cable tray)	2.5	5.0
Equipment	1.0	2.5
Lighting Fixtures	1.0	1.5

Table 1.1. Amplification factor a_p and response modification factor R_p for mechanical and electrical components. After FEMA 450/2003 [39].

Architectural Component	a_p	R_p
Interior nonstructural walls and partitions		
Plain masonry walls	1.0	1.5
All other walls and partitions	1.0	2.5
Cantilevered elements, braced or unbraced to structural frame below their centres of gravity		
Parapets and cantilevered interior nonstructural walls	2.5	2.5
Chimney and stacks laterally supported by structures	2.5	2.5
Cantilevered elements braced to structural frame above their centres of gravity		
Parapets	1.0	2.5
Chimney and stacks	1.0	2.5
Exterior nonstructural walls	1.0	2.5
Exterior nonstructural wall elements and connections		
Wall element	1.0	2.5
Body of wall-panel connection	1.0	2.5
Fasteners of the connecting system	1.25	1.0
Veneer		
High deformability elements and attachments	1.0	2.5
High deformability elements and attachments	1.0	1.5
Penthouse (except where part of the building frame)	2.5	3.5
Ceilings	1.0	2.5
Storage and laboratory cabinets	1.0	2.5
Access floor		
Special access floors	1.0	2.5
All others	1.0	1.5
Appendages and ornamentation	2.5	2.5
Signs and billboards	2.5	2.5
Other rigid components		
High deformability elements and attachments	1.0	3.5
Limited deformability elements and attachments	1.0	2.5
Low deformability elements and attachments	1.0	1.5
Other flexible components		
High deformability elements and attachments	2.5	3.5
Limited deformability elements and attachments	2.5	2.5
Low deformability elements and attachments	2.5	1.5

Table 1.2. Amplification factor a_p and response modification factor R_p for architectural components. (after FEMA 450/2003 [39])

Displacement considerations are also important in the seismic design of nonstructural components, since in the past excessive displacements and deformations caused a significant number of nonstructural failures. FEMA 450/2003 prescribes design requirements concerning interstorey drifts and relative displacement between adjacent buildings, addressed to nonstructural components installed over two or more floors of one building structure or between two building structures. This is mainly the case of architectural components, such as interior partitions and exterior wall panels, but also of mechanical and electrical components like utility and service lines (piping, HVAC ductworks, cable trays...). When a nonstructural component is attached in two points of the same supporting structure, it must be designed to accomodate a seismic relative displacement determined as follows

$$D_p = \delta_x - \delta_y \tag{1.8}$$

with the upper limit value

$$D_p \leq (X - Y)\,\frac{\Delta_a}{h_{sx}} \tag{1.9}$$

where

δ_x is the deflection of the structure at the upper attachment point (level x)

δ_y is the deflection of the structure at the lower attachment point (level y)

Δ_a is the allowable storey drift for the structure

h_{sx} is the storey height

X is the height about the base of level x

Y is the height about the base of level y

When a nonstructural component is attached in two points of adjacent structures, A and B, the former at level x and the latter at level y, the design seismic relative displacement D_p is given as

$$D_p = |\delta_{xA}| - |\delta_{yB}| \tag{1.10}$$

with the upper limit value

$$D_p \leq \frac{X\Delta_{aA}}{h_{sx}} + \frac{Y\Delta_{aB}}{h_{sx}} \tag{1.11}$$

where

δ_{xA} is the deflection of structure A at the upper attachment point (level x)

δ_{yB} is the deflection of structure B at the lower attachment point (level y)

Δ_{aA} is the allowable storey drift for structure A

Δ_{aB} is the allowable storey drift for structure B

Interstorey drifts and relative displacements between adjacent buildings, however, are only part of the displacement considerations to account for in the seismic design of nonstructural components. In particular, requirements given by Eqs. (1.8) and (1.10) do not pertain to the mechanical and electrical components having a single attachment point to the supporting structure. In this case, and in the presence of flexible anchorages, even with a large ductility capacity, the relative displacement between the component and the attachment floor should not to exceed an allowable value unless the damage of either the anchorage or the service lines connected to the component. Despite the prominency of these considerations, no provisions in this regard are included in FEMA 450/2003.

Anchorages

Anchorages or *attachments* are defined by FEMA 450/2003 as "*means by which nonstructural components and their support are secured and connected to the seismic-force-resisting system of the structure*". Anchorage detailing has a significant influence on the nonstructural component performance during earthquakes. In some cases, damage of a nonstructural component results from the failure of its anchorage due to excessive stress or deformations. In other cases, an appropriate design for anchorage means rather a significant improvement: for example, the introduction of ductility capacity in the anchorage will reduce the seismic design force on the component.

The principle established by FEMA 450/2003 is that the component forces must by transferred to the supporting structure by means of a "*continuous load path of sufficient strength and stiffness*". Hence, attachments cannot count on frictional resistance produced by the effects of gravity since components tend to move due to rocking when subjected to earthquake motions. This is often accentuated by vertical ground motions. Because frictional resistance cannot be relied upon, positive restraints must be provided, such as anchor bolts, welded connections and mechanical fasteners. Anchorages must be proportioned to carry the design force transferred by the component (Eq. (1.6)), but limiting the value of the response modification factor R_p to 1.5. This allows to provide the anchorage with overstrength when the ductility capacity of the connection is difficult to be estimated and a non-ductile failure of the anchorage is possible. For example, many bolted connections, such as large equipment anchorages, are subjected primarily to shear instead of tension. In these cases, even if the anchor steel is ductile, shear failure of the bolt may be non-ductile, particularly if the deformation of the anchor is constrained by rigid elements on either side of the joint. No specific attention, however, is paid by FEMA 450/2003 to the criteria necessary to ensure the desired ductility capacity (adequate gauge length, anchor spacing, edge distance, steel properties, etc.), which are therefore left to the designer.

Local elements of the supporting structure must be also designed for the seismic forces transferred by the component in addition to normal design loads.

Mechanical and electrical components

FEMA 450/2003 establishes two levels of earthquake safety for mechanical and electrical components depending on their importance factor I_p.

The first safety level corresponds to mechanical and electrical components with $I_p = 1.0$. In this case, the failure of the component itself poses no significant hazard and the only hazard is represented by the failure of attachments, when sliding or overturning of the component could injury people nearby. For this first category, seismic design requirements are prescribed only for supports and attachments. Among the others, components mounted on vibration isolators (rubber-in-shear, springs, or air cushions) must have a bumper restraint or snubber in each horizontal direction, as well as vertical restraints when required to resist overturning (Fig. 1.7).

The second safety level corresponds to mechanical and electrical components with $I_p = 1.5$. In this case, the failure of the component itself poses a significant hazard due to either the leakage of a hazardous content or the loss of an essential function required for post-earthquake. Examples are vessels containing highly toxic or explosive substances, fire protection equipment and uninterruptible power supplies in a hospital. For this second category, seismic design requirements are prescribed for both the components and their attachments. Mechanical and electrical components must be designed for the seismic forces and relative displacements defined in Eqs. (1.6), (1.8) and (1.10) with the intent to preserve their integrity and continuing functioning.

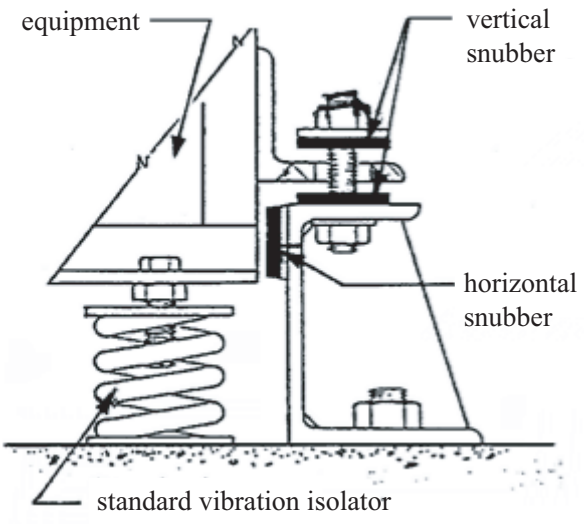

Figure 1.7. Horizontal and vertical snubbers for equipment mounted on vibration isolators.

1.4.2 New Zealand

The Standard Council of New Zealand has recently published a revised standard, "Seismic performance of engineering systems in buildings" (NZS 4219:2009) [126], specifying seismic performance levels and design criteria for engineering systems in buildings. This standard focuses only on *engineering systems*, defined as "*nonstructural systems permanently installed in a building and providing environmental control, water, gas, steam, electrical or communications services*", so it does not include architectural components and any contents not permanently attached to the building structure.

Seismic performance levels

Standard NZS 4219:2009 is set into the framework of performance-based seismic design. Components of engineering systems are classified into seven categories (Tab. 1.3) and are required to meet different seismic performance levels depending on their life safety and operational importance. The code defines three discrete limit states, which are described in the following from the highest to the lowest performance:

i. components representing a life safety hazard (categories P1, P2, P3), including those necessary for emergency evacuation (P4), must not collapse, rupture and lose support after an Ultimate Limit State (ULS) earthquake;

ii. components required for operational continuity within buildings with special post-disaster functions must be able to perform their functions after a Serviceability Limit State 2 (SLS2) earthquake;

iii. all other components must retain their structural and operational integrity without requiring repairs after a Serviceability Limit State 1 (SLS1) earthquake.

NZS4219:2009 limit states ULS and SLS1 are similar to performance levels "Life Safety" and "Operational" defined in FEMA 356. Limit state SLS2 applies only to facilities designated as essential or post-disaster, for which the operational performance level is associated to a lower probability, more severe earthquake.

Seismic design criteria

Having defined the three limit states ULS, SLS1 and SLS2, NZS 4219:2009 sets out the criteria for the seismic design of engineering systems and their restraints. Since the code is intended for a number of different figures involved into the design of engineering systems, two approaches are contemplated:

- performance-based provisions, addressed to professional structural engineers;
- prescriptive provisions, primarily addressed to designers that have no relevant experience and skills in the field of structural engineering.

Criteria	Category	Limit State
Component representing a hazard to life outside the building	P1	ULS
Component representing a hazard to a crowd of greater than 100 people within the building	P2	ULS
Component representing a hazard to individual life within the building	P3	ULS
Component necessary for the continuing function of the evacuation and life safety systems within the buildings	P4	ULS
Component required for operational continuity of essential or post-disaster facilities	P5	SLS2
Component for which the consequential damage is disproportionally great	P6	SLS1
All other components	P7	SLS1

Table 1.3. Categories and limit states for the seismic design of engineering systems components. After NZS 4219:2009 [126].

Building importance level	Criteria	Examples
1	Structures presenting a low hazard to life and property	Farm buildings, ...
2	Normal structures	Single family dwellings, ...
3	Structures that pose risks to people in crowd or contents of high value	Schools, airport terminals, commercial buildings, ...
4	Structures with essential or special post-disaster functions	Medical emergency facilities, fire and police stations, water treatment facilities, ...

Table 1.4. Building importance levels. After NZS 4219:2009 [126].

This is the most innovative aspect of NZS 4219:2009, as the code allows two grades of use depending on the professional expertise of the designer. The first grade is required for the most hazardous components (*e.g.* gas and steam piping, equipment producing heat or containing hazardous substances, brittle components,...), that need to be designed by a structural engineer. Because of his specialist skills, structural engineer is allowed to specify seismic design criteria, but he is fully responsible that engineering systems comply with the performance levels defined by the code. The second grade is admitted for standard components, that may be designed by professionals other than structural engineers such as building services engineers and systems designers. In the absence of specialist skills, the code provides prescriptive design methodologies, specifies minimum requirements of strength and stiffness and controls the details of how engineering systems are restrained in buildings. In contrast with performance-based provisions, prescriptive provisions strongly limit the designer's judgement as well as his responsibility for the effective seismic performance of the component.

Performance-based provisions Components of engineering systems and their restraints to the primary structure must be designed with adequate strength and stiffness as to comply with the requested performance levels. Like FEMA 450/2003, NZS 4219:2009 requires inertial actions due to earthquake to be determined through the equivalent static lateral force method. This approach is intended for light nonstructural components and indeed the code excludes from its scope "*individual components with a mass exceeding 20% of the combined mass of the component and the building structure and with a period of greater than 0.2 seconds*".

In alternative to calculation, testing is admitted as a means of verifying the seismic design of a component. Compared to other seismic codes, which do not deal with testing at all, this is a noteworthy innovation introduced by NZS 4219:2009. The component may be tested *in situ* in its final position in the building or set up in a separate testing laboratory, accurately replicating its boundary conditions. Earthquake hazard levels and acceptance criteria must reproduce the limit states established by the code (ULS, SLS1, SLS2).

Prescriptive provisions Prescriptive section of NZS 4219:2009 sets out a complete and detailed methodology to be used for the seismic design of a component restraining system. The design methodology consists of three steps:

i. determination of earthquake demand, that is equivalent static lateral forces and relative displacements of floors;

ii. determination of the forces on the restraining system;

iii. design of all the elements of the restraining system.

The seismic force acting on a component is determined as follows

$$F = C\,W \tag{1.12}$$

where

C is the lateral force coefficient

W is the operating weight of the component

The lateral force coefficient is taken as

$$C = 2.7 C_h\,C_p\,R_c\,Z \tag{1.13}$$

with the upper limit value

$$C \leq 3.6 \tag{1.14}$$

and where the following notation has been introduced:

C_h the floor height coefficient, equal to 3.0 for components above ground floor and to 1.0 at or below ground floor

C_p the performance factor

R_c the component risk factor

Z the zone factor

Lateral force coefficient C represents the absolute acceleration, expressed in terms of gravity acceleration, experienced by the component at its location within the supporting structure. Let us examine how it is defined.

Quantity ZR_c represents the peak ground acceleration. It accounts for site effects through the zone factor Z and for earthquake hazard level through the risk factor R_c. The latter identifies different hazard levels depending on the component category (Tab. 1.3) and the building importance level (Tab. 1.4). Values of of R_c are reported Tab. 1.5. As it can be seen, a more severe, less probable earthquake is established either for the same component category, with increasing building importance, or for the same building importance level, with increasing component category.

As a consequence of neglecting dynamic interaction, the dynamic amplification of ground motion is accounted for by means of two independent factors. The former is the floor height coefficient, C_h, which accounts for the amplification due to the structure and assumes two discrete values: 1.0 on the ground floor, where there is no amplification; 3.0 on all the floors above ground. The latter is the component amplification factor, which is taken as equal to 2.7 regardless the fundamental period of the component.

The component acceleration is finally reduced by the performance factor C_p, which accounts for the ductility capacity of the component and its restraining system. Values

		Risk factor $\mathbf{R_c}$		
Component	**Limit**	**Building importance level**		
category	**state**	**1, 2**	**3**	**4**
P1, P2, P4	ULS	1.00	1.30	1.80
P3	ULS	0.90	1.20	1.60
P5	SLS2	not applicable	not applicable	1.00
P6	SLS1		0.50	
P7	SLS1		0.25	

Table 1.5. Determination of the component risk factor R_c. After NZS 4219:2009 [126].

of C_p are given by the code and rangeand range from 0.25 (e.g. polypropylene pipes) to 0.85 (e.g. boiler on limited-ductile base fixing).

All the components of engineering systems must resist the seismic force given by Eq. (1.14). Moreover, components connected to more than one level of the supporting structure must be also able to accomodate the relative displacement between fixing points. The relative displacement D is determined from the building design displacements, where known, or it is determined as follows:

$$D = 0.025\, R_c\, H_z \tag{1.15}$$

where H_z is the height between fixing points.

Once the seismic force F_p and the relative displacement D are known, prescriptive provisions in NZS 4219:2009 provide detailed procedures to design the restraining systems. Different type of installations (linear components, floor-mounted components with rigid or flexible mounts, suspended components) and attachments (bolts, cast-in anchors, braces) are considered. In conclusion, prescriptive provisions let the engineering systems designer, even not skilled in the field of structural engineering, design components and their restraints with required minimum levels of strength and stiffness.

Other requirements

Among the general requirements indicated by NZS 4219:2009 for the seismic design of engineering systems components, three are worthy to note. The first concerns the arrangement of engineering systems within the building: their location as well as the layout of the building must be designed in order to reduce the risks due to earthquake. In this sense, NZS 4219:2009 urges a close liaison between the services, the structural and the architectural designers.

The second requirement concerns the attachments of engineering systems components. NZS4219:2009 states that components must be connected to the supporting structure so that seismic forces are transferred to the structure by means of a continuous load path of sufficient strength and stiffness. Such load path must rely on positive fixings, without consideration of frictional resistance produced by the effects of gravity.

The third requirement concerns proprietary components, that is components of standard manufacture. NZS4219:2009 states that such components must be designed by manufacturers so as to ensure the widest possible applicability regarding the building importance level, the component category and its position within the building. Once intended for a specific use, proprietary components and their restraints must be verified as complying with the limit states requested by the code. Verifications must be carried out in accordance with performance-based provisions, by either calculation or testing.

1.4.3 Europe and Italy

Seismic design requirements for nonstructural components are set out by the European Standard EN 1998-1:2004 "Design of structures for earthquake resistance – Part. 1: General rules, seismic actions and rules for buildings" (Eurocode 8) [30]. Italy has been bound to implement the content of Eurocode 8 in its latest national building code "Nuove Norme Tecniche per la Costruzioni – D.M. 14/01/2008" (NTC 2008) [90]. Due to this harmonization process, European and Italian provisions share the same formulation and can be discussed together.

An equivalent static lateral force method is adopted, which requires the nonstructural component to be verified for a horizontal seismic force

$$F_a = \frac{W_a \, S_a \, \gamma_a}{q_a} \tag{1.16}$$

acting at the component's centre of mass in the most unfavourable direction, and where the following notation has been introduced:

W_a the operating weight of the component;

S_a the seismic coefficient;

γ_a the importance factor of the component;

q_a the behaviour factor of the component;

Seismic coefficient S_a is the absolute acceleration, expressed in terms of gravity acceleration, experienced by the component within the structure and may be calculated using the expression

$$S_a = \alpha S \left(\frac{3 \, (1 + z/h)}{1 + (1 - T_a/T_1)^2} - \frac{1}{2} \right) \tag{1.17}$$

with the lower limit value

$$S_a \geq \alpha S \tag{1.18}$$

and where:

- α is the ratio between bedrock acceleration and the gravity acceleration;
- S is the soil factor, accounting for the influence of local ground conditions on the seismic action;
- T_a is the fundamental vibration period of the component;
- T_1 is the fundamental vibration period of the building in the relevant direction;
- z is the height of the nonstructural component above the foundation level;
- h is the building height measured from the foundation level.

In Eq. (1.17), quantity αS represents the peak ground acceleration and includes site effects. It is multiplied by a factor which accounts for the dynamic amplification to the component acceleration

$$\frac{3\ (1+z/h)}{1+(1-T_a/T_1)^2} - \frac{1}{2} \tag{1.19}$$

Being the equivalent static lateral force format based upon a decoupled approach, this dynamic amplification factor can be expressed as the product of two independent factors: the floor amplification factor, due to the structure, and the component amplification factor. Let these two factors be derived from formula (1.19).

To derive the floor amplification factor, we pose $T_a/T_1 = 0$ in formula (1.19), that is, we condider a rigid component. Under this assumption, the dynamic amplification factor (1.19) becomes coincident with the floor amplification factor, defined as follows

$$1 + \frac{3}{2}\,\frac{z}{h} \tag{1.20}$$

This factor varies linearly with the height of the structure and roof acceleration is conservatively taken as 2.5 times the base acceleration, regardless of the fundamental period of the structure.

The component amplification factor can be calculated as the ratio between the dynamic amplification factor (1.19) and the floor amplification factor (1.20), obtaining

$$\left(1 + \frac{3}{2}\,\frac{z}{h}\right)^{-1} \left(\frac{3\ (1+z/h)}{1+(1-T_a/T_1)^2} - \frac{1}{2}\right) \tag{1.21}$$

This factor is assumed to be a function of both the component location and the period ratio between the component and the structure.

Type of nonstructural component	$\mathbf{q_a}$
Cantilevering parapets or ornamentations Signs and billboards Chimneys, masts and tanks on legs acting as unbraced cantilevers along more than one half of their total height	1.0
Exterior and interior walls Partitions and facades Chimneys, masts and tanks on legs acting as unbraced cantilevers along less than one half of their total height, or braced or guyed to the structure at or above their centre of mass Anchorage elements for permanent cabinets and book stacks supported by the floor Anchorage elements for false (suspended) ceilings and light fixtures	2.0

Table 1.6. Values for q_a for nonstructural components. After Eurocode 8 [30].

The importance factor γ_a operates to increase the magnitude of the seismic design force F_a when required by the risk exposure of the nonstructural component. It is prescribed not be less than 1.5 for the following components: i. equipment required for life safety systems; ii. tanks and vessels containing toxic or explosive substances considered to be hazardous to the safety of the general public. In all other cases, it is assumed to be 1.0.

The behaviour factor q_a accounts for the ductility capacity of the component and its attachment in order to reduce the magnitude of the seismic design force F_a. Upper limit values of q_a are given by Eurocode 8 and are reported in Tab. 1.6.

As already pointed out, the equivalent lateral force format is intended for light nonstructural components. Such a limit is clearly indicated by the Italian code NTC 2008, which excludes from its scope "*individual components with a weight exceeding* 10% *of the total seismic weight or* 30% *of the weight of the floor where it is located.*"

1.4.4 Comparisons

The seismic design requirements provided by the assessed international building codes (FEMA 450/2003, NZS4219:2009, Eurocode 8) for nonstructural components are hereafter compared.

In all the aforementioned codes, a decoupled or systems-in-cascade approach is adopted, so that the supporting structure and the nonstructural component are decoupled and analyzed individually, neglecting their dynamic interaction. An equivalent

static lateral force method is then developed for the seismic analysis of nonstructural components.

The different formulae for the calculation of the seismic forces acting on nonstructural components can be trace back to the general format introduced in Sec. 1.3.3. Taking account of the notation used in each code, Tab. 1.7 shows how to associate the general format, given by Eq. (1.4), to the corresponding terms defined in Eqs. (1.6) after FEMA 450/2003, (1.12) and (1.13) after NZS4219:2009, (1.16) after Eurocode 8. Considering the component weight W_c, the peak ground acceleration a_g and the component behaviour factor q_c as common terms, formulations of the seismic force F_c are different depending on the definition of the floor amplification factor A_f and the component amplification factor A_c.

In general, the floor amplification factor A_f varies with the height of the supporting structure. Denoting with z the height of the floor to which the component is attached and with h the total height of the structure, both measured above the base level, this variation depends on the ratio z/h. For the sake of comparison, Fig. 1.8 shows the variation of A_f *versus* z/h according to the different building codes. In FEMA 450/2003 and Eurocode 8, we can recognize four assumptions made in the definition of the floor amplification factor:

i. the response of the supporting structure is dominated by its first mode;

ii. the first mode shape is approximated by a linear variation;

iii. floor accelerations are independent of the dynamic characteristics of the structure;

iv. the structure is assumed to be linear with a damping ratio in its first mode equal to 5%, as customary in seismic code provisions for buildings.

Due to assumptions i. and ii., A_f varies linearly with the height of the structure; due to assumptions iii. an iv., the top floor acceleration is conservatively taken as three times the base acceleration, regardless of the fundamental period of the structure. Also in NZS 4219:2009, A_f is assumed to be independent on the dynamic characteristics of the structure. In this case, however, it is taken as constant and equal to 3.0 along the height of the structure, excluding the ground floor, where $A_f = 1.0$ means no amplification.

As to the component amplification factor A_c, it is primarily affected by the dynamic characteristics of both the component and the supporting structure and the component location within the structure [115, 116]: the response of a nonstructural component located on ground or on a very rigid structure is mainly a function of the frequency content of the input ground motion; conversely, the response of a component located on a flexible structure is mainly a function of the structure natural frequencies. In view of these considerations, Eurocode 8 assumes A_c to be a function of both the ratio z/h

General format	FEMA 450/2003	NZS 4219:2009	Eurocode 8
W_c	W_p	W	W_a
a_g	$0.4\,S_{DS}\,I_p$	$Z\,R_c$	$\alpha\,S$
A_f	$1+2\,\dfrac{z}{h}$	$C_h=\begin{cases}1.0, & \dfrac{z}{h}=0\\ 3.0, & \dfrac{z}{h}>0\end{cases}$	$1+\dfrac{3}{2}\,\dfrac{z}{h}$
A_c	$a_p=\begin{cases}1.0, & T_c\le 0.06\,\mathrm{s}\\ 2.5, & T_c>0.06\,\mathrm{s}\end{cases}$	2.7	$\left(1+\dfrac{3}{2}\,\dfrac{z}{h}\right)^{-1}\left(\dfrac{3\,(1+z/h)}{1+(1-T_a/T_1)^2}-\dfrac{1}{2}\right)$
q_c	R_p	$\dfrac{1}{C_p}$	q_a
Remark (a)	$0.75\,q_c\le A_f\cdot A_c\le 4.00\,q_c$	$A_f\cdot A_c\le 3.6\,\dfrac{q_c}{a_g}$	$A_f\cdot A_c\ge 1$
Remark (b)	$W_c\le 0.25\,W_t$	$W_c\le 0.20\,W_t$	$W_c\le 0.10\,W_t$ $*$ $W_c\le 0.30\,W_f$ $*$

Table 1.7. Equivalent static lateral force method: corresponding terms between the general format, Eq. (1.4), and Eqs. (1.6) after FEMA 450/2003, (1.12) and (1.13) after NZS 4219:2009, (1.16) after Eurocode 8.
$*$ These limits are indicated by the Italian building code NTC 2008, which is a national implementation of Eurocode 8.

and the ratio T_a/T_1, where T_a and T_1 are the fundamental periods of the component and the structure, respectively. In Fig. 1.9, A_c is plotted as a function of T_a/T_1 for several values of z/h. If $T_a/T_1 = 0$, the component moves rigidly with the floor, undergoing the same acceleration, hence $A_c = 1$. The highest values of A_c are obtained when resonance between the component and the structure occurs ($T_a/T_1 = 1$). As the ratio T_a/T_1 leaves the resonance condition, A_c is significantly reduced. In particular, $A_c < 1$, that is, the component acceleration is smaller than the floor acceleration, if $T_a/T_1 > 2$ and it approaches zero as $T_a/T_1 \to \infty$. The effect of the ratio z/h is noteworthy: if $T_a/T_1 < 2$, A_c decreases with increasing z/h; on the contrary, if $T_a/T_1 > 2$, A_c increases with increasing z/h. FEMA 450/2003 includes the effect of the component flexibility in a simplified manner, whereas no account is taken of the component location. Two discrete values, 1.0 and 2.5, are prescribed for the component amplification factor A_c: the former is for rigid and rigidly attached components, the latter is for flexible components. NZS 4219:2009 is even more simplified since a single value, 2.7, is prescribed regardless the fundamental period of the component.

For the sake of comparison, the total dynamic amplification effect, which is the product of the floor amplification factor A_f and the component amplification factor A_c, is plotted in Fig. 1.10 and Fig. 1.11 *versus* the ratio z/h. Fig. 1.10 refers to a rigid component, Fig. 1.11 refers to a flexible component. As indicated in Tab. 1.7, each code establishes also lower or upper limit values for the product $A_f \cdot A_c$. In calculating these limits, a behaviour factor $q_c = 1.00$ and a peak ground acceleration $a_g = 0.5$ are assumed.

As expected, the formula with less information, *i.e.* the formula by NZS 4219:2009, tends to provide the most conservative estimates of the dynamic amplification factor in order to cover the worst possible situations. Two maximum effects, the floor amplification and the component amplification, are considered simultaneously, which is an assumption that in most cases leads to overly conservative results. As other parameters are taken into account in FEMA 450/2003 and in Eurocode 8, less simplified and conservative estimates are provided instead. In the case of a flexible nonstructural component, the dynamic amplification is strongly influenced by the ratio T_c/T_1, as indicated by the plots according to Eurocode 8: the highest value for $A_f \cdot A_c$ is obtained when resonance between the component and the structure occurs ($T_c/T_1 = 1$), whereas the dynamic amplification factor is significantly reduced when the ratio T_c/T_1 leaves the resonance condition. Hence, it seems to be useful to increase the component period T_c in order to reduce the magnitude of seismic forces. However, seismic forces are only one of the design parameters to take into account in the presence of flexible components with a large ductility capacity. Relative displacements between the component and the structure deserve even more attention since they may cause damages of either the anchorages or the service lines connected to the component. Despite the prominency of these considerations, no provisions in this regard are included in the assessed building codes.

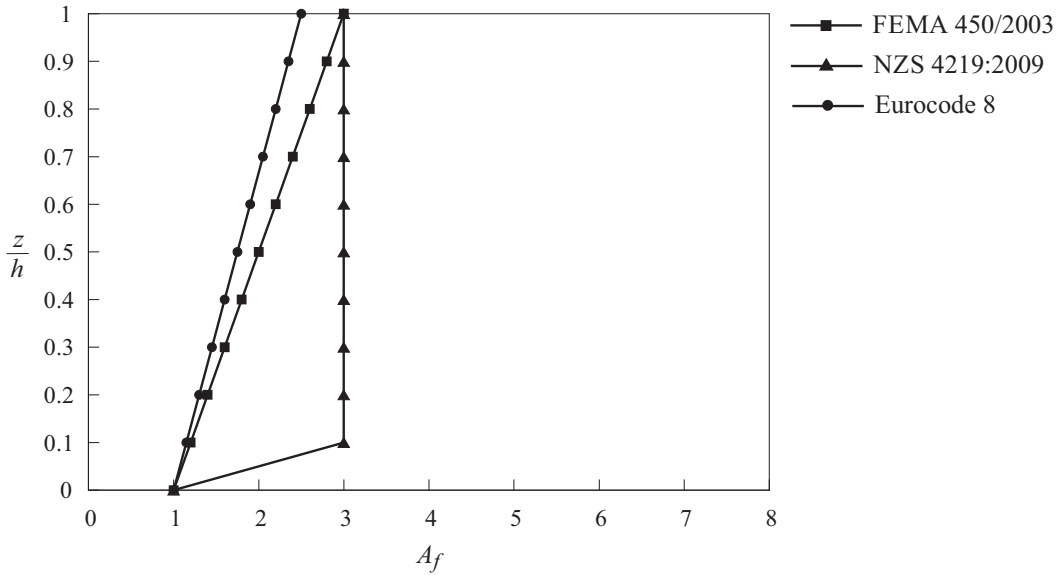

Figure 1.8. Floor amplification factor A_f: comparisons between FEMA 450/2003, NZS 4219:2009 and Eurocode 8.

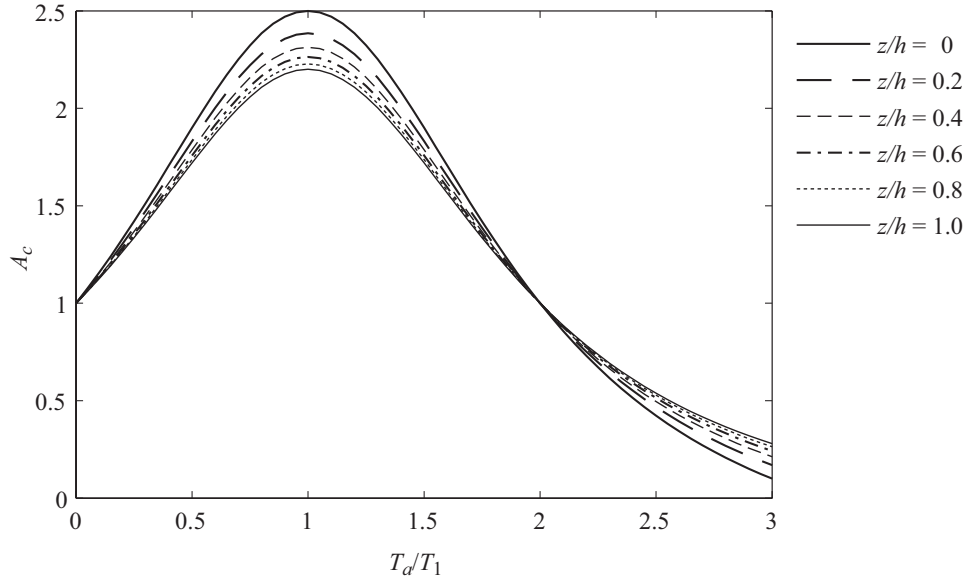

Figure 1.9. Component amplification factor A_c according to Eurocode 8: variation with the ratio between the component period T_a and the structure fundamental period T_1 for various z/h values.

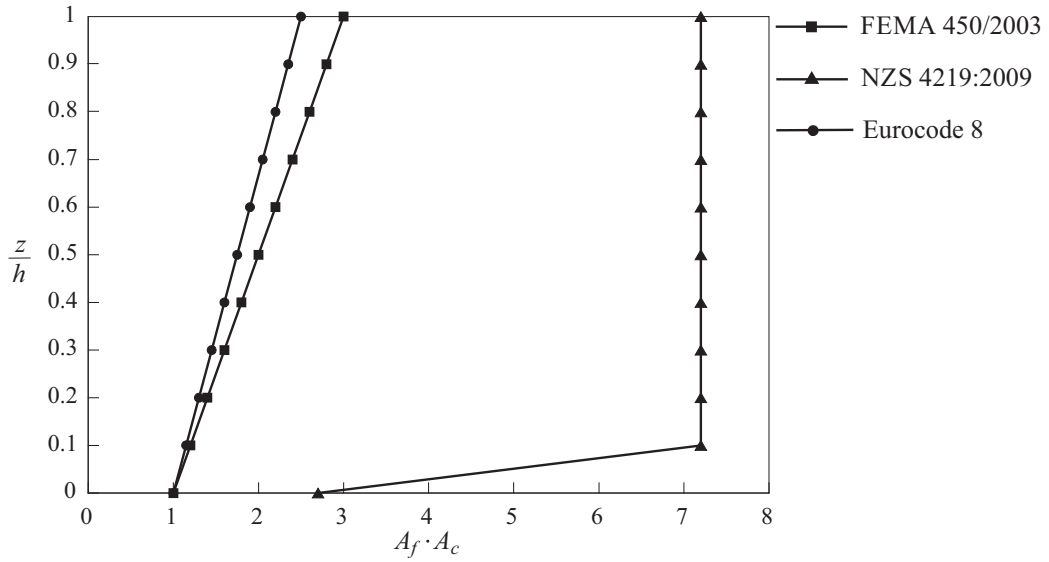

Figure 1.10. Dynamic amplification $A_f \cdot A_c$ for a rigid nonstructural component: comparison between FEMA 450/2003, NZS 4219:2009 and Eurocode 2008. It is assumed $q_c = 1.0$ and $a_g = 0.5$.

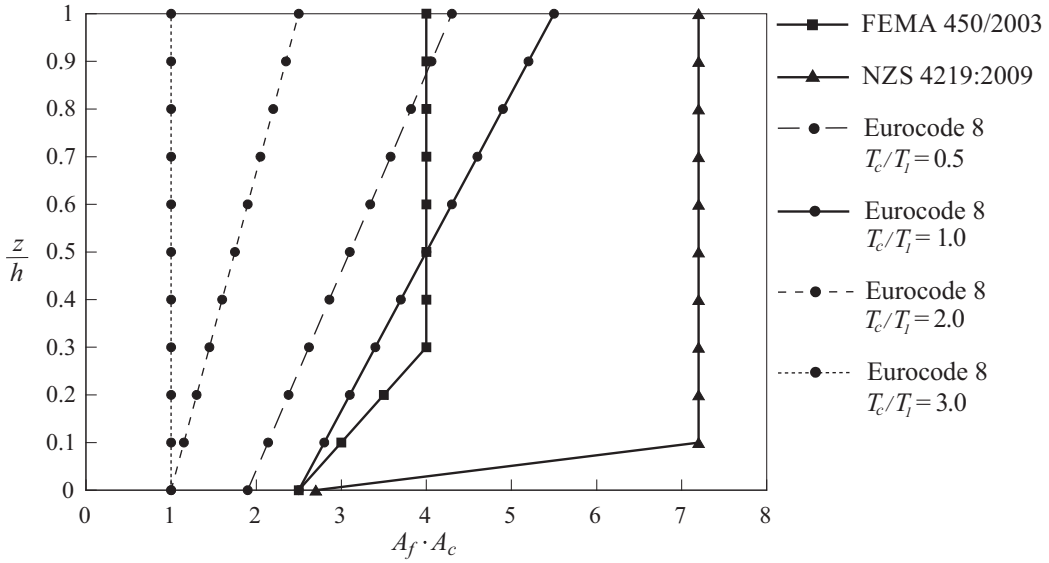

Figure 1.11. Dynamic amplification $A_f \cdot A_c$ for a flexible nonstructural component: comparison between FEMA 450/2003, NZS 4219:2009 and Eurocode 2008. It is assumed $q_c = 1.0$ and $a_g = 0.5$.

1.5 Emerging research needs

As pointed out by the comparative analysis, international building codes are intended to provide, in a form as simple as possible, conservative estimates of the seismic forces acting on nonstructural components. Owing to this, they adopt a static lateral force method, easy to implement and sufficiently accurate when designing light ordinary equipment in ordinary buildings. In the presence of either heavy equipment or an increased hazard level posed on the construction, code provisions may result to be overconservative, when not inaccurate, and require a costly and technically difficult seismic design. In such cases, less simplified and more accurate estimates are obtained by taking into account the dynamic characteristics of both the component and its supporting structure.

The weight of the nonstructural component represents a further, significant shortcoming of the equivalent static lateral force method adopted by the codes. The decoupled approach, upon which the method is based, has been proven accurate only for light nonstructural component and indeed the codes exclude heavy components from their scope. Such limits are indicated in Tab. 1.7, where W_c is the weight of the component and W_t is the combined weight of the component and the supporting structure. In addition, NTC 2008 establishes a local limit imposing the component weight not to exceed 30% of the weight of the floor where the component is located.

In a few words, seismic design requirements provided by international building codes are suitable to ordinary nonstructural components in ordinary buildings. Conversely, the seismic design of non-ordinary or hazardous nonstructural components requires improved methods to account for the dynamic interaction between the component and its supporting structure. Hence, two grades of seismic design should be recognized, depending on the professional expertise of the designer. Prescriptive simplified methodologies, specifying conservative requirements like the equivalent static lateral force method, should be addressed to designers that have no relevant skills in the field of structural engineering (mechanical engineers, electrical engineers, ...). A professional structural engineer should instead advise on non-ordinary cases, when simplified methodologies result to be inaccurate. Because of his specialist skills, the structural engineer should be allowed to specify performance-based seismic design criteria, according to his professional judgement, and to perform seismic analysis other than those prescribed by the codes.

In other terms, the seismic design of nonstructural components should involve a number of various specialities and professional figures, including service engineers and structural engineers. No one of them should have the overall responsibility for the seismic performance of nonstructural components, but an effort for coordination should be rather achieved.

Chapter 2

Seismic protection of equipment in critical facilities: a literature review

In this chapter, a single class of nonstructural components, the equipment, and a special type of constructions, the critical facilities, are considered. The significance of the equipment damage in critical facilities is shown with the evidence of vulnerability studies. A literature review about the innovative technologies for the seismic protection of equipment is presented.

2.1 Significance of equipment damage in critical facilities

Structures that host essential public and economic functions or particularly hazardous activities are designated as *critical facilities*. Owing to their special purposes, they are required to remain functional and in operation during and after a major earthquake. Typical critical facilities include:

- buildings with post-earthquake emergency functions (hospitals, fire stations, police stations, government buildings, data centers, ...);
- industrial facilities containing hazardous materials or whose failure poses catastrophic risk to a large area or a large number of people (petrochemical plants, nuclear plants, water treatment plants, ...);
- high-technologies facilities with high-precision, high-value equipment and contents (integrated circuits manufacturing factories, electronic factories, internet collocation facilities, pharmaceutical industries, ...)
- industrial plants strongly affecting the economic system on a national or a regional scale.

A correct analysis of the seismic risk posed to critical facilities should consider structural failure as well as nonstructural damage and, in particular, damage to equipment. Equipment is substantially the primary responsible of a significantly greater exposition of critical facilities than ordinary buildings to all the three categories of seismic risk: loss of life, loss of property, loss of function.

Regarding property losses, equipment represents a major portion of the total construction investment in most types of critical facilities and, as such, its damage might be the biggest contributor to the losses resulting from earthquakes [130]. As an example, Fig. 2.1 gives the distribution of the economic investments in three building categories including office buildings, hotels and hospitals. Clearly, the investment in

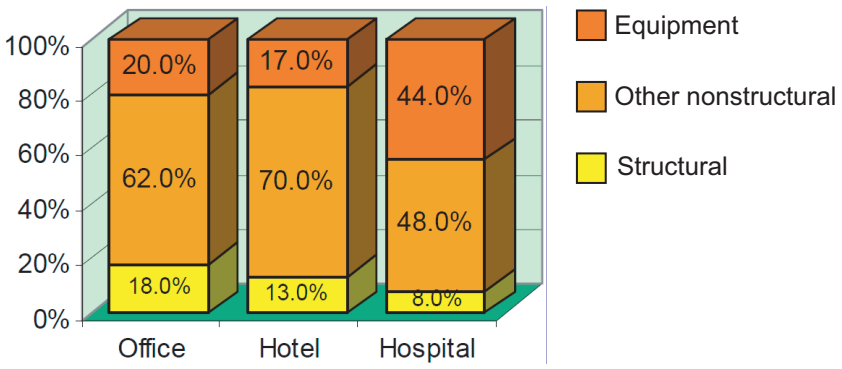

Figure 2.1. Typical investments in office buildings, hotels and hospitals. After Taghavi and Miranda [130].

equipment is far greater than that for structural components and even more in critical facilities like hospitals. It can be seen that in hospitals, the expensive medical equipment makes up 44% of the total construction investment, whereas the equipment cost reduces to 20% for office buildings and 17% for hotels. Conversely, office buildings have the largest portion of structural costs, which are 18% of the total investment, compared to 13% and 8% for hotels and hospitals, respectively. Based on these numbers, the ratio between structural cost and equipment cost is 90% and 76% for office buildings and hotels, respectively, and only 18% for hospitals. Other nonstructural components (architectural) also make up a significant portion of the total construction investment.

The greatest risk posed by the equipment damage to critical facilities is by far the loss of function. Even in the absence of structural failure, the equipment damage might cause the post-earthquake downtime of the facility and result in further and indirect life and economic losses. A case in point is the 1994 Northridge earthquake (California, USA), when many facilities were partially disabled or entirely shut down due to equipment damage in a wide variety of systems. In particular, the earthquake caused considerable service disruption to critical health care facilities and hospitals (Olive View Medical Center, the Holy Cross Medical Center, and the Indian Hills Medical Center the most damaged). Service disruptions at all of these facilities were attributed primarily to equipment failure, including fire protection piping, heating, ventilation and air conditioning (HVAC), power distribution, and control system problems. Failures were reported in diverse equipment systems such as emergency power generation, hospital communications and the medical gas system [70]. From another viewpoint, the 1999 Kocaeli earthquake (Turkey) is of particular interest because of the substantial damage and extended downtime it caused to industrial facilities in the Turkey's most heavily industrialized region. Damage to the Turkey's largest refinery and to other petrochemical plants shut down those facilities for several months and

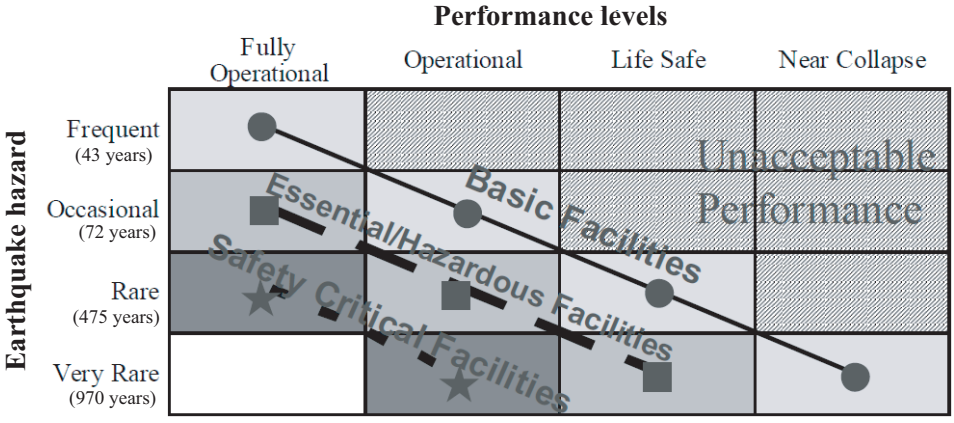

Figure 2.2. Performance objectives for various types of structures. Adapted from SEAOC Vision 2000 [127].

had regional economic consequences [70].

Unfortunately, equipment has been treated as secondary elements till recently, since the theory driving seismic codes has been to protect the structure, substantially neglecting the nonstructural components. As a result, there is a urgent need to develop effective mitigation strategies for the seismic protection of equipment in critical facilities. The primary performance objective cannot be restricted to preserve the integrity, but must insure the functionality and operational continuity of the equipment and, consequently, of the critical facility itself.

In Fig. 2.2, performance objectives prescribed by SEAOC's Vision 2000 document [127] for ordinary buildings and critical facilities are compared by means of the Performance Objective Matrix. Each design performance objective is defined by combining a performance level, that is an expected level of damage, with a seismic hazard level, characterized by a specified probability of occurrence or return period. For a same hazard level, critical facilities are required to meet enhanced performance objectives than ordinary building: *e.g.*, for a rare earthquake with a return period of 475 years, ordinary buildings can incur in extensive damage as long as life safety is protected (*Life Safe* performance level), while hazardous and critical facilities are required to suffer only minor damage compatible with operational continuity (*Operational* performance level).

From a different viewpoint, this is equivalent to say that the same Operational performance level, addressed by ordinary buildings under frequent and less intense seismic actions, must be addressed by critical facilities under less probable, and hence more severe seismic actions. Because of the incremented hazard level, standard design procedures might result inadequate to mitigate the seismic risk of critical facilities. The development of appropriate strategies and innovative technologies for the seismic protection of equipment is then strongly needed.

2.2 Innovative strategies and technologies for the seismic protection

2.2.1 Judicious placement of equipment

The international building codes discussed in Chapter 1 are intended to provide, in a form as simple as possible, conservative estimates of the seismic forces acting on nonstructural components and equipment. Owing to this, these provisions adopt a static lateral force method, easy to implement and sufficiently accurate for designing light equipment. In such cases, a judicious placement of the equipment, complying with both stiffness and structural design criteria in an effort for coordination, is sufficient to minimize the exposure to seismic accelerations and to guarantee the continuing operation.

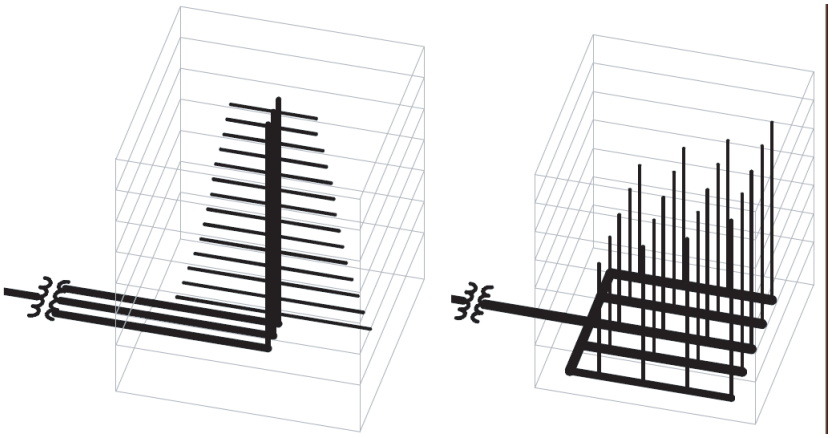

Figure 2.3. Structures for a power distribution system. (a) Standard "tree" structure of a generic power system. (b) Innovative "laid down" structure of a brush distribution system. After Parise *et al.* [101]

In this regard, Parise *et al.* [101] discussed the design and installation criteria to insure the functional reliability of electrical power systems in buildings subjected to earthquake hazard. In particular, the authors emphasize the adoption of the so-called *brush distribution approach* to reduce drastically the seismic vulnerability of electrical power systems. Proposed basic criteria are:

- minimize the mass of each component of the system (microsystem criterion);
- minimize the seismic acceleration on the component by locating it as closest as possible to ground (installation criterion).

As a result, the heaviest electrical equipment items (transformers, generators, motors, panel boards, ...) are to be located, as much as possible, on ground or underground floors. Furthermore, the electrical distribution in the upper floors should be subdivided into vertical sectors along the height of the building. A schematic of the brush distribution approach is illustrated in Fig. 2.3 and compared with the standard "tree" structure of a generic power system.

2.2.2 Equipment and raised-floor isolation systems

In the presence of either heavy equipment or an increased hazard level, provisions of international building codes may result overconservative, when not inaccurate, and require a costly and technically difficult seismic design. When this is the case, innovative technologies for the vibration control are effective and workable means to preserve integrity and operational continuity of equipment.

An effective way to protect acceleration-sensitive equipment consists in implementing an isolation system between the internal apparatus and the supporting structure.

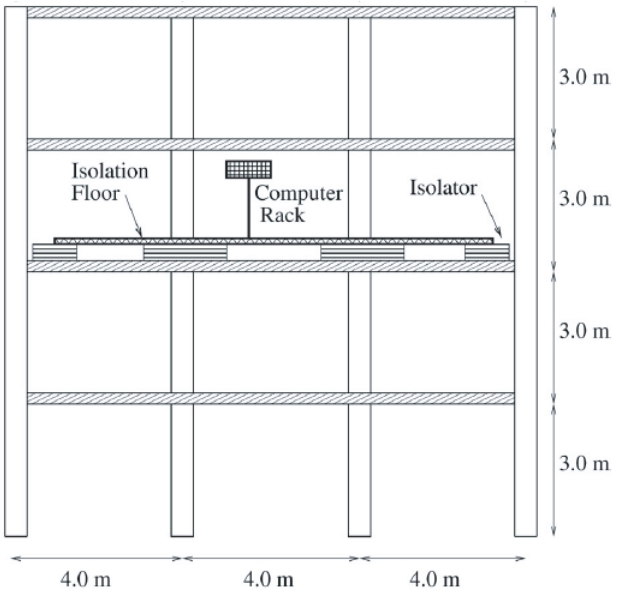

Figure 2.4. Isolated raised-floor system. After Alhan and Gavin [2].

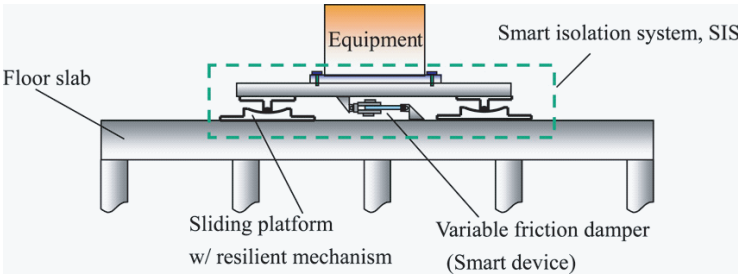

Figure 2.5. Equipment isolation system. After Lu and Lin [85].

There are two configurations proposed in literature: the apparatus to be isolated may correspond either to an individual raised floor, on which a group of several equipment is anchored (*isolated raised-floor systems* or *floor isolation systems*) [78, 154, 2, 52, 64], or an equipment itself (*equipment isolation systems*) [48, 85, 33], especially when having a large mass [23, 24]. As a result, the absolute accelerations transmitted to equipment are considerably reduced and the damages due to excessive inertial loads are prevented.

To this end, a variety of passive, semi-active and hybrid isolation systems have been studied. Passive isolation systems have been proved to be effective and practical to protect acceleration sensitive equipment from earthquake hazard [2, 52] and from microvibration, if also required [154]. When subjected to high-amplitude long-period ground motions like near-fault earthquakes, however, passive systems might suffer from low-frequency resonances leading to excessive isolator displacements and damages to equipment [48]. In order to overcome these drawbacks, researchers have proposed the

use of semi-active isolation systems, given as the combination of a passive isolation system, usually of sliding- or rolling-type, with a semi-active control device of various sort, *e.g.* variable friction devices [85] and magnetorheological dampers [33]. A hybrid platform composed of a passive layer and an actively controlled layer with a piezoelectric actuator has been proposed in [152, 153] for the protection of high-tech equipment. The platform is designed to work both as a passive isolation system, aiming at mitigating the acceleration response of the equipment during earthquakes, and as an active platform, intended to reduce the velocity response of the equipment under normal working conditions. While proved to be feasible and effective when their dynamic properties and feedback control loops are designed properly, semi-active and hybrid systems require an integrated net of sensors, processors and actuators which make them more complex than passive systems and, in the case of active control, prone to instability problems. Recent studies have therefore sought to improve the performance of passive isolation systems by exploiting the adaptive behaviour inherent in nonlinear isolators [64, 105, 106].

2.2.3 Non-conventional Tuned Mass Damper (TMD)

When tackling the problem of a supporting structure housing a series of equipment, a possible protection strategy consists in providing each equipment with an isolation system: for the sake of comparison, see Fig. 2.6 (a) and Fig. 2.6 (b). The presence of a dynamic interaction between the multiple isolated equipment, especially if heavy ones, might however prejudice the effectiveness of the vibration control. Then, to comparatively reduce the complexity of the design and increase the effectiveness of the vibration control, the following solution is proposed in Chapter 7 of this thesis: a mass already present on the structure, *e.g.* the mass of an equipment, is supposed to be converted into a Tuned Mass Damper (TMD) for the seismic protection of the supporting structure and of all of the other equipment anchored to it (Fig. 2.6 (c)). Such a TMD configuration is to be said *non-conventional* because the tuned mass is already a part of the system and keeps maintaining its own functions (structural, architectural, electrical, mechanical, ...) beyond the mere control function. Aiming at a better control performance, and since no additional weight is introduced to realize the TMD, a larger tuned mass can be chosen as compared to a conventional TMD.

Among passive strategies in the field of structural vibration control, Tuned Mass Damper (TMD) has received considerable attention over the years thanks to the major advantages it provides, such as simplicity in design, operation and maintenance, reliability and cost effectiveness [55, 125]. A conventional TMD consists of a relatively small auxiliary mass attached *ex novo* to a main structure to be protected. The connection in between finds a large variety of implementations, both linear and nonlinear,

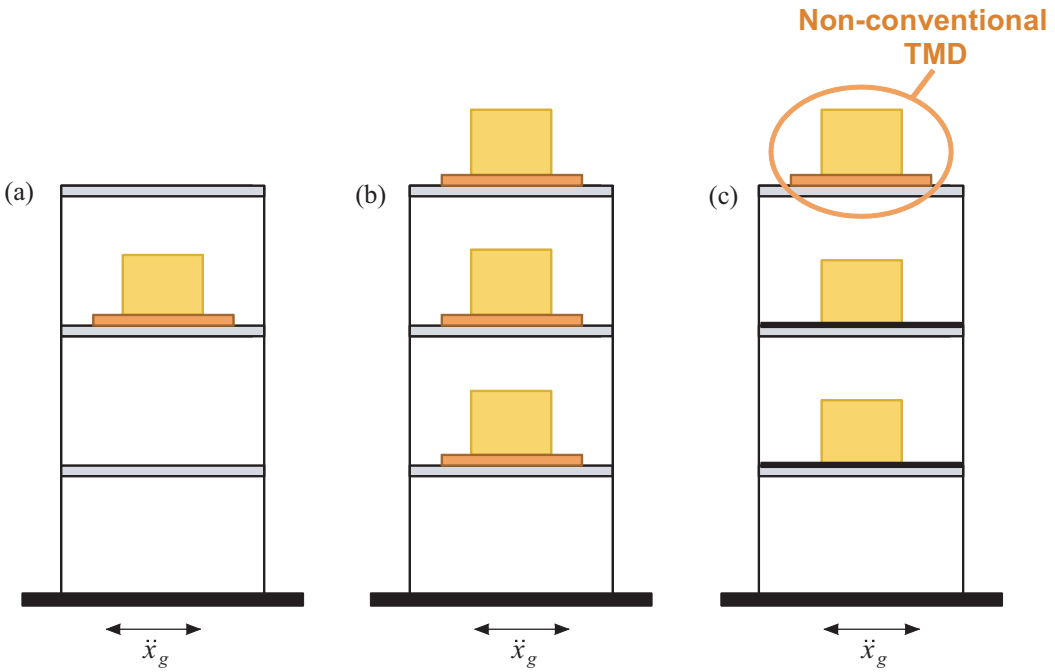

Figure 2.6. Equipment isolation and non-conventional TMD.

References	Mass ratio	Generalized mass ratio	Application
Feng, Mita [43]	1.00	–	Segmented upper stories
Chey *et al.* [12, 13]	0.18 0.46	0.20 0.60	Segmented upper stories
Villaverde [145]	0.16	–	Sliding roof system
Tiang *et al.* [133]	0.23	–	Sliding roof system
Matta, De Stefano [88]	0.17	0.76	Roof garden
Hoang *et al.* [53]	–	0.77	Seismic retrofit of a bridge
De Angelis *et al.* [22]	0.72	1.049	Industrial steel structure

Symbol – is used when cited reference does not provide sufficient information.

Table 2.1. Examples of non-conventional TMD in current literature.

in available literature and applications [118]. The principle of operation consists in inducing a vibration energy transfer from the main structure to the auxiliary mass, which dissipates the energy away vibrating out of phase with the structural motion. The purpose is to absorb most of the input energy entering into the main structure, whose dynamic response is thus reduced. The search for such a vibration interaction accounts for the name of *tuned* mass damper given to the device.

The concept of TMD, otherwise known as dynamic vibration absorber, dates back to 1909, when it was first studied by Frahm [47] and early used to attenuate the vibrations of single-degree-of-freedom mechanical systems under harmonic forces [99, 25]. The introduction of the dynamic absorber in the field of civil engineering dealt with the consideration of multi-degree-of-freedom systems and environmental loads, *i.e.* wind and earthquake, which are typically non-deterministic and possess many frequency components [21, 147]. The TMD has been widely applied since the 1970s on tall buildings and towers to mitigate wind-induced response and improve serviceability and occupant comfort [54]. Recent successful applications on pedestrian bridges also exist, where TMD is used to control human-induced vibrations (Millenium Bridge, London, UK; Solférino Bridge, Paris, France). There is not a general agreement, instead, on the TMD effectiveness in reducing the earthquake-induced response. Starting from early investigations [151, 73, 117], authors indicate three inherent limitations to the seismic effectiveness of the TMD: (i) the lack of robustness against deviations in design parameters [124, 102]; (ii) a high dependence on earthquake frequency content [79]; (iii) the impulsive character of the earthquake excitation [118]. An attempt to enhance the seismic effectiveness of the TMD consists in increasing the device mass in order to attain a better control performance [103].

In this sense, recent studies have advanced a new, non-conventional configuration in which masses already present on the structure to be protected are converted into tuned masses, retaining structural or architectural functions beyond the mere control function. Proposed systems, like segmented upper stories [43, 157, 12, 13], sliding roof systems [142, 145, 133] and roof gardens [88], are placed on the top of a building and isolated from it so that they act as a TMD for the protection of the structure below. Whereas a conventional TMD is typically taken to be a few percent of the entire structural mass, a non-conventional TMD of this sort stands out for its large mass, being in the order of 15% to 50% of the structural mass. Similar values are recognized also in applications related to steel frame structures in industrial plants [107] and a steel truss bridge [53]. Values even higher, up to 100%, are found in the aforementioned cases when the mass ratio is computed in terms of modal or generalized masses [88, 107, 53], as required by the classic formulae for the design of TMD (see Tab. 2.1). The application of the new technique is expected to be widespread: a non-conventional TMD is suitable for new constructions as well for retrofitting works since its impact on the structure is only minimal, not requiring additional weight.

Chapter 3

Setting the case study

In this chapter, a case study is set for subsequent investigations. A combined primary-secondary system is considered which consists of a supporting structure housing a single equipment. The equipment is modelled as a rigid body having a single attachment point the supporting structure (*floor-mounted block-type equipment*). In the uncontrolled configuration, the equipment is non-isolated and rigidly fixed to the attachment floor of the supporting structure; in the controlled configuration, the equipment is isolated from the attachment floor *via* a passive isolation system. Reduced order single-degree-of-freedom (SDOF) and two-degree-of-freedom (2-DOF) models are derived for design purposes, in the case of a decoupled and a coupled dynamic analysis approach, respectively.

3.1 Modelling assumptions

3.1.1 Supporting structure

In the present case study, a moment-resisting frame with N storeys is considered as a supporting structure (Fig. 3.1). The following assumptions are made.

I. With respect to the lateral stiffness and mass distribution, the structure satisfies the criteria for regularity in plan and in elevation. The analysis is thus performed using a planar model and neglecting torsional effects.

II. Columns are inextensible.

III. Floors are taken as being rigid in their own planes and masses are lumped at the centre of gravity of each floor.

IV. The structure is proportionally damped.

V. The structure is subjected to a single horizontal component of base motion.

VI. The structure remains within the elastic limit during the base excitation.

3.1.2 Equipment

In the present case study, equipment are considered whose dynamic behaviour under seismic excitation is essentially that of a rigid body and as such they are conveniently modelled. The class of *block-type equipment* comprises a significant portion of the mechanical, electrical and electronic equipment which can be found in critical facilities: emergency generators, transformers, computer cabinets, air compressors, chillers, boilers and so on.

The following assumptions are made for the equipment under consideration.

I. The equipment is floor-mounted and has a single attachment point to the supporting structure. Equipment with multiple attachment points at different floor levels are not considered.

II. For comparison purposes, two configurations are studied, as illustrated in Fig. 3.1: in the *uncontrolled configuration*, the equipment is non-isolated and rigidly anchored to the attachment floor of the supporting structure; in the *controlled configuration*, the equipment is isolated from the attachment floor *via* a passive isolation system.

III. For comparison purposes, passive isolation systems with either linear or nonlinear behaviour are studied.

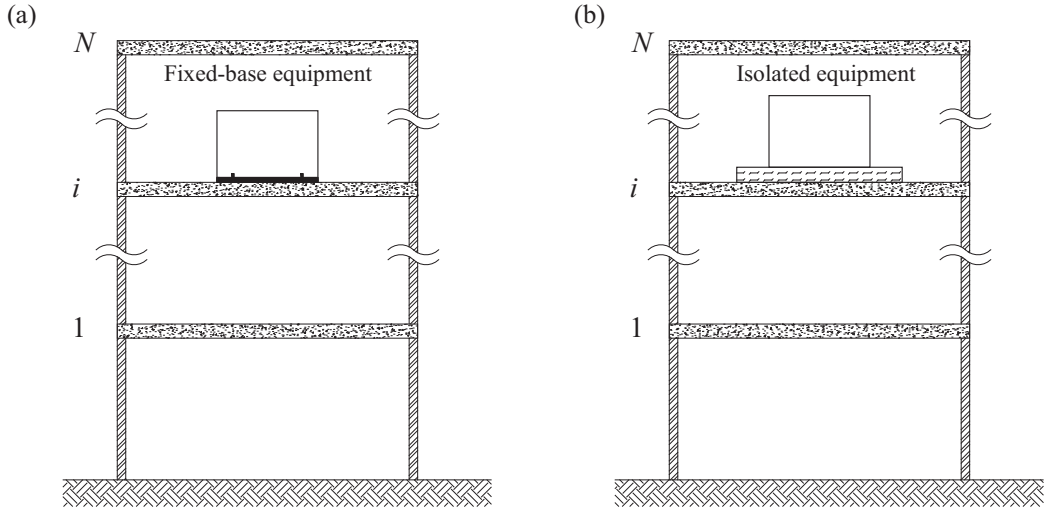

Figure 3.1. System configurations: (a) uncontrolled configuration, fixed-base equipment; (b) controlled configuration, isolated equipment.

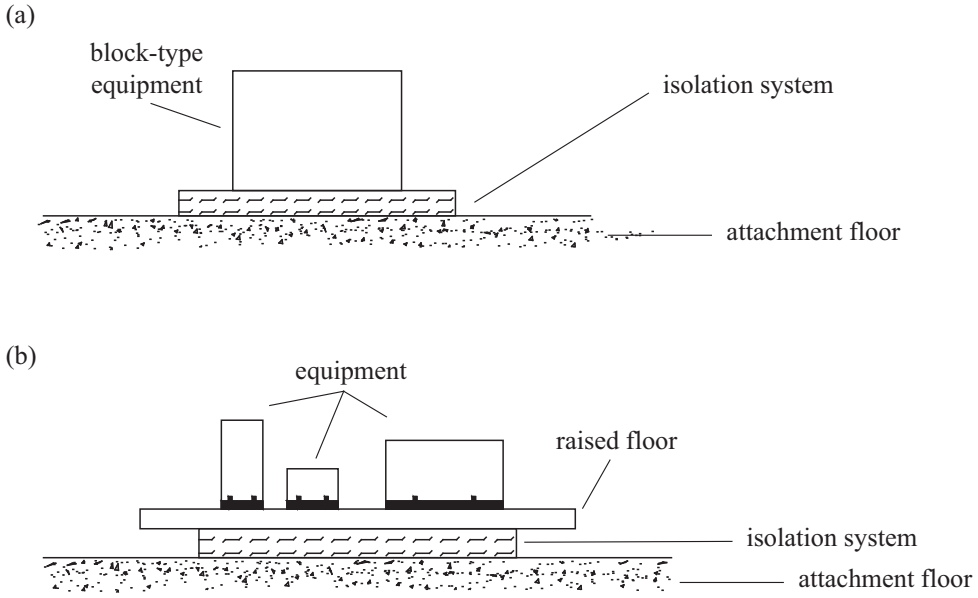

Figure 3.2. System configurations: (a) isolated block-type equipment; (b) isolated raised floor.

IV. When the equipment mass is not smaller than 10% of the total mass of the supporting structure, the dynamic interaction between the equipment and the structure is expected to be significant and it cannot be neglected unless gross errors. Hence, according to the criterion discussed in Sec. 1.3, a combined primary – secondary system approach is adopted in dynamic analysis.

V. Among the various response modes that are possible for floor-mounted block-type equipment [83, 84], this study is focused on the sliding response and its related failure modes: either excessive absolute acceleration of the equipment or excessive relative displacement between the equipment and its supporting structure. The former occurs when the shaking becomes intense enough to cause internal damage to vibration sensitive equipment, such as computers, communications systems and medical equipment. The latter primarily causes the breakage of restraints and service lines connected to the equipment.

In view of the preceding assumptions, results from the present study may be easily extended to the case of isolated raised floor systems, illustrated in Fig. 3.2 (b): in this configuration, a group of several equipment is rigidly anchored to a secondary raised floor, which is decoupled from the structure floor by means of an isolation system.

3.2 Governing equations

3.2.1 Supporting structure with fixed-base equipment

Let the equipment be non-isolated and rigidly anchored to the ith floor of the N-storey supporting structure. Due to the assumption that floor masses M_j $(j = 1, 2, \dots i \dots, N)$ are lumped at each floor level, the structure is modelled as a N-degree-of-freedom (N-DOF) system (Fig. 3.3 (a)). Note that the ith DOF has a lumped mass being the sum of the floor mass M_i and the equipment mass M_e.

The equations of motion of the structure excited by one-directional base acceleration $\ddot{x}_g(t)$ are given as

$$\overline{\mathbf{M}}\ddot{\mathbf{x}} + \mathbf{C}\dot{\mathbf{x}} + \mathbf{K}\mathbf{x} = -\overline{\mathbf{M}}\mathbf{R}\,\ddot{x}_g \tag{3.1}$$

where: $\overline{\mathbf{M}}$ is the $(N \times N)$ mass matrix of the structure incremented by the equipment mass; $\mathbf{C}$ and $\mathbf{K}$ are the $(N \times N)$ proportional damping and stiffness matrices of the structure; $\mathbf{x}(t) = \big(x_1(t)\ x_2(t)\ \dots\ x_N(t)\big)^{\mathrm{T}}$ is the displacement vector, with x_j $(j = 1, 2, \dots i \dots, N)$ denoting the lateral displacement of the jth DOF with respect to ground; $\mathbf{R}$ is the $(N \times 1)$ influence vector, whose elements are all unitary in this case. The over-dot indicates differentiation with respect to time t.

In Eq. (3.1), the incremented mass matrix $\overline{\mathbf{M}}$ can be expressed as

$$\overline{\mathbf{M}} = \mathbf{M} + \mathbf{B}_i\,\mathbf{B}_i^{\mathrm{T}}\,M_e \tag{3.2}$$

where $\mathbf{M}$ is the $(N \times N)$ mass matrix of the structure and $\mathbf{B}_i$ is a $(N \times 1)$ allocation vector given by

$$\mathbf{B}_i = (\underset{1}{0} \quad \dots \quad \underset{i}{1} \quad \dots \quad \underset{N}{0})^{\mathrm{T}} \tag{3.3}$$

3.2.2 Supporting structure with isolated equipment

Let the equipment be isolated from the ith floor of the N-storey supporting structure *via* a passive isolation system. The block-type equipment is modelled as a single-degree-of-freedom (SDOF) system having the mass lumped in its centre of gravity. It is attached to the ith DOF of the supporting structure and F denotes the total force exerted across the isolation system (Fig. 3.3 (b)).

Supporting structure and isolated equipment are considered together as a combined N+1-DOF system. The equations of motion of such a system excited by one-directional base acceleration $\ddot{x}_g(t)$ are given as

$$\mathbf{M}\ddot{\mathbf{x}} + \mathbf{C}\dot{\mathbf{x}} + \mathbf{K}\mathbf{x} = -\mathbf{M}\mathbf{R}\,\ddot{x}_g + \mathbf{B}_i\,F \tag{3.4a}$$

$$M_e\,\ddot{x}_e = -M_e\,\ddot{x}_g - F \tag{3.4b}$$

where: $\mathbf{M}$, $\mathbf{C}$, $\mathbf{K}$, $\mathbf{x}(t)$ and $\mathbf{R}$ have been previously defined; M_e is the mass of the isolated equipment; $x_e(t)$ denotes the displacement of the isolated equipment with respect to ground; F is the total force exerted across the isolation system and $\mathbf{B}_i$ is the corresponding $(N \times 1)$ allocation vector, defined in Eq. (3.3).

The definition of force F depends on the constitutive model adopted to describe the mechanical behaviour of the isolation system. Let

$$x_e(t) - x_i(t) \tag{3.5}$$

be the displacement across the isolation system, expressed as the difference between the displacement of the equipment and that of the attachment floor. In general, F is assumed to include both viscous (rate-dependent) and hysteretic (rate-independent) memory effects. Hence, it is defined as a functional $\mathcal{F}$ depending on both the current values of relative displacement and velocity and on the previous evolution of relative displacement in the time interval $[0,\, t]$:

$$F(t) = \Big[\mathcal{F}\Big(x_e - x_i,\, \dot{x}_e - \dot{x}_i,\, (x_e - x_i)|_{[0,\,t]}\Big)\Big](t) \qquad \forall\, t \in [0,\, T] \tag{3.6}$$

3.2.3 Decoupled approach: reduced order SDOF model

When a decoupled approach is allowed, the equipment is assumed to be in cascade with the supporting structure, such that it receives the input from the structure but does not modify this input. Under this assumption, the dynamic analysis of the supporting

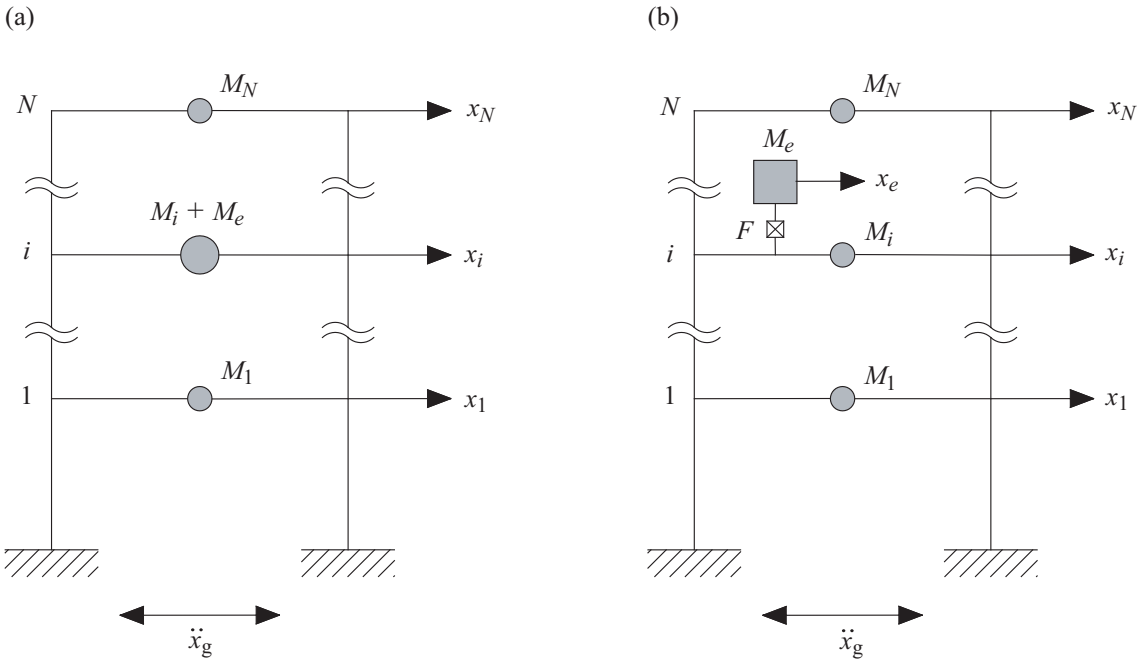

Figure 3.3. Lumped mass models: (a) supporting structure with fixed-base equipment; (b) supporting structure with isolated equipment.

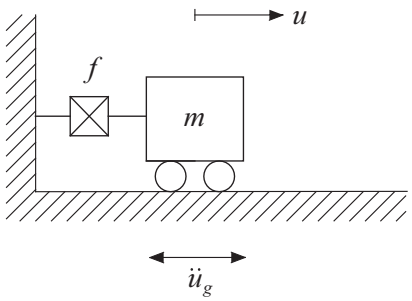

Figure 3.4. Decoupled approach: reduced order SDOF model.

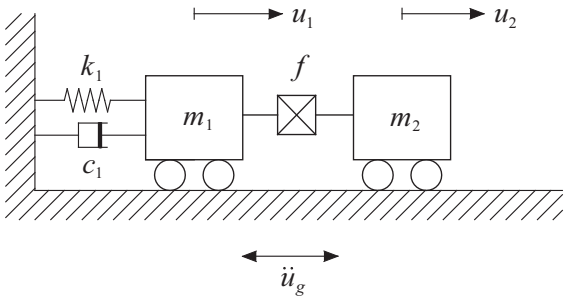

Figure 3.5. Coupled approach: reduced order 2-DOF model.

N+1-DOF system	SDOF system
$x_e - x_i$	u
M_e	m
F	f
$\ddot{x}_g + \ddot{x}_i$	$\ddot{u}_g$

Table 3.1. Response quantities and properties of the reduced order SDOF system.

structure and the equipment can be carried out independently.

In particular, the isolated equipment can be modelled as a SDOF system excited by base acceleration $\ddot{u}_g(t)$ (Fig. 3.4), being the equation of motion given as

$$m\ddot{u} = -m\ddot{u}_g - f \tag{3.7}$$

with the response quantities and properties related to those of the N+1-DOF system as shown in Tab. 3.1. It is worth noting that base acceleration $\ddot{u}_g(t)$ is equal to the absolute acceleration of the attachment floor, and relative displacement $u(t)$ is equal to the equipment displacement with respect to the attachment floor. The force f across the isolation system is defined by means of functional $\mathcal{F}$ as

$$f(t) = \left[\mathcal{F}\Big(u,\, \dot{u},\, u|_{[0,\,t]}\Big)\right](t) \qquad \forall\, t \in [0,\, T] \tag{3.8}$$

3.2.4 Coupled approach: reduced order 2-DOF model

When a coupled approach is required and the number of equations (3.4) is large, dynamic analysis of the combined N+1-DOF system is time consuming. In order to save computational time and capacities, a reduced order model of the combined system is introduced.

Consider the case when the response vector $\mathbf{x}(t)$ of the supporting structure can be approximated by a shape vector $\boldsymbol{\phi}$ and a single generalized coordinate $q(t)$:

$$\mathbf{x}(t) \approx \boldsymbol{\phi}\, q(t) \tag{3.9}$$

The shape vector $\boldsymbol{\phi}$ is a displacement profile properly defined for the structure under consideration and, in case, it may be taken equal to a natural mode shape of the structure. Substituting Eq. (3.9) into Eq. (3.4a) gives

$$\mathbf{M}\boldsymbol{\phi}\,\ddot{q} + \mathbf{C}\boldsymbol{\phi}\,\dot{q} + \mathbf{K}\boldsymbol{\phi}\,q = -\mathbf{M}\mathbf{R}\,\ddot{x}_g + \mathbf{B}_i\,F \tag{3.10}$$

Premultiplying each term in this equation by $\boldsymbol{\phi}^{\mathrm{T}}$ gives

$$\boldsymbol{\phi}^{\mathrm{T}}\mathbf{M}\boldsymbol{\phi}\,\ddot{q} + \boldsymbol{\phi}^{\mathrm{T}}\mathbf{C}\boldsymbol{\phi}\,\dot{q} + \boldsymbol{\phi}^{\mathrm{T}}\mathbf{K}\boldsymbol{\phi}\,q = -\boldsymbol{\phi}^{\mathrm{T}}\mathbf{M}\mathbf{R}\,\ddot{x}_g + \boldsymbol{\phi}^{\mathrm{T}}\mathbf{B}_i\,F \tag{3.11}$$

or

$$M^*\,\ddot{q} + C^*\,\dot{q} + K^*\,q = -M^*\Gamma\ddot{x}_g + \phi_i\,F \tag{3.12}$$

where

$$M^* = \boldsymbol{\phi}^{\mathrm{T}}\mathbf{M}\boldsymbol{\phi}, \quad C^* = \boldsymbol{\phi}^{\mathrm{T}}\mathbf{C}\boldsymbol{\phi}, \quad K^* = \boldsymbol{\phi}^{\mathrm{T}}\mathbf{K}\boldsymbol{\phi}, \quad \Gamma = \frac{\boldsymbol{\phi}^{\mathrm{T}}\mathbf{M}\mathbf{R}}{\boldsymbol{\phi}^{\mathrm{T}}\mathbf{M}\boldsymbol{\phi}} \tag{3.13}$$

and

$$\phi_i = \boldsymbol{\phi}^{\mathrm{T}}\mathbf{B}_i \tag{3.14}$$

is the ith element of the shape vector $\boldsymbol{\phi}$, *i.e.* the element at the equipment location. Eq. (3.12) may be interpreted as the equation governing the response $q(t)$ of a SDOF structure excited by applied forces $-M^*\Gamma\ddot{x}_g + \phi_i\,F$. Therefore: M^*, C^* and K^* are called the generalized mass, damping and stiffness coefficients of the structure for the prescribed shape vector $\boldsymbol{\phi}$; Γ is a participation factor that measures the degree to which shape vector $\boldsymbol{\phi}$ participates in the structural response.

Similarly, the equipment response $x_e(t)$ can be approximated as follows

$$x_e(t) \approx q_e(t) \tag{3.15}$$

that is considering only the contribution $q_e(t)$ produced by a partial applied force $-M_e\Gamma\ddot{x}_g - \phi_i\,F$.

Making use of the approximations in Eqs. (3.9) and (3.15), Eqs. (3.4a)-(3.4b) for the combined system can be rewritten as follows

$$\begin{aligned} &M^*\ddot{q} + C^*\dot{q} + K^*q = -M^*\Gamma\,\ddot{x}_g + \phi_i\,F \\ &M_e\ddot{q}_e = -M_e\Gamma\,\ddot{x}_g - \phi_i\,F \end{aligned} \tag{3.16}$$

Let these equations be compared with those governing the response of the 2-DOF system shown in Fig. 3.5. This system consists of a primary mass m_1, anchored to ground through a linear spring and a linear viscous damper, and a secondary mass m_2, attached to the former through a dissipative link. Damping and stiffness coefficients of the primary mass are denoted by c_1 and k_1, while f is the force exerted across the link. $u_1(t)$ and $u_2(t)$ are the displacement relative to ground of the primary and secondary mass, respectively. The equations of motion of such a system excited by the base acceleration $\ddot{u}_g(t)$ are given as

$$\begin{aligned} &m_1\ddot{u}_1 + c_1\dot{u}_1 + k_1u_1 = -m_1\ddot{u}_g + f \\ &m_2\ddot{u}_2 = -m_2\ddot{u}_g - f \end{aligned} \tag{3.17}$$

N+1-DOF system	Generalized 2-DOF system
q	u_1
$\boldsymbol{\phi}^\top \mathbf{M} \boldsymbol{\phi}$	m_1
$\boldsymbol{\phi}^\top \mathbf{C} \boldsymbol{\phi}$	c_1
$\boldsymbol{\phi}^\top \mathbf{K} \boldsymbol{\phi}$	k_1
q_e	u_2
M_e	m_2
F	f
$\dfrac{\boldsymbol{\phi}^\top \mathbf{M} \mathbf{R}}{\boldsymbol{\phi}^\top \mathbf{M} \boldsymbol{\phi}} \ddot{x}_g$	$\ddot{u}_g$

Table 3.2. Response quantities and properties of the reduced order 2-DOF system.

Being $u_2(t) - u_1(t)$ the relative displacement between the secondary and the primary mass, the force f is defined by means of functional $\mathcal{F}$ as

$$f(t) = \left[\mathcal{F}\Big(u_2 - u_1,\, \dot{u}_2 - \dot{u}_1,\, (u_2 - u_1)|_{[0,\,t]} \Big) \right](t) \qquad \forall\, t \in [0,\, T] \tag{3.18}$$

By comparison, it becomes apparent that Eqs. (3.16) reduce to the same form as Eqs. (3.17) when the following conditions are verified:

I. the shape vector $\boldsymbol{\phi}$ approximating the structural response is normalized so that its ith element is unity

$$\phi_i = 1 \tag{3.19}$$

II. base acceleration $\ddot{u}_g$ applied to the 2-DOF system is equal to

$$\ddot{u}_g = \Gamma\, \ddot{x}_g \tag{3.20}$$

where $\ddot{u}_g$ is the base acceleration applied to the combined N+1-DOF system.

Under these assumptions, Eqs. (3.16) may be interpreted as the equations of motion of a generalized 2-DOF system, whose response quantities and properties are related to those of the N+1-DOF system as shown in Tab. 3.2. The two coupled oscillators represent the supporting structure and the isolated equipment, respectively. As it will be stated afterwards, such a reduced order model will be particularly useful during the design phase of the isolation system.

Part II

Passive isolation systems for the seismic protection of equipment

Chapter 4

Linear isolation: optimal design and experimental investigations

In this chapter[1], a passive linear isolation system composed of High-Damping Rubber Bearings is proposed for the seismic protection of equipment. First, the optimal design problem is set and solved. Unlike previous studies, that generally decouple and analyzed the isolated equipment individually, the proposed design methodology is specifically developed to adopt a coupled approach and to account for the dynamic interaction phenomena. A multi-objective optimization procedure is developed to consider both the responses of interest: the absolute acceleration of the isolated equipment and the displacement across the isolation system. Distinctive of the procedure is the consideration of the peculiar damping properties of High-Damping Rubber Bearings in the context of a non-proportionally damped system. The seismic effectiveness of the proposed isolation system is eventually discussed in the light of extensive experimental results, obtained by means of shaking table tests under a wide selection of seismic inputs, both natural and artificial.

[1]Some of the results in this chapter have been published in the following papers:

- ♢ Reggio, A., De Angelis, M. Combined primary-secondary system approach to the design of an equipment isolation system with High-Damping Rubber Bearings. *Journal of Sound and Vibration*, 333 (9), 2386-2403, 2014.
- ♢ De Angelis, M., Perno, S., Reggio, A., De Canio, G., Ranieri, N. Shaking table tests on a passive equipment isolation system for earthquake protection. *Proceedings of 2009 ASME Pressure Vessels and Piping Division Conference (PVP2009)*, Prague, Czech Republic, July 26-30, 2009.

4.1 Linear isolation system

The proposed equipment isolation system is implemented by means of High-Damping Rubber Bearings (HDRB). Among the most economical and effective isolators, HDRB are laminated rubber bearings (elastomeric bearings) composed of high damping rubber layers alternating with steel plates, solidly joined together under high pressure and temperature through a process called *vulcanization* (Fig. 4.1). This kind of bearings takes advantage of achieving low horizontal stiffness and noticeable damping characteristics in the same device. Moreover, high vertical stiffness is achieved due to the presence of steel plates, that provide confinement, impede the bulging deformation of the rubber when it is compressed and allow to sustain static dead loads with minimal vertical deflections.

Since the high-damping rubber compound is known to possess elasticity, plasticity and viscosity, HDRB show a highly nonlinear behaviour combining both hysteresis and rate-dependence [155]. However, accurate constitutive models of the material still lack, whereas macroscopic models have been developed to describe the force-displacement relationship at the device level. As regards the cyclic simple shear behaviour, simplified macroscopic models are of two sorts. On the one hand, an equivalent linear visco-elastic model is used by defining an effective lateral stiffness, secant to the target displacement, and an equivalent viscous damping ratio, obtained by imposing the equivalence of the energy dissipated per cycle at the target displacement. This model is able to capture the rate dependent damping properties, but the linearization hypothesis is inaccurate when the device is expected to work in a wide range of lateral displacement amplitudes. On the other hand, nonlinear hysteretic models, such as the bi-linear model, are used to capture the dependence of lateral stiffness on the displacement amplitude, but they neglect the rate dependency. In recent years, few advanced mathematical models of HDRB have been developed to ameliorate the aforementioned shortcomings [134, 135]. Nevertheless, a simplified model is preferred in the present study for the sake of design applicability.

It is apparent that the choice of a simplified model for HDRB depends on the expected values of displacement amplitudes [74]. As it can be seen from the experimental curves in Fig. 4.2 (a), the shear modulus of the high damping rubber rapidly decreases at shear strains less than 50% and the behaviour of HDRB is highly nonlinear at corresponding displacement amplitudes. Over the range of $50\% - 100\%$ shear strain, shear modulus is constant and low and the behaviour of HDRB can be approximated as linear. Meanwhile, the damping is quite constant up to 200% shear strain, with values between 10% and 15% of critical depending on the applied vertical load (Fig. 4.2 (b)).

In the present study, HDRB are designed for a target shear strain of $100\% \div 150\%$ and a Kelvin-Voigt visco-elastic model is adopted for the proposed equipment isolation system. The rheological model, illustrated in Fig. 4.3, is given as the parallel of a linear

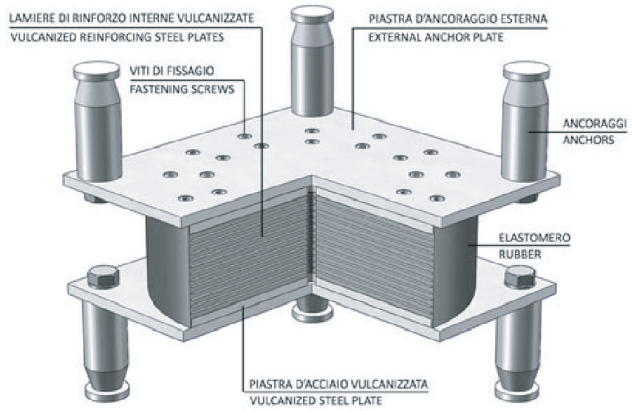

Figure 4.1. Schematic of a laminated High Damping Rubber Bearing (Algasism® HDRB by Alga S.p.a., Italy).

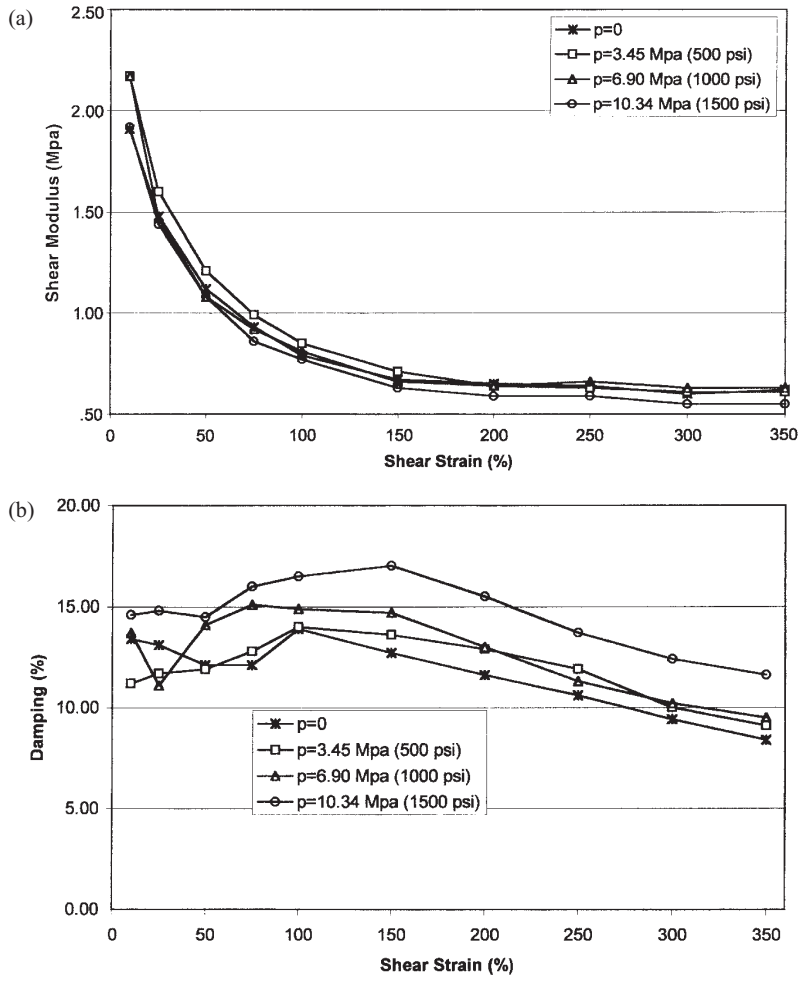

Figure 4.2. Shear modulus (a) and damping ratio (b) of HDRB *versus* shear strain. After Naeim and Kelly [92].

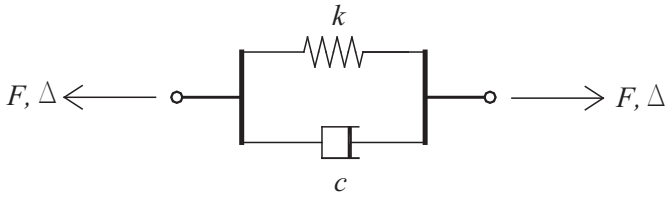

Figure 4.3. Rheological model of the equipment isolation system using HDRB: Kelvin-Voigt viscoelastic model.

spring and a linear viscous damper. The constitutive relationship for the linear spring is

$$F_{\mathrm{E}} = k\,\Delta_{\mathrm{E}} \tag{4.1}$$

where F_{E} is the force carried by the spring, Δ_{E} is the elastic displacement and k is the stiffness constant. The constitutive relationship for the linear viscous damper is

$$F_{\mathrm{V}} = c\,\dot{\Delta}_{\mathrm{V}} \tag{4.2}$$

where F_{V} is the force carried by the damper, $\dot{\Delta}_{\mathrm{V}}$ is the rate of the viscous displacement and c is the damping constant.

By equilibrium, the force F carried by the model is

$$F = F_{\mathrm{E}} + F_{\mathrm{V}} \tag{4.3}$$

By compatibility, the displacement Δ across the model is

$$\Delta = \Delta_{\mathrm{E}} = \Delta_{\mathrm{V}} \tag{4.4}$$

Substituting Eqs. (4.1) and (4.2) into Eq. (4.3) and accounting for Eq. (4.4) leads to the constitutive relationship of the Kelvin-Voigt model

$$F = k\,\Delta + c\,\dot{\Delta} \tag{4.5}$$

4.2 Coupled approach: optimal design of the equipment isolation system

Here, we consider the case when the dynamic interaction between the equipment and the supporting structure cannot be neglected: according to Sec. 3.1, the equipment mass is assumed to be not smaller than 10% of the total mass of the structure. A methodology to specify the optimal design parameters of the proposed equipment

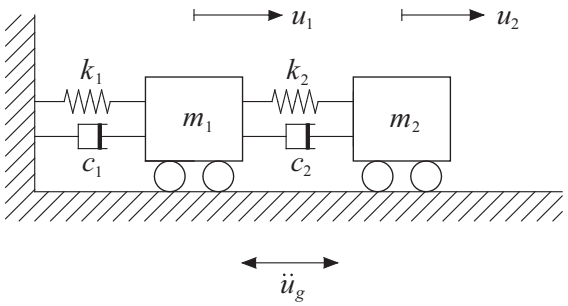

Figure 4.4. Reduced order 2-DOF model with the linear isolation system.

isolation system is first developed and eventually illustrated by means of an application.

4.2.1 Equations of motion

The dynamic interaction between the equipment and the supporting structure is taken into account and a combined primary – secondary system approach is adopted for the dynamic analysis. Eqs. (3.4) are the equations of motion of such a N+1-DOF system. They are integrated by the constitutive relationship of the equipment isolation system, modelled by the Kelvin-Voigt model in Eq. (4.5). Expressing Δ as the equipment displacement relative to the attachment floor

$$\Delta = x_e - x_i \tag{4.6}$$

we obtain

$$\begin{aligned} &\mathbf{M}\ddot{\mathbf{x}} + \mathbf{C}\dot{\mathbf{x}} + \mathbf{K}\mathbf{x} = -\mathbf{M}\mathbf{R}\,\ddot{x}_g + \mathbf{B}_i\,F \\ &M_e\ddot{x}_e = -M_e\ddot{x}_g - F \\ &F = k\,(x_e - x_i) + c\,(\dot{x}_e - \dot{x}_i) \end{aligned} \tag{4.7}$$

For the sake of design purposes, however, it is worthwhile to introduced a reduced order 2-DOF model (Fig. 4.4), whose equations of motion are

$$\begin{aligned} &m_1\ddot{u}_1 + c_1\dot{u}_1 + k_1u_1 = -m_1\ddot{u}_g + f \\ &m_2\ddot{u}_2 = -m_2\ddot{u}_g - f \\ &f = k_2\,(u_2 - u_1) + c_2\,(\dot{u}_2 - \dot{u}_1) \end{aligned} \tag{4.8}$$

As discussed earlier, response quantities and properties of the generalized 2-DOF model are related to those of the N+1-DOF model as shown in Tab. 3.2 on page 55. In addition, $k_2 = k$ and $c_2 = c$ are the stiffness and the damping coefficients of the equipment isolation system.

Aiming at identifying the parameters that govern the response of the 2-DOF system, Eqs. (4.8) can be rewritten as

$$\begin{aligned} &\ddot{u}_1 + 2\zeta_1\omega_1\dot{u}_1 + \omega_1^2 u_1 = -\ddot{u}_g + \frac{f}{m_1} \\ &\mu\ddot{u}_2 = -\mu\ddot{u}_g - \frac{f}{m_1} \\ &\frac{f}{m_1} = \mu\alpha^2\omega_1^2\left(u_2 - u_1\right) + 2\mu\zeta_2\alpha\omega_1\left(\dot{u}_2 - \dot{u}_1\right) \end{aligned} \tag{4.9}$$

Mass ratio μ, frequency ratio α, uncoupled natural frequency ω_1 and damping ratio ζ_1 of the primary oscillator and uncoupled damping ratio ζ_2 of the secondary oscillator are defined as follows

$$\mu = \frac{m_2}{m_1} \tag{4.10a}$$

$$\alpha = \frac{\omega_2}{\omega_1} \tag{4.10b}$$

$$\omega_1 = \sqrt{\frac{k_1}{m_1}} \tag{4.10c}$$

$$\zeta_1 = \frac{c_1}{2\sqrt{k_1 m_1}} \tag{4.10d}$$

$$\zeta_2 = \frac{c_2}{2\sqrt{k_2 m_2}} \tag{4.10e}$$

where $\omega_2 = \sqrt{k_2/m_2}$ is the uncoupled natural frequency of the secondary oscillator. In general, within this set of parameters: mass ratio μ and dynamic properties ω_1 and ζ_1 are known data depending on the actual configuration of the supporting structure and the isolated equipment; frequency ratio α and the damping ratio ζ_2 are the design parameters of the equipment isolation system, to be determined through an optimization procedure.

4.2.2 State-space form of equations of motion

We rewrite the equations of motion of the generalized 2-DOF model into the state-space form, *i.e.* in the form of a first-order matrix differential equation.

We first write the second-order Eqs. (4.9) in matrix form

$$\mathbf{m}\ddot{\mathbf{u}} + \mathbf{c}\dot{\mathbf{u}} + \mathbf{k}\mathbf{u} = -\mathbf{m}\mathbf{r}\,\ddot{u}_g(t) \tag{4.11}$$

where $\mathbf{m}$, $\mathbf{c}$ and $\mathbf{k}$ are the (2×2) mass, damping and stiffness matrices of the 2-DOF model; $\mathbf{u}(t) = \begin{pmatrix} u_1(t) & u_2(t) \end{pmatrix}^{\mathrm{T}}$, $\dot{\mathbf{u}}(t)$ and $\ddot{\mathbf{u}}(t)$ are the relative displacement, velocity

and acceleration vectors; $\mathbf{r}$ is the (2×1) vector of influence coefficients. Assuming that the mass matrix $\mathbf{m}$ is invertible, we can solve for $\ddot{\mathbf{u}}$ as

$$\ddot{\mathbf{u}} = -\mathbf{m}^{-1}\mathbf{c}\,\dot{\mathbf{u}} - \mathbf{m}^{-1}\mathbf{k}\,\mathbf{u} - \mathbf{r}\,\ddot{u}_g \tag{4.12}$$

Let the state vector be defined as

$$\mathbf{z} = \begin{pmatrix} \mathbf{u} \\ \dot{\mathbf{u}} \end{pmatrix} = \begin{pmatrix} u_1 \\ u_2 \\ \dot{u}_1 \\ \dot{u}_2 \end{pmatrix} \tag{4.13}$$

the state variables being the relative displacement and velocities of the 2-DOF system. Eq. (4.12) can be expressed into the state-space form as a first-order matrix differential equation

$$\dot{\mathbf{z}} = \mathbf{A}\,\mathbf{z} + \mathbf{B}\,e(t) \tag{4.14}$$

where

$$\begin{aligned} \mathbf{A} &= \begin{pmatrix} \mathbf{0} & \mathbf{I} \\ -\mathbf{m}^{-1}\mathbf{k} & -\mathbf{m}^{-1}\mathbf{c} \end{pmatrix} = \\ &= \begin{pmatrix} 0 & 0 & 1 & 0 \\ 0 & 0 & 0 & 1 \\ -\omega_1^2 - \mu\alpha^2\omega_1^2 & \mu\alpha^2\omega_1^2 & -2\zeta_1\omega_1 - 2\mu\zeta_2\alpha\omega_1 & 2\mu\zeta_2\alpha\omega_1 \\ \alpha^2\omega_1^2 & -\alpha^2\omega_1^2 & 2\zeta_2\alpha\omega_1 & -2\zeta_2\alpha\omega_1 \end{pmatrix} \end{aligned} \tag{4.15}$$

is the state matrix, function of the system parameters,

$$\mathbf{B} = \begin{pmatrix} \mathbf{0} \\ -\mathbf{r} \end{pmatrix} = \begin{pmatrix} 0 \\ 0 \\ -1 \\ -1 \end{pmatrix} \tag{4.16}$$

is the input matrix and

$$e(t) = \ddot{u}_g(t) \tag{4.17}$$

is the base acceleration applied to the 2-DOF system.

4.2.3 Seismic input and system response

In order to consider the probabilistic nature of the seismic input, ground acceleration $\ddot{u}_g(t)$ is modelled as a stationary Gaussian random process with white noise power-spectral density $S_{\ddot{u}_g}(\omega) = S_{\mathrm{W}} = \text{const}$, zero mean $\mu_{\ddot{u}_g} = 0$ and autocorrelation function $R_{\ddot{u}_g}(\tau) = 2\pi S_W \delta(\tau)$, where $\delta(\tau)$ is the Dirac's delta and $\tau = t_{j+1} - t_j$, $\forall\, j$. This choice seems to be adequate to a design phase, although it neglects the dependency on the excitation frequency content.

The system is linear and initial conditions are assumed deterministic, hence the system response $\mathbf{z}(t)$ is a stationary Gaussian multivariate process, fully defined by its mean vector $\boldsymbol{\mu}_{\mathbf{z}}$ and autocorrelation matrix $\mathbf{R}_{\mathbf{zz}}(\tau)$. Assuming a zero mean input process and zero initial conditions yields a zero mean response process $\boldsymbol{\mu}_{\mathbf{z}} = \mathbf{0}$. Moreover, since the input process has a white noise spectral density, the autocorrelation matrix $\mathbf{R}_{\mathbf{zz}}(\tau)$ of the response process can be expressed as a function of its covariance matrix $\mathbf{G}_{\mathbf{zz}}$. To sum up, the complete probability description of the response process $\mathbf{z}(t)$ is known if the covariance matrix $\mathbf{G}_{\mathbf{zz}}$ is known.

The covariance matrix of the response process is defined as

$$\mathbf{G}_{\mathbf{zz}} = \mathsf{E}\left[(\mathbf{z} - \boldsymbol{\mu}_{\mathbf{z}})\,(\mathbf{z} - \boldsymbol{\mu}_{\mathbf{z}})^{\top}\right] = \mathsf{E}\left[\mathbf{z}\mathbf{z}^{\top}\right] \tag{4.18}$$

where $\mathsf{E}[\,\cdot\,]$ denotes the expected value operator. Lin [82] has proved that $\mathbf{G}_{\mathbf{zz}}$ satisfies the following differential equation:

$$\dot{\mathbf{G}}_{\mathbf{zz}} = \mathbf{A}\mathbf{G}_{\mathbf{zz}} + \mathbf{G}_{\mathbf{zz}}\mathbf{A}^{\top} + 2\pi S_W \mathbf{B}\mathbf{B}^{\top} \tag{4.19}$$

Being $\mathbf{z}(t)$ a stationary process, $\dot{\mathbf{G}}_{\mathbf{zz}} = \mathbf{0}$ and Eq. (4.19) reduces to an algebraic equation

$$\mathbf{A}\mathbf{G}_{\mathbf{zz}} + \mathbf{G}_{\mathbf{zz}}\mathbf{A}^{\top} + 2\pi S_W \mathbf{B}\mathbf{B}^{\top} = \mathbf{0} \tag{4.20}$$

Eq. (4.20) is in the form of a Lyapunov equation and can be solved numerically to determine $\mathbf{G}_{\mathbf{zz}}$.

Once the covariance matrix of the response process is known, a good measure of the system performance is the standard deviation vector $\boldsymbol{\sigma}_{\mathbf{z}}$, which collects the individual standard deviation of all the state variables [121]. It can be readily calculated as follows

$$\boldsymbol{\sigma}_{\mathbf{z}} = \sqrt{\operatorname{diag}\left(\mathbf{G}_{\mathbf{zz}}\right)} \tag{4.21}$$

where $\operatorname{diag}(\,\cdot\,)$ indicates a vector composed of the diagonal elements of a matrix. Since the response process has zero mean, the standard deviation vector $\boldsymbol{\sigma}_{\mathbf{z}}$ reduces to

$$\boldsymbol{\sigma}_{\mathbf{z}} = \sqrt{\operatorname{diag}\left(\mathsf{E}\left[\mathbf{z}\mathbf{z}^{\top}\right]\right)} \tag{4.22}$$

that is, the vector collecting the Root-Mean-Square (RMS) of state variables.

Besides the state vector $\mathbf{z}(t)$, which describes the dynamics of the 2-DOF system in terms of relative displacements and velocities, we are interested in calculating the absolute acceleration vector $\ddot{\mathbf{u}}_a(t)$. From Eq. (4.12), it follows

$$\ddot{\mathbf{u}}_a = \ddot{\mathbf{u}} + \mathbf{r}\,\ddot{u}_g(t) = -\mathbf{m}^{-1}\mathbf{c}\dot{\mathbf{u}} - \mathbf{m}^{-1}\mathbf{k}\mathbf{u} \tag{4.23}$$

The absolute acceleration vector can be expressed in terms of state vector as

$$\ddot{\mathbf{u}}_a = \mathbf{C}_{\ddot{\mathbf{u}}_a}\,\mathbf{z} = \Big(-\mathbf{m}^{-1}\mathbf{k} \quad -\mathbf{m}^{-1}\mathbf{c}\Big)\,\mathbf{z} \tag{4.24}$$

where $\mathbf{C}_{\ddot{\mathbf{u}}_a}$ is called output influence matrix. The covariance matrix $\mathbf{G}_{\ddot{\mathbf{u}}_a\ddot{\mathbf{u}}_a}$ of the absolute acceleration vector can then be obtained from the covariance matrix $\mathbf{G}_{\mathbf{zz}}$ of the state vector as

$$\mathbf{G}_{\ddot{\mathbf{u}}_a\ddot{\mathbf{u}}_a} = \mathsf{E}\left[\ddot{\mathbf{u}}_a\ddot{\mathbf{u}}_a^\top\right] = \mathsf{E}[\mathbf{C}_{\ddot{\mathbf{u}}_a}\,\mathbf{z}\mathbf{z}^\top\mathbf{C}_{\ddot{\mathbf{u}}_a}^\top] = \mathbf{C}_{\ddot{\mathbf{u}}_a}\,\mathsf{E}\left[\mathbf{z}\mathbf{z}^\top\right]\mathbf{C}_{\ddot{\mathbf{u}}_a}^\top = \mathbf{C}_{\ddot{\mathbf{u}}_a}\mathbf{G}_{\mathbf{zz}}\mathbf{C}_{\ddot{\mathbf{u}}_a}^\top \tag{4.25}$$

In a similar way as Eq. (4.22), we calculate the standard deviation vector $\boldsymbol{\sigma}_{\ddot{\mathbf{u}}_a}$ as follows

$$\boldsymbol{\sigma}_{\ddot{\mathbf{u}}_a} = \sqrt{\operatorname{diag}\left(\mathbf{G}_{\ddot{\mathbf{u}}_a\ddot{\mathbf{u}}_a}\right)} \tag{4.26}$$

4.2.4 Optimization

The optimization procedure is specifically developed to account for the damping properties of HDRB. For a target shear strain of 100% – 150%, the equivalent damping ratio of HDRB is experimentally found to range from 0.10 to 0.15 (see Fig. 4.2 (b)). Based on this finding, the damping ratio in the first complex mode of the generalized 2-DOF system can be assumed to be constant and equal to $\eta_1 = 0.12$. This is equivalent to say that only one design parameter, the frequency ratio α, is varied to find the optimal value, while the damping ratio ζ_2 results from the complex modal analysis of the system, complying with the required value of η_1.

In order to investigate the sensitivity of the system response to the design parameter α, a series of numerical simulations is shown in Figs. 4.5 – 4.8. To represent the system response, the following non-dimensional variables are introduced:

$$\ddot{U}_{a1} = \frac{\sigma_{\ddot{u}_{a1}\,\mathrm{IE}}}{\sigma_{\ddot{u}_{a1}\,\mathrm{FBE}}} \tag{4.27a}$$

$$\ddot{U}_{a2} = \frac{\sigma_{\ddot{u}_{a2}\,\mathrm{IE}}}{\sigma_{\ddot{u}_{a2}\,\mathrm{FBE}}} \tag{4.27b}$$

$$U_1 = \frac{\sigma_{u_1\,\mathrm{IE}}}{\sigma_{u_1\,\mathrm{FBE}}} \tag{4.27c}$$

$$U_{21} = \frac{\sigma_{u_{21}\,\mathrm{IE}}}{\sigma_{u_1\,\mathrm{FBE}}} \tag{4.27d}$$

In Eqs. (4.27), standard deviation $\sigma_\cdot$ coincides with RMS $\sqrt{\mathsf{E}\left[(\cdot)^2\right]}$. Then, non-dimensional variables represent the RMS ratios of system responses between the controlled and the uncontrolled configurations: subscript IE indicates the controlled configuration, where the equipment is isolated from the supporting structure; subscript FBE indicates the uncontrolled configuration, where the equipment is fixed-base and rigidly anchored to the supporting structure. RMS ratios $\ddot{U}_{a1}$ and $\ddot{U}_{a2}$ refer to the absolute accelerations $\ddot{u}_{a1} = \ddot{u}_1 + \ddot{u}_g$ and $\ddot{u}_{a2} = \ddot{u}_2 + \ddot{u}_g$ of the supporting structure and the equipment, respectively; U_1 refers to the displacement u_1 of the supporting structure; U_{21} refers to the displacement $u_{21} = u_2 - u_1$ of the equipment relative to the supporting structure.

Sensitivity analyses are conducted by varying the parameter α, while holding the other parameters[2] at fixed values ($\zeta_1 = 0.02$, $\eta_1 = 0.12$). Mass ratio μ ranges from 0.1 to 2.0. Two limit cases are recognized in Figs. 4.5 – 4.8: on the one hand, $\alpha \to \infty$ corresponds to the FBE configuration and indeed $\ddot{U}_{a1}$, $\ddot{U}_{a2}$ and U_1 tend to unity, while U_{21} tends to zero; on the other hand, $\alpha \to 0$ corresponds to a complete decoupling of the equipment from the supporting structure and this leads to $\ddot{U}_{a2}$ tending to zero and U_{21} tending to infinity. Values of α between the two limits indicate variously designed equipment isolation systems.

It can be noted from numerical results that $\ddot{U}_{a2}$ monotonically decreases as parameter α decreases and assumes values below unity. This means that the equipment absolute acceleration can always be reduced, as compared to the FBE configuration, by weakening the coupling with the supporting structure. Meanwhile, the equipment relative displacement is expected to increase, as shown by U_{21}. In passing, it is interesting to examine the response of the supporting structure too. A range of values for α exists where $\ddot{U}_{a1}$ and U_1 are less than unity, that is, the absolute acceleration and the displacement of the supporting structure are reduced compared to the FBE configuration. As mass ratio μ increases, this range of values significantly expands.

Aiming at preserving integrity and serviceability of the isolated equipment, two RMS ratios are considered for design purposes: the absolute acceleration $\ddot{U}_{a2}$ of the equipment and its displacement U_{21} relative to the supporting structure. In fact, both these quantities may lead to the failure of the equipment: excessive absolute accelerations, or excessive inertial loads, should be avoided to prevent internal damages to vibration sensitive apparati; meanwhile, practical considerations associated with the presence of service lines and of a limited space of installation require the relative displacement of the equipment to be within an allowable threshold as well.

Since there is a conflict in achieving the minimum absolute acceleration $\ddot{U}_{a2}$ and, at the same time, limiting the relative displacement U_{21}, compromises have to be made. A multi-objective optimization problem is defined which takes into account both the

[2]RMS ratios in Eqs. (4.27) depend on α, ζ_1, η_1, μ and are independent on ω_1.

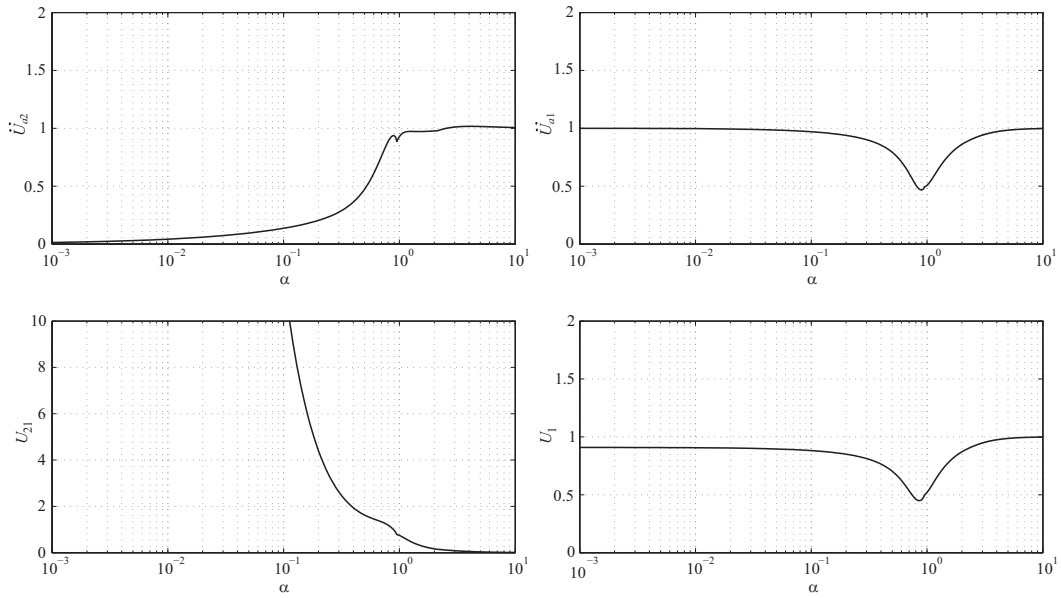

Figure 4.5. RMS response ratios *versus* design parameter α: (a) absolute acceleration $\ddot{U}_{a2}$ of the equipment; (b) displacement U_{21} of the equipment relative to the supporting structure; (c) absolute acceleration $\ddot{U}_{a1}$ of the supporting structure; (d) displacement U_1 of the supporting structure relative to ground. It is assumed: $\mu = 0.10$, $\zeta_1 = 0.02$, $\eta_1 = 0.12$.

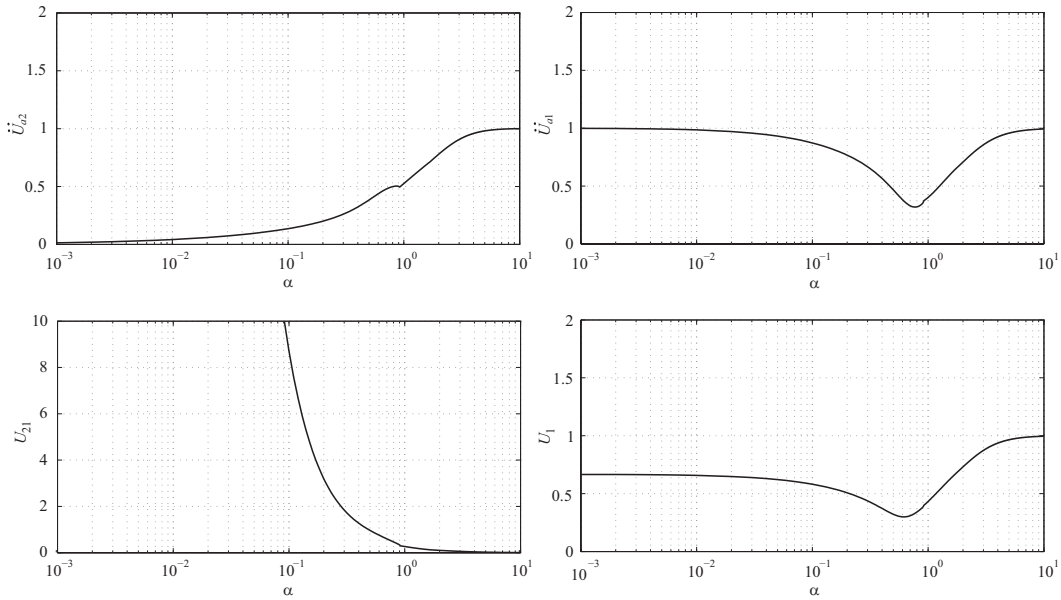

Figure 4.6. RMS response ratios *versus* design parameter α: (a) absolute acceleration $\ddot{U}_{a2}$ of the equipment; (b) displacement U_{21} of the equipment relative to the supporting structure; (c) absolute acceleration $\ddot{U}_{a1}$ of the supporting structure; (d) displacement U_1 of the supporting structure relative to ground. It is assumed: $\mu = 0.50$, $\zeta_1 = 0.02$, $\eta_1 = 0.12$.

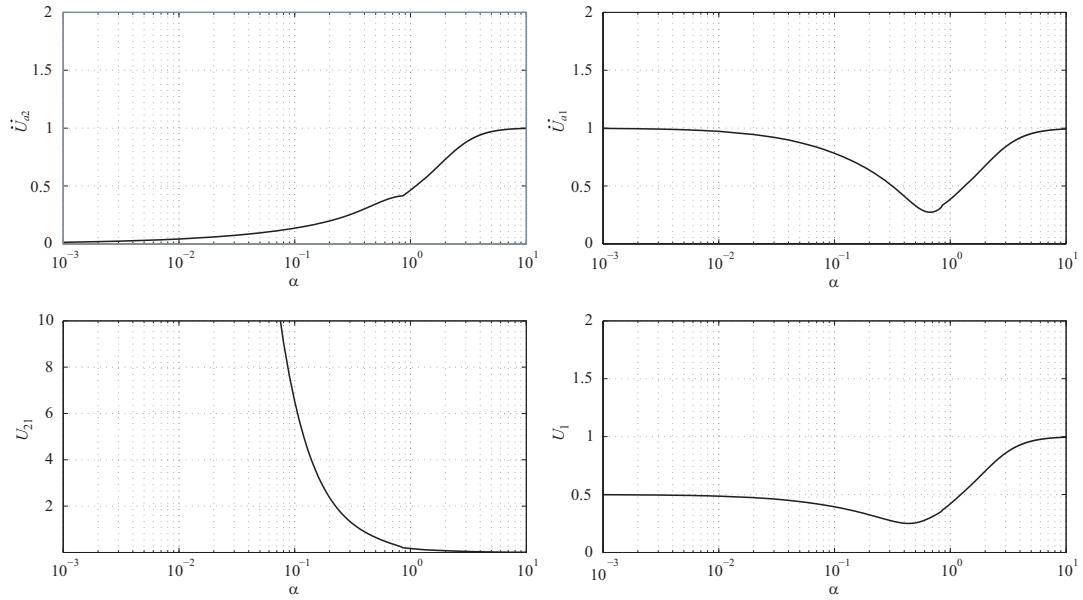

Figure 4.7. RMS response ratios *versus* design parameter α: (a) absolute acceleration $\ddot{U}_{a2}$ of the equipment; (b) displacement U_{21} of the equipment relative to the supporting structure; (c) absolute acceleration $\ddot{U}_{a1}$ of the supporting structure; (d) displacement U_1 of the supporting structure relative to ground. It is assumed: $\mu = 1.00$, $\zeta_1 = 0.02$, $\eta_1 = 0.12$.

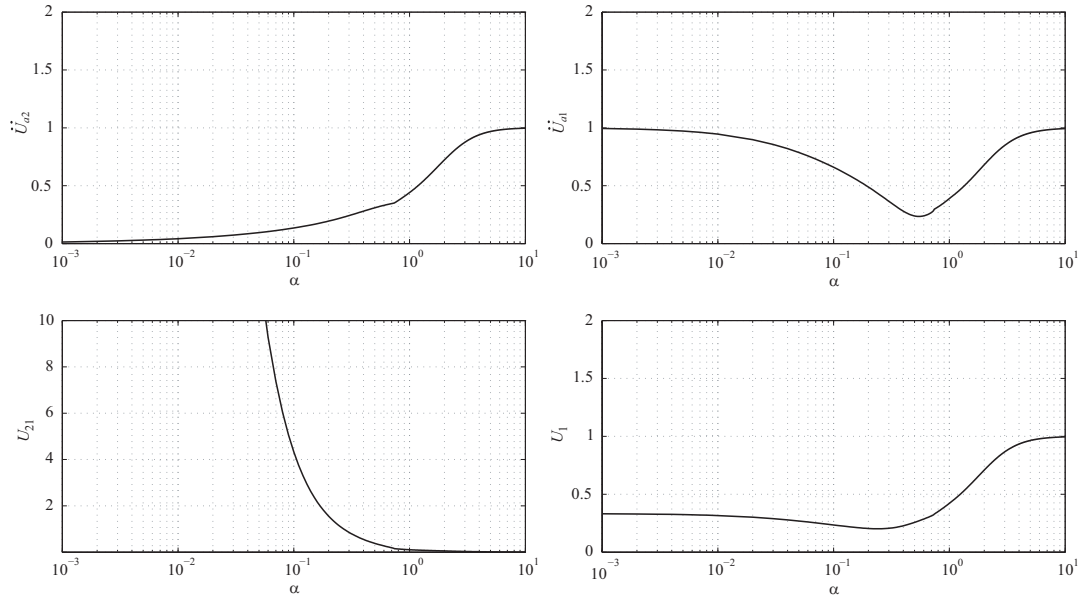

Figure 4.8. RMS response ratios *versus* design parameter α: (a) absolute acceleration $\ddot{U}_{a2}$ of the equipment; (b) displacement U_{21} of the equipment relative to the supporting structure; (c) absolute acceleration $\ddot{U}_{a1}$ of the supporting structure; (d) displacement U_1 of the supporting structure relative to ground. It is assumed: $\mu = 2.00$, $\zeta_1 = 0.02$, $\eta_1 = 0.12$.

criteria:

$$\min_{\alpha} J(\alpha), \quad J(\alpha) = p\,\ddot{U}_{a2}(\alpha) + (1-p)\,U_{21}(\alpha) \tag{4.28}$$

The objective function $J(\alpha)$ has the form of a weighted sum, where $p \in [0,1]$ is the weight assigned to the equipment absolute acceleration and its complement to one is the weight assigned to the equipment relative displacement. The weight p requires to make a trade-off between the absolute acceleration and the relative displacement of the equipment. In this study, $p = 0.85$ is assigned, preferring the goal of reducing the equipment acceleration, but limiting the relative displacement as well. The optimal value α_{opt} is selected by solving the equation

$$\frac{\partial J(\alpha)}{\partial \alpha} = 0 \tag{4.29}$$

through a numerical search algorithm.

4.3 Application

Here, we provide an application to illustrate the methodology proposed for the optimal design of an equipment isolation system using HDRB. The illustrative application refers to steel frame structures in industrial plants, which mostly house heavy equipment (*e.g.*, see Fig. 4.9).

A 1:5 scale physical model is considered. The supporting structure (Fig. 4.10) is a two-storey steel frame and a block-type equipment is supposed to be isolated on the second floor. The steel frame consists of L cross-section beams and columns and two square plates, one for each floor. Floor dimensions are 0.60 m × 0.60 m and total height is 2.40 m, with an inter-story height of 1.20 m (Fig. 4.10 (a)). Two cross bracings are arranged in the yz-plane so that the frame motion is in the x-direction only, the same as the one of base excitation, avoiding out of plane displacements (Fig. 4.10 (b)). Total floor masses are $M_1 = 89.7$ kg and $M_2 = 97.2$ kg, where subscripts 1 and 2 indicate the first and the second floor, respectively. The equipment mass is assumed to be $M_e = 334$ kg.

Modal analysis of the supporting structure

A preliminary finite element model of the steel frame is developed to evaluate its dynamic behaviour by using the general purpose Structural Analysis Program SAP2000 v.10.0.4 (Computers & Structures Inc. 2007) [18].

Since the frame satisfies the criteria for regularity in plan and elevation, as to lateral stiffness and mass distribution, and it is supposed to be base-excited in the x-direction only, the analysis is limited to the xz-plane. Axial deformation is neglected in all structural members and floors are taken as rigid in their own planes. Masses are lumped at the centre of mass of each floor, which is also the geometric centre.

Figure 4.9. Industrial steel frame structure housing a heavy equipment.

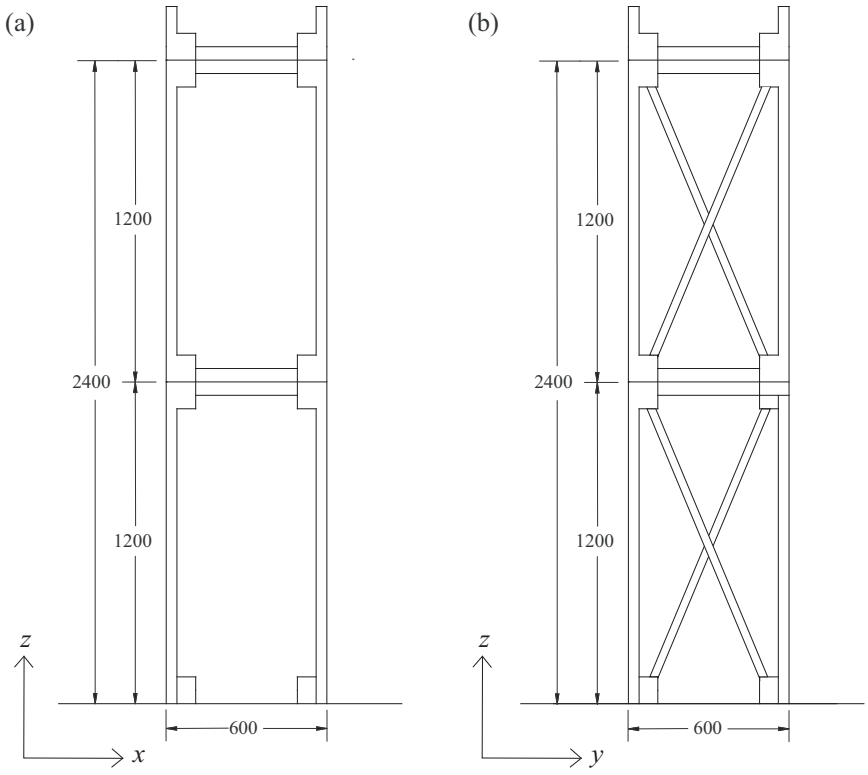

Figure 4.10. Application: 1:5 scale physical model of the supporting structure. (a) View in the xz-plane. (b) View in the yz-plane. Unit: mm.

Each floor has a single dynamic degree of freedom, the lateral displacement in the x-direction, hence the frame is modelled as a 2-DOF system. The mass matrix of the frame is regarded as a diagonal matrix

$$\mathbf{M}\ [\mathrm{kg}] = \begin{pmatrix} 89.7 & 0 \\ 0 & 97.2 \end{pmatrix} \tag{4.30}$$

The stiffness matrix is

$$\mathbf{K}\ [\mathrm{N/m}] = 10^5 \cdot \begin{pmatrix} 6.0273 & -2.9467 \\ -2.9467 & 2.8295 \end{pmatrix} \tag{4.31}$$

The frame is assumed to be classically damped and the viscous damping matrix is obtained as proportional to the mass matrix, or

$$\mathbf{C} = a\,\mathbf{M} \tag{4.32}$$

Constant a is determined so that the damping ratio of the first mode is 0.02. It yields $a = 1.3443$ and the viscous damping matrix is

$$\mathbf{C}\ [\mathrm{Ns/m}] = \begin{pmatrix} 120.58 & 0 \\ 0 & 130.66 \end{pmatrix} \tag{4.33}$$

The influence vector of the frame is

$$\boldsymbol{\tau} = \begin{pmatrix} 1 \\ 1 \end{pmatrix} \tag{4.34}$$

Modal frequencies, damping ratios and participating mass ratios of the steel frame are reported in Tab. 4.1. The matrix made up of the mode-shape vectors of the frame is given by

$$\boldsymbol{\Phi} = (\boldsymbol{\phi}_1 \quad \boldsymbol{\phi}_2) = \begin{pmatrix} 0.507 & 0.879 \\ 0.862 & -0.477 \end{pmatrix} \tag{4.35}$$

Mode	Frequency [rad/s]	Frequency [Hz]	Damping ratio	Participating mass ratio
I	33.61	5.35	0.0200	0.9381
II	92.20	14.67	0.0073	0.0619

Table 4.1. Application: modal frequencies, damping ratios and participating mass ratios of the supporting structure.

Reduced order 2-DOF model

The dynamic response of the steel frame is governed by its first mode, as indicated by a modal participating mass ratio of 0.9381. In order to introduced the reduced order 2-DOF model (Eq. (4.8)), the response vector $\mathbf{x}(t)$ of the frame is approximated by its first mode-shape vector $\boldsymbol{\phi}_1$ and the modal amplitude $q_1(t)$

$$\mathbf{x}(t) \approx \boldsymbol{\phi}_1 \, q_1(t) \tag{4.36}$$

The mode-shape vector $\boldsymbol{\phi}_1$ is normalized with respect to the element corresponding to the location of the isolated equipment. Being the latter supposed to be on the second floor, the normalized mode-shape vector is given as

$$\widetilde{\boldsymbol{\phi}}_1 = \begin{pmatrix} 0.588 \\ 1.000 \end{pmatrix} \tag{4.37}$$

Now, generalized properties m_1, c_1 and k_1 of the primary oscillator are calculated as shown in Tab. 3.2 on page 55. Generalized mass m_1 is given as the modal mass of the frame

$$m_1 = \widetilde{\boldsymbol{\phi}}_1^{\top} \, \mathbf{M} \, \widetilde{\boldsymbol{\phi}}_1 = 128.18 \;\; \text{kg} \tag{4.38}$$

Similarly, generalized viscous damping constant c_1 and stiffness k_1 are given as the modal damping coefficient

$$c_1 = \widetilde{\boldsymbol{\phi}}_1^{\top} \, \mathbf{C} \, \widetilde{\boldsymbol{\phi}}_1 = 172.31 \;\; \text{Ns/m} \tag{4.39}$$

and the modal stiffness

$$k_1 = \widetilde{\boldsymbol{\phi}}_1^{\top} \, \mathbf{K} \, \widetilde{\boldsymbol{\phi}}_1 = 1.4477 \cdot 10^5 \;\; \text{N/m} \tag{4.40}$$

respectively. The modal participation factor of the frame is calculated as

$$\Gamma = \frac{\widetilde{\boldsymbol{\phi}}_1^{\mathrm{T}} \, \mathbf{M} \, \boldsymbol{\tau}}{\widetilde{\boldsymbol{\phi}}_1^{\mathrm{T}} \, \mathbf{M} \, \widetilde{\boldsymbol{\phi}}_1} = 1.170 \tag{4.41}$$

In this case, generalized properties in Eqs. (4.38) – (4.41) are equal to the modal properties of the supporting structure due to the first-mode assumption in Eq. (4.36).

According to Tab. 3.2 on page 55, the mass of the secondary oscillator is equal to the mass of the equipment to be isolated: $m_2 = M_e = 334$ kg.

On the basis of the aforementioned quantities, known data of the problem are calculated as follows. Mass ratio is

$$\mu = \frac{m_2}{m_1} = 2.606 \tag{4.42}$$

Uncoupled natural frequency and damping ratio of the primary oscillator are

$$\omega_1 = \sqrt{\frac{k_1}{m_1}} = 33.61 \;\; \text{rad/s} \tag{4.43}$$

and

$$\zeta_1 = \frac{c_1}{2\sqrt{k_1\, m_1}} = 0.02 \tag{4.44}$$

respectively. The damping ratio in the first complex mode of the generalized 2-DOF system is assumed to be constant and equal to $\eta_1 = 0.12$. As a consequence, the uncoupled damping ratio ζ_2 of the secondary oscillator results from the complex modal analysis of the system. The frequency ratio α is then the design parameter to be selected according to the proposed optimization procedure.

Optimization

In Fig. 4.11, the RMS response ratios of the reduced order 2-DOF model and the objective function $J(\alpha)$ are shown *versus* the design parameter α for the present application. The minimum of $J(\alpha)$ identifies the optimal value $\alpha_{\text{opt}} = 0.430$. The damping ratio $\zeta_2 = 0.2379$ is consequently obtained by requiring $\eta_1 = 0.12$. As highlighted by the curve for $\ddot{U}_{a2}$, these parameters lead to a significant reduction (70%) of the equipment absolute acceleration, while the relative displacement U_{21} between the equipment and the supporting structure is within an allowable range. It has to be pointed out that also the response of the supporting structure is reduced, in terms of both displacement U_1 and absolute acceleration $\ddot{U}_{a1}$, with reductions amounting to nearly 80%. This implies that the proposed isolation system, designed for the seismic protection of equipment, is actually able to protect the supporting structure as well.

Optimal design of HDRB

The optimal value $\alpha_{\text{opt}} = 0.430$ is used to design the equipment isolation system implementing HDRB. The optimal stiffness of the isolation system is found to be

$$k_{2\,\text{opt}} = \alpha_{\text{opt}}^2\, \omega_1^2\, m_2 = 6.976 \cdot 10^4 \ \text{N/m} \tag{4.45}$$

Let the isolation system be composed of $n_{\text{HDRB}} = 4$ bearings. The optimal horizontal stiffness of a single bearing is then found to be

$$k_{H\,\text{opt}} = \frac{k_{2\,\text{opt}}}{n_{\text{HDRB}}} = 1.7441 \cdot 10^4 \ \text{N/m} \tag{4.46}$$

The prototypes of HDRB were manufactured in circular shape with a high-damping rubber compound, whose shear modulus is

$$G_{r\,100\%} = 0.36 \ \text{MPa} \tag{4.47}$$

when shear strain is 100%. The total thickness of the rubber

$$t_r = 54 \ \text{mm} \tag{4.48}$$

was set on the basis of manufacturing requirements, whereas the diameter of rubber layers d_r was designed to realize the optimal stiffness $k_{H\,\text{opt}}$. Being the horizontal

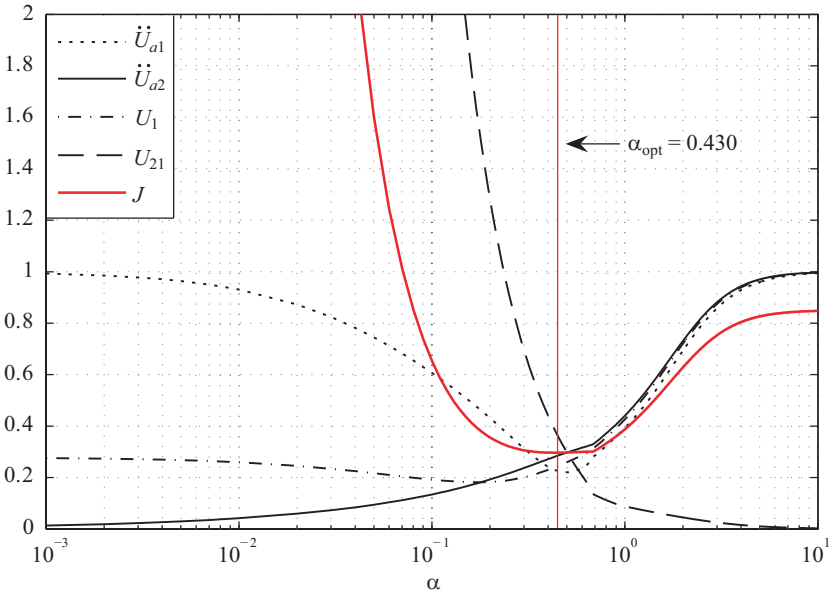

Figure 4.11. Application: optimal design of the equipment isolation system implementing HDRB. RMS response ratios and objective function J *vs* frequency ratio α. It is assumed: $\mu = 2.606$, $\zeta_1 = 0.02$, $\eta_1 = 0.12$. For the objective function: $p = 0.85$. It is obtained: $\alpha_{opt} = 0.430$, $\zeta_2 = 0.2379$.

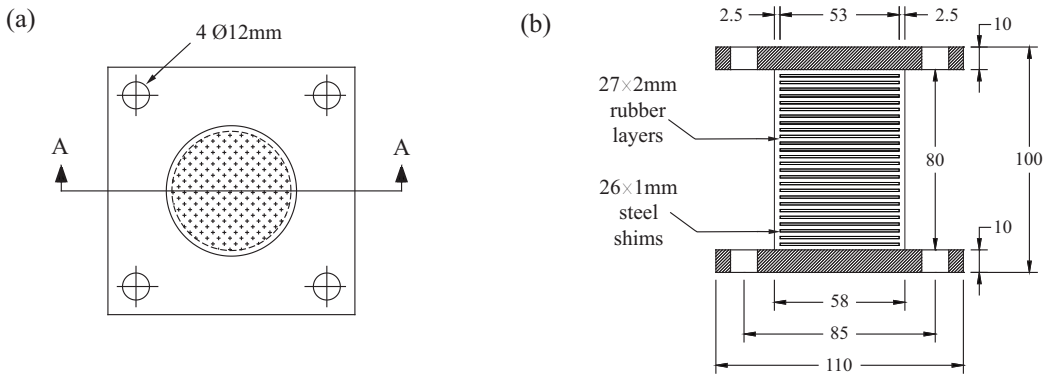

Figure 4.12. Application: details of HDRB. (a) Plane view. (b) Section A-A. Unit: mm.

stiffness of the bearing given by the formula

$$k_H = \frac{G_r\, A_r}{t_r} \tag{4.49}$$

where A_r is the full cross-sectional area of the elastomer, the optimal stiffness yields

$$A_{r\,\mathrm{opt}} = \frac{k_{H\,\mathrm{opt}}\, t_r}{G_{r\ 100\%}} = 2.6161 \cdot 10^{-3}\ \ \mathrm{m}^2 \tag{4.50}$$

and therefore

$$d_{r\,\mathrm{opt}} = \sqrt{\frac{4\, A_{r\,\mathrm{opt}}}{\pi}} = 58\ \ \mathrm{mm} \tag{4.51}$$

Details of manufactured HDRB are shown in Fig. 4.12 (a) and (b). The bearings consist of 27 2-mm-thick thin rubber layers and 26 1-mm-thick steel shims. Total rubber thickness is 54 mm, while the height of the bearing – excluding the end plates – is 80 mm. Total diameter is 58 mm, including 53 mm of shim diameter and 5 mm of cover. Oversize end plates permit the bearings to be bolted to structural elements.

4.4 Shaking table tests

4.4.1 Experimental model

Shaking table tests were performed on the 1:5 scale model illustrated in Figs. 4.13 – 4.16, realized to reproduce the system designed in Sec. 4.3. The model is composed of a two-story steel frame and a rigid mass located on the second floor, made of three integrated rectangular steel plates: the former represents the supporting structure, the latter has the role of a block-type equipment, whose mass is $M_e = 334$ kg. The experimental model was tested in three different configurations:

- (BF) bare frame without equipment;
- (FBE) frame with fixed-base equipment;
- (IE) frame with isolated equipment.

In the (BF) configuration, the steel frame was tested in the absence of the mass on the second floor (Fig. 4.13). Frame columns were welded to steel base plates; each of such plates was bolted to the shaking table by means of 4 30-mm-diameter steel bolts, so as to realize a clamp (Fig. 4.13 (b) and (c)).

In the uncontrolled configuration (FBE), the mass was anchored to the second floor of the frame by means of four steel beams having HEA120 cross-section, bolted to each other to realize a rigid connection (Figs. 4.14).

In the controlled configuration (IE), the mass was isolated from the second floor of the frame *via* a passive isolation system implementing HDRB (Figs. 4.15 and 4.16). The isolation system, composed of four bearings placed symmetrically to the x-direction of base excitation, realizes the optimal parameters designed in Sec. 4.3.

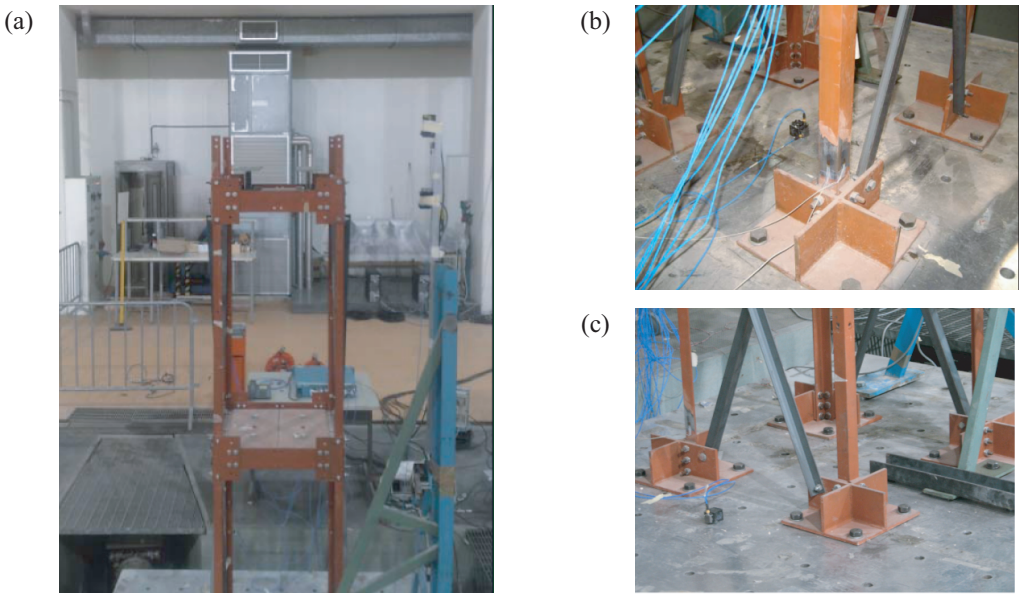

Figure 4.13. Experimental model for shaking table tests, bare frame (BF) configuration. (a) General view of the model. (b) and (c) Details of clamps at the base of frame columns.

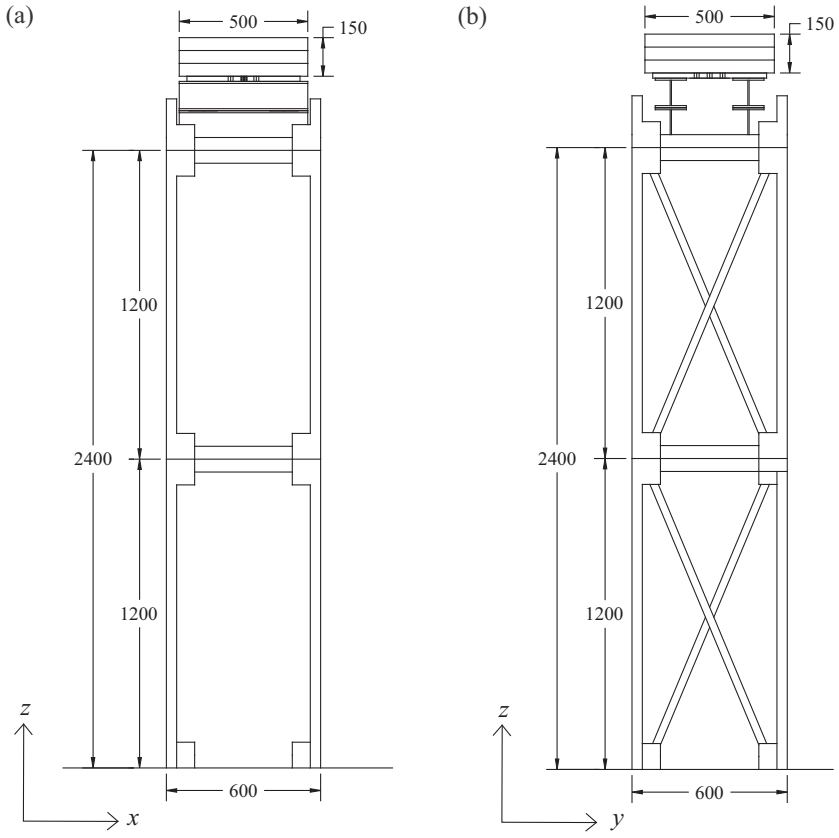

Figure 4.14. Experimental model for shaking table tests, uncontrolled configuration (FBE). (a) View in the xz-plane. (b) View in the yz-plane. Unit: mm.

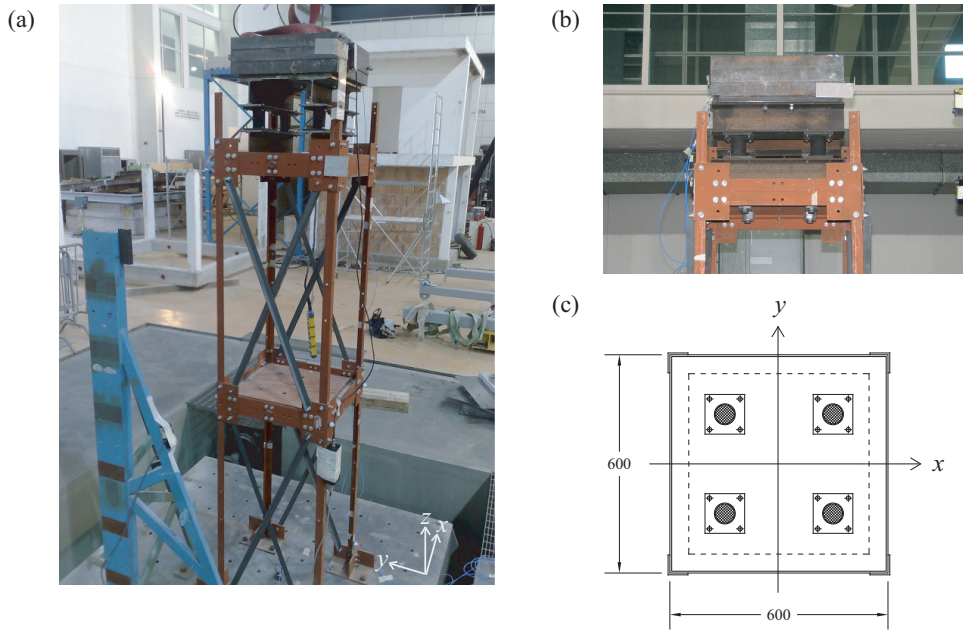

Figure 4.15. Experimental model for shaking table tests, controlled configuration (IE). (a) General view of the model. (b) Detail of the isolation system implementing HDRB, view in the xz-plane. (c) In-plane arrangement of HDRB. Unit: mm.

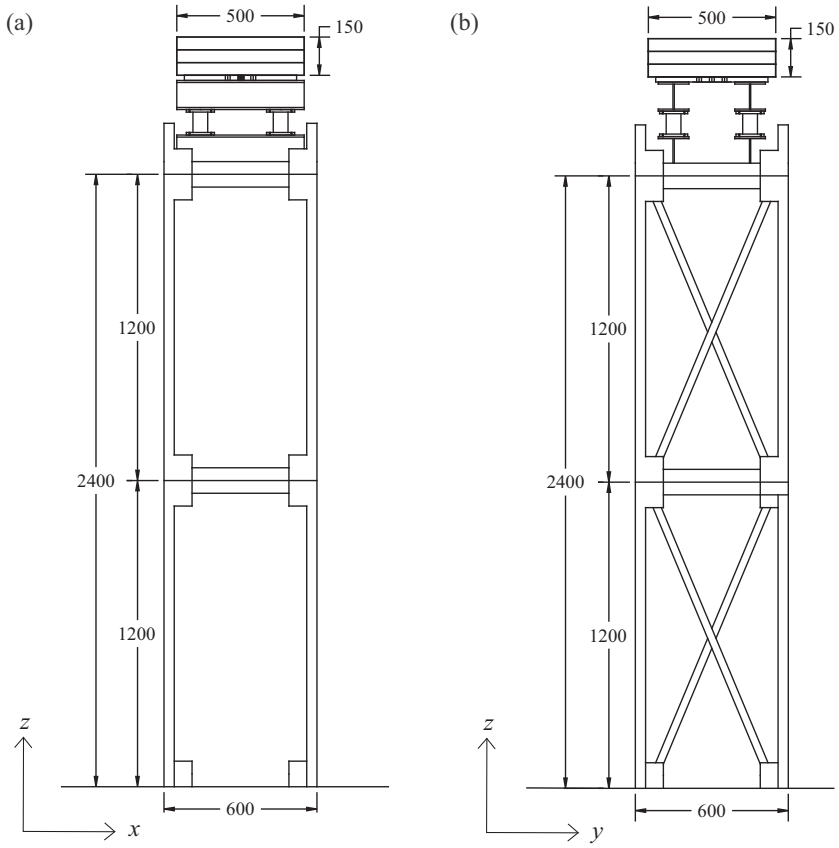

Figure 4.16. Experimental model for shaking table tests, controlled configuration (IE). (a) View in the xz-plane. (b) View in the yz-plane. Unit: mm.

4.4.2 Test setup

Tests were carried out on a six-degree-of-freedom shaking table (Fig. 4.17) in the MAT-QUAL Laboratory of ENEA (Italian National Agency for New Technologies, Energy and the Environment), "Casaccia" Research Center in Rome, Italy. The 2.0 m $\times$ 2.0 m shaking table, manufactured by the MTS Corporation (USA), has the following characteristics: operating frequency range $0 \div 100$ Hz; maximum acceleration $\pm 5\,g$, where g is the acceleration due to gravity; maximum velocity ± 1 m/s; maximum displacement ± 0.30 m; maximum tested specimen mass of 1 ton when its center of gravity is 1 m high.

The shaking table is driven by oil-filled actuators, four in the horizontal direction and four in the vertical direction (Fig. 4.18). As the input, the table can receive displacement or velocity or else acceleration time-histories and it is controlled by a real-time digital system controller. The system controller is used for pre-tuning, system operation and test execution and provides feed-back and adaptive compensation techniques for high fidelity and faithfully reproduction of the desired table motions. The shaking table and its reaction mass, a concrete block weighing several tons, are isolated from the surrounding structure through a series of compressed air bearings.

The experimental model was equipped with the following measurement instrumentation (Fig. 4.19):

- n.11 Piezotronic PCB piezoelectric accelerometers, two on the shaking table, three on each floor and three on the rigid mass (Fig. 4.20);
- n.3 optoNCDT 1607 laser displacement transducers, one on each floor and one on the rigid mass (Fig. 4.21);
- n.4 strain gauges, to measure strains at the base of two frame columns (Fig. 4.13 (b)).

On each floor and on the mass, accelerometers were arranged as to measure accelerations in both the x- and the y-direction and to detect any torsional motion that might occur. Two accelerometers were also placed at the center of the shaking table, in order to measure the actual acceleration time history generated by the shaking table. Laser transducers were used to measure the displacements relative to the shaking table in the x-direction. For doing this, an auxiliary metallic frame was installed on the shaking table and it was employed as a benchmark for displacement measures (Fig. 4.21 (a)). The auxiliary frame was verified to be rigid enough, having unitary transmissibility with respect to base acceleration in the frequency range of interest. The displacement responses of the second floor and the mass were further processed to obtain by difference the relative displacement of the mass.

Output signals were acquired with a sampling frequency of 200 Hz by means of a MTS 469D unit.

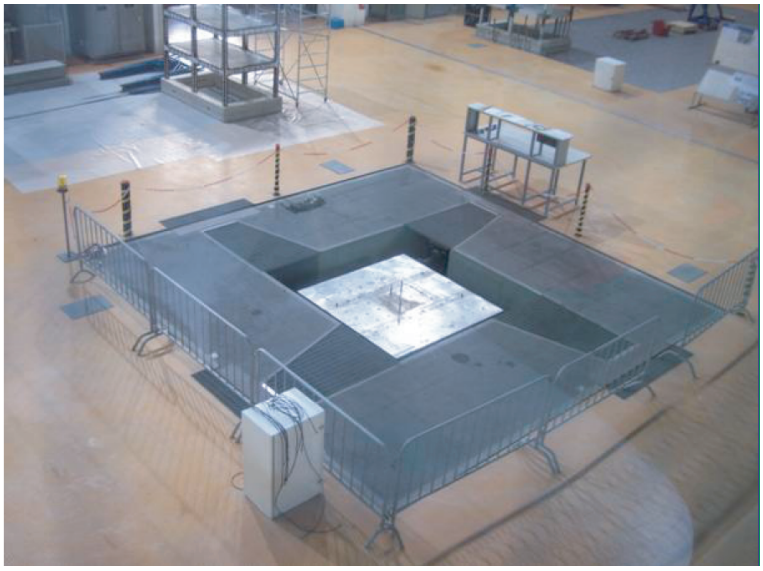

Figure 4.17. Six-degree-of-freedom shaking table in the MAT-QUAL Laboratory (ENEA, "Casaccia" Research Center, Rome).

(a)

(b)

Figure 4.18. Six-degree-of-freedom shaking table in the MAT-QUAL Laboratory of ENEA, "Casaccia" Research Center, Rome. (a) and (b) Details of oil-driven actuators.

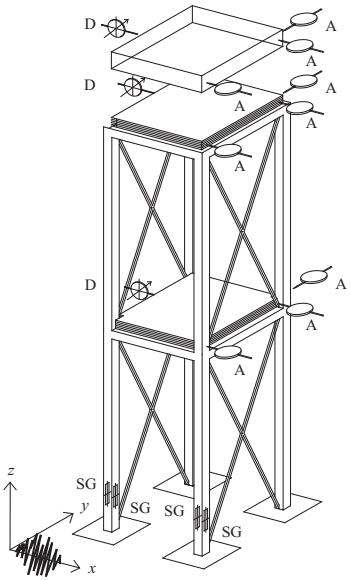

Figure 4.19. Arrangement of measurement sensors on the experimental model. Legend: A = piezoelectric accelerometer; D = laser displacement transducer; SG = strain gauge.

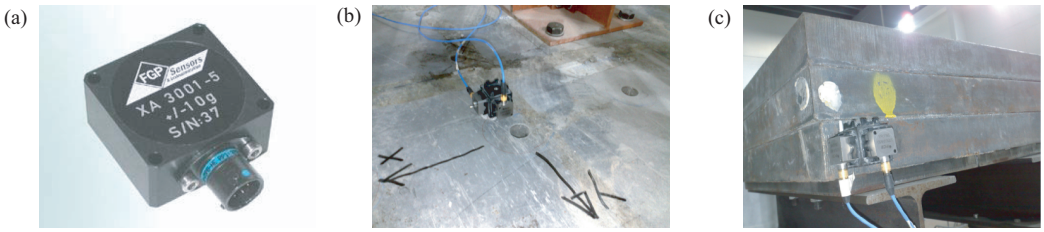

Figure 4.20. Piezotronic PCB piezoelectric accelerometers. (a) Detail of the sensor. (b) Sensors on the shaking table. (c) Sensors on the isolated mass.

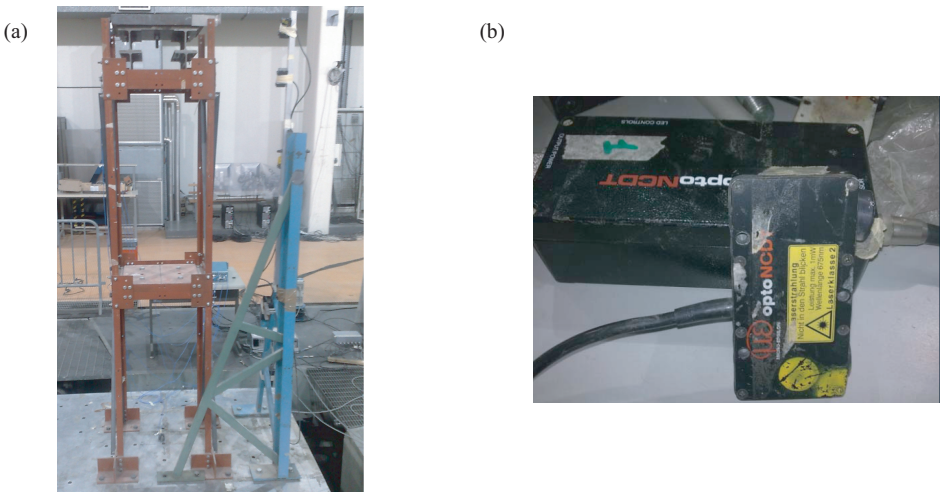

Figure 4.21. OptoNCDT 1607 laser displacement transducers. (a)The experimental model and the auxiliary metallic frame supporting laser displacement transducers. (b) Detail of the transducer.

4.4.3 Program of the tests

Shaking table tests were performed in all the model configurations and consisted of both dynamic identification tests and seismic tests.

Dynamic identification tests made use of random white noise (constant power spectral density between 1 Hz and 20 Hz) and sine sweep accelerograms (variable frequency ranging from 1 Hz to 20 Hz at a rate of 1 Hz/s). Tests were repeated at different peak ground acceleration (PGA) levels, aiming at identifying any system nonlinearities.

Seismic tests were performed under a wide selection of ground acceleration time histories in order to assess the influence of input duration and frequency content on the effectiveness of the proposed equipment isolation system. Both an artificial accelerogram and four natural accelerograms, recorded during historical earthquakes and selected from the database of the Pacific Earthquake Engineering Research Center [100], were used. Detailed information about these seismic inputs is given below:

- artificial accelerogram generated to match the elastic response spectra given by the European Standard EN 1998-1:2005 (Eurocode 8) for 5% viscous damping and C type soil [30].
- Imperial Valley Earthquake (May 19, 1940), magnitude 6.95, record from El Centro Array Station, NS component, PGA 0.313 g.
- Tokachi-oki earthquake (May 16, 1968), magnitude 7.90, record from Hachinohe Station, NS component, PGA 0.229 g.
- Northridge earthquake (January 17, 1994), magnitude 6.69, record from Sylmar Station - Olive View Medical Center, NS component, PGA 0.843 g.
- Kobe earthquake (January 16, 1995), magnitude 6.90, record from KJMA Station, NS component, PGA 0.821 g.

Selected earthquake records have been widely used in earthquake engineering research. Among them, records from Kobe (KJMA) and Northridge (Sylmar) earthquakes are characterized by one or more dominant long-period pulses, so they are typically classified as near-fault ground motions [15]. Records from Imperial Valley (El Centro) and Tokachi-oki (Hachinohe) earthquakes are instead broad-frequency-band excitations, so they are used to represent far-field ground motions.

The time scale of seismic inputs was compressed in order to achieve the equivalence of the acceleration response between the reduced-scale model and the corresponding full-scale system. Considering the geometric scaling factor $\lambda_G = 0.2$ of the model, its time scaling factor is determined as $\lambda_T = \sqrt{\lambda_G} = 0.447$. Fig. 4.22 compares acceleration time histories and elastic response spectra (5% viscous damping) of the time-scaled inputs, with PGA values normalized to 1.00 g. The figure shows that, due to the existence of long-period pulse-like components, the near-fault ground motions (Kobe, Northridge), induces relatively larger spectral acceleration values for systems whose scaled vibration period is greater than 0.5s.

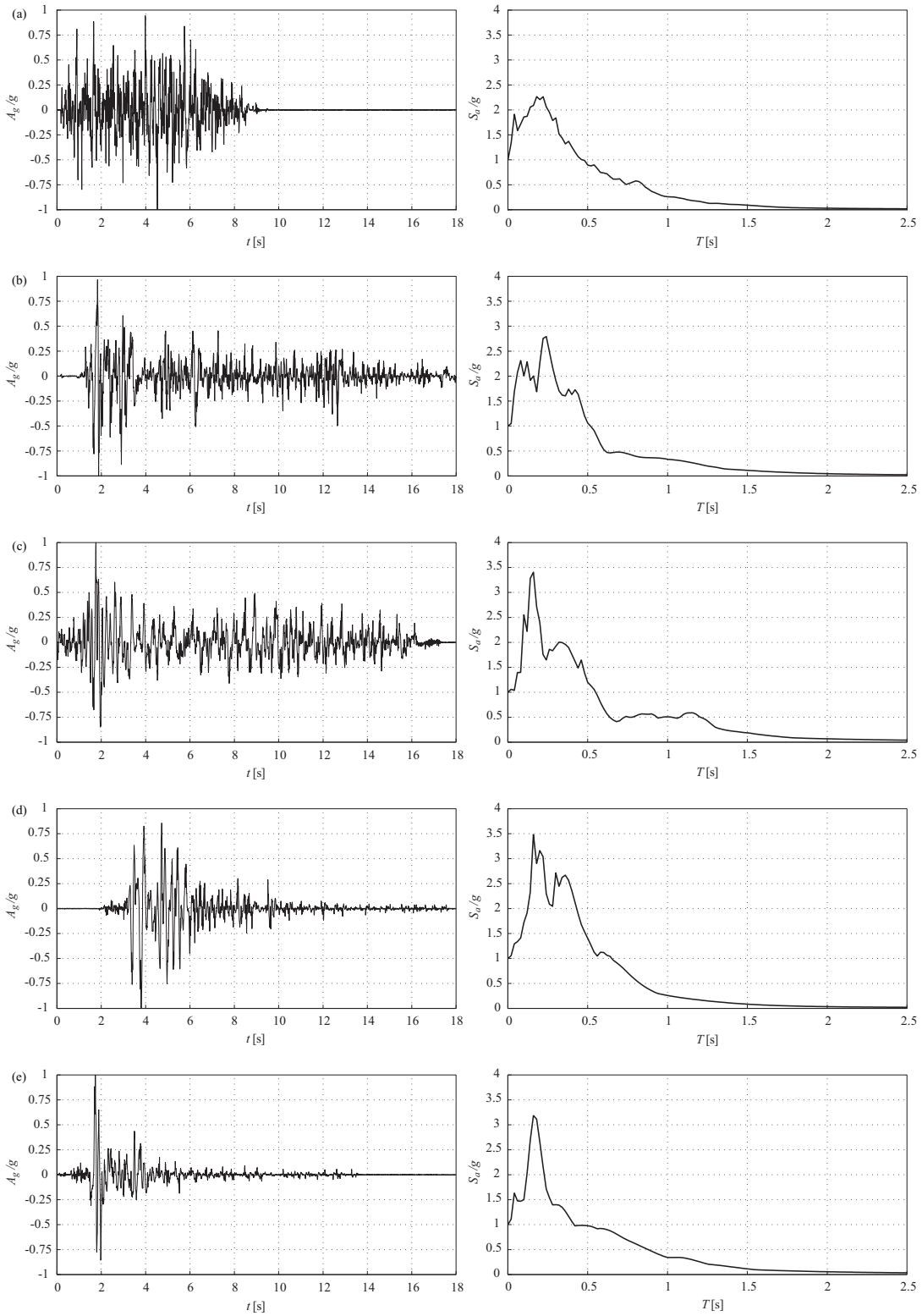

Figure 4.22. Time-scaled seismic inputs: acceleration time histories and elastic response spectra (5% damping) with PGA values normalized to 1.00 g. (a) Eurocode 8. (b) El Centro. (c) Hachinohe. (d) Kobe. (e) Northridge.

Seismic tests were carried out at different PGA levels for each accelerogram, never exceeding the elastic limit of the frame as well as the allowable shear strain of the HDRB. Tab. 4.2 summarizes the seismic tests performed in the (IE) configuration and indicates the actual PGA value measured in each test.

Accelerogram	**PGA [g]**		**Accelerogram**	**PGA [g]**	
	nominal	**measured**		**nominal**	**measured**
El Centro	0.70	0.54	Hachinohe	0.10	0.09
	0.90	0.64		0.30	0.26
	1.00	0.68		0.50	0.46
	1.10	0.75		0.70	0.65
	1.20	0.79		0.90	0.85
	1.30	0.85		1.10	1.04
	1.40	0.90		1.30	1.23
	1.50	0.99		1.50	1.47
	1.80	1.18		1.70	1.69
	2.00	1.44		1.80	1.82
Kobe	0.10	0.12	Northridge	0.10	0.13
	0.30	0.30		0.50	0.52
	0.50	0.47		0.70	0.72
	0.70	0.65		0.90	0.91
	0.90	0.79		1.10	1.06
	1.10	0.94		1.30	1.25
	1.30	1.14		1.50	1.50
	1.50	1.35		1.60	1.58
Eurocode 8	0.20	0.20			
	0.40	0.35			
	0.60	0.54			
	0.80	0.68			
	1.00	0.82			
	1.20	0.95			
	1.40	1.11			
	1.60	1.24			
	2.00	1.53			

Table 4.2. List of the seismic tests in the (IE) configuration.

4.5 Analysis of results

4.5.1 Identification of dynamic properties

Previous to the seismic tests, dynamic properties and frequency response functions of the experimental model were identified [71] in all the tested configurations (BF, FBE, IE) to validate the assumptions made in the design phase.

A random white noise accelerogram (constant power spectral density between 1 Hz and 20 Hz, PGA ranging from $0.10\,g$ to $1.56\,g$) was used to excite the experimental model and the absolute acceleration responses were measured in the x-direction on each floor and on the mass.

Identified modal frequencies and damping ratios are listed in Tab. 4.3. As expected, modal properties are different depending on the tested configuration. In (BF) and (FBE) configurations, the experimental model exhibits an indefinitely linear elastic behaviour, hence frequencies and damping ratios are constant with increasing PGA. The first natural frequency of the bare frame, 5.06 Hz, results to be close to the value 5.35 Hz assumed in the design phase (*see* Tab. 4.1). In (IE) configuration, nonlinearities in the lateral behaviour of HDRB makes the results depend on the excitation level. In this regard, Fig. 4.23 illustrates the results obtained from the dynamic characterization tests performed on the isolation system. In Fig. 4.23 (a), the effective horizontal stiffness k_H of a single bearing is shown *versus* the maximum shear strain $\gamma_{\max}$ achieved in each test. The displacement responses of the isolated mass, D_{III}, and of the second floor (the attachment floor), D_{II}, are first processed to calculate by difference the isolator displacement Δ:

$$\Delta = D_{\mathrm{III}} - D_{\mathrm{II}} \tag{4.52}$$

Test configuration	PGA [g]	$\gamma_{\max}$	I mode		II mode		III mode	
			f [Hz]	η	f [Hz]	η	f [Hz]	η
BF	0.20	-	5.06	0.0200	16.72	0.0061	-	-
FBE	0.20	-	2.63	0.0200	15.25	0.0035	-	-
IE	0.10	0.02	2.71	0.0378	10.46	0.1487	17.87	0.0319
	0.15	0.03	2.63	0.0461	10.01	0.1177	17.48	0.0256
	0.52	0.19	2.29	0.0858	8.23	0.1192	16.87	0.0246
	1.02	0.44	2.09	0.1220	7.47	0.1390	16.57	0.0276
	1.32	0.53	2.02	0.1380	7.23	0.1296	16.45	0.0286
	1.56	0.60	1.97	0.1552	7.22	0.1414	16.39	0.0241

Table 4.3. Identified modal frequencies and damping ratios in (BF), (FBE) and (IE) configurations. In (IE) configuration, modal properties are shown *vs* PGA and maximum shear strain $\gamma_{\max}$ of HDRB.

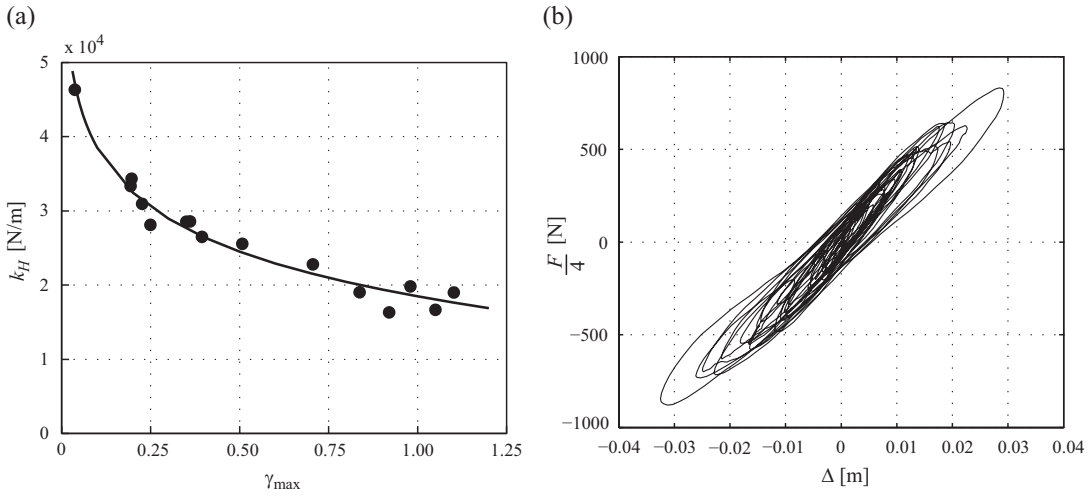

Figure 4.23. Experimental characterization of a single HDRB: (a) horizontal stiffness k_H *vs* the maximum shear strain $\gamma_{\max}$; (b) force – displacement cycles when $\gamma_{\max} = 0.60$.

When the maximum value $\Delta_{\max}$ is reached, the effective horizontal stiffness k_H and the maximum shear strain $\gamma_{\max}$ are both calculated. The former is given as the stiffness secant to the $\Delta_{\max}$

$$k_H = \frac{1}{4}\frac{F(\Delta_{\max})}{\Delta_{\max}} \tag{4.53}$$

F being the total force carried by the isolation system. The latter is given by

$$\gamma_{\max} = \frac{\Delta_{\max}}{t_r} \tag{4.54}$$

where t_r is the thickness of the rubber. Up to $\gamma_{\max} = 0.80$, HDRB show a nonlinear softening behaviour since k_H decreases with increasing shear strain. Around the design shear strain level $\gamma_{\max} = 1.00$, k_H is constant and comparable to the optimal value (Eq. (4.46)) adopted in the design phase. In this range, the HDRB system can be modelled as linear with a sufficient accuracy. Fig. 4.23 (b) illustrates the force – displacement cycles obtained for a single bearing from the test when $\gamma_{\max} = 0.60$.

Natural frequencies and damping ratios in (IE) configuration are shown in Tab. 4.3 *versus* the PGA level and the HDRB maximum shear strain $\gamma_{\max}$. As PGA and $\gamma_{\max}$ increase, the model exhibits decreasing frequencies due to the HDRB nonlinear softening behaviour. Damping ratios, considerably higher than in (BF) and (RC) configurations, are almost constant instead. In particular, the identified second modal damping ratio, ranging from 0.1177 to 0.1414, is comparable with the value 0.12 assumed in the design phase. Recorded responses were further processed through the discrete Fourier transform (DFT), computed with a fast Fourier transform (FFT) algorithm, to obtain the experimental frequency response functions. The latter were then compared with the frequency response functions of the identified numerical models. Such a comparison is shown in Fig. 4.24 for the (IE) configuration, where functions refer to the floor

absolute accelerations A_k (k = I, II) and the absolute acceleration A_{III} of the isolated mass with respect to ground acceleration A_g. A very good agreement of the curves indicates the accuracy of the identification results. In Fig. 4.25, the dynamic properties of the model are highlighted by comparing identified frequency response functions in all the tested configurations. In the uncontrolled configuration (FBE), significant amplifications can be seen for both the first and the second modes. In the controlled configuration (IE), however, these values are greatly reduced thanks to an increase in the modal damping ratios, as indicated above.

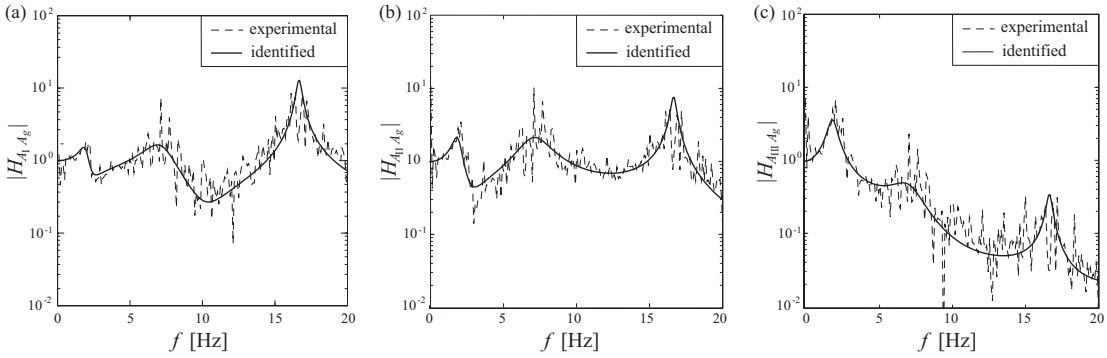

Figure 4.24. Experimental and identified frequency response functions of the model in the IE configuration: (a) first floor absolute acceleration A_{I}; (b) second floor absolute acceleration A_{II}; (c) absolute acceleration A_{III} of the isolated mass.

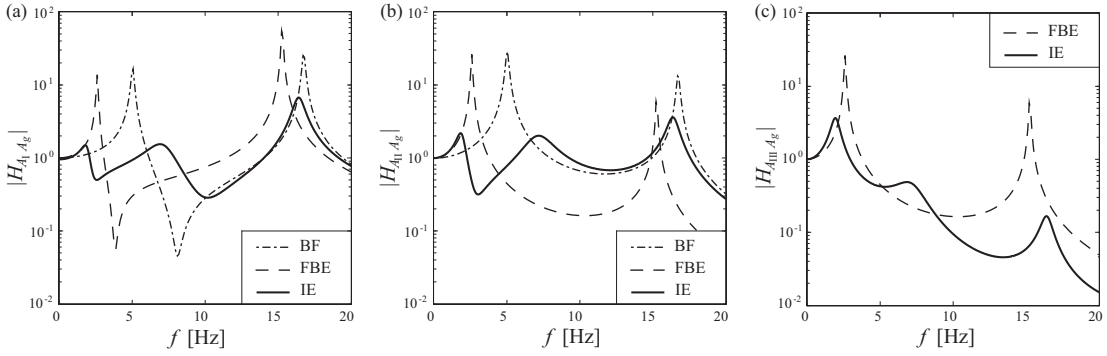

Figure 4.25. Identified frequency response functions of the model in BF, FBE and IE configurations:(a) first floor absolute acceleration A_{I}; (b) second floor absolute acceleration A_{II}; (c) absolute acceleration A_{III} of the isolated mass.

4.5.2 Evaluation of seismic effectiveness

In order to asses the seismic effectiveness of the proposed equipment isolation system implementing HDRB, a series of seismic tests was performed on the experimental model in the controlled (IE) and the uncontrolled (FBE) configurations. Seismic effectiveness is evaluated in terms of both RMS and peak response by means of performance indices. Once chosen a response quantity of interest, the performance index is defined as the ratio of the response value between the controlled and the uncontrolled configurations.

With regard to the isolated mass, relevant response quantities are its absolute acceleration A_{III} and its displacement relative to the attachment floor. Whilst the former is directly measured during the tests, the latter is calculated by difference as indicated in Eq. (4.52). Performance indices are expressed in terms of RMS responses as

$$I_1 = \frac{\mathrm{RMS}\left(A_{\mathrm{III\,IE}}\right)}{\mathrm{RMS}\left(A_{\mathrm{III\,FBE}}\right)} \tag{4.55}$$

$$I_2 = \frac{\mathrm{RMS}\left(\Delta_{\mathrm{IE}}\right)}{\mathrm{RMS}\left(D_{\mathrm{III\,FBE}}\right)} \tag{4.56}$$

For index I_1, a value smaller than one implies the effectiveness of the designed isolation system in reducing the absolute acceleration of the mass. Meanwhile, index I_2, which represents the relative displacement Δ of the isolated mass divided by its displacement D_{III} in the uncontrolled configuration, should be within an allowable threshold.

In order to ensure strength and serviceability, the dynamic response of the supporting structure is monitored as well. With regard to the frame, response quantities of interest are floor absolute accelerations A_k and displacements D_k ($k = \mathrm{I},\ \mathrm{II}$) relative to the shaking table. Base shear T_b and bending moment M_b are also considered since they are representative of the overall internal loads in the structural members. Base shear T_b is computed by summing the inertial forces acting on each mass. Base bending moment M_b is computed by summing the moments of the inertial forces about the base of the frame. Performance indices are expressed in terms of RMS responses as follows

$$I_{3,\,4} = \frac{\mathrm{RMS}\left(A_{k\,\mathrm{IE}}\right)}{\mathrm{RMS}\left(A_{k\,\mathrm{FBE}}\right)} \qquad k = \mathrm{I},\ \mathrm{II} \tag{4.57}$$

$$I_{5,\,6} = \frac{\mathrm{RMS}\left(D_{k\,\mathrm{IE}}\right)}{\mathrm{RMS}\left(D_{k\,\mathrm{FBE}}\right)} \qquad k = \mathrm{I},\ \mathrm{II} \tag{4.58}$$

$$I_7 = \frac{\mathrm{RMS}\left(T_{b\,\mathrm{IE}}\right)}{\mathrm{RMS}\left(T_{b\,\mathrm{FBE}}\right)} \tag{4.59}$$

$$I_8 = \frac{\mathrm{RMS}\left(M_{b\,\mathrm{IE}}\right)}{\mathrm{RMS}\left(M_{b\,\mathrm{FBE}}\right)} \tag{4.60}$$

Note that for indices $I_3 - I_8$, a value smaller than one implies that the dynamic response of the supporting structure is reduced in the (IE) configuration as compared to the (FBE) configuration.

Similarly to $I_1 - I_8$, performance indices $J_1 - J_8$ are defined in terms of peak responses as well. Values of $I_1 - I_8$ and $J_1 - J_8$ due to the seismic tests are shown in Fig. 4.26 and Tab. 4.4, respectively. For a given accelerogram, indices are reported *versus* the PGA level and the maximum shear strain $\gamma_{\max}$ of HDRB, which is computed as indicated by Eq. (4.54). A comparative analysis of the results highlights the following remarks.

Generally speaking, seismic tests prove the effectiveness of the proposed equipment isolation system. Performance indices for the isolated mass indicate considerable percentage reductions of the dynamic response as compared to the (FBE) configuration, in terms of both RMS and peak values. Some differences, however, can be noticed by comparing different seismic inputs. The best results are attained under the Eurocode spectrum-compatible and El Centro accelerograms: the absolute acceleration A_{III} of the isolated mass is suppressed down to 70% – 80% regardless the PGA level, as indicated by indices I_1 and J_1. This outstanding performance is due to the agreement between the seismic excitation and the input adopted in the design phase: both the accelerograms are broad-band excitations whose frequency content can be properly represented by a random white noise in the frequency range of interest for the experimental model (1 Hz – 20 Hz). For the other far-field ground motion (Hachinohe accelerogram), reductions of A_{III} are smaller, ranging from 50% to 70% as to RMS and peak values. A better control performance is attained with increasing PGA up to $\gamma_{\max} \cong 0.80$; after that, HDRB show an approximately linear behaviour and indices I_1 and J_1 remain almost constant.

In the case of near-fault ground motions (Kobe and Northridge accelerograms), the seismic excitation notably differs from the design input because of its frequency content, which is typically narrow-band, and its impulsive character. We then examine how these features affect the performance of the proposed isolation system. Indices I_1 and J_1 show that the system is still able to suppress down the absolute acceleration of the isolated mass, but it could be less effective to reduce the peak values. In fact, for Kobe accelerogram, RMS A_{III} is reduced by 80% while peak A_{III} is reduced by 50% – 70%. Conversely, for Northridge accelerogram, reductions decrease down to 30% – 35% in terms of both RMS and peak values.

Aiming at an exhaustive evaluation of the proposed isolation system, we now consider the displacement Δ of the isolated mass with respect to the attachment floor. As already stated, this quantity should be limited for the sake of safety and functionality. In the present study, any overcoming of an allowable threshold for Δ can be monitored by means of the maximum shear strain $\gamma_{\max}$ of HDRB. The limit value, having been set as $\gamma_{\max} = 1.00$, was never exceeded during the shaking table tests, as seen in Tab. 4.4.

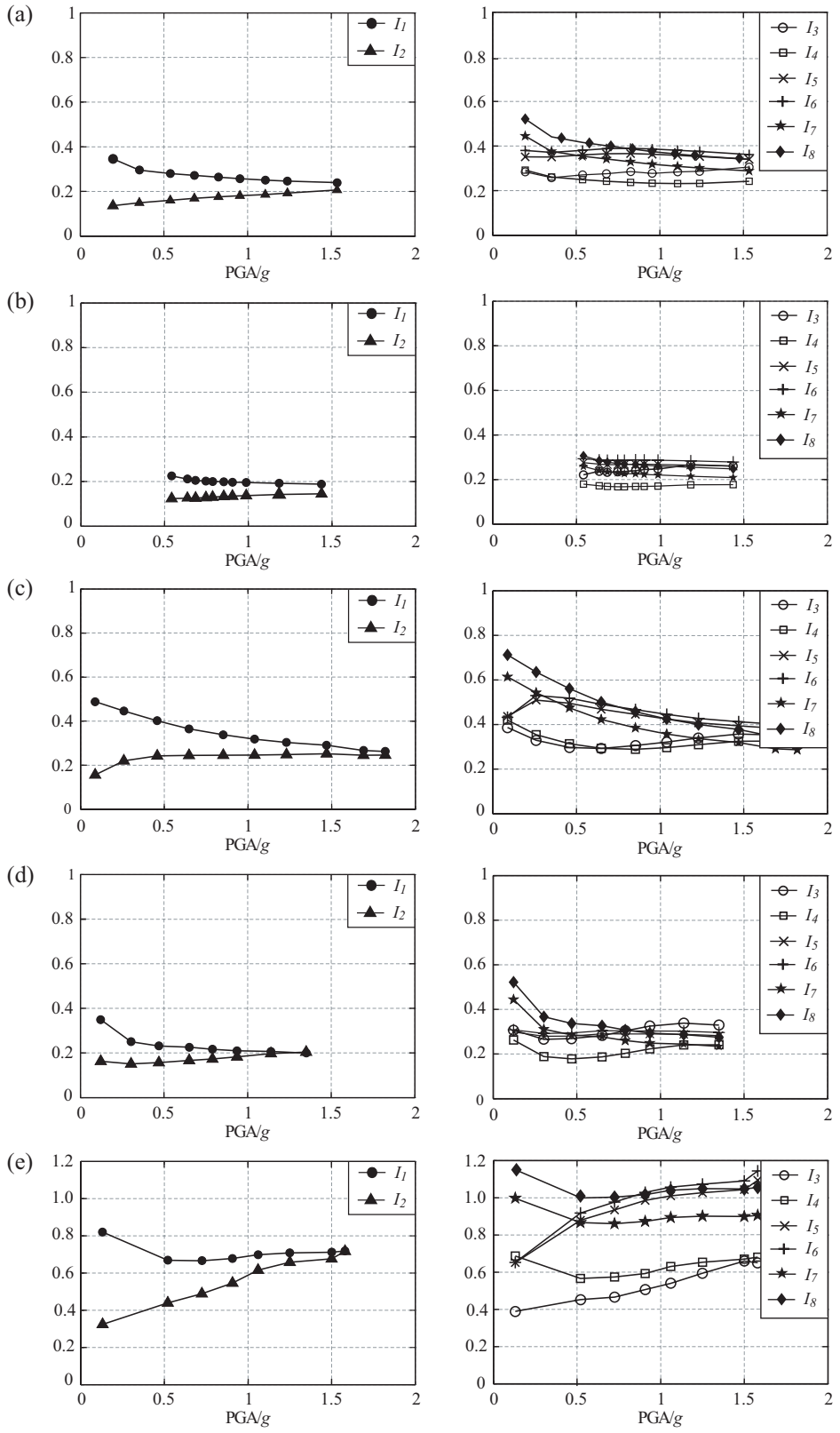

Figure 4.26. Performance indices in terms of RMS responses, I_1 – I_2 for the isolated mass, I_3 – I_8 for the supporting structure. For a given accelerogram, indices are shown *versus* PGA level: (a) Eurocode 8; (b) El Centro; (c) Hachinohe; (d) Kobe; (e) Northridge;

Accelerogram	PGA [g]	γ_{max}	J_1	J_2	J_3	J_4	J_5	J_6	J_7	J_8
EC8	0.20	0.04	0.371	0.161	0.305	0.376	0.423	0.458	0.298	0.384
	0.35	0.11	0.339	0.207	0.286	0.334	0.425	0.464	0.291	0.363
	0.54	0.17	0.328	0.221	0.261	0.306	0.440	0.474	0.278	0.347
	0.68	0.24	0.315	0.230	0.263	0.316	0.432	0.466	0.265	0.334
	0.82	0.32	0.308	0.246	0.268	0.329	0.412	0.445	0.256	0.320
	0.95	0.40	0.302	0.255	0.278	0.344	0.405	0.439	0.260	0.310
	1.11	0.49	0.300	0.265	0.299	0.367	0.402	0.428	0.256	0.303
	1.24	0.59	0.302	0.280	0.304	0.394	0.393	0.419	0.254	0.300
	1.53	0.82	0.297	0.310	0.323	0.437	0.371	0.392	0.252	0.292
El Centro	0.54	0.17	0.274	0.187	0.299	0.260	0.397	0.425	0.258	0.297
	0.64	0.22	0.266	0.188	0.319	0.258	0.387	0.414	0.238	0.280
	0.68	0.25	0.261	0.191	0.318	0.261	0.381	0.403	0.237	0.278
	0.75	0.28	0.261	0.194	0.334	0.249	0.372	0.396	0.236	0.276
	0.79	0.31	0.263	0.199	0.348	0.275	0.366	0.388	0.243	0.281
	0.85	0.35	0.266	0.203	0.362	0.294	0.359	0.383	0.243	0.279
	0.90	0.38	0.265	0.204	0.370	0.311	0.351	0.376	0.238	0.273
	0.99	0.41	0.264	0.208	0.378	0.328	0.349	0.370	0.233	0.267
	1.18	0.52	0.266	0.220	0.393	0.358	0.335	0.357	0.230	0.258
	1.44	0.60	0.261	0.226	0.372	0.365	0.324	0.345	0.225	0.252
Hachinohe	0.09	0.03	0.603	0.241	0.605	0.659	0.702	0.737	0.584	0.669
	0.26	0.12	0.467	0.273	0.416	0.491	0.630	0.653	0.449	0.515
	0.46	0.21	0.438	0.294	0.362	0.471	0.558	0.596	0.373	0.438
	0.65	0.32	0.420	0.315	0.394	0.483	0.511	0.555	0.332	0.406
	0.85	0.44	0.409	0.339	0.462	0.506	0.490	0.525	0.312	0.375
	1.04	0.58	0.399	0.368	0.474	0.615	0.481	0.505	0.313	0.350
	1.23	0.73	0.395	0.391	0.517	0.686	0.480	0.492	0.314	0.347
	1.47	0.88	0.384	0.407	0.540	0.759	0.475	0.485	0.329	0.339
	1.69	0.98	0.346	0.400	0.527	0.722	0.456	0.466	0.307	0.313
	1.82	1.00	0.343	0.386	0.538	0.720	0.454	0.460	0.314	0.314
Kobe	0.12	0.06	0.554	0.311	0.385	0.515	0.555	0.613	0.491	0.584
	0.30	0.19	0.458	0.332	0.431	0.388	0.539	0.575	0.373	0.458
	0.47	0.31	0.393	0.318	0.390	0.312	0.469	0.517	0.319	0.386
	0.65	0.44	0.356	0.318	0.380	0.363	0.452	0.487	0.286	0.343
	0.79	0.56	0.331	0.317	0.414	0.402	0.432	0.460	0.278	0.320
	0.94	0.62	0.310	0.320	0.471	0.428	0.414	0.438	0.267	0.307
	1.14	0.84	0.298	0.330	0.548	0.460	0.392	0.414	0.260	0.296
	1.35	0.92	0.276	0.314	0.498	0.441	0.403	0.410	0.265	0.289
Northridge	0.13	0.04	0.862	0.443	0.535	0.935	0.881	0.810	0.835	0.918
	0.52	0.23	0.649	0.503	0.793	0.683	1.028	1.040	0.708	0.731
	0.72	0.36	0.665	0.567	0.764	0.772	1.050	1.062	0.673	0.741
	0.91	0.51	0.674	0.623	0.775	0.754	1.025	1.041	0.678	0.736
	1.06	0.71	0.679	0.705	0.774	0.835	1.008	1.020	0.683	0.746
	1.25	0.84	0.688	0.709	0.773	0.789	0.996	0.998	0.691	0.731
	1.50	0.98	0.675	0.718	0.874	0.758	0.977	0.975	0.663	0.715
	1.58	1.10	0.671	0.756	0.833	0.791	0.977	0.980	0.642	0.692

Table 4.4. Performance indices in terms of peak responses, J_1 – J_2 for the isolated mass, J_3 – J_8 for the supporting structure. Given the accelerogram, indices are shown *versus* PGA level and the maximum shear strain γ_{max} of HDRB.

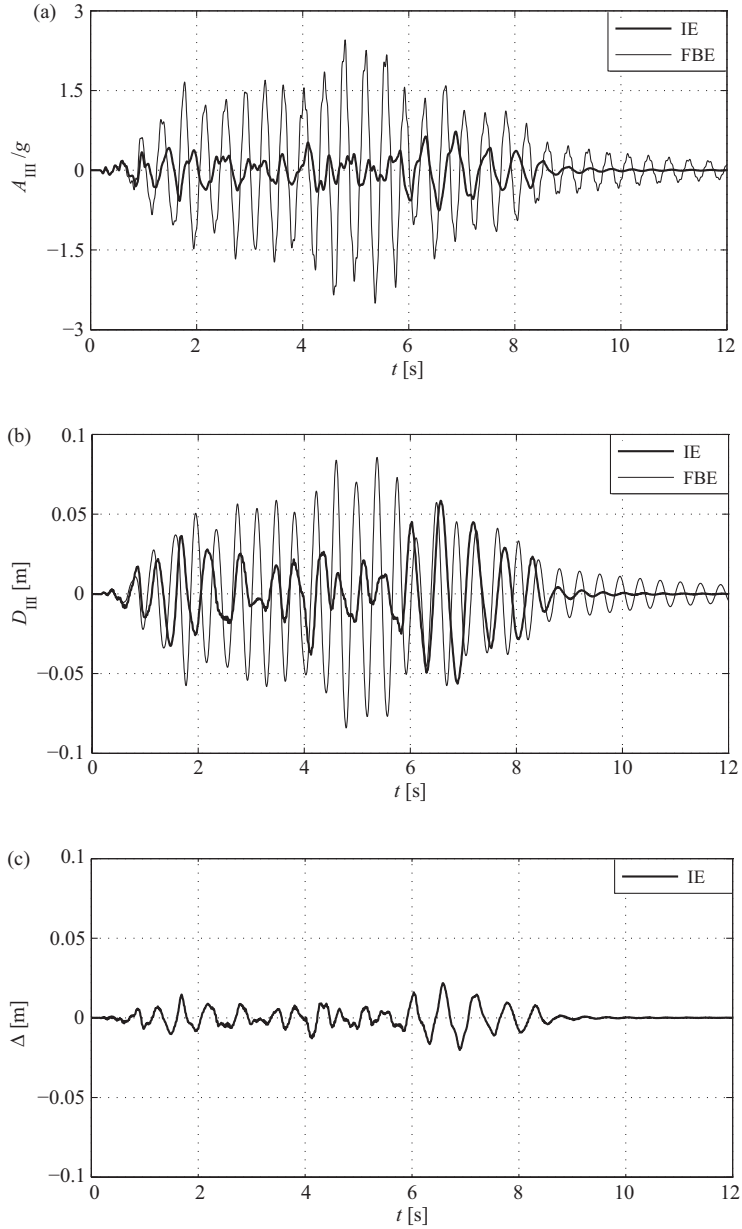

Figure 4.27. Time history responses of the isolated mass due to Eurocode 8 spectrum-compatible accelerogram, time scaling factor $\lambda_T = 0.447$, PGA = 0.95 g: (a) absolute acceleration A_{III}; (b) displacement D_{III} relative to ground; (c) displacement Δ relative to the attachment floor.

Non-dimensional indices I_2 and J_2 are then used to analyze how Δ varies with PGA level. In this regard, only Northridge accelerogram differs from the other seismic input since, as PGA increases, Δ tends to increase rather than to remain constant.

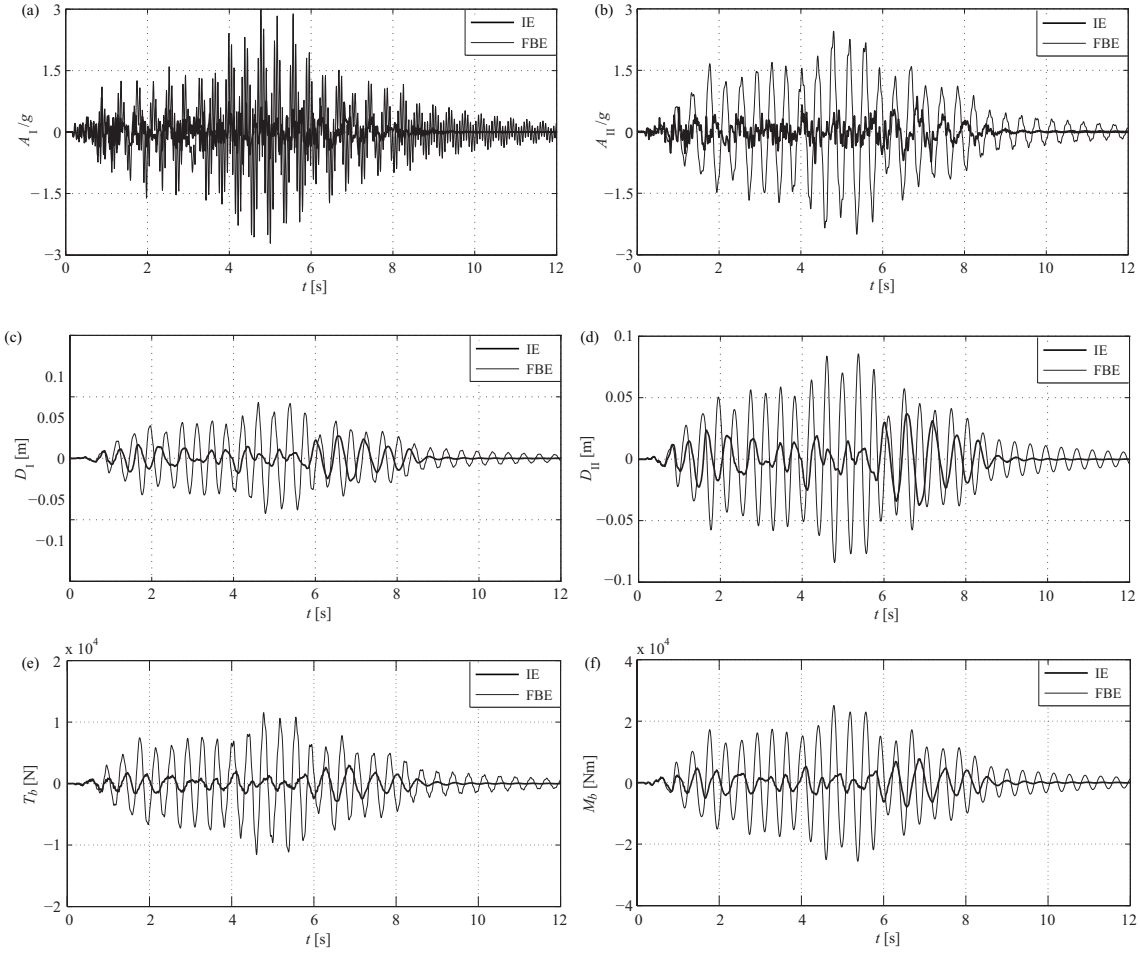

Figure 4.28. Time history responses of the supporting structure due to Eurocode 8 spectrum-compatible accelerogram, time scaling factor $\vartheta_T = 0.447$, PGA = 0.95 g: (a) first floor absolute acceleration A_{I}; (b) second floor absolute acceleration A_{II}; (c) first floor displacement D_{I} relative to ground; (d) second floor displacement D_{II} relative to ground; (e) base shear T_b (f) base bending moment M_b.

Significant observations can also be made from indices I_3 – I_8 and J_3 – J_8, which refer to the dynamic response of the supporting structure. It is worthy to note that reducing the coupling between the mass and the structure advantageously reduces the structural response as well. The greatest reductions are recognized for floor accelerations and amount to 70% – 80% in terms of RMS values and to 50% – 70% in terms of peak values, depending on the seismic input. Floor displacements and actions at the base of the frame (shear and bending moment) are suppressed down by 60% – 70% in terms of both RMS and peak values, indicating considerable reductions of overall internal loads in structural members. Once again, however, previous results do not

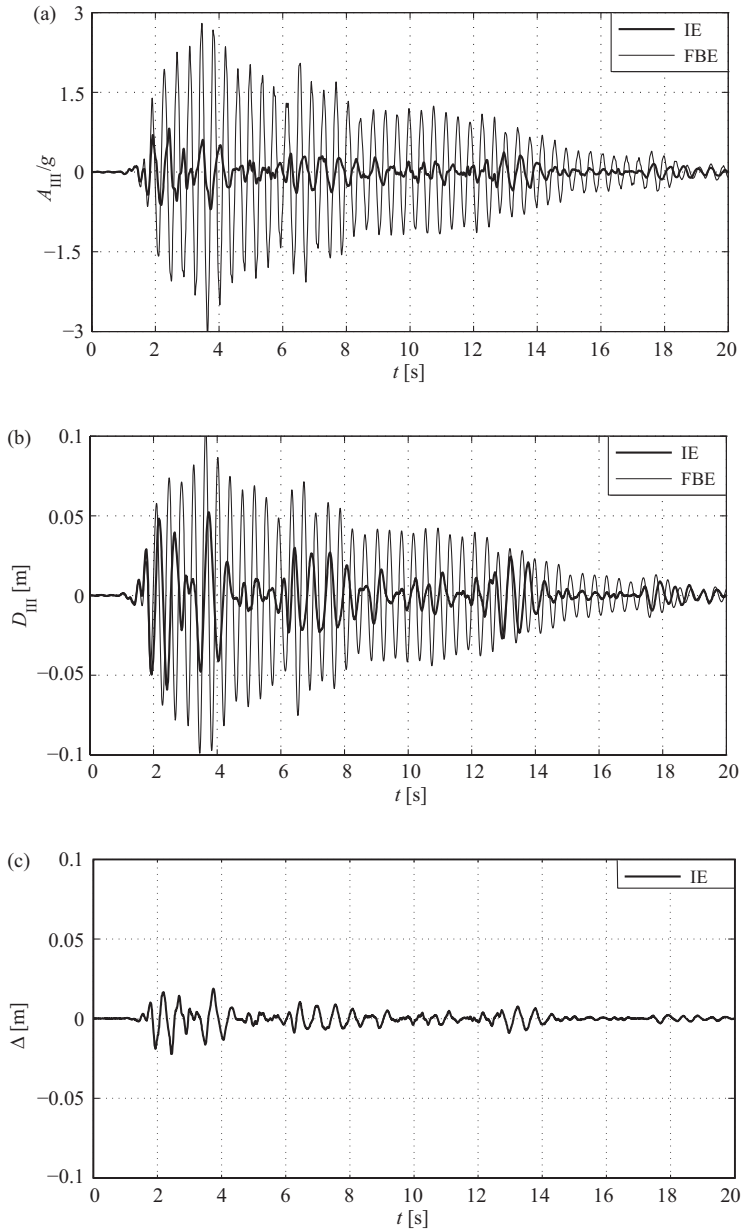

Figure 4.29. Time history responses of the isolated mass due to El Centro accelerogram, time scaling factor $\vartheta_T = 0.447$, PGA = 0.99 g: (a) absolute acceleration $A_{\rm III}$; (b) displacement $S_{\rm III}$ relative to ground; (c) displacement Δ relative to the attachment floor.

apply to Northridge accelerogram: reductions in floor accelerations decrease down to 40% – 50% in terms of RMS values and to 20% – 30% in terms of peak values, whereas floor displacements and base bending moment result to be even amplified compared

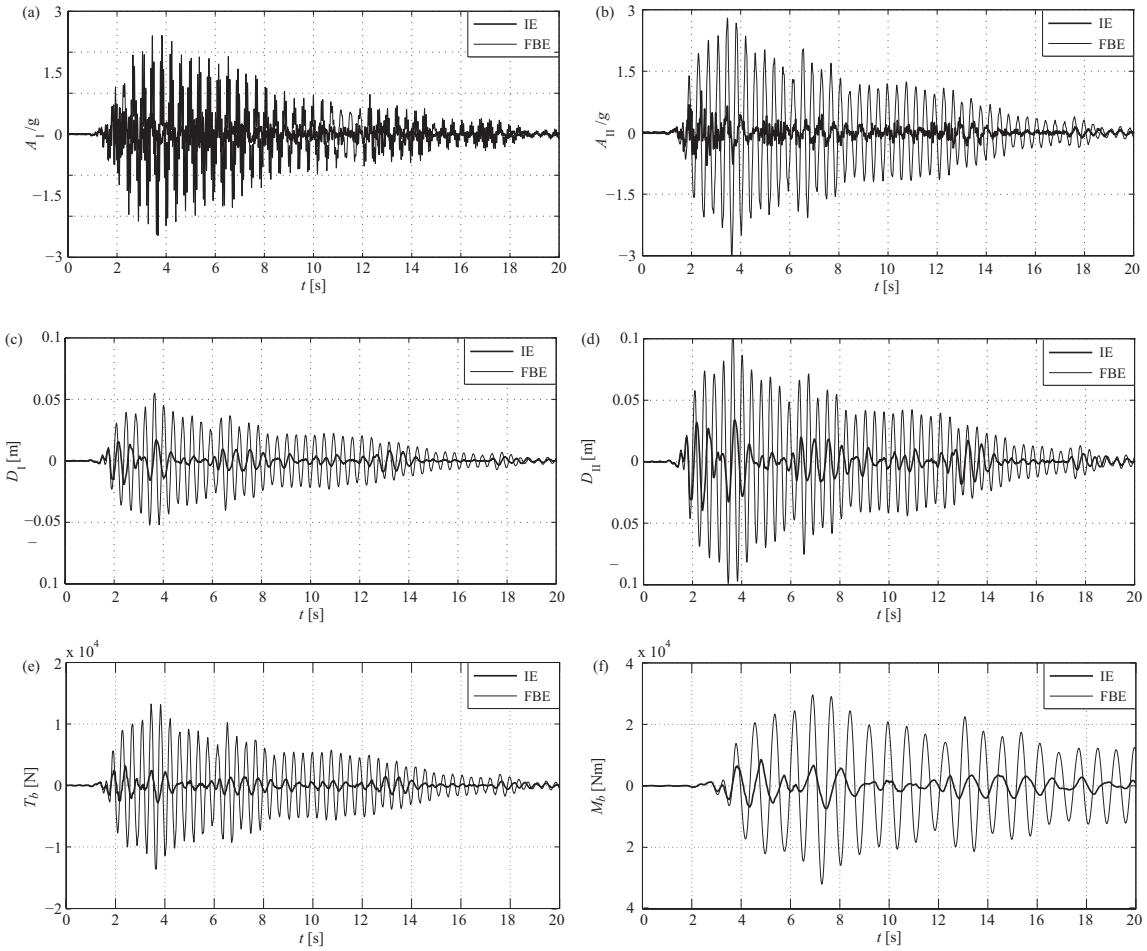

Figure 4.30. Time history responses of the supporting structure due to El Centro accelerogram, time scaling factor $\vartheta_T = 0.447$, PGA = 0.99 g: (a) first floor absolute acceleration $A_{\rm I}$; (b) second floor absolute acceleration $A_{\rm II}$; (c) first floor displacement $D_{\rm I}$ relative to ground; (d) second floor displacement $D_{\rm II}$ relative to ground; (e) base shear T_b (f) base bending moment M_b.

with the (FBE) configuration (I_5, I_6, $I_8 > 1$; J_5, $J_6 > 1$).

A deeper insight of the differences between seismic inputs comes from a careful analysis of time history responses. Figures 4.27 – 4.36 illustrate the time history responses of the isolated mass and the supporting structure in (FBE) and (IE) configurations under selected input accelerograms, which share approximately the same PGA level ($\cong 1.00\ g$). As it can be seen, the proposed equipment isolation system is effective to suppress down the responses since the beginning of the excitations, in the presence of both far-field and near-fault ground motions, distinctive features can be recognized for Northridge accelerogram.

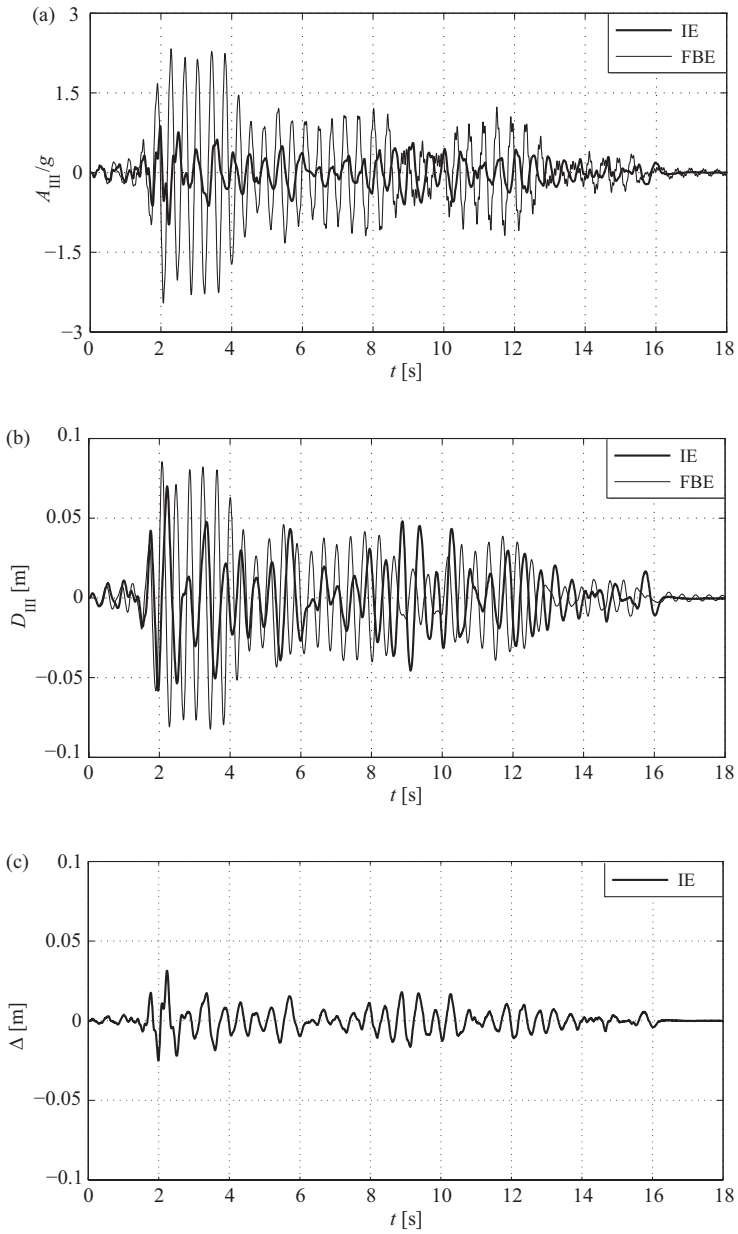

Figure 4.31. Time history responses of the isolated mass due to Hachinohe accelerogram, time scaling factor $\vartheta_T = 0.447$, PGA $= 1.04\ g$: (a) absolute acceleration A_{III}; (b) displacement S_{III} relative to ground; (c) displacement Δ relative to the attachment floor.

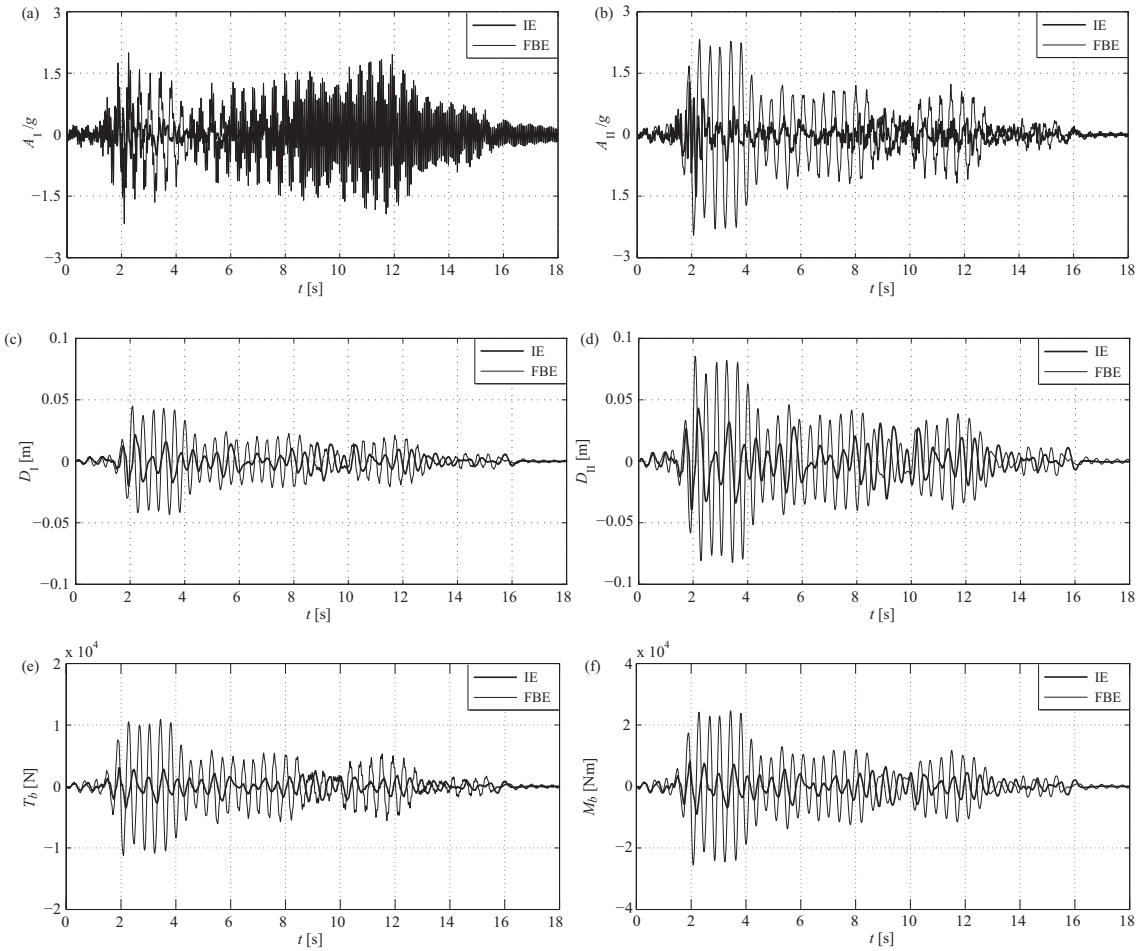

Figure 4.32. Time history responses of the supporting structure due to Hachinohe accelerogram, time scaling factor $\vartheta_T = 0.447$, PGA = 1.04 g: (a) first floor absolute acceleration A_{I}; (b) second floor absolute acceleration A_{II}; (c) first floor displacement D_{I} relative to ground; (d) second floor displacement D_{II} relative to ground; (e) base shear T_b (f) base bending moment M_b.

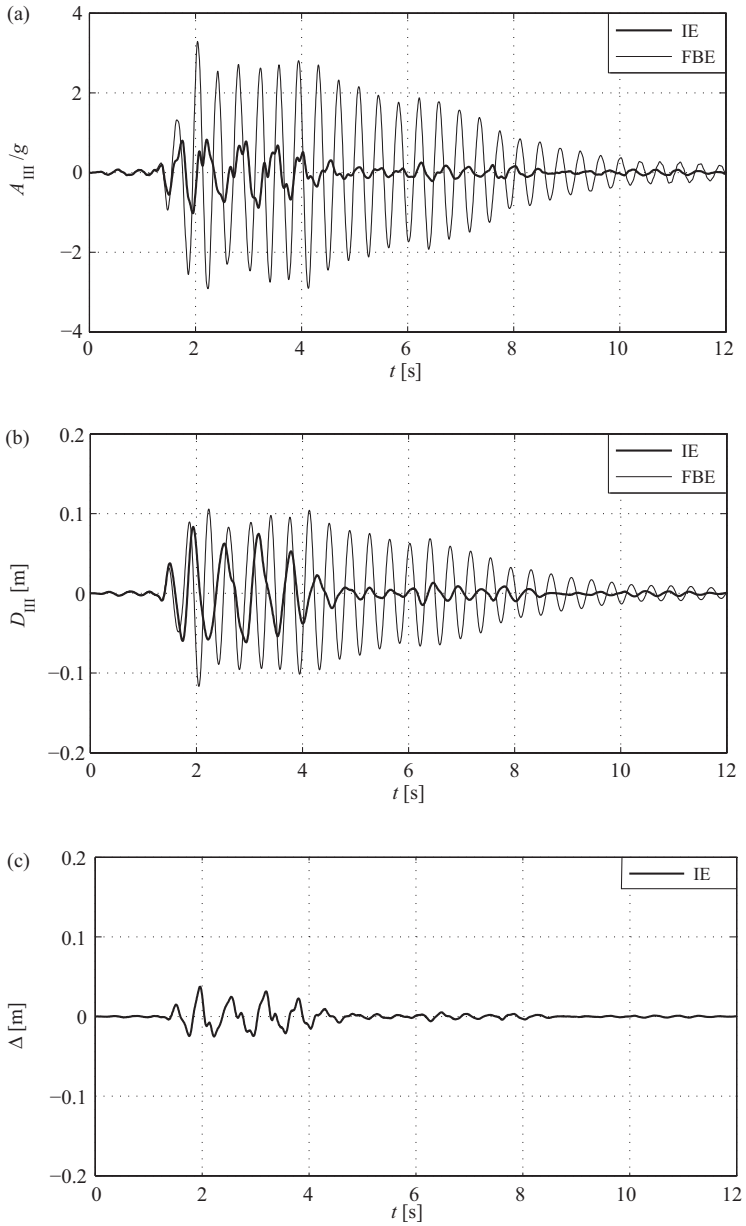

Figure 4.33. Time history responses of the isolated mass due to Kobe accelerogram, time scaling factor $\vartheta_T = 0.447$, PGA $= 0.94\ g$: (a) absolute acceleration A_{III}; (b) displacement S_{III} relative to ground; (c) displacement Δ relative to the attachment floor of the supporting structure.

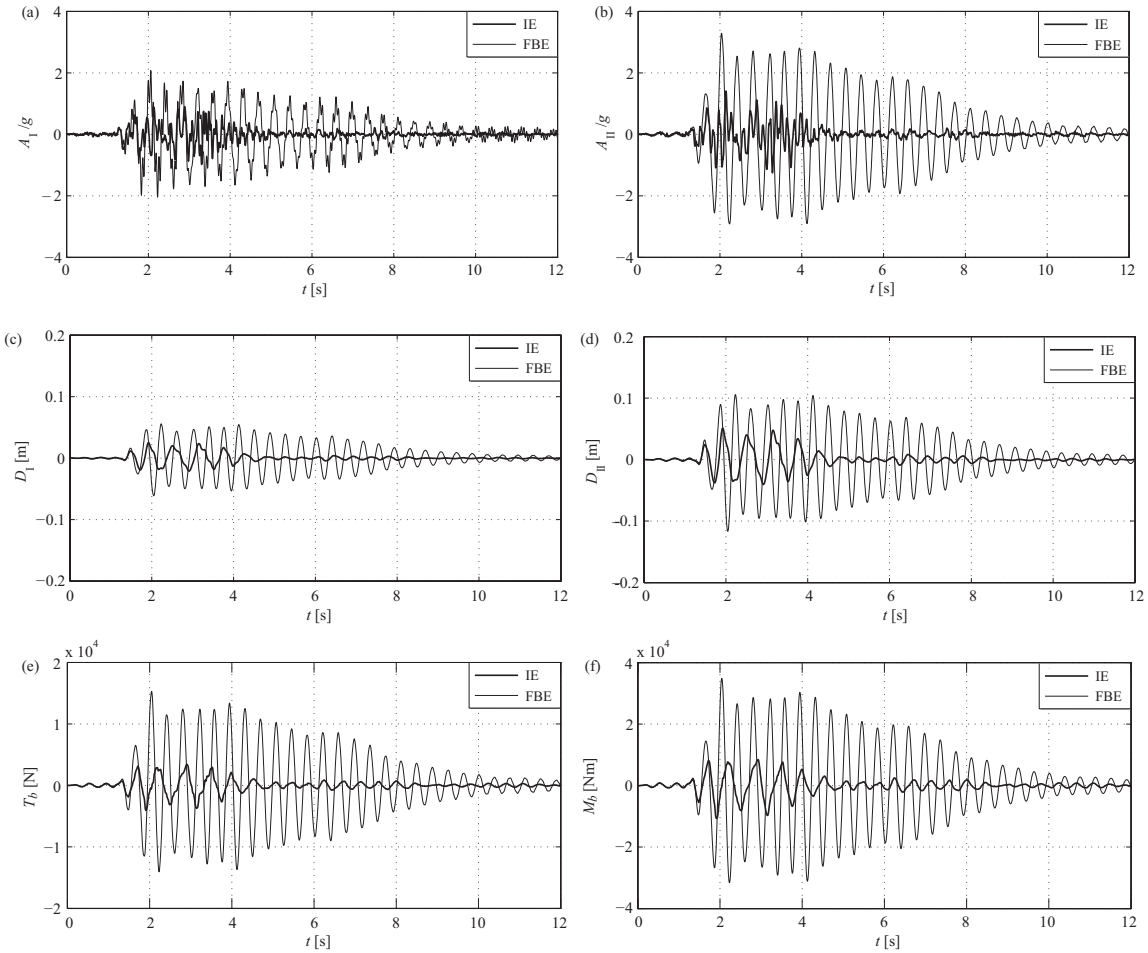

Figure 4.34. Time history responses of the supporting structure due to Kobe accelerogram, time scaling factor $\vartheta_T = 0.447$, PGA = 0.94 g: (a) first floor absolute acceleration A_{I}; (b) second floor absolute acceleration A_{II}; (c) first floor displacement D_{I} relative to ground; (d) second floor displacement D_{II} relative to ground; (e) base shear T_b (f) base bending moment M_b.

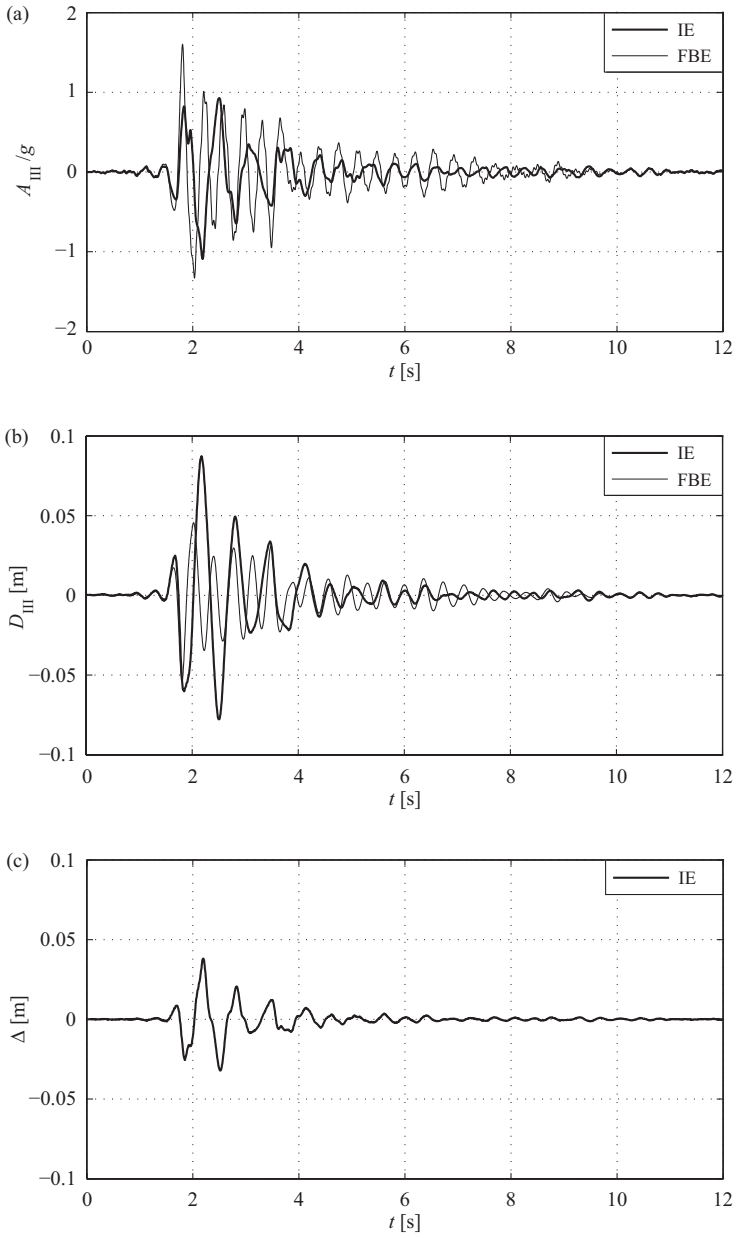

Figure 4.35. Time history responses of the isolated mass due to Northridge accelerogram, time scaling factor $\lambda_T = 0.447$, PGA $= 1.06\ g$: (a) absolute acceleration A_{III}; (b) displacement D_{III} relative to ground; (c) displacement Δ relative to the attachment floor of the supporting structure.

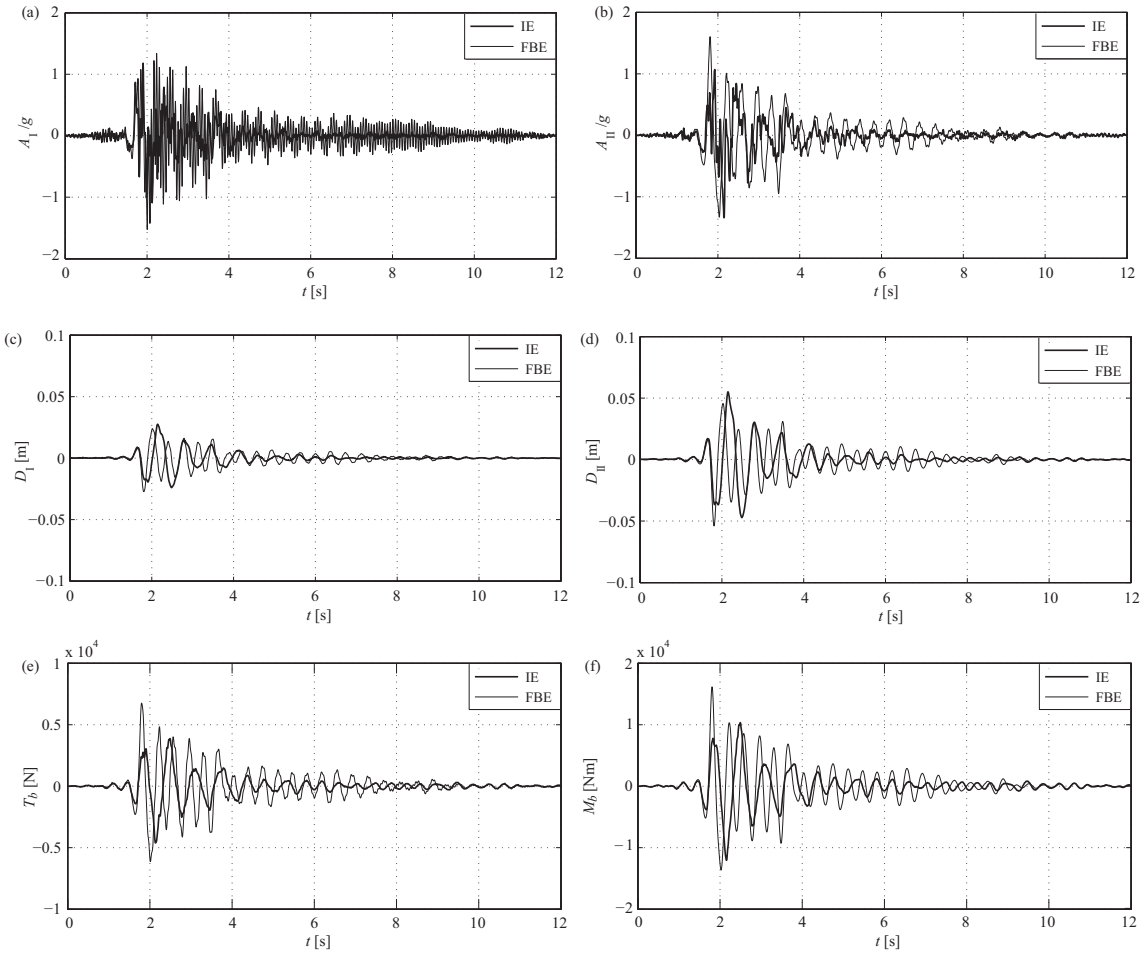

Figure 4.36. Time history responses of the supporting structure due to Northridge accelerogram, time scaling factor $\lambda_T = 0.447$, PGA = 1.50 g: (a) first floor absolute acceleration A_{I}; (b) second floor absolute acceleration A_{II}; (c) first floor displacement D_{I} relative to ground; (d) second floor displacement D_{II} relative to ground; (e) base shear T_b (f) base bending moment M_b.

Chapter 5

Nonlinear hysteretic isolation: constitutive modelling

In this chapter[1], an innovative isolation system with nonlinear hysteretic behaviour is proposed and studied. Referred to as *High Damping Rolling Pendulum* (HDRP) isolators, this novel class is suited to the seismic protection of equipment under horizontal motion by virtue of its attractive mechanical properties, summarized as follows: the decoupling between an elastic restoring force, to provide a re-centering mechanism, and a hysteretic restoring force, to provide rate-independent damping; a nonlinear geometric stiffness suitable to achieve multiple performance objectives throughout the course of motion; a high energy dissipation capability to limit the horizontal displacements induced by severe earthquake. The study first addresses the problem of formulating a constitutive relationship for the isolation system and an integrable hysteresis model, derived from the mathematical Duhem operator, is adopted owing to its versatility and analytical tractability.

[1]Some of the results in this chapter have been published in the following papers:

♢ Reggio, A., De Angelis, M. Optimal design of an equipment isolation system with nonlinear hysteretic behaviour. *Earthquake Engineering and Structural Dynamics*, 42 (13), 1907-1930, 2013.

♢ Reggio, A., De Angelis, M. A passive isolation system with nonlinear hysteretic behaviour: modelling and numerical investigations. *Proceedings of the XX Congresso AIMETA Associazione Italiana di Meccanica Teorica e Applicata*, Bologna, Italy, September 12-15, 2011.

5.1 Characteristics of nonlinear isolation

According to the linear theory of vibration isolation [25, 109], a passive linear isolator attenuates transmitted vibrations above an excitation frequency Ω that exceeds the value $\sqrt{2}\,\omega_0$, where ω_0 is the undamped natural frequency of the isolator. The damping, which is beneficial in reducing the resonance peak, tends instead to increase transmitted vibrations for $\Omega > \sqrt{2}\,\omega_0$. The effectiveness of an isolator can then be improved by lowering its natural frequency: the lower the isolator stiffness and hence the natural frequency, the wider the frequency range of isolation. In addition, lowering the damping ratio may be an advantage too. However, a smaller stiffness results in a larger static displacement and this trade-off between isolation and static displacement is a well-known problem, in particular when isolating vertical motions [10]. Furthermore, the isolator spectrum contains dangerous low-frequency components that may lead to resonant-like behaviour when the system is subjected to severe environmental disturbances such as shocks, impact loads and near-fault ground motions [68]. To overcome these limits, a growing interest in the study of nonlinear isolation has arisen. A comprehensive assessment of the recent developments in this field has been provided by Ibrahim [58].

The effects of nonlinearity on the isolator performance are various depending on the type of nonlinearity (in stiffness or in damping) and the type of excitation (force or base excitation) [1, 87].

In general, an isolator with softening stiffness characteristics is found to be superior to one with hardening stiffness characteristics: soft nonlinearity causes a reduction in the resonance frequency and the isolation may be improved, whereas hard nonlinearity, shifting the resonance frequency on the right of the linear value, increases transmitted vibrations towards high frequencies [104]. Recently, researchers have developed nonlinear isolators made from elements with positive stiffness in parallel with elements with negative stiffness. By choosing appropriate geometry and pre-stress for negative-stiffness elements, much of the positive stiffness at the static equilibrium position can be cancelled and a so-called *quasi-zero-stiffness* isolator is realized. This mechanism aims to obtain, on the one hand, a high static stiffness and hence small static displacements, on the other hand, a low dynamic stiffness and hence a wide frequency range of vibration isolation [9].

Under harmonic excitations, nonlinear isolators may experience irregular dynamic behaviours like jump phenomena, period-doubling bifurcations and non-periodic (chaotic) motion [114]. In the case of nonlinear visco-elastic isolators, however, it was proved that the jump width, or the unstable zone, reduces and may even be entirely eliminated by increasing the isolator damping coefficient [104]. Likewise, numerical studies revealed that the suitable choice of a large damping coefficient can completely suppress the transitions from a periodic harmonic solution to period-doubling bifurcations and

to chaotic response [76].

A number of nonlinear systems have been proposed and developed for the base isolation of structures from earthquake ground motions [58]. Basically, they can be classified into two main categories:

i. laminated-rubber bearing isolators, with and without lead core;

ii. frictional-type, sliding or rolling, isolators.

The first category, which has already found several practical implementations, shows a strongly nonlinear behaviour, combining both hysteresis and rate-dependence, during the large deformation range and a nonlinear modelling is required in such cases. An equivalent linear visco-elastic model, however, is considered as accurate in usual applications, as earlier stated in Sec. 4.1.

The second category is still in the stage of development, but it is finding more and more applications in recent years. Because the stick and the slip phases take place alternately depending on the magnitude of the shear forces on the sliding surfaces, the dynamic behaviour of friction-base isolators is highly nonlinear. Excellent isolation performance is achieved in conventional sliding systems if the friction coefficient is small, due to the reduction in the transmitted acceleration. Conversely, if the friction coefficient is large, the structure is isolated only during large earthquakes and the sliding system is not activated by small to moderate earthquakes.

Fenz and Constantinou [44, 45] have recently developed novel multi-spherical sliding bearings with adaptive stiffness and adaptive damping. These bearings are fully passive devices consisting of multiple spherical sliding surfaces, whose radii and friction coefficients are designed to be different. As a result, the bearings exhibit a nonlinear force-displacement relationship that is said *adaptive* since stiffness and effective friction change to predictable values at controllable displacement amplitudes, determined *a priori* by the design engineer. The design idea is to exploit the adaptive behaviour, *i.e.* several sliding regimes throughout the course of motion, to separately optimize the isolation system for multiple levels of input and multiple performance objectives.

The passive adaptive behaviour permits also the isolation system to withstand a wider range of earthquakes with different characteristics. Notably, recent studies have shown the favorable response of passive adaptive isolation systems over the linear ones to alleviate the excessive displacement problem caused by near-fault earthquakes with strong long-period components [86].

5.2 High Damping Rolling Pendulum (HDRP) isolators

A novel class of bearings with nonlinear hysteretic behaviour, referred to as *High Damping Rolling Pendulum* (HDRP) isolators, is here proposed for the seismic protection of equipment under horizontal motion. Characteristic of the new isolators is to be of a rolling-based type and to incorporate hysteretic elements to provide damping. As an example, a bearing that could be ascribed to the class is the one developed at ENEA (Italian National Agency for New Technologies, Energy and the Environment), "Casaccia" Research Center, under the the name of "Earlyprot" (Italian Patent no. ITRM2006A000141 [29]).

More in general, the study presented herein is addressed to exploit, rather than a specific implementation, the mechanical properties distinctive of the new class, which can be summarized as follows:

- the decoupling between an elastic restoring force, to provide a re-centering mechanism, and a hysteretic restoring force, to provide rate-independent damping;
- a nonlinear geometric stiffness suitable to achieve multiple performance objectives throughout the course of motion;
- a high energy dissipation capability to limit the horizontal displacements induced by severe earthquake.

5.2.1 Technical features of Earlyprot Isolator ©ENEA

A prototype of the Earlyprot isolator is illustrated in Figs. 5.1, 5.2 and 5.3. The isolation bearing consists of an internal rolling pendulum assembly placed between two facing square steel plates (Fig. 5.2 (b)). The rolling body is represented by a Ball Transfer Unit (BTU) fixed to the upper plate (Fig. 5.2 (c)). The BTU has a solid steel housing incorporating a hardened ball cup and an internal raceway made of small supporting balls. The height of the BTU is 103 mm and the diameter of the load ball is 76 mm. The latter is designed to ensure precise rolling and a full load-bearing capability of 20000 N. The BTU is to roll against a concave surface inserted in the lower plate (Fig. 5.2 (d)). The rolling surface is made of hardened steel with a diameter of 400 mm and a radius of curvature of 2000 mm. The rolling friction coefficient between the load ball and the concave surface is estimated in the order of 10^{-3} depending on load and speed.

Arc elements of steel wire rope are arranged around the rolling pendulum assembly in number of seven along each side (Fig. 5.3 (a)), fastened to the upper and lower plates by means of clamps (Fig. 5.3 (b)). The steel wire rope is referred to under the denomination "6x19 + IWRC 7x7" and has an ordinary right hand lay and a diameter of 13 mm (Fig. 5.3 (c)). The rope construction consists of 6 outer strands, each made of 19 wires, and an internal Independent Wire Rope Core composed by 7 strands, each made of 7 wires (Fig. 5.3 (d)). The length of the rope elements is only chosen to allow for ± 200 mm as the maximum rolling displacement.

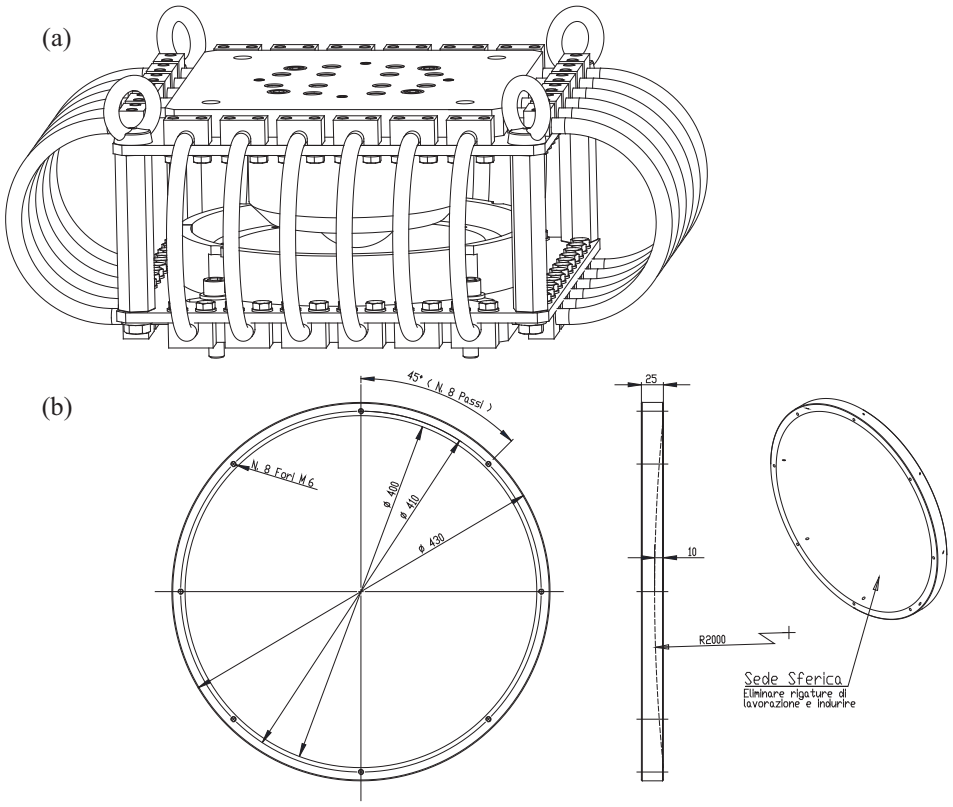

Figure 5.1. "Earlyprot" isolator ©ENEA, Patent no.ITRM2006A000141 (Italy). Technical drawings: (a) axonometric projection of the isolator; (b) plan and lateral views of the concave rolling surface.

5.2.2 Mechanical properties of rolling pendulum

The use of rolling-based isolators is proved to achieve outstanding isolation performance. The rolling mechanism offers the minimum possible degree of coupling between the isolated object and its base since a far lower friction coefficient is present if compared to the sliding mechanism. As a consequence, rolling approaches the most the ideal isolation concept which requires a total horizontal object-base separation [65].

Flat rolling bearings are the simplest form of rolling-based isolators, though significant drawbacks limit their real technical feasibility: they lack effective re-centering mechanism and buffer and cannot rely on actual damping sources [81, 80, 67]. These drawbacks have been attempted to be overcome by way of: elastic self-center devices, like rubber springs [49]; gravity-based re-centering mechanisms, like elliptical rolling rods [69] or spherical bodies rolling against concave plates in a rolling-pendulum system [156]; additional elements, like metallic yield dampers [65], integrated into the isolation system to provide supplemental damping; a nonlinear geometrical stiffness, like due to eccentric rolling isolators [17], in order to increase the isolation period and limit the displacements.

In continuity with the previous literature, Earlyprot isolator combines a rolling pendulum configuration with integrated steel wire rope elements: the former guarantees the re-centering, the latter provide nonlinear stiffness and supplemental damping.

(a) (b)

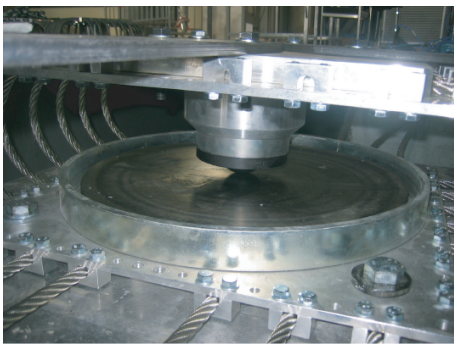

(c) (d)

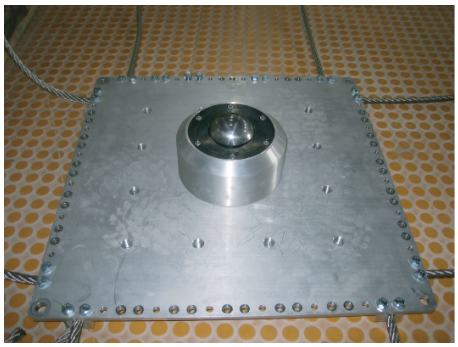

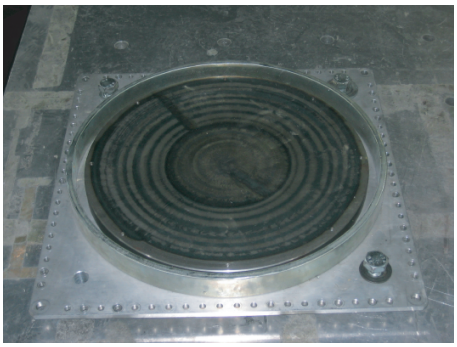

Figure 5.2. "Earlyprot" isolator ©ENEA, Patent no.ITRM2006A000141 (Italy). Layout (1): (a) view of the complete device; (b) detail of the ball transfer unit on the concave rolling surface; (c) ball transfer unit; (d) concave rolling surface.

(a) (b)

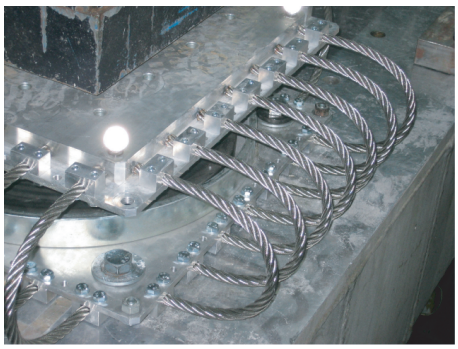

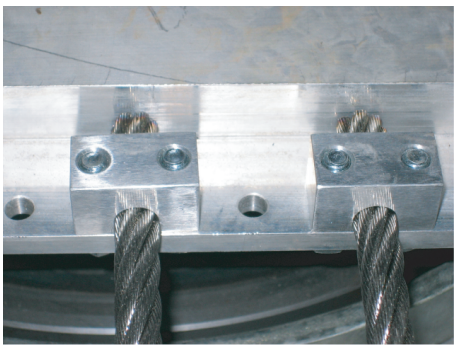

(c) (d)

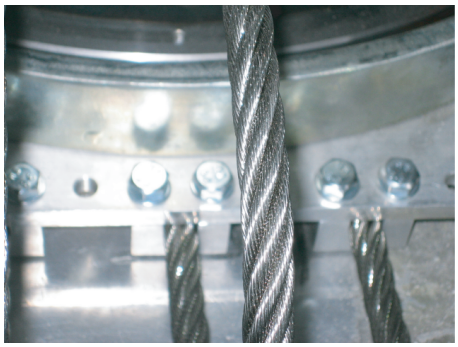

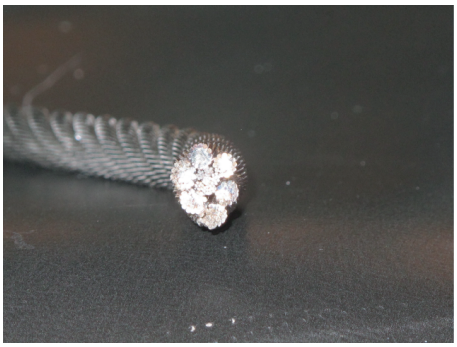

Figure 5.3. "Earlyprot" isolator ©ENEA, Patent no.ITRM2006A000141 (Italy). Layout (2): (a) view of the steel wire ropes on one side of the isolator; (b) detail of the clamps attaching the wire ropes to the rolling pendulum; (c) detail of the wire rope construction: right-hand ordinary lay; (d) detail of the wire rope cross-section.

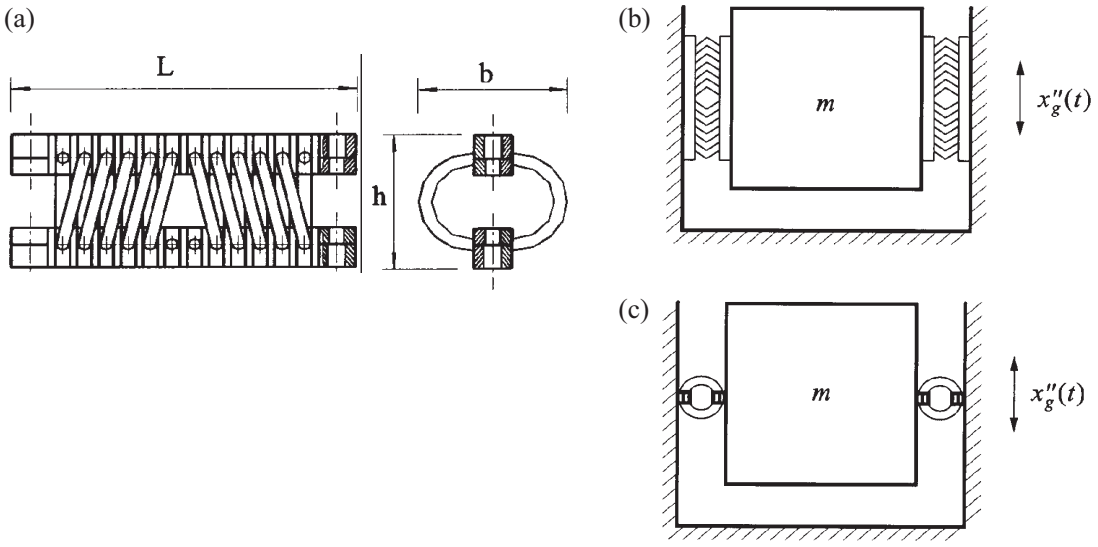

Figure 5.4. Helical wire rope isolator. (a) Schematic diagram. (b) Shear deformation mode. (c) Roll deformation mode. After Ni *et al.* [96].

5.2.3 Mechanical properties of steel wire ropes

According to the patent of Earlyprot isolator and the purpose of its inventor, wire rope elements are integrated into the device only as buffer elements for the sake of a fail-safe mechanism. Nevertheless, in the opinion of the author writing, their role in terms of stiffness and damping contribution is significant and cannot be neglected in a correct design methodology of the isolator.

In this regard, a mechanical analogy could be established between the behaviour of the wire rope arc elements integrated into the Earlyprot isolator and the widely used helical wire-rope vibration isolators (Fig. 5.4 (a)). In particular, the behaviour of the arc elements orthogonal to the motion direction can be correlated with the shear deformation mode wire-rope isolators, whereas the behaviour of the arc elements parallel to the motion direction can be correlated with the roll deformation mode of wire-rope isolators (Fig. 5.4 (b)). As for the wire-rope isolators, then, specific dynamic characteristic are to be set by the selection of the diameter of the wire rope, the number of strands, the cable length and the cable twist or lay [96, 97].

In view of the preceding analogy, wire rope arc elements in the Earlyprot isolators are expected to exhibit a significant nonlinear hysteretic behaviour. From the damping viewpoint, inherent rubbing and sliding friction between the wire rope strands provides rate independent hysteretic damping and could allow a good energy dissipation performance. From the stiffness viewpoint, wire rope elements are characterized by softening stiffness at small displacements. At large displacements, geometric effects due to tension deformation of the rope make the stiffness gradually increase and change into a hardening one.

5.3 Development of the constitutive model

The HDRP isolator has physical and geometrical nonlinearities. Physical nonlinearities are due to the presence of friction forces in both the rolling pendulum, to a smaller extent, and the steel wire ropes, to a larger extent. The rolling friction and, even more, the inherent rubbing friction between individual wire rope strands act as a source of hysteretic damping. Geometrical nonlinearities deal with the tension deformation of wire ropes, which show a hardening lateral stiffness at large displacements.

In view of the preceding considerations, an analytical model with nonlinear hysteretic characteristics is developed to represent the constitutive behaviour of the HDRP isolator. A phenomenological model is derived that describes from a macroscopic point of view the restoring force *versus* displacement relationship of the isolator.

5.3.1 Hysteresis

The term *hysteresis* etymologically originates from the ancient Greek word ὑστέρεσυς which means *to lag behind*. It seems it was first used at the end of the nineteenth century to indicate a delayed magnetization of ferromagnetic materials.

Nowadays, hysteresis is generally defined as a *rate independent memory effect* [146]. To explain this concept, let us consider Fig. 5.5. Two scalar variables, $u(t)$ and $w(t)$, which depend continuously on time t, are illustrated: $u(t)$ is the independent, or *input*, variable, while $w(t)$ is the dependent, or *output*, variable of a hysteretic system. If $u(t)$ increases from u_1 to u_2, the couple $(u(t), w(t))$ moves along the curve ABC; conversely, if $u(t)$ decreases from u_2 to u_1, then (u, w) moves along the curve CDA. Moreover, if $u(t)$ inverts its movement when $u_1 < u(t) < u_2$, then $(u(t), w(t))$ moves into the interior of the region bounded by the major loop $ABCDA$. Note that, whenever $u_1 < u(t) < u_2$, $w(t)$ is not determined only by the value of $u(t)$ at the same instant;

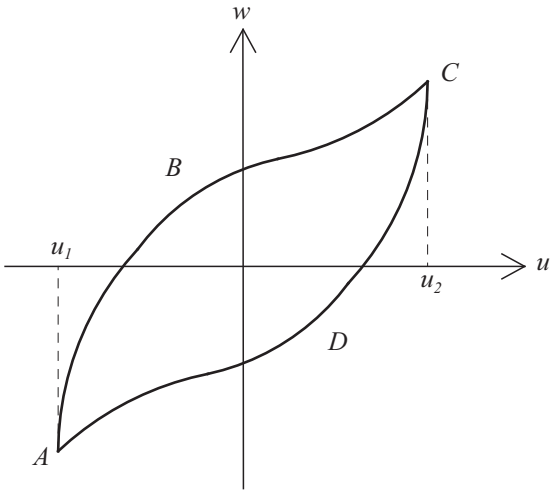

Figure 5.5. Continuous hysteresis loop.

indeed $w(t)$ depends on the previous evolution of $u(t)$ and possibly on the initial state of the system. Due to this *memory* or *hereditary* effect, the output variable appears as a multi-valued function of the input variable. In addition, the path of $(u(t), w(t))$ is required to be invariant with respect to any increasing time homeomorphism, i.e. at any instant t, $w(t)$ depends just on the range of restriction $u : [0, t] \to \mathbf{R}$ and on the order in which values have been attained. Hence, there is no dependence on the input velocity and this property, named *rate independence*, is considered as the main feature of hysteresis since it excludes any viscous-type memory effect. This property is evidenced also by the graphic representation of hysteresis in the input-output plane, where the multi-valued function is described, for a continuous input signal, by a closed loop named *hysteresis loop*. Unlike the input-output loop shown by viscous systems, the hysteresis loop does not depend on the input frequency and it is non-vanishing at asymptotically low frequency.

Hysteresis phenomena occur in several fields of physics and engineering such as ferromagnetism, ferroelectricity, superconductivity and phase transitions. In mechanics, hysteresis deals with nonlinear systems whose output, represented by a force or stress, depends in a rate independent way on the history of input, represented by a displacement or strain. Moreover, this kind of behaviour leads to energy dissipation, as in friction and plasticity. Thanks to the inherent damping characteristics, hysteresis is more and more often incorporated in supplemental damping and isolation devices like metallic and friction dampers, magneto-rheological dampers, wire rope isolators [94], subject, in recent years, of a great deal of theoretical and experimental investigations. A deep focus on hysteresis in mechanical systems, with emphasis on the modelling on a macroscopic scale and the analysis of the dynamic response, can be found in the special volume edited by Vestroni and Noori [140].

From a mathematical point of view, the concept of *hysteresis operator* provides a functional framework for hysteresis relations [146]. Given the input $u(t)$ and output $w(t)$ variables, both function of time t, a hysteresis operator is a functional $\mathcal{F}$ characterized by two properties:

i. memory: at any t, $w(t)$ depends not only on $u(t)$, but also on the previous evolution of u in the interval $[0, t]$ and possibly on the initial state of the system $w(0) = w_0$, that is

$$w(t) = \Big[\mathcal{F}\big(u|_{[0,\,t]},\, w_0\big)\Big](t) \qquad \forall\, t \in [0,\, T] \tag{5.1}$$

ii. rate independence: $w(t)$ is invariant with respect to changes of the time scale. So we have:

$$\begin{aligned} &\forall\ (u, w_0) \in \mathrm{Dom}(\mathcal{F}), \quad \forall\, t \in [0,\, T] \\ &\text{if } s : [0,\, T] \longrightarrow [0,\, T] \text{ is an increasing homeomorphism} \\ &\text{then } \Big[\mathcal{F}\big(u \circ s,\, w_0\big)\Big](t) = \Big[\mathcal{F}\big(u,\, w_0\big)\Big](s(t)) \end{aligned} \tag{5.2}$$

An alternative formulation of the hysteresis operator is provided when the state of the system is not completely characterized by the couple $(u(t),\, w(t))$, but also by one or more variables $\xi(t)$, named *inner variables* since they may not be accessible to direct observation. In this case, hysteresis operator $\mathcal{F}$ acts as follows: first, the value of the inner variable $\xi(t)$ is evaluated, in dependence of the input $u|_{[0,\,t]}$ and the initial value $\xi(0) = \xi_0$; then, $\xi(t)$ is transformed into the output variable $w(t)$. Hence,

$$\begin{aligned} &w(t) = \Big[\mathcal{F}\big(u|_{[0,\,t]},\, \xi_0\big)\Big](t) \\ &\text{is equivalent to} \\ &\xi(t) = \Big[\Phi\big(u|_{[0,\,t]},\, \xi_0\big)\Big](t) \quad \text{and} \quad w(t) = \mathcal{T}(\xi(t)) \end{aligned} \tag{5.3}$$

where Φ is the hysteresis operator and $\mathcal{T}$ is a transform without memory.

In past decades, several analytical models have been presented to describe hysteretic processes. Among the ones commonly used in mechanics, it is worth mentioning: the Play model (rigid plasticity with kinematic strain-hardening), the Stop model (elasto-plasticity without strain-hardening) and the standard Duhem operator as examples of the formulation (5.1), where inner variables are missing; the Prandtl-Ishlinskiĭ (elasto-plasticity with kinematic strain-hardening) and the Preisach operators as examples of the formulation (5.3), where inner variables are present. Although hysteresis is often the macroscopic effect of complex phenomena occurring at a microscopic scale, the models adopted in mechanics are more usually defined at the scale of the system on a phenomenological base [140].

5.3.2 Duhem hysteresis operator

In its standard form, the Duhem hysteresis operator [28] establishes a mapping $\mathcal{F} : (u,\, w) \to w$ that solves a Cauchy problem of the form [146]:

$$\dot{w}(t) = g_1\big(u(t),\, w(t)\big)\, \dot{u}(t)^+ - g_2\big(u(t),\, w(t)\big)\, \dot{u}(t)^- \qquad \text{in } (0,\, T) \tag{5.4a}$$

$$w(0) = w_0 \tag{5.4b}$$

where the over-dot denotes the time derivative, g_1 and g_2 are continuous functions in the $(u,\, w)$ plane and

$$\dot{u}(t)^+ = \frac{1}{2}\Big(|\dot{u}(t)| + \dot{u}(t)\Big) \tag{5.5a}$$

$$\dot{u}(t)^- = \frac{1}{2}\Big(|\dot{u}(t)| - \dot{u}(t)\Big) \tag{5.5b}$$

By setting

$$g\big(u,\, w,\, \mathrm{sign}(\dot{u})\big) = \begin{cases} g(u,\, w,\, 1) := g_1(u,\, w) & \dot{u} \geq 0 \\ g(u,\, w,\, -1) := g_2(u,\, w) & \dot{u} < 0 \end{cases} \tag{5.6}$$

Eq. (5.4b) can be rewritten in the compact form

$$\dot{w}(t) = g\big(u(t),\, w(t),\, \mathrm{sign}(\dot{u}(t))\big) \tag{5.7}$$

It is worth noting that the output $w(t)$ governed by Eq. (5.7) is not directly dependent on the entire history of $u(t)$ through $[0,\, t]$; instead it depends only on the local history since the last change of $\mathrm{sign}(\dot{u})$ and on the value of the output at this switching instant (*local memory*) [95]. Although the standard Duhem operator represents hysteresis with local memory, it can be generalized by replacing the describing functions g_1, g_2 by operators with memory in order to model hysteresis systems with inner variables too.

Among the several differential models of hysteresis that can be reduced to the Duhem operator, in its standard or its generalized form, it must be mentioned the Bouc-Wen model [5, 6], the Dahl's friction model and the Coleman-Hodgdon ferromagnetic hysteresis model [146].

5.3.3 Integrable Duhem hysteresis model

By eliminating the time dependence, Eq. (5.4b) can be rewritten in incremental form:

$$\mathrm{d}w = g_1(u,\, w)\,\mathrm{d}u^{+} - g_2(u,\, w)\,\mathrm{d}u^{-} \tag{5.8}$$

Under suitable regularity conditions, two systems of curves are obtained by integrating the functions g_1 and g_2: they represent the paths of evolution of the couple $(u,\, w)$ for increasing and decreasing u, respectively. These two families of ascending and descending curves may span the whole $(u,\, w)$ plane.

The Duhem operator then offers the potential of formulating novel differential models of hysteresis by prescribing specific expressions for the describing functions g_1 and g_2. According to this approach, Ni *et al.* [98] formulated an integrable hysteresis model that allows for the description of the nonlinear behaviour of wire rope isolators. Due to the mechanical analogy with the HDRP isolator, the model by Ni *et al.* is considered in the present thesis and its development is shown herein.

The ascending and descending describing functions are prescribed in the forms

$$g_1(u,\, w) = \frac{\mathrm{d}\overline{w}_1(u)}{\mathrm{d}u} + h_{w1}(w - \overline{w}_1)\, h_{u1}(u) \tag{5.9a}$$

$$g_2(u,\, w) = \frac{\mathrm{d}\overline{w}_2(u)}{\mathrm{d}u} + h_{w2}(w - \overline{w}_2)\, h_{u2}(u) \tag{5.9b}$$

where $\overline{w}_1(u)$, $\overline{w}_2(u)$, $h_{w1}(w-\overline{w}_1)$, $h_{w2}(w-\overline{w}_2)$, $h_{u1}(u)$ and $h_{u2}(u)$ are arbitrary continuous and differentiable functions. Substituting Eqs. (5.9a) and (5.9b) into Eq. (5.4b)

and integrating Eq. (5.4b) yields

$$G_{w1}(w-\overline{w}_1) = G_{u1}(u), \qquad \dot{u} \geq 0 \tag{5.10a}$$

$$G_{w2}(w-\overline{w}_2) = G_{u2}(u), \qquad \dot{u} < 0 \tag{5.10b}$$

where

$$G_{w1}(w-\overline{w}_1) = \int_0^{w-\overline{w}_1} \frac{\mathrm{d}z}{h_{w1}(z)} \tag{5.11a}$$

$$G_{u1}(u) = \int_{-u_r}^{u} h_{u1}(z)\,\mathrm{d}z \tag{5.11b}$$

$$G_{w2}(w-\overline{w}_2) = \int_0^{w-\overline{w}_2} \frac{\mathrm{d}z}{h_{w2}(z)} \tag{5.11c}$$

$$G_{u2}(u) = \int_{u_r}^{u} h_{u2}(z)\,\mathrm{d}z \tag{5.11d}$$

where $u_r > 0$ is the residual hysteresis input that satisfies $w(u_r) = 0$.

Most hysteretic systems exhibit symmetric hysteresis loops about the origin under symmetric input sequence. For this kind of hysteresis, there is a generic relation $g_2(u,\, w) = g_1(-u,\, -w)$ and the integrable Duhem hysteresis model is characterized only by the functions $\overline{w}(u)$, $h_w(w-\overline{w})$ and $h_u(u)$. Let us assume

$$\overline{w}(u) = k_l u + k_{nl} u^3 \tag{5.12a}$$

$$h_w(w-\overline{w}) = \frac{\gamma}{\beta} - \gamma(w-\overline{w}) \tag{5.12b}$$

$$h_u(u) = 1 \tag{5.12c}$$

which correspond to the ascending and descending describing functions

$$g_1(u,\, w) = k_l + 3k_{nl}u^2 + \frac{\gamma}{\beta} - \gamma\left(w - klu - k_{nl}u^3\right) \tag{5.13a}$$

$$g_2(u,\, w) = g_1(-u,\, -w) \tag{5.13b}$$

With the functions in Eq. (5.13), the hysteresis loop curves are determined as

$$w = \begin{cases} w^+ = k_l u + k_{nl}u^3 + \dfrac{1}{\beta}\Big(1 - \mathrm{e}^{-\gamma\,(u+u_r)}\Big), & \dot{u} \geq 0 \\[2ex] w^- = k_l u + k_{nl}u^3 - \dfrac{1}{\beta}\Big(1 - \mathrm{e}^{\gamma\,(u-u_r)}\Big), & \dot{u} < 0 \end{cases} \tag{5.14}$$

where k_l, k_{nl}, β and γ are the parameters of the model.

5.3.4 Constitutive model of the HDRP isolator

We derive the constitutive model of the HDRP isolator starting from the integrable Duhem hysteresis model developed by Ni *et al.* in the framework of the standard Duhem hysteresis operator.

The hysteretic damping occurring in the HDRP isolator is due to the presence of friction forces. A differential model of hysteresis, like the Duhem model, has been preferred to Coulomb-type friction models since it makes use of smooth functions instead of the signum function, which should lead to strongly nonlinear equations of motion. All the same, the local memory feature of the Duhem model is suitable to represent the dependence of friction forces on the sign of velocity. The HDRP model finally comprises the influence of possible viscous damping too.

In the place of the input u and the output w variables, we consider the displacement Δ and the force F across the HDRP isolator, respectively. The total restoring force is expressed as the sum of a hysteretic force F_{DM}, to be described by the Duhem model, and a viscous force F_{V}

$$F = F_{\mathrm{DM}} + F_{\mathrm{V}} \tag{5.15}$$

According to the Duhem model, the hysteretic force can be decoupled, in turn, into a purely elastic component F_{E} and a hysteretic component F_{H}

$$F_{\mathrm{DM}} = F_{\mathrm{E}} + F_{\mathrm{H}} \tag{5.16}$$

The total restoring force can then be expressed as

$$F = F_{\mathrm{E}} + F_{\mathrm{H}} + F_{\mathrm{V}} \tag{5.17}$$

where

$$F_{\mathrm{E}} = k_l\,\Delta + k_{nl}\,\Delta^3 \tag{5.18}$$

is the nonlinear purely elastic force, being k_l and k_{nl} the stiffness coefficients of the linear and of the cubic terms, respectively,

$$F_{\mathrm{H}} = \begin{cases} {F_{\mathrm{H}}}^{+} = \dfrac{1}{\beta}\left(1 - \mathrm{e}^{-\gamma\,(\Delta+\Delta_r)}\right), & \dot{\Delta} \geq 0 \\ {F_{\mathrm{H}}}^{-} = -\dfrac{1}{\beta}\left(1 - \mathrm{e}^{\gamma\,(\Delta-\Delta_r)}\right), & \dot{\Delta} < 0 \end{cases} \tag{5.19}$$

is the nonlinear hysteretic force, depending on the two parameters β and γ and the value of the residual hysteresis displacement Δ_r,

$$F_{\mathrm{V}} = c\dot{\Delta} \tag{5.20}$$

is the linear viscous force, depending on the damping constant c.

The constitutive relationship defined for the HDRP isolator can be represented by the rheological model depicted in Fig. 5.6, composed of a nonlinear spring, a hysteretic

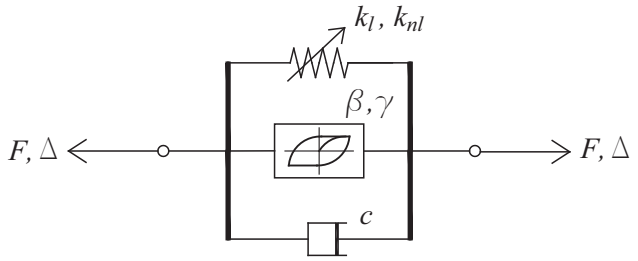

Figure 5.6. Rheological model of the HDRP isolator.

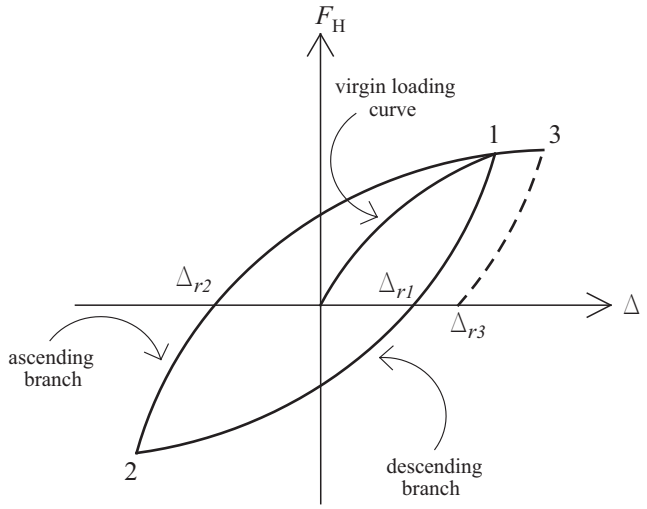

Figure 5.7. Hysteresis loops and residual hysteresis displacements for the HDRP model.

element and a linear viscous damper arranged in parallel. Five parameters (k_l, k_{nl}, β, γ, c) govern the model.

Determination of the residual hysteresis displacement

From Eqs. (5.19), it is gathered that the form of both the ascending and the descending branches of the hysteresis loop is independent of a shift of displacement Δ [8]. As apparent in Fig. 5.7, this shift is quantified by the residual hysteresis displacement $\Delta_r > 0 : F_H\big(-\text{sgn}(\dot{\Delta})\Delta_r\big) = 0$, *i.e.* the residual displacement, taken in absolute value, when unloading the system from the actual state to zero hysteretic force.

To obtain the residual hysteresis displacement, we consider, one at a time, the virgin loading curve and the ascending and the descending branches of both an asymmetric and of a symmetric hysteresis loop.

Virgin loading curve The virgin loading curve is the loading curve from the virgin state ($\Delta = 0$, $F_H = 0$). It represents also the skeleton curve for all the hysteresis loops the system may undergo. On the virgin loading curve, the residual hysteresis displacement is trivially null.

Descending branch The descending branch is the unloading branch from a state with positive hysteretic force (Fig. 5.8). To obtain the residual hysteresis displacement Δ_r^- on the descending branch, we consider the velocity reversal point given by the couple $(\Delta_{i1},\, F_{\mathrm{H}_{i1}})$, where the velocity is reversed from $\dot{\Delta} > 0$ to $\dot{\Delta} < 0$.

It is required

$$F_{\mathrm{H}}^{-}(\Delta_{i1}) = F_{\mathrm{H}}^{+}(\Delta_{i1}) = F_{\mathrm{H}_{i1}} \tag{5.21}$$

where $F_{\mathrm{H}_{i1}}$ is assumed to be known and

$$F_{\mathrm{H}}^{-}(\Delta_{i1}) = -\frac{1}{\beta}\left(1 - \mathrm{e}^{\gamma\,(\Delta_{i1} - \Delta_r^-)}\right) \tag{5.22}$$

with Δ_r^- to be determined. Solving Eq. (5.21) for Δ_r^- yields

$$\Delta_r^- = \frac{\gamma\,\Delta_{i1} - \ln(1 + \beta\,F_{\mathrm{H}i1})}{\gamma} \tag{5.23}$$

Ascending branch The ascending branch is the unloading branch from a state with negative hysteretic force (Fig. 5.8). To obtain the residual hysteresis displacement Δ_r^+ on the ascending branch, we consider the velocity reversal point given by the couple $(\Delta_{i2},\, F_{\mathrm{H}i2})$, where the velocity is reversed from $\dot{\Delta} < 0$ to $\dot{\Delta} > 0$.

It is required

$$F_{\mathrm{H}}^{+}(\Delta_{i2}) = F_{\mathrm{H}}^{-}(\Delta_{i2}) = F_{\mathrm{H}i2} \tag{5.24}$$

where F_{H2} is assumed to be known and

$$F_{H}^{+}(\Delta_{i2}) = \frac{1}{\beta}\left(1 - \mathrm{e}^{-\gamma\,(\Delta_{i2} + \Delta_r^+)}\right) \tag{5.25}$$

with Δ_r^+ to be determined. Solving Eq. (5.24) for Δ_r^+ yields

$$\Delta_r^+ = -\frac{\gamma\,\Delta_{i2} + \ln(1 - \beta\,F_{Hi2})}{\gamma} \tag{5.26}$$

Symmetric hysteresis loop On a hysteresis loop that is symmetric with respect to the origin (Fig. 5.9), we have

$$|\Delta_{i1}| = |\Delta_{i2}| = \Delta_i \tag{5.27a}$$

$$|F_{\mathrm{H}i1}| = |F_{\mathrm{H}i2}| = F_{\mathrm{H}i} \tag{5.27b}$$

$$\Delta_r^+ = \Delta_r^- = \Delta_r \tag{5.27c}$$

Let us consider the velocity reversal point given by the couple $(\Delta_i,\, F_{\mathrm{H}i})$. It is required

$$F_{\mathrm{H}}^{+}(\Delta_i) = F_{\mathrm{H}}^{-}(\Delta_i) = F_{\mathrm{H}i} \tag{5.28}$$

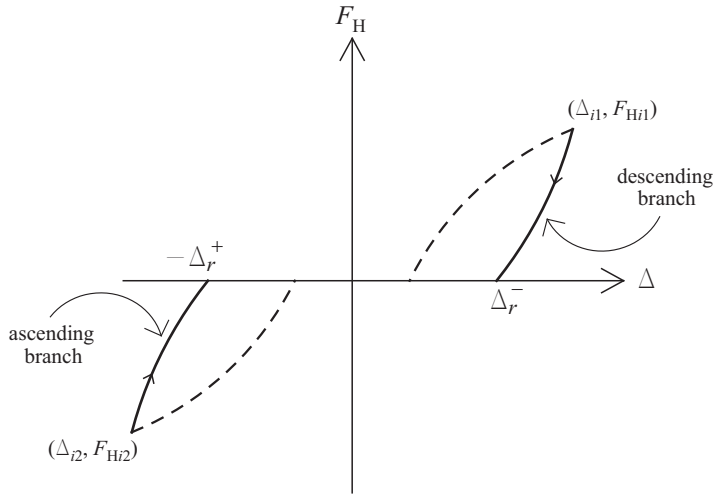

Figure 5.8. Ascending and descending branches of an asymmetric hysteresis loop.

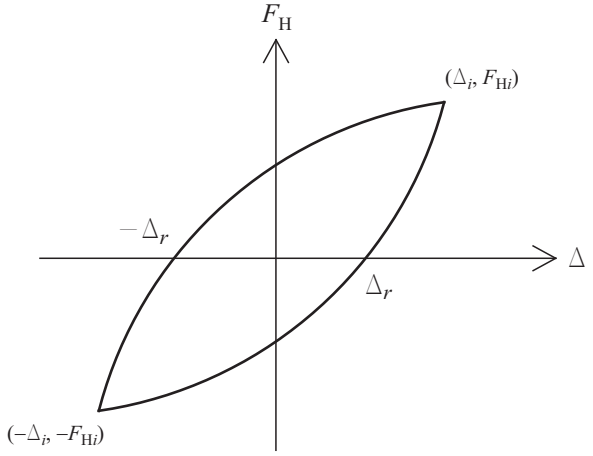

Figure 5.9. Ascending and descending branches of a symmetric hysteresis loop.

By substituting the expressions for $F_{\mathrm{H}}^{+}(\Delta_i)$ and $F_{\mathrm{H}}^{-}(\Delta_i)$ into Eq. (5.28), it follows

$$\frac{1}{\beta}\left(1-\mathrm{e}^{-\gamma\,(\Delta_i+\Delta_r)}\right)=-\frac{1}{\beta}\left(1-\mathrm{e}^{\gamma\,(\Delta_i-\Delta_r)}\right) \tag{5.29}$$

with Δ_r to be determined. Solving Eq. (5.29) for Δ_r yields:

$$\Delta_r=-\Delta_i+\frac{1}{\gamma}\ln\left(\frac{1+e^{2\gamma\Delta_i}}{2}\right) \tag{5.30}$$

Determination of the nominal yielding point

Unlike classical elastoplasticity models, which provide for a yielding surface, the Duhem hysteresis model and then the model defined for the HDRP isolator do not identify a sharp discontinuity between elastic and plastic states. In this case, yielding is a phenomenon that occurs when the system is loaded from the virgin state on. Anyway, since hysteretic force F_{H} is a bounded function, a nominal yielding point can be determined as shown hereafter in this paragraph.

We compute the stiffness tangent to each stage of the force–displacement loop by taking the first derivative of the total restoring force F with respect to displacement Δ

$$\frac{\partial F}{\partial \Delta} = \frac{\partial F_{\mathrm{E}}}{\partial \Delta} + \frac{\partial F_{\mathrm{H}}}{\partial \Delta} \tag{5.31}$$

where

$$\frac{\partial F_E}{\partial \Delta} = k_l + 3k_{nl}\Delta^2 \tag{5.32}$$

is the stiffness term associated to the purely elastic force and

$$\frac{\partial F_{\mathrm{H}}}{\partial \Delta} = \begin{cases} \dfrac{\partial F_{\mathrm{H}}^{+}}{\partial \Delta} = \left(\dfrac{\gamma}{\beta}\,\mathrm{e}^{-\gamma\Delta_r}\right)\mathrm{e}^{-\gamma\Delta}, & \dot{\Delta} \geq 0 \\ \dfrac{\partial F_{\mathrm{H}}^{-}}{\partial \Delta} = \left(\dfrac{\gamma}{\beta}\,\mathrm{e}^{-\gamma\Delta_r}\right)\mathrm{e}^{\gamma\Delta}, & \dot{\Delta} < 0 \end{cases} \tag{5.33}$$

is the stiffness term associated to the hysteretic force. Eqs. (5.32) and (5.33) indicate that the force–displacement loop is symmetric with respect to the origin.

The stiffness term associated to the purely elastic force F_{E} is given as the superposition of a constant function, whose stiffness coefficient is k_l, and of a quadratic function of displacement Δ, whose stiffness coefficient is k_{nl}. The sign of k_{nl} denotes the stiffness behaviour, which can be hardening ($k_{nl} > 0$), softening ($k_{nl} < 0$) or even linear ($k_{nl} = 0$). In the present study, we assume k_l to be a positive real number and k_{nl} to be a non-negative real number

$$k_l \in \mathbb{R}^{+} \tag{5.34a}$$

$$k_{nl} \in \mathbb{R}_0^{+} \tag{5.34b}$$

The stiffness term associated to the hysteretic force F_{H} is a function of both the displacement Δ and the residual hysteresis displacement Δ_r. In particular, it decreases with increasing Δ, thus denoting a nonlinear softening behaviour of F_{H}. To determine the nominal yielding hysteretic force $F_{\mathrm{H}y}$ and displacement Δ_y, we consider the virgin loading curve by assuming $\Delta_r = 0$ and $\dot{\Delta} > 0$. The tangent stiffness to the virgin state ($\Delta = 0$, $F_{\mathrm{H}} = 0$) is

$$\left.\frac{\partial F_{\mathrm{H}}}{\partial \Delta}\right|_{\Delta=0} = \left.\frac{\gamma}{\beta}\,\mathrm{e}^{-\gamma\Delta}\right|_{\Delta=0} = \frac{\gamma}{\beta} \tag{5.35}$$

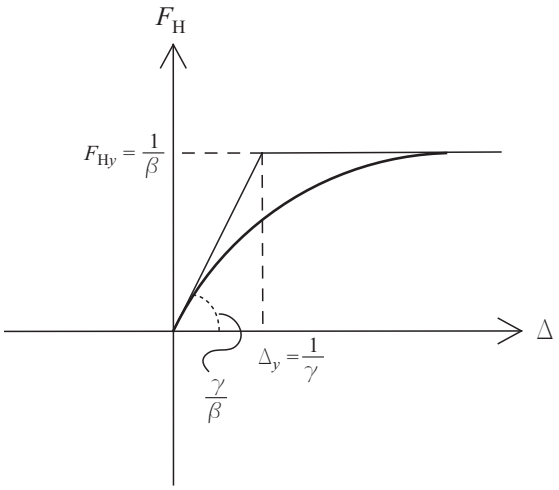

Figure 5.10. Hysteretic force F_{H}: determination of the nominal yielding point.

whereas the tangent stiffness when $\Delta \to \infty$ is computed as

$$\lim_{\Delta\to\infty} \frac{\partial F_{\mathrm{H}}}{\partial \Delta} = \lim_{\Delta\to\infty} \frac{\gamma}{\beta}\, \mathrm{e}^{-\gamma\Delta} = 0 \tag{5.36}$$

Eq. (5.35) and Eq. (5.36) can be considered as the stiffness of an associated elasto-plastic limit case, in the elastic and in the plastic range, respectively. The point where this stiffness experiences a discontinuity is taken as the nominal yielding point (see Fig. 5.35). Hence, the nominal yielding hysteretic force is computed as

$$\begin{aligned} F_{\mathrm{H}y} &:= \lim_{\Delta\to\infty} F_{\mathrm{H}} = \\ &= \lim_{\Delta\to\infty} \frac{1}{\beta}\left(1 - \mathrm{e}^{-\gamma\,\Delta}\right) = \\ &= \frac{1}{\beta} \end{aligned} \tag{5.37}$$

Being

$$F_{\mathrm{H}y} = \left(\left.\frac{\partial F_{\mathrm{H}}}{\partial \Delta}\right|_{\Delta=0} \right) \Delta_y \tag{5.38}$$

it follows that the nominal yielding displacement is given by

$$\Delta_y := \left(\left.\frac{\partial F_{\mathrm{H}}}{\partial \Delta}\right|_{\Delta=0} \right)^{-1} F_{\mathrm{H}y} = \frac{1}{\gamma} \tag{5.39}$$

From Eq. (5.37) and (5.39), parameters β and γ must be positive real numbers

$$\beta,\ \gamma \quad \in \mathbb{R}^{+} \tag{5.40}$$

Determination of the inflection points

As to the total restoring force F, the stiffness behaviour is affected by the combination of the softening effect due to the hysteretic component F_{H} and the hardening effect due to the cubic purely elastic component F_{E}. As a result, the total restoring force F shows a peculiar behaviour that is called *soft-hardening* and is shown in Fig. (5.11): for small amplitudes, the model exhibits softening behaviour, which gradually changes into hardening behaviour for increasing amplitudes. This kind of hysteretic behaviour is known in Literature as a distinctive feature of wire-rope vibration isolators [96, 97].

By properly choosing the values of parameter k_{nl}, β and γ, the total restoring force F may have three inflection points, marked by numbers 1, 2 and 3 on the curve depicted in Fig. 5.12. Owing to the symmetry about the origin, one inflection point (see point 1) is trivially located at the origin. In addition, two inflection points divide the softening section from the hardening section, on the ascending branch (see point 2) and on the descending branch (see point 3), respectively.

To determine the displacement Δ_{fl} at the non-trivial inflection point, we compute the second derivative of the total restoring force F with respect to displacement Δ

$$\frac{\partial^2 F}{\partial \Delta^2} = \frac{\partial^2 F_E}{\partial \Delta^2} + \frac{\partial^2 F_H}{\partial \Delta^2} \tag{5.41}$$

where

$$\frac{\partial^2 F_E}{\partial \Delta^2} = 6 k_{nl} \Delta \tag{5.42}$$

and

$$\frac{\partial^2 F_H}{\partial \Delta^2} = \begin{cases} \dfrac{\partial^2 F_{\mathrm{H}}^{+}}{\partial \Delta^2} = -\left(\dfrac{\gamma^2}{\beta}\,\mathrm{e}^{-\gamma\Delta_r}\right)\mathrm{e}^{-\gamma\Delta}, & \dot{\Delta} \geq 0 \\ \dfrac{\partial^2 F_{\mathrm{H}}^{-}}{\partial \Delta^2} = \left(\dfrac{\gamma^2}{\beta}\,\mathrm{e}^{-\gamma\Delta_r}\right)\mathrm{e}^{\gamma\Delta}, & \dot{\Delta} < 0 \end{cases} \tag{5.43}$$

We consider the virgin loading curve by assuming $\Delta_r = 0$ and $\dot{\Delta} > 0$ and we require

$$\left.\frac{\partial^2 F}{\partial \Delta^2}\right|_{\Delta=\Delta_{fl}} = 0 \tag{5.44}$$

obtaining

$$\Delta_{fl} = \frac{1}{\gamma}\,\mathrm{W}\left(\frac{1}{6}\,\frac{\gamma^3}{\beta\, k_{nl}}\right) \tag{5.45}$$

where $\mathrm{W}(x)$ indicates the Lambert's W function of x. Lambert's W function is a transcendent, non elementary function that is defined in the inverse form as the function solving the equation

$$y\, e^{y} = x \quad \text{where} \quad y = \mathrm{W}(x)$$

For any real number $x \geq 0$, Lambert's W is a real, single-valued function [20]. It can be computed through a recursive scheme as done by the MATLAB function *lambertw* [132].

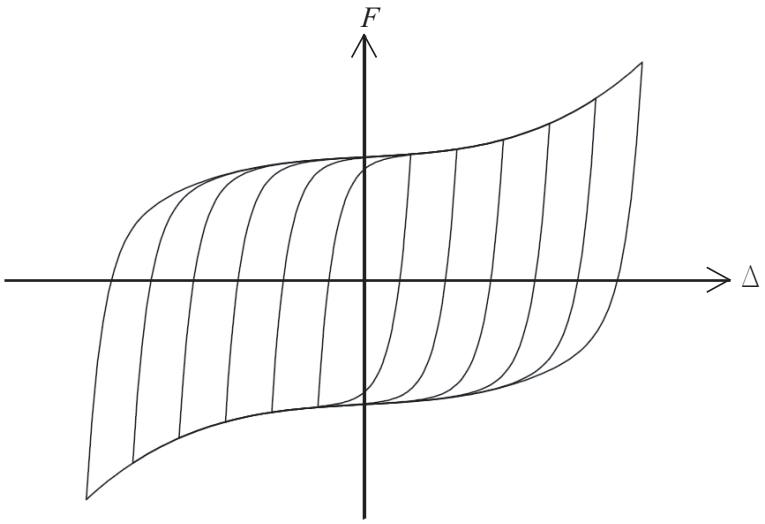

Figure 5.11. Soft-hardening hysteretic behaviour.

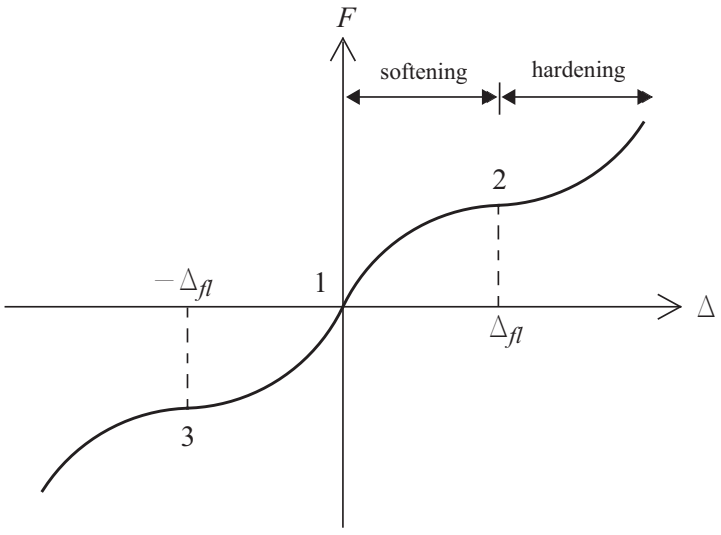

Figure 5.12. Total restoring force F: inflection points.

Chapter 6

Nonlinear hysteretic isolation: optimal design and numerical investigations

In this chapter[1], the constitutive model previously developed is adopted for the optimal design of an equipment isolation system with nonlinear hysteretic behaviour. Both a single-degree-of-freedom model, suited for a decoupled dynamic analysis, and a two-degree-of-freedom model, suited for a coupled dynamic analysis, are used for design purposes. Two optimization criteria are defined, involving the reduction of the peak equipment absolute acceleration to a threshold value allowable for full operation and the maximization of a properly defined energy performance index. The methodology is proved to account, in a synthetic and effective way, for both the different response quantities of the equipment (absolute acceleration and relative displacement) and the energy dissipation in the isolation system. Numerical simulations are used to predict the response characteristics of the nonlinear hysteretic isolation system. Direct numerical integration of the equations of motion is performed by using the fourth-order fixed-step Runge-Kutta scheme. A real application referring to a full scale physical model is eventually provided, first to illustrate the optimal design methodology and second to assess the seismic effectiveness of the proposed equipment isolation system.

[1]Some of the results in this chapter have been published in the following papers:

♢ Reggio, A., De Angelis, M. Optimal design of an equipment isolation system with nonlinear hysteretic behaviour. *Earthquake Engineering and Structural Dynamics*, 42 (13), 1907-1930, 2013.

♢ Reggio A., De Angelis M. Optimal design of a passive nonlinear isolation system for the seismic protection of equipment. *Proceedings of EACS 2012 - V European Conference on Structural Control*, Genova, Italy, June 18-20, 2012.

6.1 Decoupled approach: reduced order SDOF model

6.1.1 Equations of motion

Let us consider the equation of motion given by Eq. (3.7) for the reduced order SDOF model. Let $u(t)$ and f be the displacement and the total restoring force across the isolation system, respectively. Let the force f be described by the nonlinear hysteretic constitutive model given by Eqs. (5.17)-(5.20) in Sec 5.3.4. The system of interest is depicted in Fig. 6.1 and its equation of motion is drawn in the form

$$m\ddot{u} = -m\ddot{u}_g - f \tag{6.1a}$$

$$f = k_l\, u + k_{nl}\, u^3 + f_{\mathrm{H}} + c\,\dot{u} \tag{6.1b}$$

$$f_{\mathrm{H}} = \begin{cases} f_{\mathrm{H}}^{+} = \dfrac{1}{\beta}\left(1 - \mathrm{e}^{-\gamma\,(u+u_r)}\right), & \dot{u} \geq 0 \\ f_{\mathrm{H}}^{-} = -\dfrac{1}{\beta}\left(1 - \mathrm{e}^{\gamma\,(u-u_r)}\right), & \dot{u} < 0 \end{cases} \tag{6.1c}$$

where m is the mass of the isolated equipment; $\beta,\ \gamma \in \mathbb{R}^+$ and $k_l,\ k_{nl},\ c \in \mathbb{R}_0^+$ are the parameters of the constitutive model; $u_r \in \mathbb{R}_0^+$ is the residual hysteresis displacement.

To attempt a more general description of the problem, Eqs. (6.1) are non-dimensionalized by setting the following characteristic values of frequency, displacement and force

$$\begin{aligned} \omega^* &= \sqrt{\frac{k_0}{m}} && \text{with } k_0 = k_l + \frac{\gamma}{\beta} \\ u^* &= \frac{m\,a_g}{k_0} && \text{with } a_g = \max_t \left[\left|\ddot{u}_g(t)\right|\right] \\ f^* &= m\,a_g \end{aligned} \tag{6.2}$$

It is worth noting that, being k_0 the stiffness tangent to the virgin loading curve of the constitutive model for $u = 0$ (see Eqs. (5.31)–(5.33) in Sec. 5.3.4), ω^* is the circular

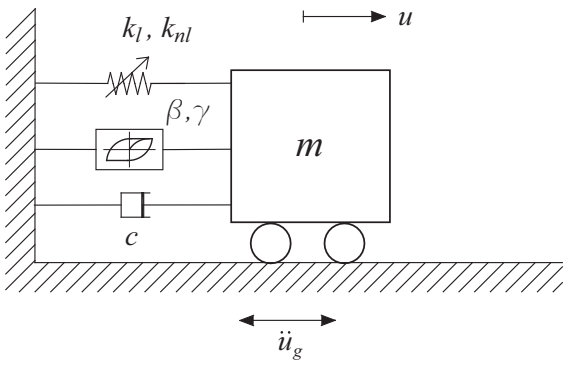

Figure 6.1. SDOF model with the nonlinear hysteretic isolation system.

frequency of the nonlinear isolation for small-amplitude oscillations. The following non-dimensional variables are thus assumed

$$\hat{t} = \omega^* \, t, \qquad \hat{u} = \frac{u}{u^*}, \qquad \hat{u}_r = \frac{u_r}{u^*}, \qquad \hat{f} = \frac{f}{f^*} \tag{6.3}$$

while differentiation with respect to the non-dimensional time $\hat{t}$ is expressed as

$$\frac{\mathrm{d}}{\mathrm{d}\hat{t}} = \frac{\mathrm{d}}{\mathrm{d}t} \frac{\mathrm{d}t}{\mathrm{d}\hat{t}} = \frac{1}{\omega^*} \frac{\mathrm{d}}{\mathrm{d}t} \tag{6.4}$$

Substituting Eqs. (6.3) and (6.4) into Eqs. (6.1) yields

$$\begin{aligned} & m\omega^{*2} u^* \, \hat{u}'' = -m\ddot{u}_g - f^* \, \hat{f} \\ & f^* \, \hat{f} = k_l u^* \, \hat{u} + k_{nl} u^{*3} \, \hat{u}^3 + f_{\mathrm{H}} + c \, \omega^* u^* \, \hat{u}' \\ & f_{\mathrm{H}} = \begin{cases} f_{\mathrm{H}}^+ = \dfrac{1}{\beta} \left(1 - \mathrm{e}^{-\gamma u^* \, (\hat{u} + \hat{u}_r)} \right), & \hat{u}' \geq 0 \\ f_{\mathrm{H}}^- = -\dfrac{1}{\beta} \left(1 - \mathrm{e}^{\gamma u^* \, (\hat{u} - \hat{u}_r)} \right), & \hat{u}' < 0 \end{cases} \end{aligned} \tag{6.5}$$

with symbol $'$ denoting differentiation with respect to the non-dimensional time $\hat{t}$. Letting Eqs. (6.5) be divided by the characteristic force f^*, the non-dimensional form of the equation of motion is obtained

$$\begin{aligned} & \frac{m\omega^{*2} u^*}{f^*} \, \hat{u}'' = -\frac{m\ddot{u}_g}{f^*} - \hat{f} \\ & \hat{f} = \frac{k_l u^*}{f^*} \, \hat{u} + \frac{k_{nl} u^{*3}}{f^*} \, \hat{u}^3 + \frac{f_{\mathrm{H}}}{f^*} + \frac{c \, \omega^* u^*}{f^*} \, \hat{u}' \\ & \frac{f_{\mathrm{H}}}{f^*} = \begin{cases} \dfrac{f_{\mathrm{H}}^+}{f^*} = \dfrac{1}{f^* \beta} \left(1 - \mathrm{e}^{-\gamma u^* \, (\hat{u} + \hat{u}_r)} \right), & \hat{u}' \geq 0 \\ \dfrac{f_{\mathrm{H}}^-}{f^*} = -\dfrac{1}{f^* \beta} \left(1 - \mathrm{e}^{\gamma u^* \, (\hat{u} - \hat{u}_r)} \right), & \hat{u}' < 0 \end{cases} \end{aligned} \tag{6.6}$$

After introducing the following non-dimensional parameters

$$\begin{aligned} & \hat{k}_l = \frac{k_l}{k_0}, \qquad \hat{k}_{nl} = k_{nl} \frac{(m \, a_g)^2}{k_0^3}, \qquad \zeta_0 = \frac{c}{2\sqrt{m k_0}} \\ & \hat{\beta} = \beta \, m a_g, \qquad \hat{\gamma} = \gamma \, \frac{m a_g}{k_0} \end{aligned} \tag{6.7}$$

and defining the non-dimensional base acceleration as

$$\hat{u}_g''(\hat{t}) = \frac{\ddot{u}_g(t)}{a_g} \tag{6.8}$$

Eqs. (6.6) can be rewritten as

$$\hat{u}'' = -\hat{u}_g'' - \hat{f} \tag{6.9a}$$

$$\hat{f} = \hat{k}_l\,\hat{u} + \hat{k}_{nl}\,\hat{u}^3 + \hat{f}_{\mathrm{H}} + 2\zeta_0\,\hat{u}' \tag{6.9b}$$

$$\hat{f}_{\mathrm{H}} = \begin{cases} \hat{f}_{\mathrm{H}}^{+} = \dfrac{1}{\hat{\beta}}\left(1 - \mathrm{e}^{-\hat{\gamma}\,(\hat{u}+\hat{u}_r)}\right), & \hat{u}' \geq 0 \\ \hat{f}_{\mathrm{H}}^{-} = -\dfrac{1}{\hat{\beta}}\left(1 - \mathrm{e}^{\hat{\gamma}\,(\hat{u}-\hat{u}_r)}\right), & \hat{u}' < 0 \end{cases} \tag{6.9c}$$

Remark 1 *Due to the introduced non-dimensionalization, non-dimensional stiffness* $\hat{k}_0$ *tangent to the virgin loading curve at* $\hat{u} = 0$ *is unitary. It is defined*

$$\left.\frac{\partial \hat{f}}{\partial \hat{u}}\right|_{\hat{u}=0,\,\hat{u}_r=0} = \hat{k}_l + \frac{\hat{\gamma}}{\hat{\beta}} := \hat{k}_0 \tag{6.10}$$

Substituting non-dimensional parameters (6.7) *into Eq.* (6.10) *and recalling dimensional stiffness* $k_0 = k_l + \gamma/\beta$*, it is obtained*

$$\begin{aligned} \hat{k}_0 &= \frac{k_l}{k_0} + \gamma\,\frac{m a_g}{k_0}\,\frac{1}{\beta m a_g} = \\ &= \frac{1}{k_0}\left(k_l + \frac{\gamma}{\beta}\right) \\ &= \frac{k_0}{k_0} = \\ &= 1 \end{aligned} \tag{6.11}$$

A constraint between non-dimensional parameters $\hat{k}_l$, $\hat{\beta}$, $\hat{\gamma}$ *thus follows from Eq.* (6.11)

$$\hat{k}_l + \frac{\hat{\gamma}}{\hat{\beta}} = 1 \tag{6.12}$$

Remark 2 *Due to the introduced non-dimensionalization, the peak value of non-dimensional base acceleration is unitary. It is obtained*

$$\begin{aligned} \hat{a}_g &= \max_{\hat{t}}\left[\left|\hat{u}_g''(\hat{t})\right|\right] = \\ &= \max_{t}\left[\left|\frac{\ddot{u}_g(t)}{a_g}\right|\right] = \\ &= \frac{a_g}{a_g} = \\ &= 1 \end{aligned} \tag{6.13}$$

6.1.2 Energy balance

The equation of relative energy balance [136] can be obtained by multiplying both members of Eq. (6.9a) by relative velocity $\hat{u}'$ and integrating over time, yielding

$$E_k(\hat{t}) = E_i(\hat{t}) - E_E(\hat{t}) - E_H(\hat{t}) - E_V(\hat{t}) \tag{6.14}$$

where

$$E_k(\hat{t}) = \int_0^{\hat{t}} \hat{u}''\,\hat{u}'\,\mathrm{d}\tau = \frac{1}{2}\,\hat{u}'^2(\hat{t}) \tag{6.15}$$

is the relative kinetic energy,

$$E_i(\hat{t}) = \int_0^{\hat{t}} -\hat{u}_g''\,\hat{u}'\,\mathrm{d}\tau \tag{6.16}$$

is the input energy,

$$E_E(\hat{t}) = \int_0^{\hat{t}} (\hat{k}_l\,\hat{u} + \hat{k}_{nl}\,\hat{u}^3)\,\hat{u}'\,\mathrm{d}\tau = \frac{1}{2}\,\hat{k}_l\,\hat{u}^2(\hat{t}) + \frac{1}{4}\,\hat{k}_{nl}\,\hat{u}^4(\hat{t}) \tag{6.17}$$

is the pure elastic strain energy,

$$E_H(\hat{t}) = \int_0^{\hat{t}} \hat{f}_{\mathrm{H}}\,\hat{u}'\,\mathrm{d}\tau \tag{6.18}$$

is the strain energy due to the hysteretic force $\hat{f}_H$,

$$E_V(\hat{t}) = \int_0^{\hat{t}} 2\zeta_0\,\hat{u}'^2\,\mathrm{d}\tau \tag{6.19}$$

is the viscous damping energy.

Energy $E_H(\hat{t})$ is in turn composed by the sum of a recoverable elastic energy $E_{HE}(\hat{t})$ plus an irrecoverable energy $E_{HD}(\hat{t})$ dissipated on hysteresis loops

$$E_H(\hat{t}) = E_{HE}(\hat{t}) + E_{HD}(\hat{t}) \tag{6.20}$$

Making use of the nominal elastic-perfectly plastic constitutive relationship associated with $\hat{f}_H$ and of the nominal elastic stiffness, given as

$$\left.\frac{\partial \hat{f}_H}{\partial \hat{u}}\right|_{\hat{u}=0,\,\hat{u}_r=0} = \frac{\hat{\gamma}}{\hat{\beta}} \tag{6.21}$$

it is obtained

$$E_{HE}(\hat{t}) = \frac{1}{2}\,\frac{\hat{f}_H^2(\hat{t})}{\hat{\gamma}/\hat{\beta}} \tag{6.22}$$

and consequently

$$E_{HD}(\hat{t}) = E_H(\hat{t}) - E_{HE}(\hat{t}) \tag{6.23}$$

6.2 Decoupled approach: optimal design of the equipment isolation system

Here, we specifically develop an optimal design methodology for the equipment isolation system with nonlinear hysteretic behaviour.

Since a decoupled approach is adopted, the dynamic analysis of the equipment is carried out independently from the supporting structure and the floor acceleration time history is assumed as the base seismic input. However, without loss of generality for the purposes of this study, we neglect the filter effect of the structure and we make use of the ground acceleration time history as the base input.

The proposed optimization criteria involve both the reduction of the equipment peak responses and the maximization of a properly defined energy index. The methodology is proved to account, in a synthetic and effective way, both for the response quantities of the equipment (displacement and acceleration) and for the energy dissipation in the isolation system.

6.2.1 Multi-objective performance-based seismic design

The current practice for linear isolation systems is to set the value of the acceleration transmitted in the Design Based Earthquake (DBE) and to design the isolation system to have sufficient displacement capacity to meet the demand of the Maximum Considered Earthquake (MCE). The drawback of such systems is the trade-off between isolation performance and displacement demand: reducing the displacement demand in the MCE with increased stiffness and damping worsens the isolation performance in the DBE and vice versa. Moreover, the performance of linear isolation systems for more frequent, low intensity events is typically not considered in the design process. As a result, they may either not activate for minor events, if designed with sufficient stiffness and damping for larger earthquakes, or not re-center, if they do activate [45].

In the case of nonlinear isolation systems, multiple performance objectives, that is multiple performance levels at different intensities of ground shaking, can rather be achieved by separately optimizing the system parameters, in accordance to the principles of *multi-objective performance-based seismic design*. The tangent stiffness associated to a nonlinear model varies during the course of motion depending on the model parameters. The stiffness can then be designed to change to predictable values at calculable and controllable displacement amplitudes, so that the system exhibits adaptive behaviour, yet is completely passive.

The proposed nonlinear hysteretic isolation system shows a soft-hardening stiffness behaviour that is well-suited to a multi-objective performance-based seismic design. The works by Kelly [75] and Hall [51] indicate that to control displacements in large earthquakes while still maintaining good performance in low-to-moderate earthquakes

requires designing an isolation system that: (a) is very stiff with low damping at low-level shaking; (b) softens with increasing damping in the DBE; (c) stiffens at and beyond the MCE. This desirable behavior can be achieved with properly designed parameters of the proposed nonlinear hysteretic model.

To realize a multi-objective performance-based seismic design, two performance levels are selected. Each of them states an acceptable risk of incurring specific levels of damage and consequential losses (*performance level*) at an established level of seismic hazard (*hazard level*) [40]. Target performance objectives are the following:

- for the DBE, an *Operational level* is required, which means that the structure remains safe to occupy. As to nonstructural components, they remain secured and do not represent a risk of injuries or life-threats. As to the equipment damage, all the systems necessary for critical or essential functions of the facility are required to be fully operational.

- for the MCE, a *Life-Safety level* is required, which means that the structure still retains a significant margin against collapse, yet undergoing considerable structural and nonstructural damage. Nonstructural elements of the structure, while secured and not presenting falling hazards, are severely damaged and equipment cannot function.

Since two performance levels are assumed, two-fold are the criteria defined for the optimal design of the equipment isolation system:

- for the Operational level, the continuing functioning of acceleration-sensitive equipment is guaranteed by preventing the excessive inertial loads caused by the shaking. An optimization criterion is defined that consists in reducing the equipment acceleration response to a threshold value allowable for the full operation.

- for the Life-Safety level, life threats and injuries are avoided by preventing excessive motion and restraint breakage of the isolated equipment. An optimization criterion is defined that consists in increasing the stiffness of the isolation system in order to limit the equipment displacement.

Both the performance levels and the optimization criteria are achievable through the soft-hardening stiffness behaviour of the proposed nonlinear hysteretic model: the purpose of the softening section can be to reduce the equipment acceleration response to an earthquake within the design level, so as to guarantee its full operation; the purpose of the hardening section can be to suppress the displacement across the isolation system in a severe earthquake exceeding the design level, so as to secure the safety of the isolated equipment. By properly design the model parameters, the designer can set the value of the displacement $\hat{u}_{fl}$ at the inflection point, where the nonlinear isolation system switches from the acceleration control to the displacement control (Fig. 6.2). In

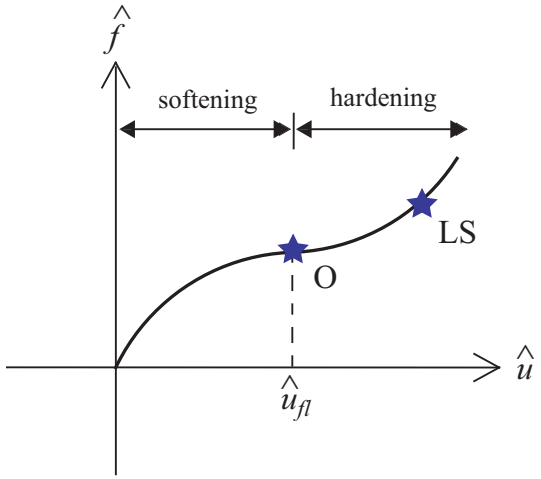

Figure 6.2. Soft-hardening stiffness behaviour and multi-objective performance-based seismic design of the isolation system: Operational (O) level; Life Safety (LS) level.

addition, a further stiffness hardening can be used as an ultimate fail-safe mechanism for the isolated equipment, if subjected to even more severe earthquakes.

6.2.2 Seismic input

In the first phase of the study, the optimal design of the nonlinear hysteretic isolation system is addressed by considering only one performance objective, the Operational one. Corresponding design seismic input should be defined in terms of its probability of exceedance and depends on the local hazard. It is then defined according to the latest Italian building code "Nuove Norme Tecniche per la Costruzioni – D.M. 14/01/2008" (NTC 2008) [90].

One set of seven artificial accelerograms was generated by the software SIMQKE [139] (http://bsing.ing.unibs.it/g̃elfi/software/simqke/) to match the response spectrum given by the code for the assigned performance objective. The case study referred to the "*Stato Limite di Danno*" performance objective, equivalent to the Operational level in the Italian code classification, for a critical facility ("*classe d'uso IV*") with a nominal life of 100 years. This leads to a design seismic action with a mean return period T_R of 201 years and a Peak Ground Acceleration (PGA) of 0.273 g. A pseudo-acceleration elastic response spectrum is evaluated for L'Aquila site, C-type soil, 5% viscous damping and a behaviour factor $q = 1$ (Fig. 6.3).

Given a set of seven artificial records, the average of the response quantities from all of the analyses is used as the design value of the action effect in the relevant verifications, according to the Italian code's provisions.

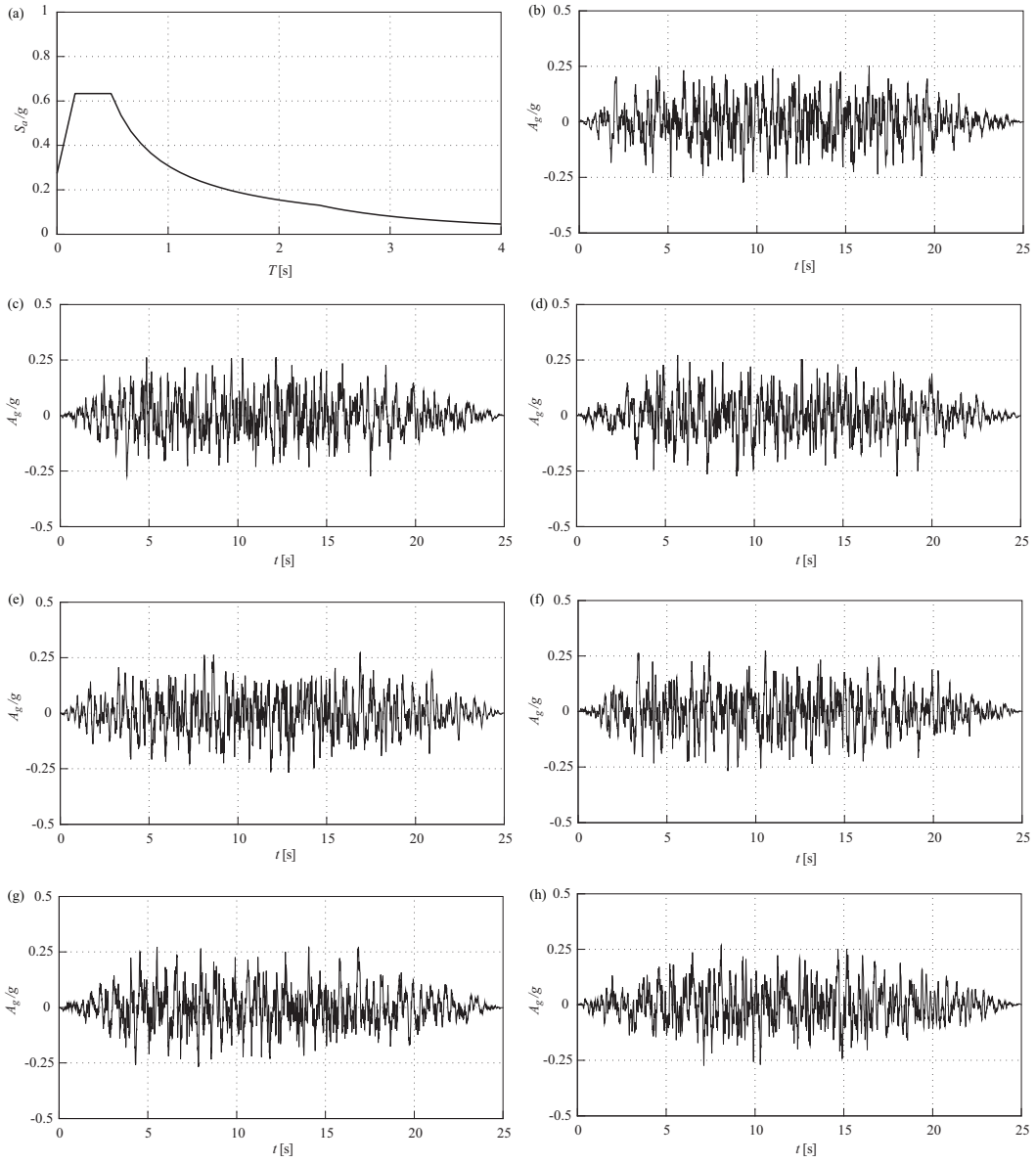

Figure 6.3. Design seismic input according to the Italian building code NTC 2008. (a) Pseudo-acceleration elastic response spectrum. (b) Acceleration time history n.1. (c) Acceleration time history n.2. (d) Acceleration time history n.3. (e) Acceleration time history n.4. (f) Acceleration time history n.5. (g) Acceleration time history n.6. (h) Acceleration time history n.7.

6.2.3 Optimization

The optimization procedure developed for the Operational level aims at selecting the parameters that govern the softening section of the nonlinear hysteretic model: the initial tangent stiffness k_0 and the non-dimensional parameter $\hat{\beta}$. Non-dimensional stiffness coefficients $\hat{k}_l$ and $\hat{k}_{nl}$ as well as the viscous damping ratio ζ_0 are considered as known data, whereas non-dimensional parameter $\hat{\gamma}$ is required to comply with the constraint from Eq. (6.12). To a first approximation, the hardening coefficient $\hat{k}_{nl}$ is assumed to be null and as a consequence, non-dimensional parameter $\hat{k}_l$ takes on the meaning of the ratio between post- and pre-yielding stiffness. A small damping ratio $\zeta_0 = 0.01$ is taken into account for numerical stability reason.

The sensitivity of the equipment response to the design parameters is investigated in the contour plots in Fig. 6.4. Design parameters k_0 and $\hat{\beta}$ are converted into those more meaningful to the nonlinear isolation design: the period $T_0 = 2\pi\sqrt{m/k_0}$ of the isolation system for small-amplitude oscillations; the non-dimensional hysteretic force at nominal yielding $\hat{f}_{\mathrm{H}y} = 1/\hat{\beta}$. The peak values of non-dimensional absolute acceleration $\hat{u}''_a$ and displacement $\hat{u}$ are illustrated. In order to make the responses comparable between variously designed isolation systems, $\hat{u}$ is normalized by the squared period T_0^2 and by the non-dimensional displacement at the nominal yielding $\hat{u}_y$. A stiffness ratio $\hat{k}_l = 0.05$ is assumed in the analyses.

Aiming at preserving the serviceability of the isolated equipment by preventing excessive inertial loads, an optimization criterion is defined which consists in reducing the equipment absolute acceleration $\hat{u}''_a$ to a threshold value allowable for full operation. The latter is set as

$$\max_{\hat{t}} \left|\hat{u}''_a(\hat{t})\right| = \frac{\max_t \left|\ddot{u}_a(t)\right|}{a_g} = 0.2 \tag{6.24}$$

i.e., the peak absolute acceleration transmitted to the equipment is required to be 20% of PGA a_g. In Fig. 6.4 (a), where the peak of $\hat{u}''_a$ is shown *versus* the design parameters T_0 and $\hat{f}_{\mathrm{H}y}$, it can be noticed that all the couples $\left(T_0,\ \hat{f}_{\mathrm{H}y}\right)$ belonging to a contour line comply with the requirement in Eq. (6.24), hence a further design criterion is needed to obtain a unique optimal solution.

In order to fully exploit the high energy dissipation capability owned by the hysteretic isolation system, an energy criterion is introduced [55]. The proposed idea is that the more is dissipated of the input energy transmitted by the earthquake, the more effective and economic is the isolation system performance. In this sense, the following energy performance index, named *Hysteresis Energy Dissipation Index*, is defined

$$EDI_{\mathrm{H}} = \frac{\max_{\hat{t}} \left[E_{\mathrm{HD}}(\hat{t})\right]}{\max_{\hat{t}} \left[E_i(\hat{t})\right]} \tag{6.25}$$

where E_{HD} is the irrecoverable energy dissipated through hysteresis in the isolation system and E_i is the input energy to the equipment. E_{HD} and E_i are given by Eqs. (6.23)

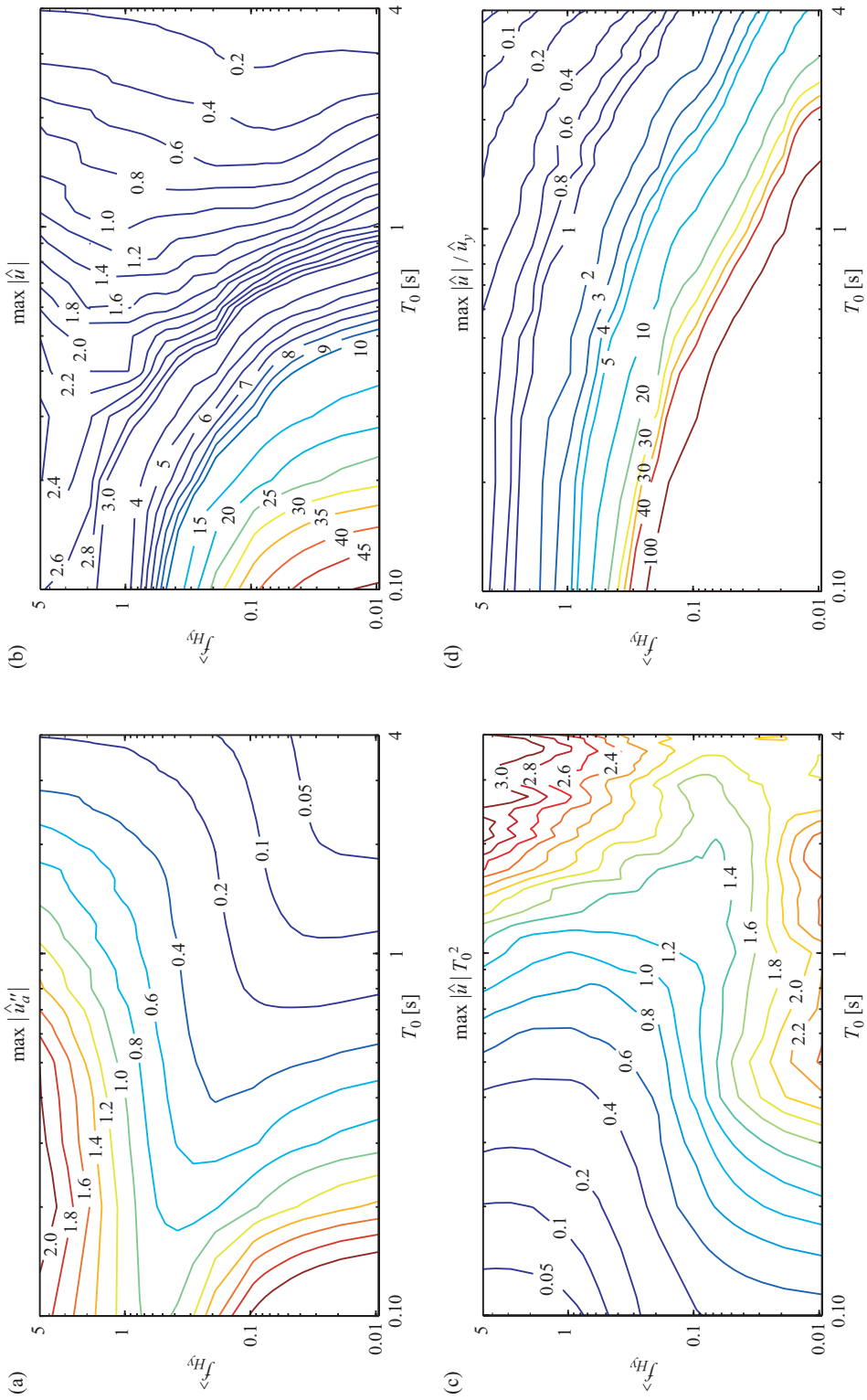

Figure 6.4. SDOF model, peak non-dimensional responses *vs* period T_0 and hysteretic force at nominal yielding f_{Hy}. (a) Absolute acceleration $\hat{u}_a''$. (b) Displacement $\hat{u}$. (c) Normalized displacement $\hat{u}\,T_0^2$. (d) Displacement ratio $\hat{u}/\hat{u}_y$. It is assumed: $\hat{k}_l = 0.05$, $\hat{k}_{nl} = 0.00$, $\zeta_0 = 0.01$.

and (6.16), respectively, and their peak values over time are considered to compute EDI_{H}. It is apparent that maximizing EDI_{H} means to maximize the hysteresis energy dissipation capability owned by the isolation system with respect to the equipment input energy. The upper limit value of E_{HD} is one, meaning that the whole input energy is dissipated through hysteresis.

Fig. 6.5 shows the sensitivity of index EDI_{H} to design parameters T_0 and $\hat{f}_{\mathrm{H}y}$. In addition, the variation of two other energy performance indices is illustrated. The one is the *Viscous Energy Dissipation Index*, defined as

$$EDI_{\mathrm{V}} = \frac{\max_{\hat{t}} \left[E_{\mathrm{V}}(\hat{t}) \right]}{\max_{\hat{t}} \left[E_i(\hat{t}) \right]} \tag{6.26}$$

where E_{V} is the viscous damping energy, given by Eq. (6.19). The other one is the *Kinetic Energy Index*, defined as

$$EI_{\mathrm{k}} = \frac{\max_{\hat{t}} \left[E_k(\hat{t}) \right]}{\max_{\hat{t}} \left[E_i(\hat{t}) \right]} \tag{6.27}$$

where E_k is the relative kinetic energy of the isolated equipment, given by Eq. (6.16). Looking at the contour plots, some clear trends can be observed. Contour lines for EDI_{H} are arranged according to an almost elliptical shape and a similar trend is found for EDI_{V} and EI_k too. It is noticed that an increase of EDI_{H} implies a decrease of EDI_{V} since a different distribution of energy dissipation is attained between hysteresis and viscous damping. Furthermore, an increase of EDI_{H} generally reduces also the kinetic energy index EI_k, that is the energy quota associated to the motion of the isolated equipment.

Given the significance of the energy performance index EDI_{H}, the proposed optimization procedure consists in determining, among the different couples $\left(T_0,\, \hat{f}_{\mathrm{H}y}\right)$ complying with the acceleration requirement in Eq. (6.24), the one that maximizes EDI_{H}. The procedure is illustrated in Fig. 6.6. The contour line where the acceleration requirement is satisfied is highlighted in Fig. 6.6 (a) and then transferred as a dashed line in Fig. 6.6 (c). It becomes apparent from Fig. 6.6 (c) that a same isolation performance in terms of equipment absolute acceleration $\hat{u}''_a$ corresponds to a wide range of values of normalized displacement $\hat{u}\, T_0^2$, depending on the design parameters. Hence, the energy criterion acts as follows. If we envelop the points where EDI_{H} is maximized at each different value of acceleration $\hat{u}''_a$, we obtain the curve traced as a continous line in Fig. 6.6 (b) and transferred as a dashed line in Fig. 6.6 (c). The intersection between this curve and the curve where the acceleration requirement is satisfied identifies the optimal design point, that is the couple $\left(T_{0\,\mathrm{opt}},\, \hat{f}_{\mathrm{H}y\,\mathrm{opt}}\right)$ complying with Eq. (6.24) and maximizing EDI_{H} at the same time. Such optimal design parameters lead also to minimize the displacement $\hat{u}\, T_0^2$, being the same acceleration $\hat{u}''_a$ (Fig. 6.6 (c)).

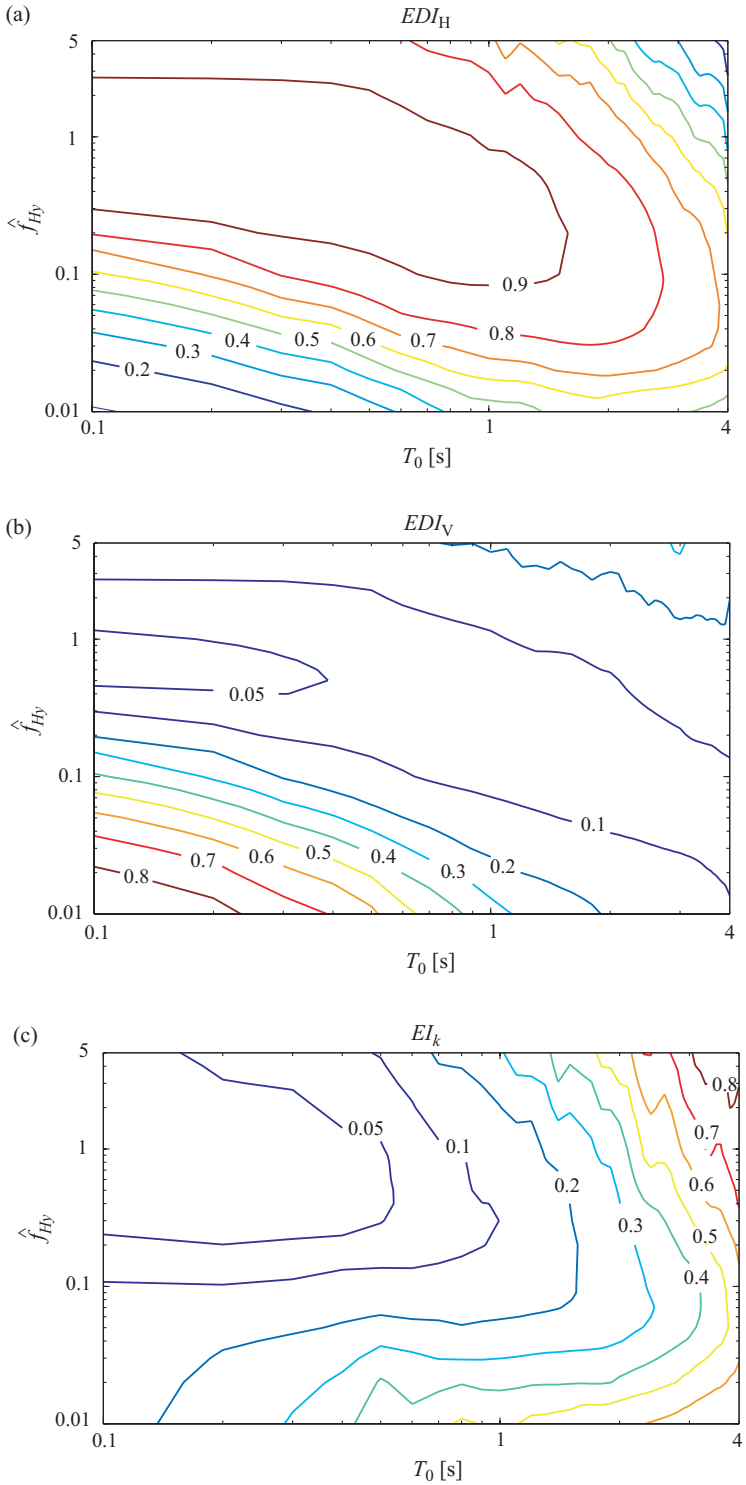

Figure 6.5. SDOF model, energy indices *vs* period T_0 and hysteretic force at nominal yielding f_{Hy}. (a) EDI_{H}. (b) EDI_{V}. (c) EI_k. It is assumed: $\hat{k}_l = 0.05$, $\hat{k}_{nl} = 0.00$, $\zeta_0 = 0.01$.

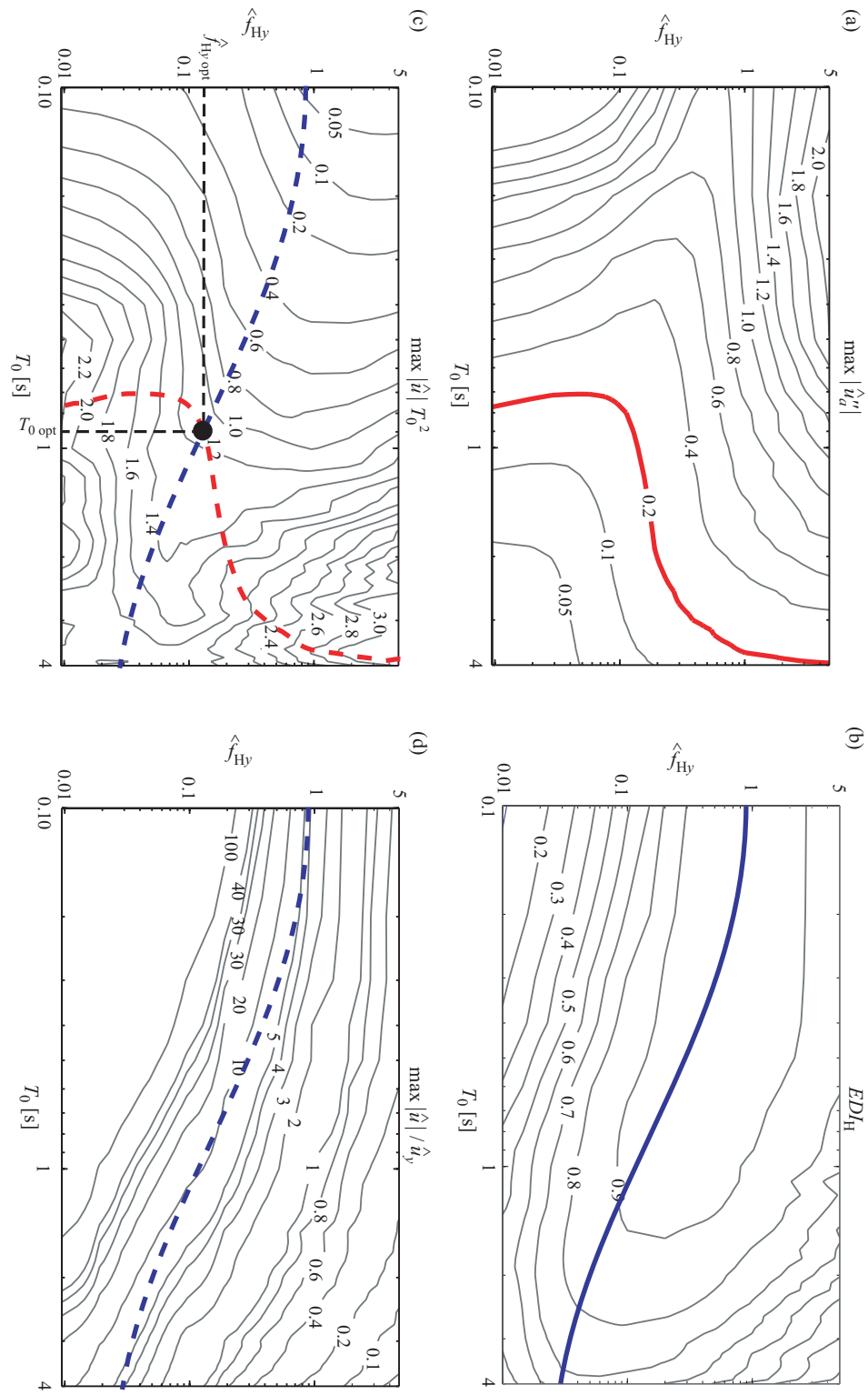

Figure 6.6. Optimal design of the equipment isolation system with nonlinear hysteretic behaviour, Operational level. (a) Acceleration criterion. (b) Energy criterion. (c) Combination of both criteria to identify the optimal design parameters $T_{0\,opt}$ and F_{Hyopt}. (d) Energy criterion and ductility demand to the isolation system.

In conclusion, the proposed optimization procedure is able to combine, at one time, the primary criterion of reducing the inertial loads on the isolated equipment with the further one of limiting its displacement. In fact, practical considerations associated with the presence of service lines and the space of installation require the equipment displacement to be within an allowable threshold. Moreover, the procedure allows the most effective end economic use of the nonlinear hysteretic isolation system. In Fig. 6.6 (d), the design curve for EDI_{H} is traced as a dashed line on the contour plot for the ratio $\hat{u}/\hat{u}_y$. Since the latter represents the ductility demand to the isolation system, it is worth noting that the design curve corresponds nearly to $\hat{u}/\hat{u}_y \cong 10$, indicating a full exploitation of the energy dissipation capability of the isolation system.

6.2.4 Parametric analyses

We investigate the sensitivity of the nonlinear hysteretic isolation system to the parameter $\hat{k}_l$, *i.e.* to the ratio between post- and pre-yielding stiffness. Sensitivity analysis is conducted by considering three values of $\hat{k}_l$ (0.01, 0.05, 0.25) and determining the optimal design parameters and the responses of the isolated equipment according to the proposed optimization procedure. Afterwards, the optimal nonlinear hysteretic isolation system is compared, as to design and performance, with an optimal isolation system with linear visco-elastic behaviour. In the linear case, the optimization procedure is carried out by setting the same acceleration requirement as in the nonlinear case (Eq. (6.24)) and investigating the sensitivity of the system to a viscous damping ratio ζ_0 ranging between 0.01 and 0.20. The results of parametric analyses are illustrated in Fig. 6.7: for the nonlinear system, they are shown *versus* the stiffness ratio $\hat{k}_l$; for the linear system, they are shown *versus* the viscous damping ratio ζ_0.

As the stiffness ratio $\hat{k}_l$ increases, the optimal design parameters of the nonlinear isolation system show the following trends: the initial period $T_{0\,\mathrm{opt}}$ increases while the nominal yielding hysteretic force $\hat{f}_{hy\,\mathrm{opt}}$ decreases or, in other terms, the isolation system tends to be more flexible and less dissipative. This is confirmed by the responses of the isolated equipment: being equal the isolation performance in terms of peak equipment acceleration $\hat{u}''_a$, both the normalized displacement $\hat{u}\,T_0^2$ and the kinetic energy index EI_k increase with increasing $\hat{k}_l$. Conversely, the optimization criterion based on the maximization of the energy dissipation index EDI_{H} caused the ductility demand $\hat{u}/\hat{u}_y$ to be almost constant and equal to 10 for $\hat{k}_l$ between 0.05 and 0.25. For $\hat{k}_l = 0.01$, the ductility demand is even greater, up to 15. In general, and unless specific design prescription, a value of $\hat{k}_l$ as low as possible may be recognized as favourable for the nonlinear hysteretic isolation system.

From the comparison with the optimal linear isolation system, the following remarks are pointed out. On the one hand, the isolation performance in terms of peak equipment acceleration is the same for both the systems since the same optimization criterion has been adopted ($\max_{\hat{t}} \left|\hat{u}''_a\right| = 0.2$). On the other hand, the linear isolation system undergoes greater normalized displacements $\hat{u}\,T_0^2$ and greater values of the

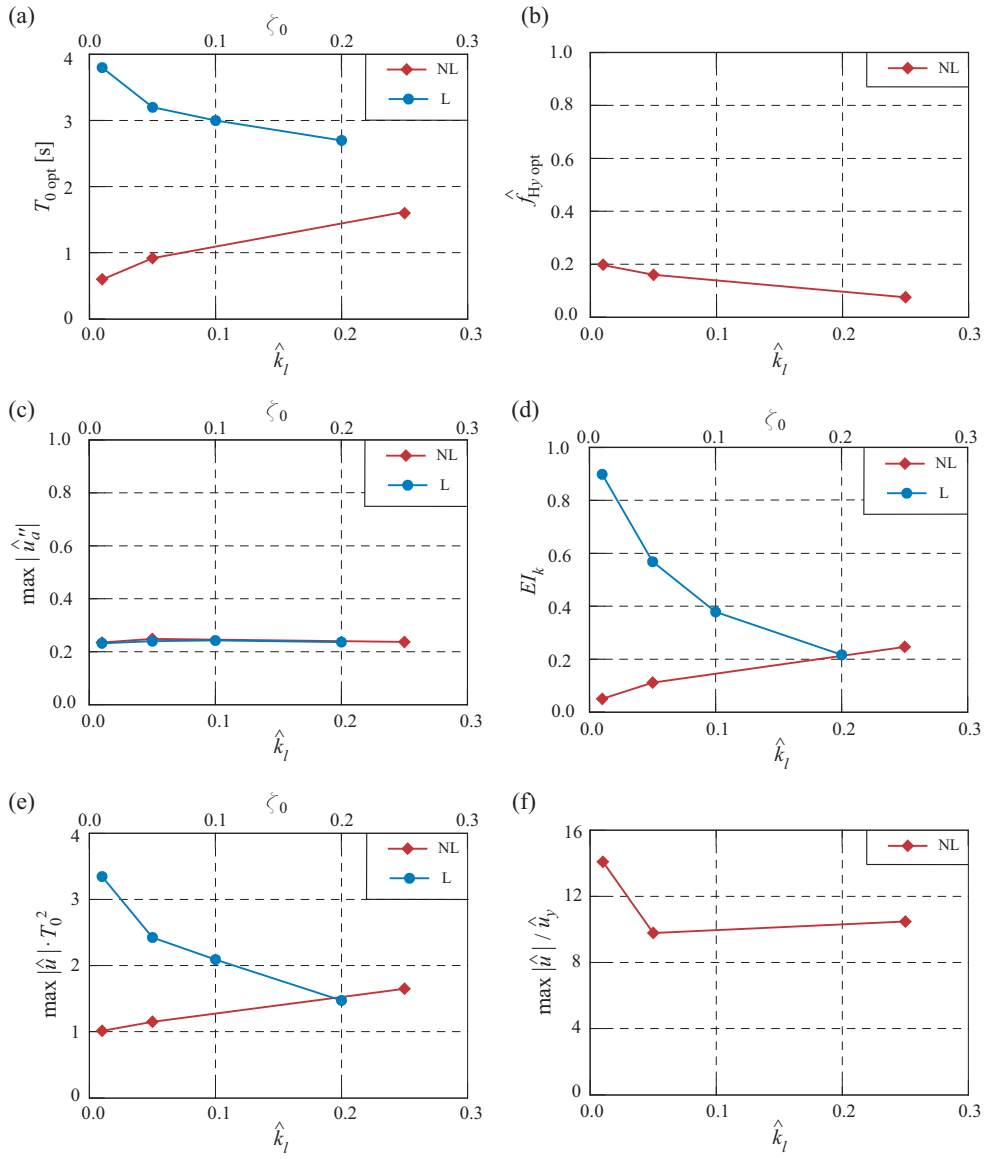

Figure 6.7. SDOF model, comparisons between the optimal design of the nonlinear (NL) and the linear (L) isolation systems. For the nonlinear system, it is assumed $\hat{k}_{nl} = 0.00$, $\zeta_0 = 0.01$ and results are shown *vs* the stiffness ratio $\hat{k}_l$. For the linear system, results are shown *vs* the viscous damping ratio ζ_0. (a) Optimal period $T_{0\,\mathrm{opt}}$. (b) Optimal hysteretic force at nominal yielding $\hat{f}_{Hy\,\mathrm{opt}}$. (c) Peak absolute acceleration $\hat{u}_a''$. (d) Kinetic energy index EI_k. (e) Peak normalized displacement $\hat{u}\,T_0^2$. (f) Peak displacement ratio $\hat{u}/\hat{u}_y$.

kinetic energy index EI_k. As the viscous damping ratio ζ_0 increases, however, both $\hat{u}\,T_0^2$ and EI_k decrease, down to become comparable with the average values given for the nonlinear isolation system when $\zeta_0 = 0.20$.

In conclusion, it is worth noting that the optimal design period $T_{0\,\mathrm{opt}}$ for the linear isolation system is more than twice greater than the one for the nonlinear system. This means that the nonlinear system is able to achieve the same isolation performance as the linear system, yet having a much higher initial stiffness. Hence, the nonlinear isolation system outperforms the linear one also in static conditions, since it could benefit from a higher initial stiffness to limit its static displacement as well.

6.3 Decoupled approach: seismic analyses

The optimal design of the nonlinear hysteretic isolation system is carried out by assuming, as the seismic input, a set of seven artificial accelerograms matching the response spectrum given by the code. Since this kind of input is typically a broad-band excitation, the effectiveness of the isolation system is assessed for the different frequency content of natural earthquakes by means of numerical analyses. Comparisons with an optimal isolation system with linear visco-elastic behaviour are eventually provided.

6.3.1 Natural earthquakes

Four natural accelerograms (Fig. 6.8), recorded during historical earthquakes and selected from the database of the Pacific Earthquake Engineering Research Center [100], were used in the seismic analyses. Detailed information about these seismic inputs is given below:

- Imperial Valley Earthquake (May 19, 1940), record from El Centro Array Station, NS component.
- Tokachi-oki earthquake (May 16, 1968), record from Hachinohe Station, NS component.
- Northridge earthquake (January 17, 1994), record from Sylmar Station - Olive View Medical Center, NS component.
- Kobe earthquake (January 16, 1995), record from KJMA Station, NS component.

Selected earthquake records have been widely used in earthquake engineering research. Among them, records from Kobe (KJMA) and Northridge (Sylmar) earthquakes are characterized by one or more dominant long-period pulses, so they are typically classified as near-fault ground motions [15]. Records from Imperial Valley (El Centro) and Tokachi-oki (Hachinohe) earthquakes are instead broad-frequency-band excitations, so they are used to represent far-field ground motions. Since the seismic analyses are performed in non-dimensional terms by making use of Eqs. (6.9), the seismic inputs are non-dimensionalized accordingly by using the characteristics values given in Eq. (6.2). Due to the non-dimensionalization, the PGA of the seismic inputs is unitary.

6.3.2 Evaluation of seismic effectiveness

In this subsection, it is investigated the influence of input frequency content on the seismic effectiveness of the nonlinear hysteretic isolation system. The isolation system is designed according to the proposed optimization procedure and its performance is compared under the design input as well as natural accelerograms. Fig. 6.9 illustrates the results of the numerical analyses, carried out by considering three values of the parameter $\hat{k}_l$ (0.01, 0.05, 0.25), and the following observations can be made.

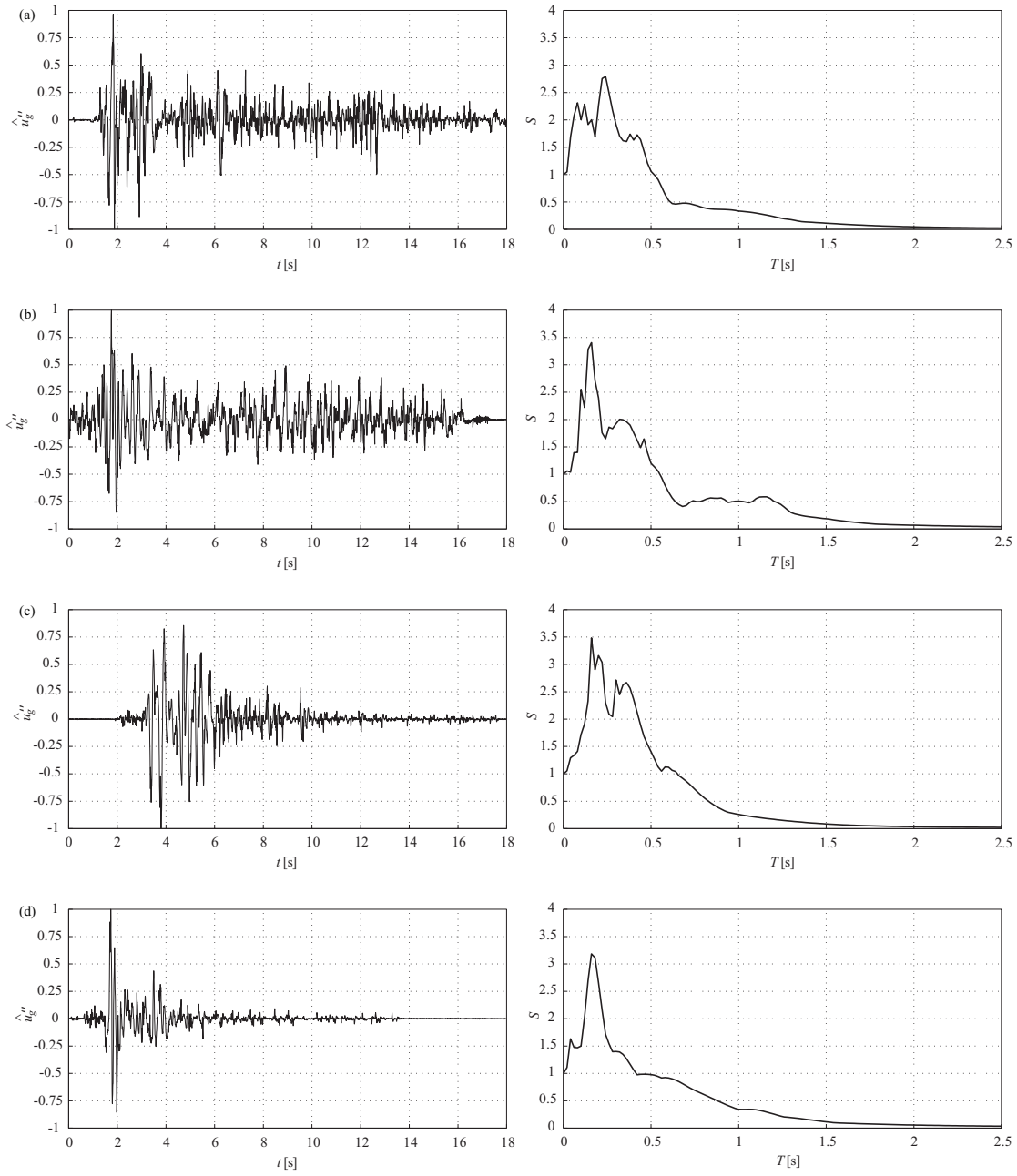

Figure 6.8. Natural earthquakes: accelerograms and elastic response spectra (5% damping) with unitary non-dimensional PGA. (a) El Centro. (b) Hachinohe. (c) Kobe. (d) Northridge.

As to the isolation performance, El Centro and Kobe accelerograms are comparable to the design input over all the spanned range of $\hat{k}_l$: the peak absolute acceleration $\hat{u}_a''$ transmitted to the equipment is reduced to the optimal value 0.2 and the normalized displacement $\hat{u}\,T_0^2$ slightly increases with increasing $\hat{k}_l$. Conversely, for Hachinohe and Northridge accelerograms, values of both $\hat{u}_a''$ and $\hat{u}\,T_0^2$ are almost comparable to the design ones only when $\hat{k}_l < 0.05$, while they become much higher with increasing $\hat{k}_l$.

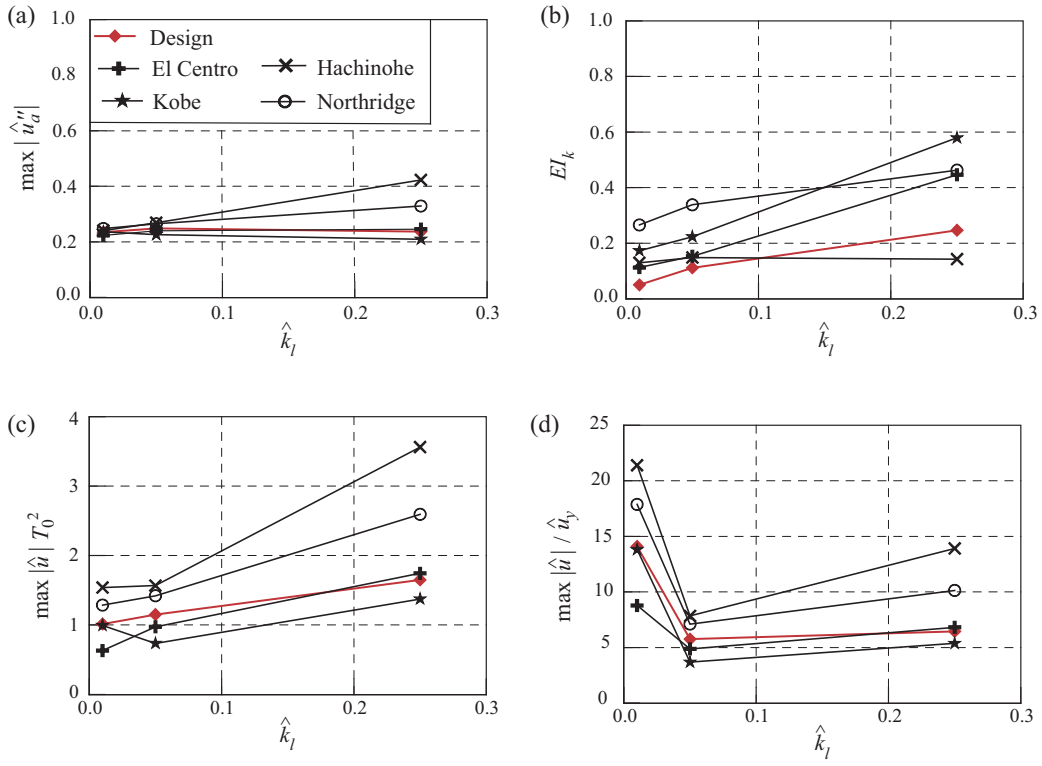

Figure 6.9. SDOF model, seismic effectiveness of the optimal nonlinear isolation system: comparisons between the design input and the scaled natural accelerograms. (a) Peak absolute acceleration $\hat{u}_a''$. (b) Kinetic energy index EI_k. (c) Peak normalized displacement $\hat{u}\,T_0^2$. (d) Peak displacement ratio $\hat{u}/\hat{u}_y$. It is assumed: $\hat{k}_{nl} = 0.00$, $\zeta_0 = 0.01$.

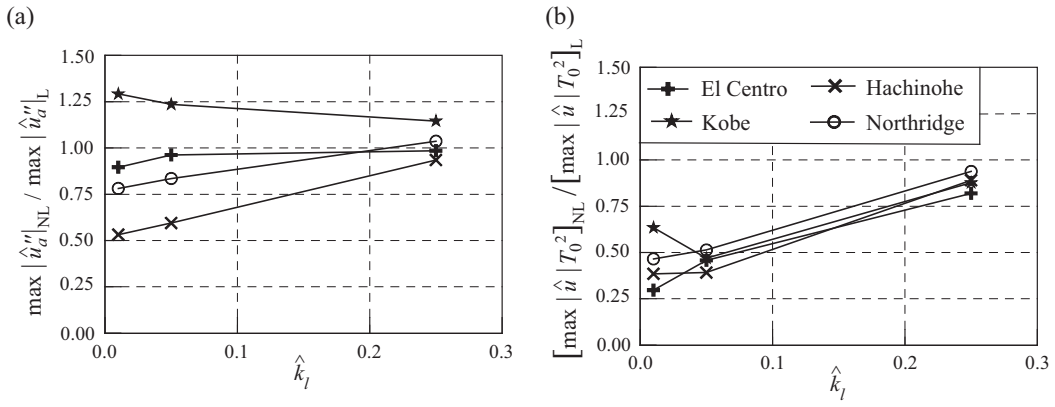

Figure 6.10. SDOF model, seismic effectiveness of the optimal nonlinear and linear isolation systems. (a) Ratio of peak absolute acceleration $\hat{u}_a''$. (b) Ratio of peak normalized displacement $\hat{u}\,T_0^2$. For the nonlinear system, it is assumed: $\hat{k}_{nl} = 0.00$, $\zeta_0 = 0.01$. For the linear system, it is assumed: $\zeta_0 = 0.10$.

As a consequence, also the ductility demand $\hat{u}/\hat{u}_y$ show the same trend. It must therefore be concluded that the frequency content of the seismic input might affect the effectiveness of the isolation system depending on the value of the ratio $\hat{k}_l$ between the post- to pre- yielding stiffness: the higher is $\hat{k}_l$, the greater is this influence, as far as becomes a crucial issue for an effective seismic design. A value of $\hat{k}_l$ as low as possible is then recognized as favourable for the nonlinear hysteretic isolation system.

6.3.3 Comparisons with linear isolation

In this subsection, the performance achieved under the different natural accelerograms by the nonlinear system with hysteretic behaviour is compared to that of a linear system with visco-elastic behaviour. The latter is designed by setting the same design input and the same acceleration requirement as for the nonlinear system, while assuming a viscous damping ratio ζ_0 equal to 0.10, a standard value for elastomeric bearings.

For the purpose of comparison, Fig. 6.10 illustrates the ratios of the equipment peak absolute acceleration $\hat{u}''_a$ and normalized displacement $\hat{u}\,T_0^2$ between the nonlinear and the linear cases. Values of these ratios below unity indicate, therefore, that the nonlinear system is outperforming the linear one.

The analysis of the results highlights the following remarks. Although a same optimization criterion is adopted for both the systems in terms of acceleration response, the accelerations transmitted by the nonlinear system are smaller under three out of four accelerograms (El Centro, Hachinohe, Northridge). Reductions amount up to $40\% - 50\%$ under Hachinohe accelerogram and for values of the parameter $\hat{k}_l$ less than 0.1. In only one case (Kobe), the isolation performance of the linear system is better than that of the nonlinear system.

In addition to the acceleration requirement, limiting the displacements is indeed a crucial point in implementing an isolation system for the sake of safety and functionality. The nonlinear system results to undergo smaller equipment displacements, with a performance comparable under the different seismic input. Reductions are particularly significant $(50\% - 70\%)$ when $\hat{k}_l$ is less than 0.1, while they tend to decrease as $\hat{k}_l$ increases. This is due to the fact that, as $\hat{k}_l$ increases, the contribution of the elastic component in the total restoring force increases, at the expense of the hysteretic component and of the energy dissipation capabilities owned by the nonlinear system due to hysteresis.

6.4 Coupled approach: reduced order 2-DOF model

6.4.1 Equations of motion

Let us consider the equation of motion given by Eqs. (3.17) for the reduced order 2-DOF model. Let $u_2(t) - u_1(t)$ and f be the displacement and the total restoring force across the isolation system, respectively. Let the force f be described by the nonlinear hysteretic constitutive model given by Eqs. (5.17)-(5.20) in Sec 5.3.4. The system of interest is depicted in Fig. 6.11 and its equations of motion are drawn in the form

$$m_1\ddot{u}_1 + c_1\dot{u}_1 + k_1 u_1 = -m_1\ddot{u}_g + f \tag{6.28a}$$

$$m_2\ddot{u}_2 = -m_2\ddot{u}_g - f \tag{6.28b}$$

$$f = k_l\,(u_2 - u_1) + k_{nl}\,(u_2 - u_1)^3 + f_{\mathrm{H}} + c\,(\dot{u}_2 - \dot{u}_1) \tag{6.28c}$$

$$f_{\mathrm{H}} = \begin{cases} f_{\mathrm{H}}^{+} = \dfrac{1}{\beta}\left(1 - \mathrm{e}^{-\gamma\,(u_2 - u_1 + u_r)}\right), & (\dot{u}_2 - \dot{u}_1) \geq 0 \\ f_{\mathrm{H}}^{-} = -\dfrac{1}{\beta}\left(1 - \mathrm{e}^{\gamma\,(u_2 - u_1 - u_r)}\right), & (\dot{u}_2 - \dot{u}_1) < 0 \end{cases} \tag{6.28d}$$

where $m_1,\ k_1,\ c_1$ are the generalized mass, stiffness and damping coefficients of the supporting structure; m_2 is the mass of the isolated equipment; $\beta,\ \gamma \in \mathbb{R}^+$ and $k_l,\ k_{nl},\ c \in \mathbb{R}_0^+$ are the parameters of the nonlinear hysteretic constitutive model; $u_r \in \mathbb{R}_0^+$ is the residual hysteresis displacement. To attempt a more general description of the problem, Eqs. (6.28) are non-dimensionalized by setting the following characteristic values of frequency, displacement and force

$$\begin{aligned} \omega^* &= \sqrt{\frac{k_0}{m_2}} && \text{with } k_0 = k_l + \frac{\gamma}{\beta} \\ u^* &= \frac{m_2\,a_g}{k_0} && \text{with } a_g = \max_t\left[\left|\ddot{u}_g(t)\right|\right] \\ f^* &= m_2\,a_g \end{aligned} \tag{6.29}$$

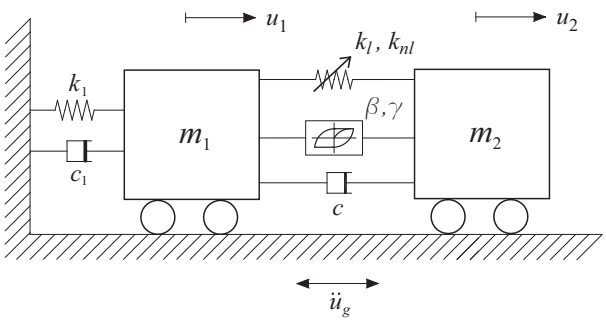

Figure 6.11. 2-DOF model with the nonlinear hysteretic isolation system.

It is worth noting that, being k_0 the stiffness tangent to the virgin loading curve of the model for $u_2 - u_1 = 0$, ω^* is the uncoupled dimensional circular frequency of the nonlinear isolation for small-amplitude oscillations. The following non-dimensional variables are then assumed

$$\hat{t} = \omega^* t, \qquad \hat{u}_1 = \frac{u_1}{u^*}, \qquad \hat{u}_2 = \frac{u_2}{u^*}, \qquad \hat{u}_r = \frac{u_r}{u^*}, \qquad \hat{f} = \frac{f}{f^*} \tag{6.30}$$

while differentiation with respect to the non-dimensional time $\hat{t}$ is expressed as indicated earlier in Eq. (6.4) and denoted with symbol $'$. After introducing the following non-dimensional parameters

$$\begin{aligned}
&\mu = \frac{m_2}{m_1}, \qquad \zeta_1 = \frac{c_1}{2\sqrt{m_1 k_1}}, \\
&\lambda = \frac{T_0}{T_1} \qquad \text{with} \quad T_0 = 2\pi\sqrt{k_0/m_2} \quad \text{and} \quad T_1 = 2\pi\sqrt{k_1/m_1}, \\
&\hat{k}_l = \frac{k_l}{k_0}, \qquad \hat{k}_{nl} = k_{nl}\frac{(m_2\, a_g)^2}{k_0^3}, \qquad \zeta_0 = \frac{c}{2\sqrt{m_2 k_0}} \\
&\hat{\beta} = \beta\, m_2 a_g, \qquad \hat{\gamma} = \gamma\, \frac{m_2 a_g}{k_0}
\end{aligned} \tag{6.31}$$

and defining the non-dimensional base acceleration as given in Eq. (6.8), the non-dimensional form of the equations of motion results to be

$$\frac{1}{\mu}\,\hat{u}_1'' + \frac{2\zeta_1\lambda}{\mu}\,\hat{u}_1' + \frac{\lambda^2}{\mu}\,\hat{u}_1 = -\frac{1}{\mu}\,\hat{u}_g'' + \hat{f} \tag{6.32a}$$

$$\hat{u}_2'' = -\hat{u}_g'' - \hat{f} \tag{6.32b}$$

$$\hat{f} = \hat{k}_l\,(\hat{u}_2 - \hat{u}_1) + \hat{k}_{nl}\,(\hat{u}_2 - \hat{u}_1)^3 + \hat{f}_{\mathrm{H}} + 2\zeta_0\,(\hat{u}_2' - \hat{u}_1') \tag{6.32c}$$

$$\hat{f}_{\mathrm{H}} = \begin{cases} \hat{f}_{\mathrm{H}}^{+} = \dfrac{1}{\hat{\beta}}\left(1 - \mathrm{e}^{-\hat{\gamma}\,(\hat{u}_2 - \hat{u}_1 + \hat{u}_r)}\right), & (\hat{u}_2' - \hat{u}_1') \geq 0 \\ \hat{f}_{\mathrm{H}}^{-} = -\dfrac{1}{\hat{\beta}}\left(1 - \mathrm{e}^{\hat{\gamma}\,(\hat{u}_2 - \hat{u}_1 - \hat{u}_r)}\right), & (\hat{u}_2' - \hat{u}_1') < 0 \end{cases} \tag{6.32d}$$

Remark 3 *The constraints stated in Eqs.* (6.12) *and* (6.13) *for the non-dimensional equations of the SDOF model, hold also for the non-dimensional equations of the 2-DOF model.*

6.4.2 Energy balance

The equations of relative energy balance for the 2-DOF model are obtained by considering one degree of freedom at a time.

First, we consider the equation of motion of the supporting structure, Eq. (6.32a). The equation of relative energy balance is obtained by multiplying both members by the relative velocity $\hat{u}_1'$ and integrating over time, yielding

$$E_{k1}(\hat{t}) + E_{\mathrm{V}1}(\hat{t}) + E_{\mathrm{E}1}(\hat{t}) = E_{i1}(\hat{t}) + E_f(\hat{t}) \tag{6.33}$$

where

$$E_{k1}(\hat{t}) = \int_0^{\hat{t}} \frac{1}{\mu}\, \hat{u}_1''\, \hat{u}_1'\, \mathrm{d}\tau = \frac{1}{2\mu}\, \hat{u}_1'^2(\hat{t}) \tag{6.34}$$

is the relative kinetic energy,

$$E_{\mathrm{V}1}(\hat{t}) = \int_0^{\hat{t}} \frac{2\zeta_1\lambda}{\mu}\, \hat{u}_1'^2\, \mathrm{d}\tau \tag{6.35}$$

is the viscous damping energy,

$$E_{\mathrm{E}1}(\hat{t}) = \int_0^{\hat{t}} \frac{\lambda^2}{\mu}\, \hat{u}_1\, \hat{u}_1'\, \mathrm{d}\tau = \frac{\lambda^2}{2\mu}\, \hat{u}_1^2 \tag{6.36}$$

is the elastic strain energy,

$$E_{i1}(\hat{t}) = \int_0^{\hat{t}} -\frac{1}{\mu}\, \hat{u}_g''\hat{u}_1'\, \mathrm{d}\tau \tag{6.37}$$

is the input energy,

$$E_f(\hat{t}) = \int_0^{\hat{t}} \hat{f}\hat{u}_1'\, \mathrm{d}\tau \tag{6.38}$$

is the energy flow transmitted by the equipment to the supporting structure through the isolation system.

Secondly, we consider the equation of motion of the equipment, Eq. (6.32b), and we multiply both members by the relative velocity $\hat{u}_2'$

$$\hat{u}_2''\, \hat{u}_2' = -\hat{u}_g''\, \hat{u}_2' - \hat{f}\, \hat{u}_2' \tag{6.39}$$

Eq. (6.39) can be then rewritten in the form

$$\hat{u}_2''\, \hat{u}_2' = -\hat{u}_g''\, \hat{u}_2' - \hat{f}\, (\hat{u}_2' - \hat{u}_1') - \hat{f}\, \hat{u}_1' \tag{6.40}$$

By integrating Eq. (6.40) over time, we obtain the equation of relative energy balance

$$E_{k2}(\hat{t}) = E_{i2}(\hat{t}) - E_f(\hat{t}) - E_{\mathrm{E}2}(\hat{t}) - E_{\mathrm{H}2}(\hat{t}) - E_{\mathrm{V}2}(\hat{t}) \tag{6.41}$$

where

$$E_{k2}(\hat{t}) = \int_0^{\hat{t}} \hat{u}_2'' \, \hat{u}_2' \, \mathrm{d}\tau = \frac{1}{2} \, \hat{u}_2'^2(\hat{t}) \tag{6.42}$$

is the relative kinetic energy,

$$E_{i2}(\hat{t}) = \int_0^{\hat{t}} -\hat{u}_g'' \, \hat{u}_2' \, \mathrm{d}\tau \tag{6.43}$$

is the input energy, $E_f(\hat{t})$ is the energy flow between the equipment and the supporting structure, as defined in Eq. (6.38),

$$\begin{aligned} E_{\mathrm{E2}}(\hat{t}) &= \int_0^{\hat{t}} \left(\hat{k}_l \, (\hat{u}_2 - \hat{u}_1) + \hat{k}_{nl} \, (\hat{u}_2 - \hat{u}_1)^3 \right) (\hat{u}_2' - \hat{u}_1') \, \mathrm{d}\tau = \\ &= \frac{1}{2} \, \hat{k}_l \left(\hat{u}_2(\hat{t}) - \hat{u}_1(\hat{t}) \right)^2 + \frac{1}{4} \, \hat{k}_{nl} \left(\hat{u}_2(\hat{t}) - \hat{u}_1(\hat{t}) \right)^4 \end{aligned} \tag{6.44}$$

is the pure elastic strain energy,

$$E_{\mathrm{H2}}(\hat{t}) = \int_0^{\hat{t}} \hat{f}_{\mathrm{H}} \, (\hat{u}_2' - \hat{u}_1') \, \mathrm{d}\tau \tag{6.45}$$

is the strain energy due to the hysteretic force $\hat{f}_H$

$$E_{\mathrm{V2}}(\hat{t}) = \int_0^{\hat{t}} 2\zeta_0 \, (\hat{u}_2' - \hat{u}_1')^2 \, \mathrm{d}\tau \tag{6.46}$$

is the viscous damping energy.

Energy $E_{\mathrm{H2}}(\hat{t})$ is in turn composed by the sum of a recoverable elastic energy $E_{\mathrm{HE2}}(\hat{t})$ plus an irrecoverable energy $E_{HD2}(\hat{t})$ dissipated on hysteresis loops

$$E_{\mathrm{H2}}(\hat{t}) = E_{\mathrm{HE2}}(\hat{t}) + E_{\mathrm{HD2}}(\hat{t}) \tag{6.47}$$

Making use of the nominal elastic-perfectly plastic constitutive relationship associated with $\hat{f}_{\mathrm{H}}$ and of the nominal elastic stiffness, given as

$$\left. \frac{\partial \hat{f}_{\mathrm{H}}}{\partial (\hat{u}_2 - \hat{u}_1)} \right|_{(\hat{u}_2 - \hat{u}_1)=0, \, \hat{u}_r=0} = \frac{\hat{\gamma}}{\hat{\beta}} \tag{6.48}$$

it is obtained

$$E_{\mathrm{HE2}}(\hat{t}) = \frac{1}{2} \, \frac{\hat{f}_{\mathrm{H}}^2(\hat{t})}{\hat{\gamma}/\hat{\beta}} \tag{6.49}$$

and consequently

$$E_{\mathrm{HD2}}(\hat{t}) = E_{\mathrm{H2}}(\hat{t}) - E_{\mathrm{HE2}}(\hat{t}) \tag{6.50}$$

6.5 Coupled approach: optimal design of the equipment isolation system

In Sec. 6.2, we have developed, in the framework of a decoupled approach, an optimal design methodology for the equipment isolation with nonlinear hysteretic behaviour. In the present section, we extend the methodology to the case of a coupled approach. When the dynamic interaction between the equipment and the supporting structure is expected to be significant, this approach allows to account for it: the structure, or primary subsystem, and the equipment, or secondary subsystem, are considered as coupled parts of a primary – secondary system and analyzed together.

The same performance objective and the same artificial seismic input as in Sec. 6.2.2 are assumed for design purposes. A similar optimization procedure involving both the reduction of the peak equipment absolute acceleration and the maximization of the energy dissipation in the isolation system is proposed. Although the parameter space results to be augmented as compared to the decoupled approach, two are still recognized as the design parameters for the Operational performance level: the ratio λ between the uncoupled natural periods of the equipment and of the supporting structure; the non-dimensional hysteretic force $\hat{f}_{\mathrm{H}y} = 1/\hat{\beta}$ at the nominal yielding of the isolation system. Known data of the problem are: the mass ratio μ between the equipment and the structure; the uncoupled natural period T_1 and viscous damping ratio ζ_1 of the structure; non-dimensional stiffness coefficients $\hat{k}_l$ and $\hat{k}_{nl}$ and the viscous damping ratio ζ_0 of the isolation system. Meanwhile, non-dimensional parameter $\hat{\gamma}$ is required to comply with the constraint from Eq. (6.12).

In Fig. 6.12, the peak values of the equipment absolute acceleration $\hat{u}''_{a2}$ and of the equipment displacement $\left(\hat{u}_2 - \hat{u}_1\right)$ relative to the supporting structure are illustrated *versus* the design parameters λ and $\hat{f}_{\mathrm{H}y}$. In order to make the response comparable between different systems, the relative displacement is normalized, on the one hand, by multiplying the squared period T_0^2, on the other hand, by dividing by the value $\left(\hat{u}_2 - \hat{u}_1\right)_y$ corresponding to the nominal yielding. As an example, the following set of known data is assumed: $T_1 = 0.5$ s, $\zeta_1 = 0.02$, $\mu = 0.50$, $\hat{k}_l = 0.05$, $\hat{k}_{nl} = 0.00$, $\zeta_0 = 0.01$. To a first approximation, the hardening coefficient $\hat{k}_{nl}$ is considered to be null and, as a consequence, non-dimensional parameter $\hat{k}_l$ takes on the meaning of the ratio between the post- and the pre-yielding stiffness. A small damping ratio ζ_0 is taken into account for numerical stability reason.

For the sake of completeness, contour plots in Fig. 6.13 show the sensibility to the design parameters of the supporting structure responses: the peak non-dimensional absolute acceleration $\hat{u}''_{a1}$ and the peak non-dimensional displacement $\hat{u}_1$, normalized by multiplying the squared period T_0^2.

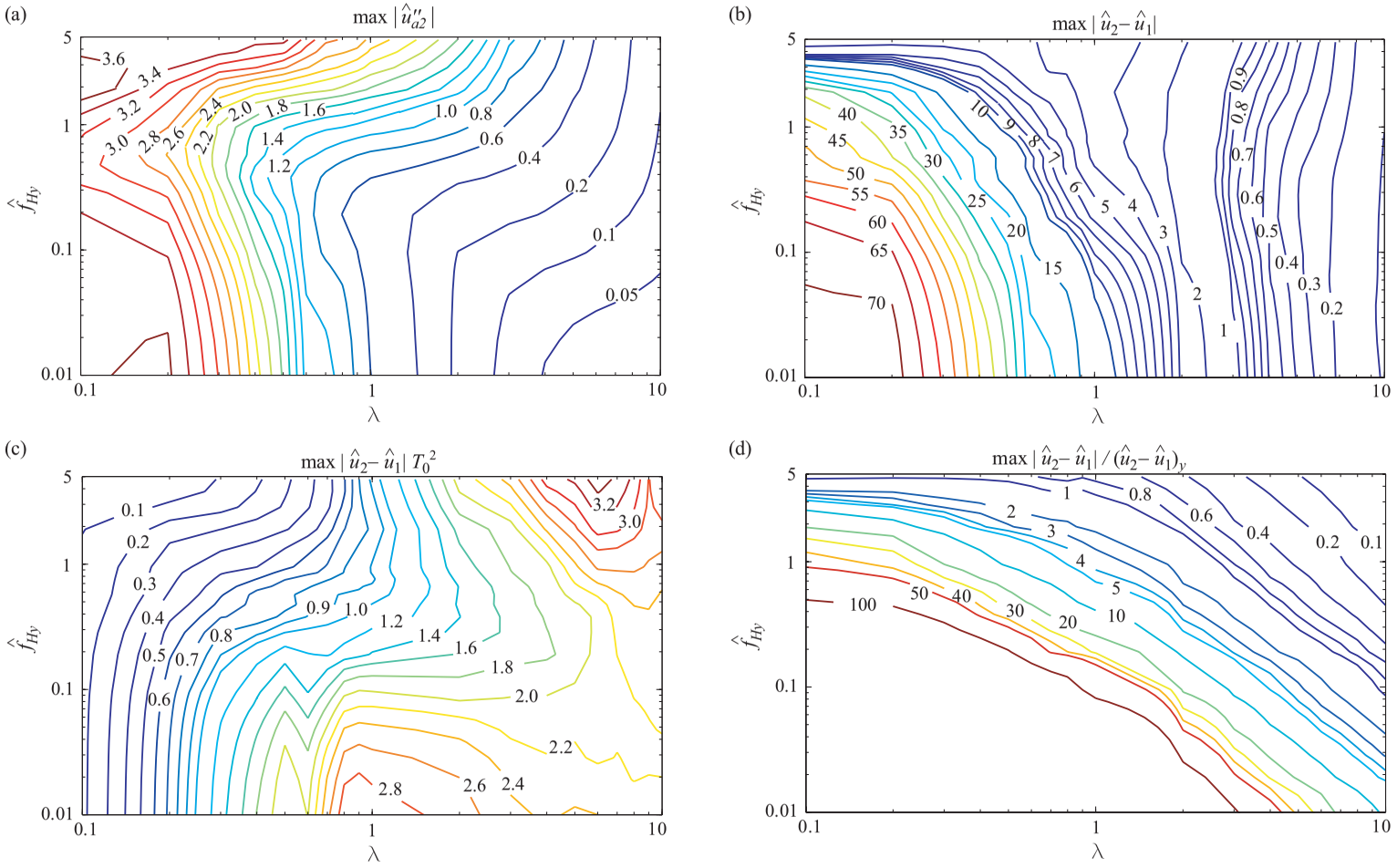

Figure 6.12. 2-DOF model, peak non-dimensional responses of the equipment *vs* period ratio λ and hysteretic force at nominal yielding $\hat{f}_{Hy}$. (a) Absolute acceleration $\hat{u}''_{a2}$. (b) Relative displacement $(\hat{u}_2 - \hat{u}_1)$ with respect to the supporting structure. (c) Normalized relative displacement $(\hat{u}_2 - \hat{u}_1)\, T_0^2$. (d) Relative displacement ratio $(\hat{u}_2 - \hat{u}_1)/(\hat{u}_2 - \hat{u}_1)_y$. It is assumed: $T_1 = 0.5$ s, $\zeta_1 = 0.02$, $\mu = 0.50$, $\hat{k}_l = 0.05$, $\hat{k}_{nl} = 0.00$, $\zeta_0 = 0.01$.

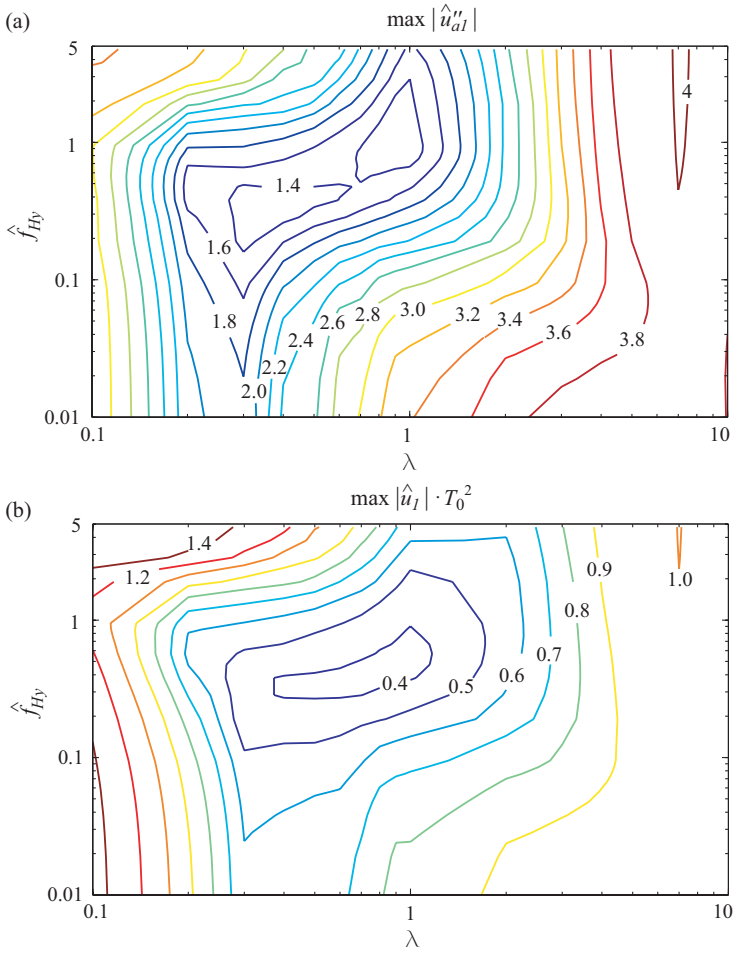

Figure 6.13. 2-DOF model, peak non-dimensional responses of the supporting structure *vs* period ratio λ and hysteretic force at nominal yielding $\hat{f}_{Hy}$. (a) Absolute acceleration $\hat{u}''_{a1}$. (b) Normalized displacement $\hat{u}_1\, T_0^2$. It is assumed: $T_1 = 0.5$ s, $\zeta_1 = 0.02$, $\mu = 0.50$, $\hat{k}_l = 0.05$, $\hat{k}_{nl} = 0.00$, $\zeta_0 = 0.01$.

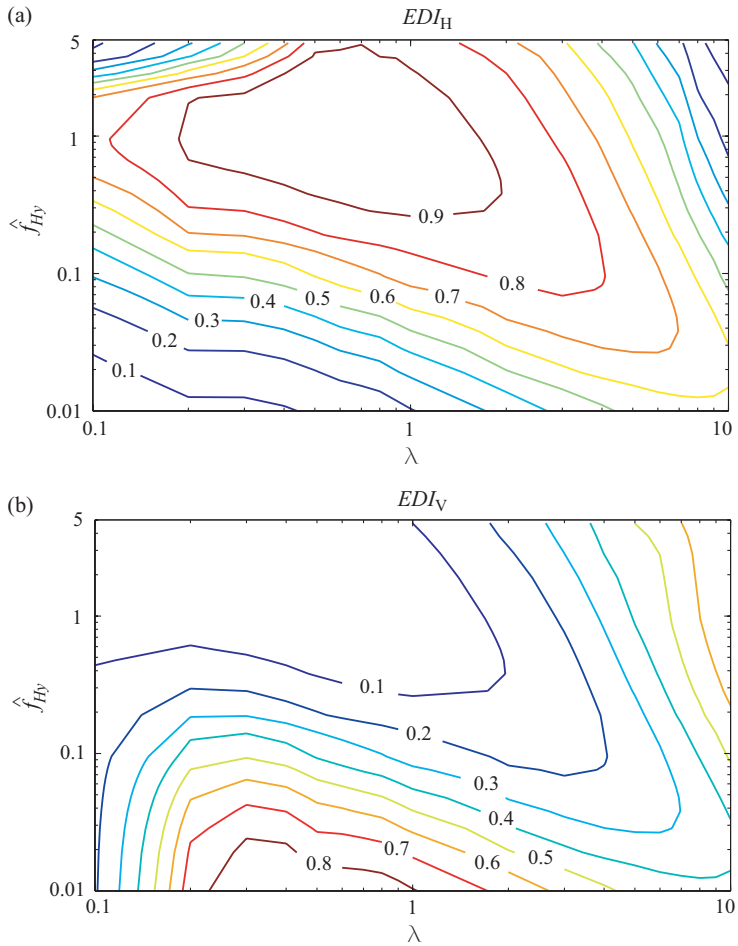

Figure 6.14. 2-DOF model, energy indices *vs* period ratio λ and hysteretic force at nominal yielding $\hat{f}_{Hy}$. (a) EDI_{H}. (b) EDI_{V}. It is assumed: $T_1 = 0.5$ s, $\zeta_1 = 0.02$, $\mu = 0.50$, $\hat{k}_l = 0.05$, $\hat{k}_{nl} = 0.00$, $\zeta_0 = 0.01$.

The same optimization procedure adopted for the decoupled approach is here extended to the coupled approach. On the one hand, with the aim of protecting the isolated equipment from excessive inertial loads, the peak absolute acceleration transmitted to it is required to be 20% of PGA a_g

$$\max_{\hat{t}} \left|\hat{u}''_{a2}(\hat{t})\right| = \frac{\max_t \left|\ddot{u}_{a2}(t)\right|}{a_g} = 0.2 \tag{6.51}$$

On the other hand, the energy dissipation capability of the hysteretic isolation

system is fully exploited through the maximization of the hysteresis energy dissipation index EDI_{H}. The definition of EDI_{H}, given in Eq. (6.25) for the SDOF model, is extended to the 2-DOF model as follows

$$EDI_{\mathrm{H}} = \frac{\max_{\hat{t}} \left[E_{\mathrm{HD2}}(\hat{t}) \right]}{\max_{\hat{t}} \left[E_{i2}(\hat{t}) - E_f(\hat{t}) \right]} \tag{6.52}$$

where E_{HD2} is the irrecoverable energy dissipated through hysteresis in the isolation system and $(E_{i2} - E_f)$ is the "net" input energy to the equipment, *i.e.* the total input energy E_{i2} deducted the energy flow E_f from the equipment to the supporting structure. In Fig. 6.14, the sensitivity of index EDI_{H} to the design parameters is shown. For comparison purposes, the figure illustrates also the viscous energy dissipation index EDI_{V}, whose definition is given for the 2-DOF model as follows

$$EDI_{\mathrm{V}} = \frac{\max_{\hat{t}} \left[E_{\mathrm{V2}}(\hat{t}) \right]}{\max_{\hat{t}} \left[E_{i2}(\hat{t}) - E_f(\hat{t}) \right]} \tag{6.53}$$

As earlier noticed, the joint indices EDI_{H} and EDI_{V} are representative of the distribution, between hysteresis and viscous damping, of the energy dissipation into the isolation system.

The optimization procedure is illustrated in Fig. 6.15. The contour line where the acceleration requirement is satisfied is highlighted as a red continuous line in Fig. 6.15 (a). It becomes apparent that a same isolation performance in terms of equipment peak absolute acceleration $\hat{u}''_{a2}$ may correspond to a wide range of values of normalized peak displacement $\left(\hat{u}_2 - \hat{u}_1\right) T_0^2$, depending on the design parameters. Hence, the energy criterion acts as follows. If we envelop the points where EDI_{H} is maximized for each value (*i.e.* contour line) of peak acceleration $\hat{u}''_{a2}$, we obtain the curve traced as a blue continous line in Fig. 6.15 (b). In Fig. 6.15 (c), the design curve for EDI_{H} (the blue one) and the design curve for $\hat{u}''_{a2}$ (the red one) are traced as dashed lines. The intersection between them identifies the optimal design point, that is the couple $(\lambda_{\mathrm{opt}},\, f_{\mathrm{H}y\,\mathrm{opt}})$ complying with Eq. (6.51) and maximizing EDI_{H} at the same time; such optimal design parameters lead also to minimize the displacement $\left(\hat{u}_2 - \hat{u}_1\right) T_0^2$ among the all points on the same contour line for peak acceleration $\hat{u}''_{a2}$.

Moreover, the procedure allows the most effective and economic use of the nonlinear hysteretic isolation system. In 6.15 (d), the design curve for EDI_{H} is traced as a dashed line on the contour plot for the relative displacement ratio $\left(\hat{u}_2 - \hat{u}_1\right) / \left(\hat{u}_2 - \hat{u}_1\right)_y$. Since the latter represents the ductility demand to the isolation system, it is worth noting that the design curve corresponds nearly to $\left(\hat{u}_2 - \hat{u}_1\right) / \left(\hat{u}_2 - \hat{u}_1\right)_y \cong 10$ indicating a full exploitation of the energy dissipation capability of the isolation system.

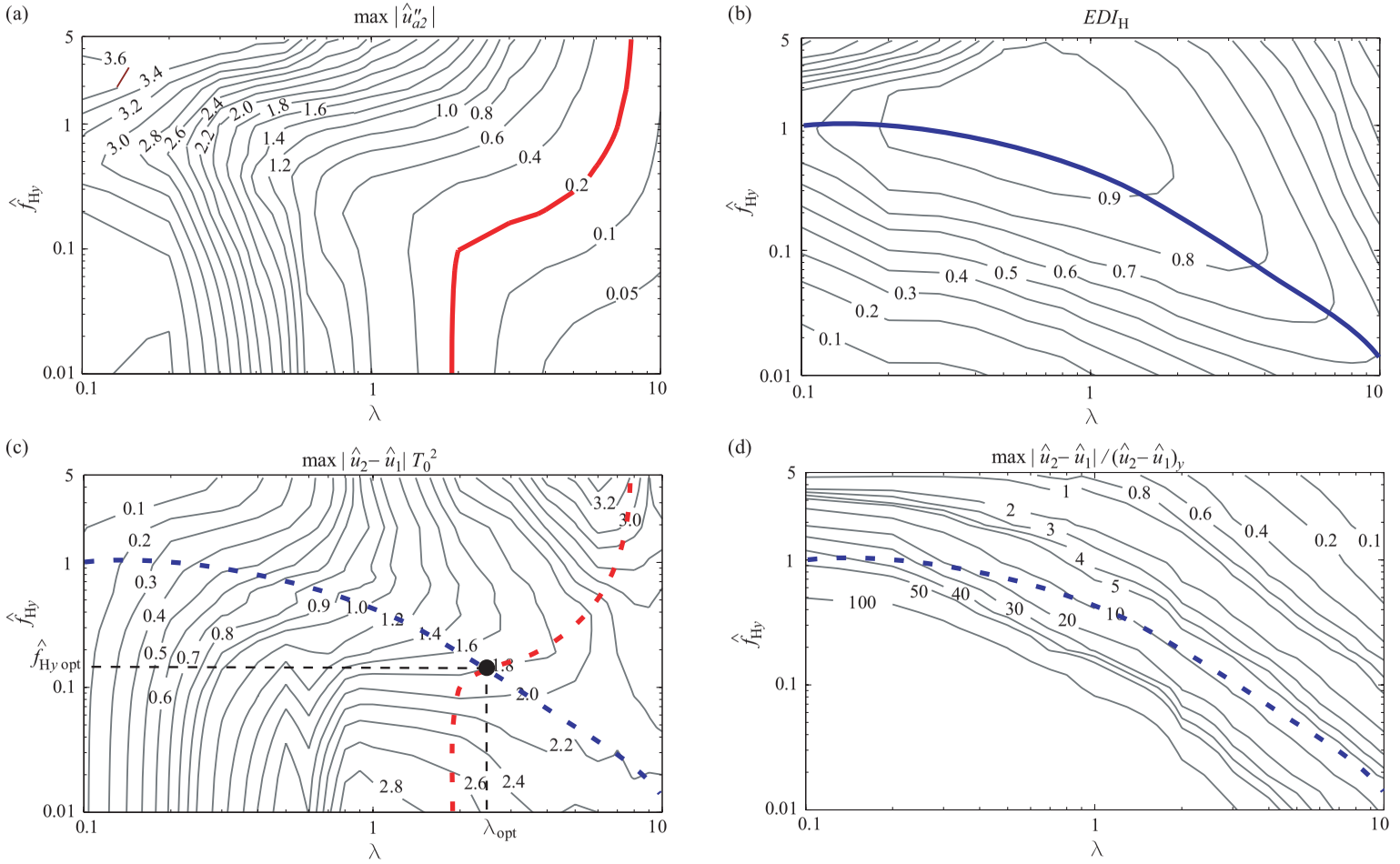

Figure 6.15. Optimal design of the equipment isolation system with nonlinear hysteretic behaviour, Operational level. (a) Acceleration criterion. (b) Energy criterion. (c) Combination of both criteria to identify the optimal design parameters λ_{opt} and $\hat{f}_{\mathrm{Hy\,opt}}$. (d) Energy criterion and ductulity demand to the isolation sytem.

6.6 Application

Here, we provide an application to illustrate the methodology previously developed for the optimal design of an equipment isolation system with nonlinear hysteretic behaviour.

A full scale physical model is considered. The supporting structure (Fig. 6.16(a)) is a two-storey one-bay steel frame, 3.00 m long, 2.40 m wide and 4.00 m high, with an interstorey height of 2.00 m. The frame consists of HEA cross-section beams and columns and it is provided with L cross-section bracings in the direction orthogonal to the one of base excitation, in order to avoid out of plane displacements. Total floor masses M_1 and M_2, where subscripts 1 and 2 indicate the first and the second floor respectively, are 4932 kg.

A block-type equipment weighing 3400 kg is supposed to be mounted on the first floor of the frame (Fig. 6.16(b)) and isolated from it by means of the nonlinear hysteretic isolation system. Since the mass ratio between the equipment and the supporting structure is significant and as such is expected to be their dynamic interaction, a coupled approach is adopted in the optimal design of the isolation system.

6.6.1 Optimal design

Modal analysis of the supporting structure

A preliminary finite element model of the steel frame is developed to evaluate its dynamic behaviour by using the general purpose Structural Analysis Program SAP2000 v.10.0.4 (Computers & Structures Inc. 2007) [18].

The frame is regular in plan and in elevation and it is supposed to be base-excited

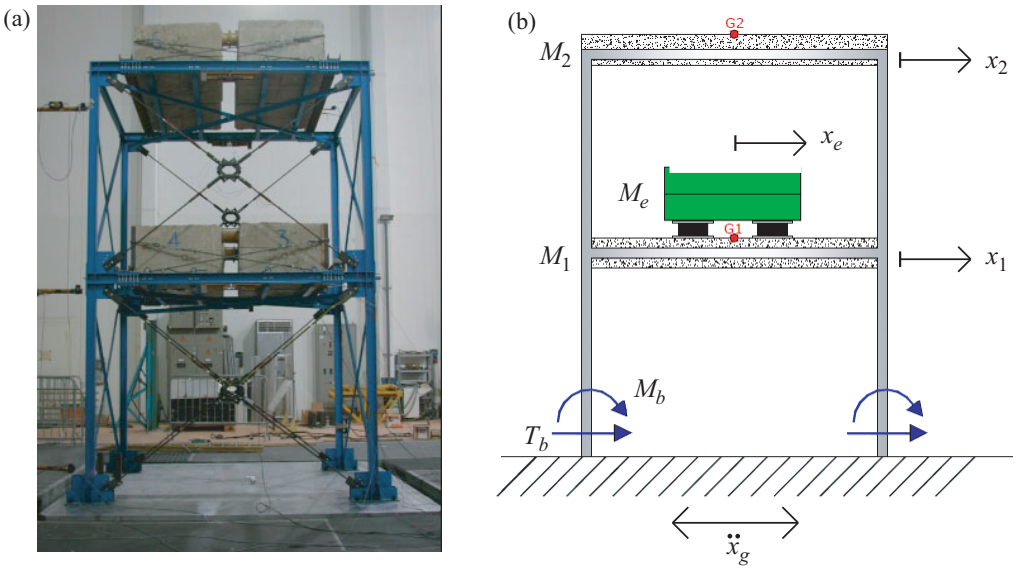

Figure 6.16. Application. (a) Full scale physical model of the supporting structure. (b) Controlled configuration.

in the x-direction only, then the analysis is performed using a planar model. Axial deformation is neglected in all structural members and floors are taken as rigid in their own planes. Masses are lumped at the centre of mass of each floor, which is also the geometric centre. Each floor has a single dynamic degree of freedom, the lateral displacement in the x-direction, hence the frame is modelled as a 2-DOF system. The mass matrix of the frame is regarded as a diagonal matrix

$$\mathbf{M}\ [\text{kg}] = \begin{pmatrix} 4932 & 0 \\ 0 & 4932 \end{pmatrix} \tag{6.54}$$

The stiffness matrix is

$$\mathbf{K}\ [\text{N/m}] = 10^6 \cdot \begin{pmatrix} 8.4289 & -5.8815 \\ -5.8815 & 5.8652 \end{pmatrix} \tag{6.55}$$

The frame is assumed to be proportionally damped and the viscous damping matrix is formulated in the Rayleigh form

$$\mathbf{C} = a\,\mathbf{M} + b\,\mathbf{K} \tag{6.56}$$

Constants a and b are determined so that the damping ratio of the first mode is 0.011 and of the second mode is 0.044. It yields the viscous damping matrix

$$\mathbf{C}\ [\text{Ns/m}] = 10^4 \cdot \begin{pmatrix} 1.4246 & -1.0154 \\ -1.0154 & 0.9820 \end{pmatrix} \tag{6.57}$$

The influence vector of the frame is

$$\boldsymbol{\tau} = \begin{pmatrix} 1 \\ 1 \end{pmatrix} \tag{6.58}$$

Modal frequencies, damping ratios and participating mass ratios of the steel frame are reported in Tab. 6.1. The matrix made up of the mode-shape vectors is given by

$$\boldsymbol{\Phi} = (\boldsymbol{\phi}_1 \quad \boldsymbol{\phi}_2) = \begin{pmatrix} -0.2825 & -0.3507 \\ -0.3507 & 0.2825 \end{pmatrix} \tag{6.59}$$

Mode	Frequency [Hz]	Frequency [rad/s]	Period [s]	Damping ratio	Participating mass ratio
I	2.41	15.12	0.42	0.011	0.9885
II	8.22	51.67	0.12	0.044	0.0115

Table 6.1. Application: modal frequencies, periods, damping ratios and participating mass ratios of the supporting structure.

Reduced order 2-DOF model

The dynamic response of the steel frame is governed by its first mode, as indicated by a modal participating mass ratio of 0.9885. In order to introduced the reduced order 2-DOF model, the response vector $\mathbf{x}(t)$ of the frame is approximated by its first mode-shape vector $\boldsymbol{\phi}_1$ and the modal amplitude $q_1(t)$

$$\mathbf{x}(t) \approx \boldsymbol{\phi}_1 \, q_1(t) \tag{6.60}$$

The mode-shape vector $\boldsymbol{\phi}_1$ is normalized with respect to the element corresponding to the location of the isolated equipment. Being the latter supposed to be on the first floor, the normalized mode-shape vector is given as

$$\widetilde{\boldsymbol{\phi}}_1 = \begin{pmatrix} 1.000 \\ 1.241 \end{pmatrix} \tag{6.61}$$

Now, generalized properties m_1, c_1 and k_1 of the supporting structure are calculated as shown in Tab. 3.2 on page 55. Generalized mass m_1 is given as the modal mass of the frame

$$m_1 = \widetilde{\boldsymbol{\phi}}_1^{\top} \, \mathbf{M} \, \widetilde{\boldsymbol{\phi}}_1 = 12533 \;\; \text{kg} \tag{6.62}$$

Similarly, generalized viscous damping constant c_1 and stiffness k_1 are given as the modal damping coefficient

$$c_1 = \widetilde{\boldsymbol{\phi}}_1^{\top} \, \mathbf{C} \, \widetilde{\boldsymbol{\phi}}_1 = 4169 \;\; \text{Ns/m} \tag{6.63}$$

and the modal stiffness

$$k_1 = \widetilde{\boldsymbol{\phi}}_1^{\top} \, \mathbf{K} \, \widetilde{\boldsymbol{\phi}}_1 = 2.8650 \cdot 10^6 \;\; \text{N/m} \tag{6.64}$$

respectively. The modal participation factor of the frame is calculated as

$$\Gamma = \frac{\widetilde{\boldsymbol{\phi}}_1^{\mathrm{T}} \, \mathbf{M} \, \boldsymbol{\tau}}{\widetilde{\boldsymbol{\phi}}_1^{\mathrm{T}} \, \mathbf{M} \, \widetilde{\boldsymbol{\phi}}_1} = 0.8821 \tag{6.65}$$

In this case, generalized properties in Eqs. (6.62) – (6.65) are equal to the modal properties of the supporting structure due to the first-mode assumption in Eq. (6.60).

According to Tab. 3.2 on page 55, the mass of the secondary oscillator is equal to the mass of the equipment to be isolated: $m_2 = M_e = 3400$ kg.

On the basis of the aforementioned quantities, the known data of the optimal design problem are calculated as follows. Mass ratio is $\mu = m_2/m_1 = 0.2713$. As to the supporting structure, the uncoupled natural frequency is $\omega_1 = \sqrt{k_1/m_1} = 15.12$ rad/s (or natural period $T_1 = 0.42$ s) and the uncoupled damping ratio is $\zeta_1 = c_1/\left(2\sqrt{k_1 \, m_1}\right) = 0.011$. As to the isolation system, non-dimensional parameters $\hat{k}_l = 0.05$, $\hat{k}_{nl} = 0.00$ and $\zeta_0 = 0.01$ are assumed.

Optimization

The optimization procedure and the design seismic input described in Sec. 6.5 are applied. As a result, the optimal design parameters $\lambda_{\text{opt}} = 2.40$ and $\hat{f}_{\text{Hy opt}} = 0.095$ are identified. Dimensional parameters are then computed and indicated in Tab. 6.2.

Non-dimensional							Dimensional				
μ	ζ_1	$\hat{k}_l$	$\hat{k}_{nl}$	ζ_0	λ_{opt}	$\hat{f}_{\text{Hy opt}}$	T_1 [s]	T_0 [s]	k_l [N/m]	k_{nl} [N/m^3]	f_{Hy} [N]
0.2713	0.011	0.05	–	0.010	2.40	0.095	0.42	1.00	6605	–	866

Table 6.2. Non-dimensional and dimensional parameters of the optimal design.

6.6.2 Numerical simulations

To assess the seismic effectiveness of the equipment isolation system here designed, a series of numerical simulations is performed under a wide selection of ground acceleration time histories. Comparisons with an optimal isolation system with linear visco-elastic behaviour are eventually provided.

Natural earthquakes

Four natural accelerograms, recorded during historical earthquakes and selected from the database of the PEER Center [100], are used fo the seismic analyses: Northridge 17/01/1994, Sylmar Station NS; Kobe 17/01/1995, KJMA Station NS; Tokachi-oki 16/05/1968, Hachinohe Station NS; Imperial Valley 18/05/1940, El Centro Station NS. Detailed information about these seismic inputs is given in Sec. 6.3.

Natural accelerograms are scaled to obtain the same spectral pseudo-acceleration of the design spectrum in correspondence of the fundamental period $T_1 = 0.42$ s of the supporting structure. (Fig. 6.17).

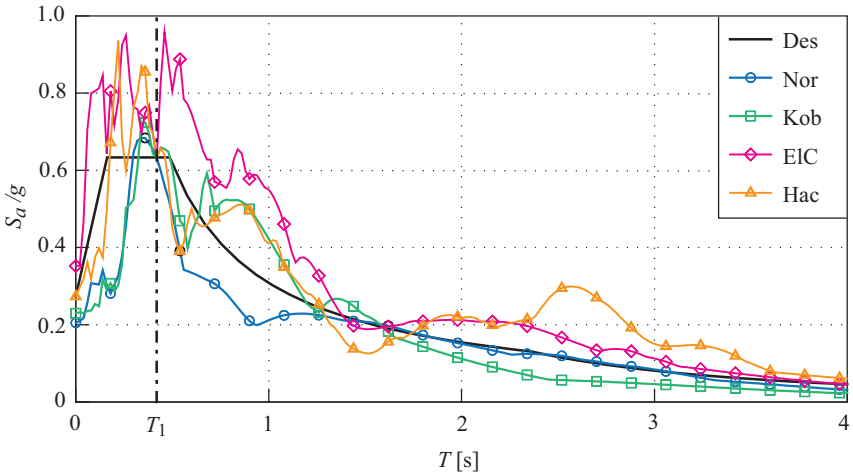

Figure 6.17. Elastic pseudo-acceleration response spectra (5% damping) of design input and scaled natural accelerograms.

Evaluation of seismic effectiveness

For comparison purposes, two configurations are considered:

- the uncontrolled configuration (Fixed-Base Equipment, FBE), where the equipment is non-isolated and rigidly fixed to the attachment floor of the supporting structure;
- the controlled configuration (Non-Linear isolation, NL), where the equipment is isolated from the attachment floor *via* the nonlinear hysteretic isolation system.

Seismic effectiveness is evaluated in terms of both root-mean-square (RMS) and peak responses by means of performance indices. Once chosen a response quantity of interest, the performance index is defined as the ratio of the response value between the controlled and the uncontrolled configurations.

With regard to the isolated mass, relevant response quantities are its absolute acceleration $\ddot{x}_{ae}$ and its displacement $\Delta = x_e - x_1$ relative to the attachment floor. Performance indices are expressed in terms of RMS responses as

$$I_1 = \frac{\mathrm{RMS}\left(\ddot{x}_{ae\,\mathrm{NL}}\right)}{\mathrm{RMS}\left(\ddot{x}_{ae\,\mathrm{FBE}}\right)} \qquad I_2 = \frac{\mathrm{RMS}\left(\Delta_{\mathrm{NL}}\right)}{\mathrm{RMS}\left(x_{e\,\mathrm{FBE}}\right)}$$

For index I_1, a value smaller than one implies the effectiveness of the nonlinear hysteretic isolation system in reducing the absolute acceleration of the mass. Meanwhile, index I_2, which represents the relative displacement Δ of the isolated mass divided by its displacement x_e in the uncontrolled configuration, should be within an allowable threshold.

In order to ensure strength and serviceability, the dynamic response of the supporting structure is monitored as well. With regard to the frame, response quantities of interest are floor absolute accelerations $\ddot{x}_k$ and floor displacements x_k relative to ground ($k = 1,\ 2$). Base shear T_b and bending moment M_b are also considered since representative of the overall internal loads in the structural members. Base shear T_b is computed by summing the inertial forces acting on each mass. Base bending moment M_b is computed by summing the moments of the inertial forces about the base of the frame. Performance indices are expressed in terms of RMS responses as follows

$$I_{3,\,4} = \frac{\mathrm{RMS}\left(\ddot{x}_{k\,\mathrm{NL}}\right)}{\mathrm{RMS}\left(\ddot{x}_{k\,\mathrm{FBE}}\right)} \qquad I_{5,\,6} = \frac{\mathrm{RMS}\left(x_{k\,\mathrm{NL}}\right)}{\mathrm{RMS}\left(x_{k\,\mathrm{FBE}}\right)} \qquad k = 1,\ 2$$

$$I_7 = \frac{\mathrm{RMS}\left(T_{b\,\mathrm{NL}}\right)}{\mathrm{RMS}\left(T_{b\,\mathrm{FBE}}\right)} \qquad I_8 = \frac{\mathrm{RMS}\left(M_{b\,\mathrm{NL}}\right)}{\mathrm{RMS}\left(M_{b\,\mathrm{FBE}}\right)}$$

Note that for indices I_3 – I_8, a value smaller than one implies that the dynamic response of the supporting structure is reduced in the (NL) configuration as compared to the (FBE) configuration.

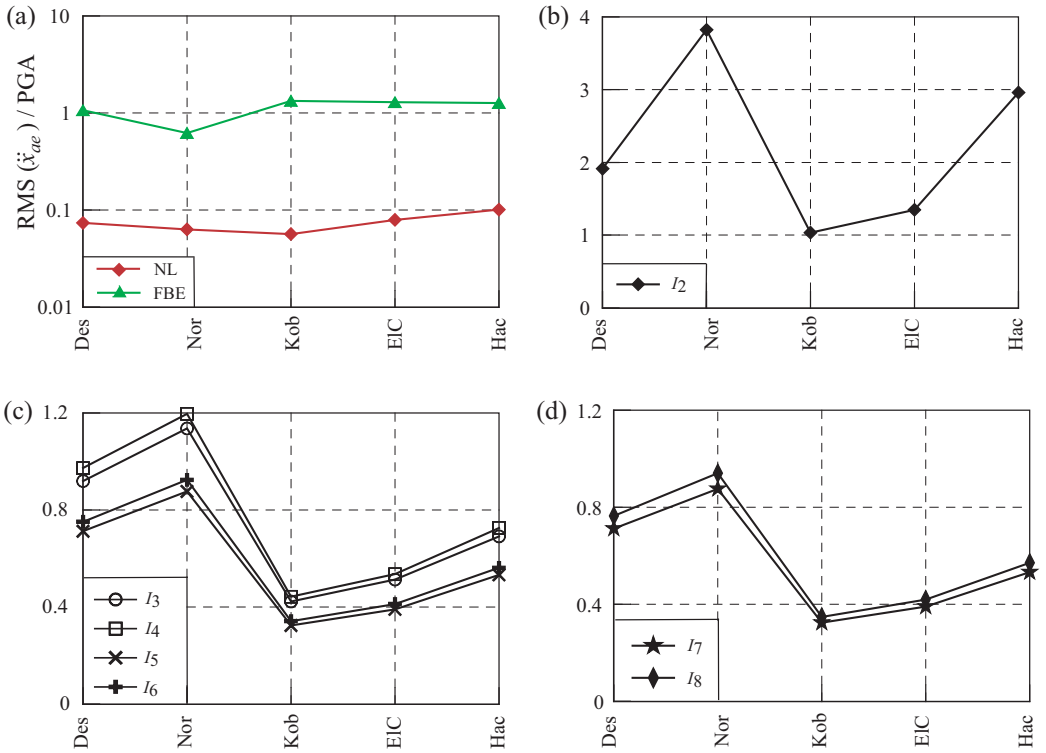

Figure 6.18. Nonlinear hysteretic isolation (NL) *vs* fixed-base equipment (FBE): performance indices in terms of RMS responses.

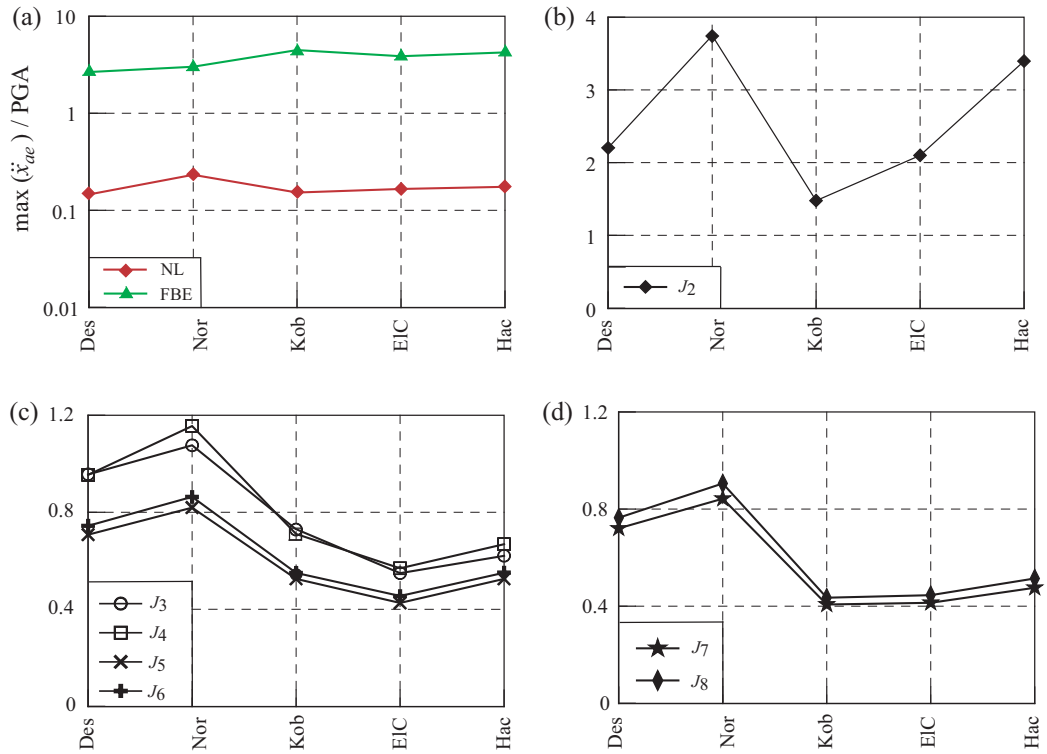

Figure 6.19. Nonlinear hysteretic isolation (NL) *vs* fixed-base equipment (FBE): performance indices in terms of peak responses.

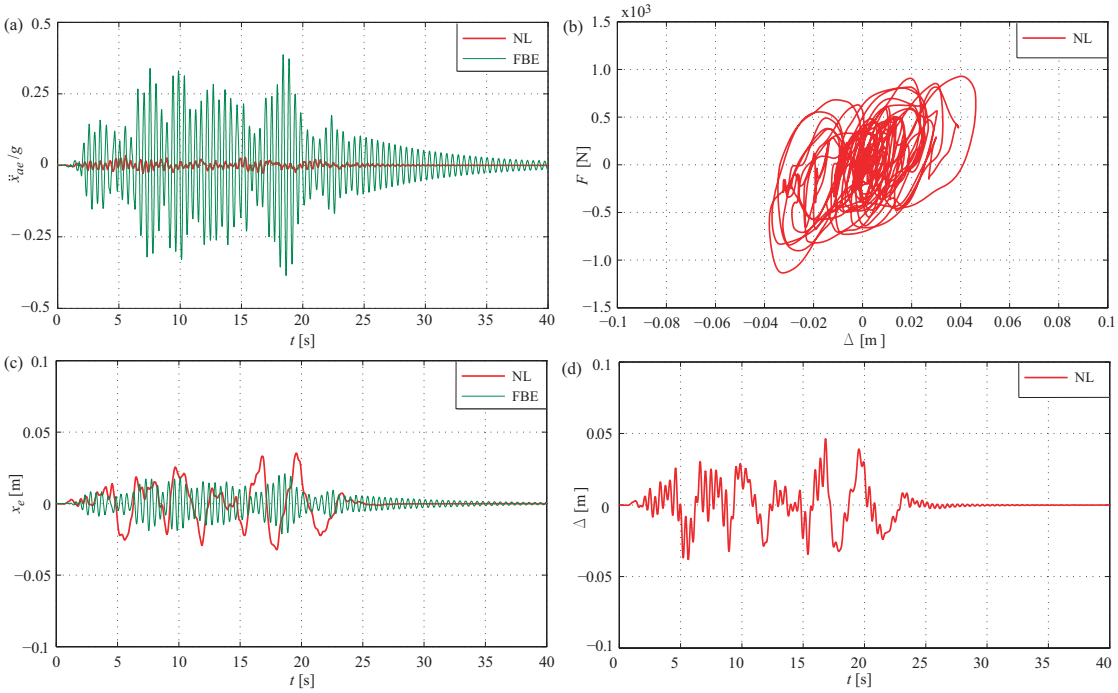

Figure 6.20. Responses of the isolated equipment due to the design accelerogram, PGA $= 0.273\ g$. (a) Absolute acceleration $\ddot{x}_e$. (b) Force-displacement loops in the nonlinear hysteretic isolation system. (c) Displacement x_e. (d) Relative displacement Δ.

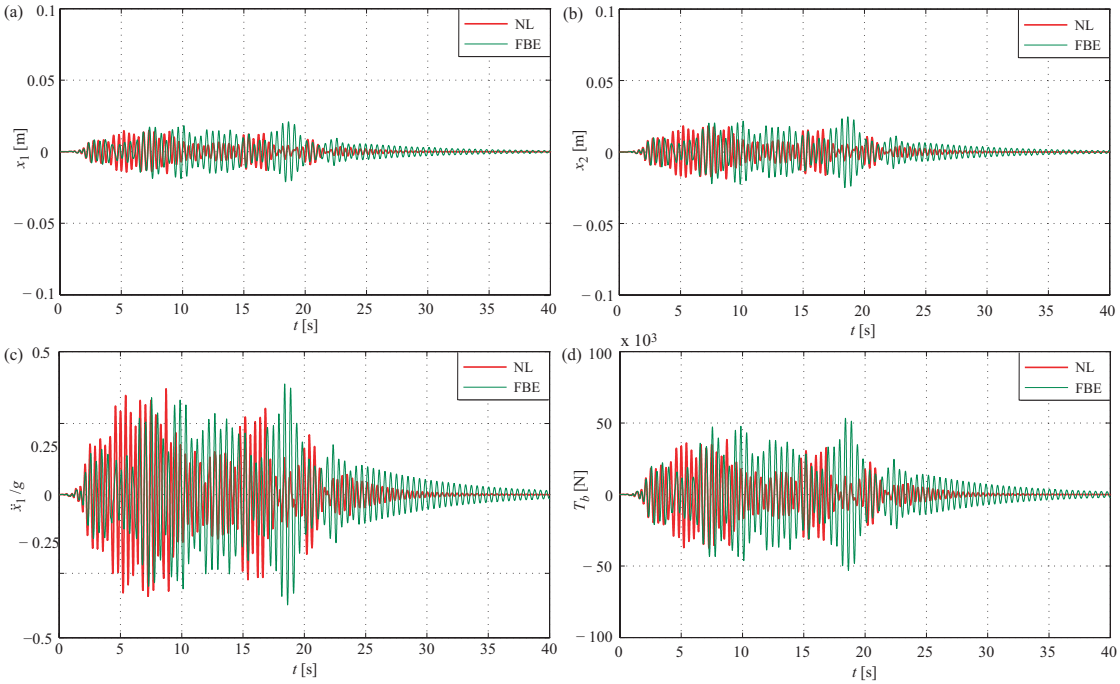

Figure 6.21. Responses of the supporting structure to the design accelerogram, PGA $= 0.273\ g$. (a) First floor displacement x_1. (b) Second floor displacement x_2. (c) First floor absolute acceleration $\ddot{x}_1$. (d) Base shear T_b.

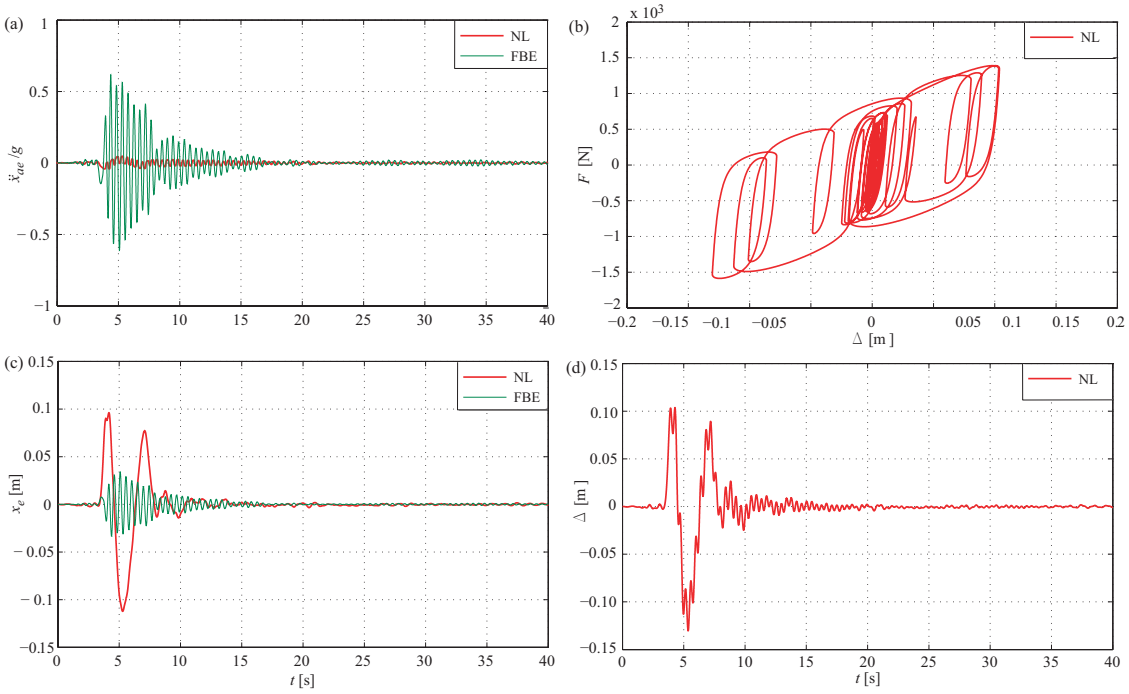

Figure 6.22. Responses of the isolated equipment due to Northridge accelerogram, PGA = 0.205 g. (a) Absolute acceleration $\ddot{x}_e$. (b) Force-displacement loops in the nonlinear hysteretic isolation system. (c) Displacement x_e. (d) Relative displacement Δ.

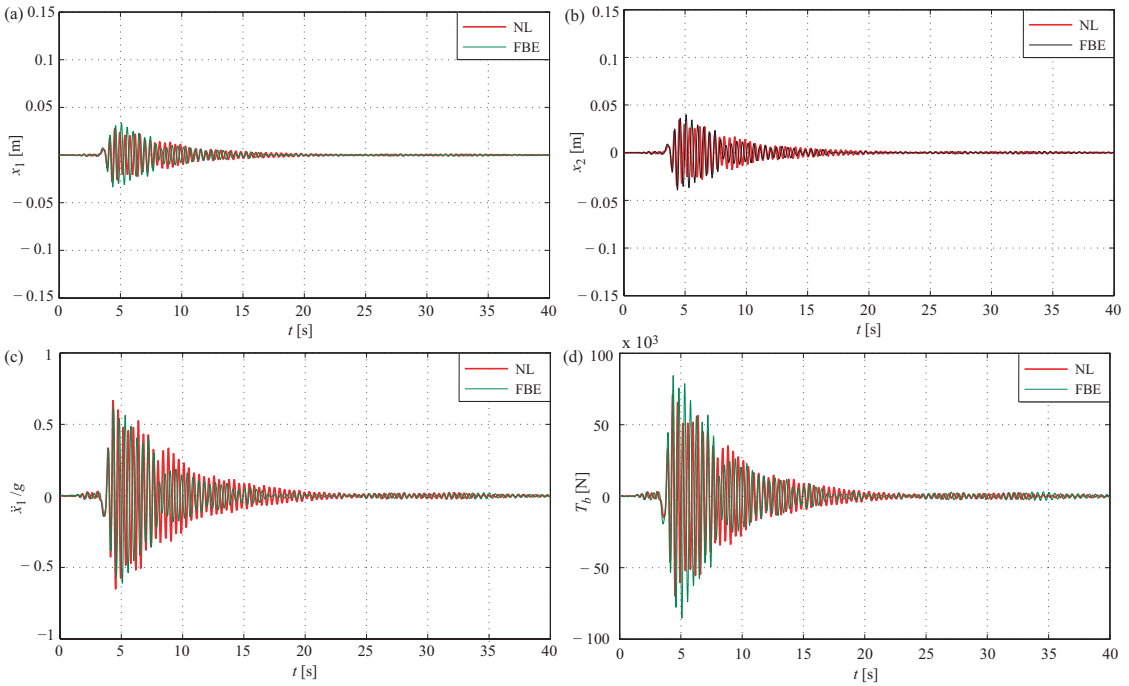

Figure 6.23. Responses of the supporting structure to Northridge accelerogram, PGA = 0.205 g. (a) First floor displacement x_1. (b) Second floor displacement x_2. (c) First floor absolute acceleration $\ddot{x}_1$. (d) Base shear T_b.

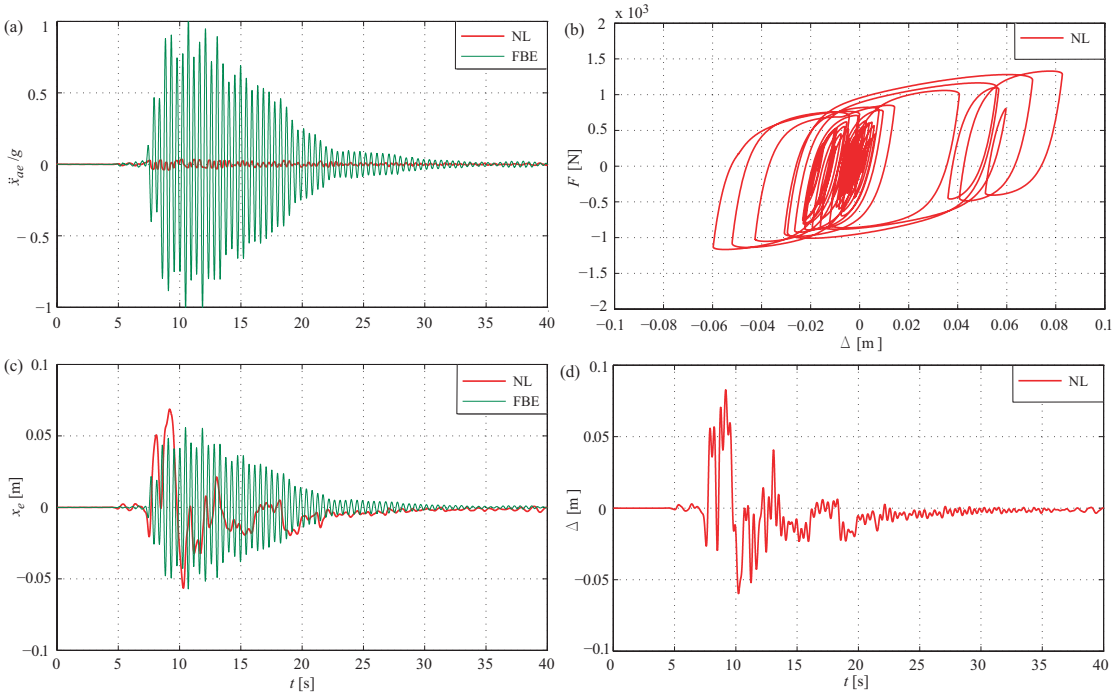

Figure 6.24. Responses of the isolated equipment due to Kobe accelerogram, PGA $= 0.230\ g$. (a) Absolute acceleration $\ddot{x}_e$. (b) Force-displacement loops in the nonlinear hysteretic isolation system. (c) Displacement x_e. (d) Relative displacement Δ.

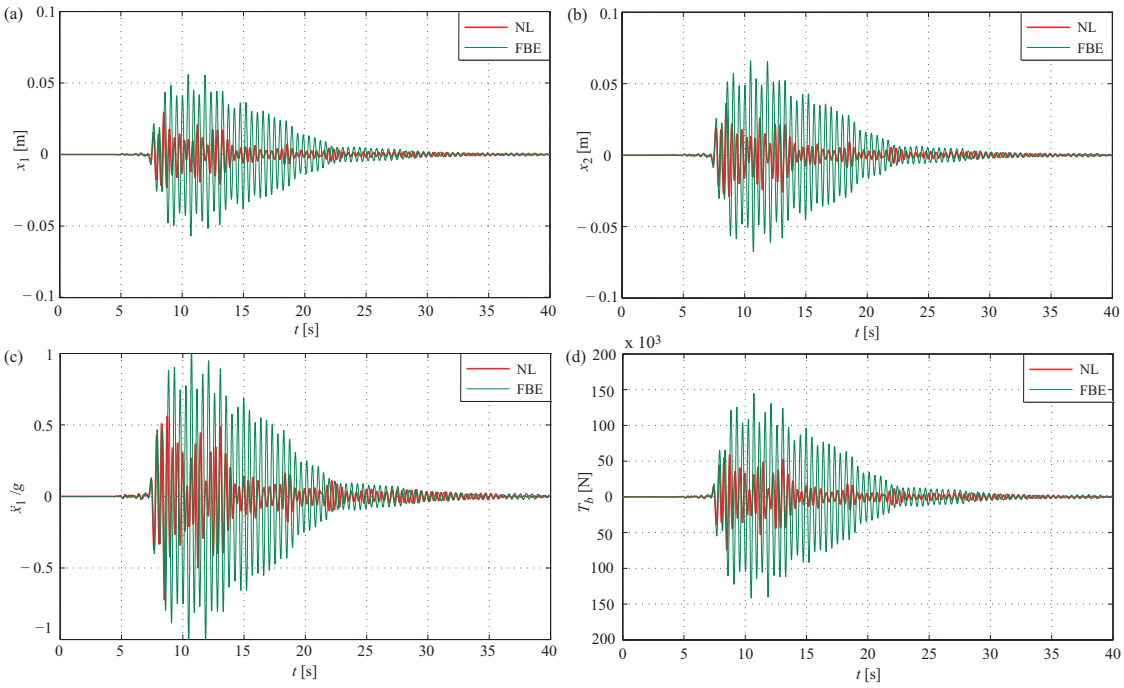

Figure 6.25. Responses of the supporting structure to Kobe accelerogram, PGA $= 0.230\ g$. (a) First floor displacement x_1. (b) Second floor displacement x_2. (c) First floor absolute acceleration $\ddot{x}_1$. (d) Base shear T_b..

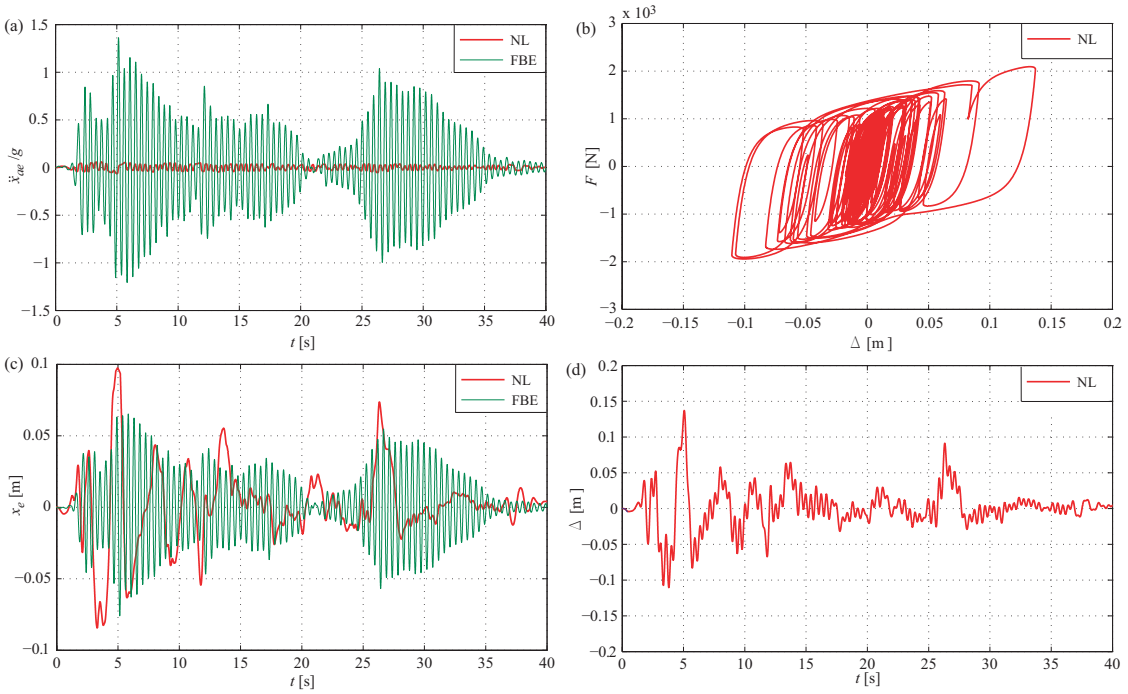

Figure 6.26. Responses of the isolated equipment due to El Centro accelerogram, PGA = 0.352 g. (a) Absolute acceleration $\ddot{x}_e$. (b) Force-displacement loops in the nonlinear hysteretic isolation system. (c) Displacement x_e. (d) Relative displacement Δ.

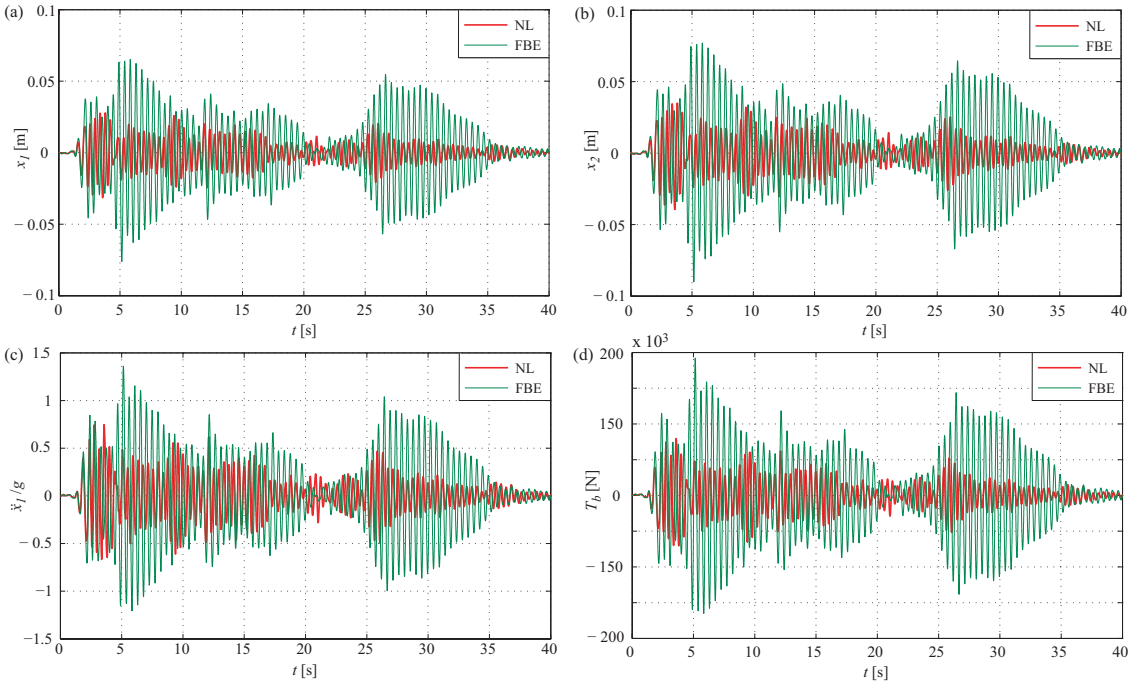

Figure 6.27. Responses of the supporting structure to El Centro accelerogram, PGA = 0.352 g. (a) First floor displacement x_1. (b) Second floor displacement x_2. (c) First floor absolute acceleration $\ddot{x}_1$. (d) Base shear T_b.

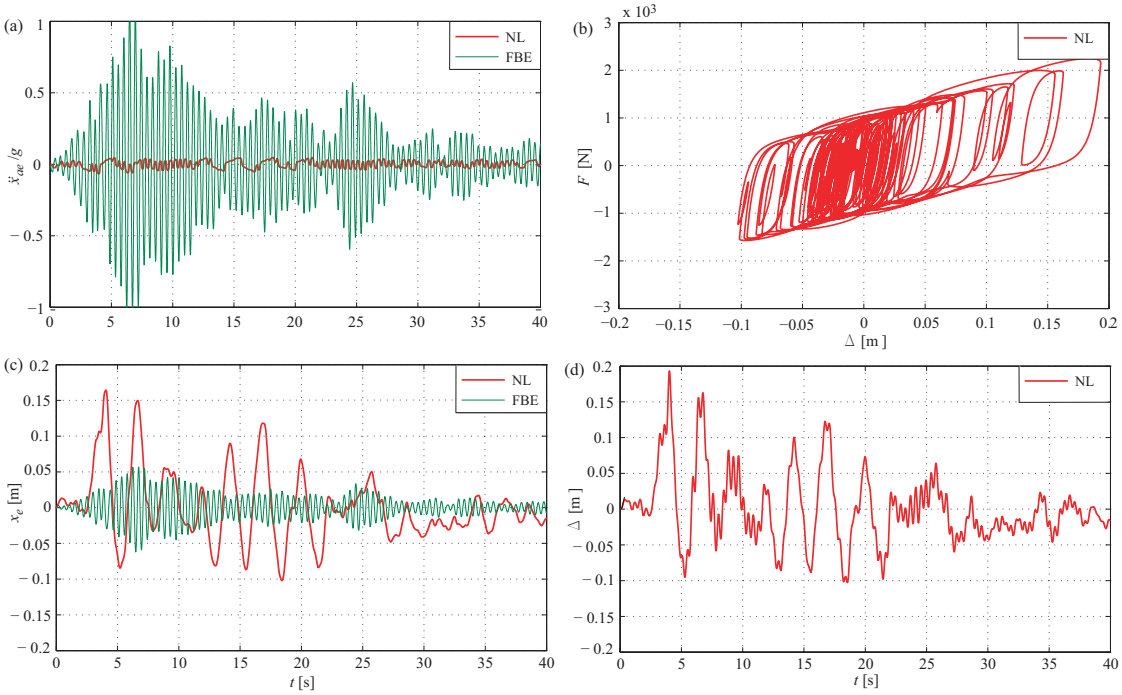

Figure 6.28. Responses of the isolated equipment due to Hachinohe accelerogram, PGA $= 0.273\ g$. (a) Absolute acceleration $\ddot{x}_e$. (b) Force-displacement loops in the nonlinear hysteretic isolation system. (c) Displacement x_e. (d) Relative displacement Δ.

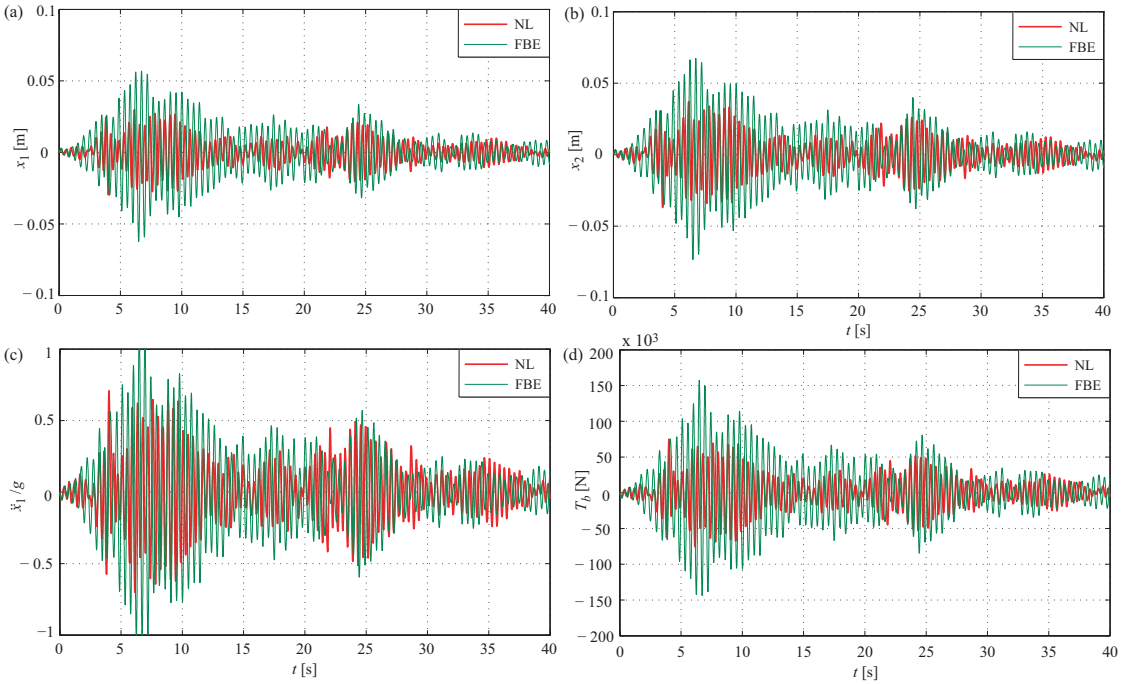

Figure 6.29. Responses of the supporting structure to Hachinohe accelerogram, PGA $= 0.273\ g$. (a) First floor displacement x_1. (b) Second floor displacement x_2. (c) First floor absolute acceleration $\ddot{x}_1$. (d) Base shear T_b.

Similarly to I_1 – I_8, performance indices J_1 – J_8 are defined in terms of peak responses as well. Values of I_1 – I_8 and J_1 – J_8 due to the seismic tests are shown in Figs. 6.18 and 6.19, respectively. The time history responses of the isolated equipment and the supporting structure in (NL) and (FBE) configurations are illustrated in Figs. 6.20 – 6.29.

As it can be noticed, the proposed nonlinear hysteretic isolation system is remarkably effective to suppress down the equipment acceleration response as compared to the (FBE) configuration. Reductions are quantified in Fig. 6.18 and 6.19, where both the peak and the RMS values of $\ddot{x}_{ae}$ are normalized to PGA for the different scaled inputs used in the seismic analyses. Reductions are greater than 95% in terms of both peak and RMS values and no substantial differences could be noticed between excitations with different frequency content. Furthermore, the optimal design criterion given by Eq. (6.51) is satisfied in the seismic analyses: the peak absolute acceleration transmitted to the equipment is limited to 20% of PGA not only for the design seismic input, but also for the scaled natural accelerograms.

Significant observations can also be made from indices I_3 – I_8 and J_3 – J_8, which refer to the dynamic response of the supporting structure. It is worthy to note that reducing the coupling between the mass and the structure advantageously reduces the structural response as well. The greatest reductions are recognized for floor displacements and the actions at the base of the frame (shear T_b and bending moment M_b), amounting to 50% – 60% in terms of both RMS and peak values. Smaller value are found for floor accelerations (30% – 50%). In the case of design and Northridge accelerograms, reductions decrease down in terms of both RMS and peak values. The acceleration response of the supporting structure results to be even amplified as compared with the (FBE) configuration (I_3, $I_4 > 1$; J_3, $J_4 > 1$).

The force-displacement loops obtained for the nonlinear hysteretic isolation system are illustrated in Figs. 6.20 – 6.29. As required in the design phase, no hardening effect can be noticed and a post- to pre-yielding ratio of about 0.05 can be recognized.

Comparisons with linear isolation system

The proposed nonlinear hysteretic isolation system is compared, as to the seismic effectiveness, with an optimal isolation system with linear visco-elastic behaviour (Linear isolation, L). In the linear case, the optimization procedure is carried out by setting the same acceleration requirement as in the nonlinear case (Eq. (6.51)) and assuming a viscous damping factor ζ_0 equal to 0.10, which is a standard value for elastomeric bearings. This leads to an isolation period $T_0 = 3.65$ s, as shown in Tab. 6.3.

Figs. 6.30 and 6.31 illustrate the comparisons between the optimal nonlinear hysteretic and the optimal linear isolation systems by means of performance indices. The latter are expressed in terms of RMS values as

$$IL_1 = \frac{\text{RMS}\left(\ddot{x}_{ae\,\text{NL}}\right)}{\text{RMS}\left(\ddot{x}_{ae\,\text{L}}\right)} \qquad IL_2 = \frac{\text{RMS}\left(\Delta_{\text{NL}}\right)}{\text{RMS}\left(\Delta_{\text{L}}\right)}$$

Non-dimensional							Dimensional				
μ	ζ_1	$\hat{k}_l$	$\hat{k}_{nl}$	ζ_0	λ_{opt}	$\hat{f}_{\text{H}y\,\text{opt}}$	T_1 [s]	T_0 [s]	k_l [N/m]	k_{nl} [N/m^3]	$f_{\text{H}y}$ [N]
0.2713	0.011	0.05	–	0.010	2.40	0.095	0.42	1.00	6605	–	866
0.2713	0.011	–	–	0.100	8.80	–	0.42	3.65	9826	–	–

Table 6.3. Non-dimensional and dimensional parameters of the optimal design problem: comparisons between the linear (L) and the nonlinear hysteretic (NL) isolation systems.

for the isolated equipment, and as

$$IL_{3,4} = \frac{\text{RMS}\left(\ddot{x}_{k\,\text{NL}}\right)}{\text{RMS}\left(\ddot{x}_{k\,\text{L}}\right)} \qquad IL_{5,6} = \frac{\text{RMS}\left(x_{k\,\text{NL}}\right)}{\text{RMS}\left(x_{k\,\text{L}}\right)} \qquad k = 1,\ 2$$

$$IL_7 = \frac{\text{RMS}\left(T_{b\,\text{NL}}\right)}{\text{RMS}\left(T_{b\,\text{L}}\right)} \qquad IL_8 = \frac{\text{RMS}\left(M_{b\,\text{NL}}\right)}{\text{RMS}\left(M_{b\,\text{L}}\right)}$$

for the supporting structure. Similarly to IL_1 – IL_8, performance indices JL_1 – JL_8 are defined in terms of peak responses as well. The time history responses of the isolated equipment and the supporting structure in (NL) and (L) configurations are illustrated in Figs. 6.32 – 6.36.

From the comparisons, the following remarks are pointed out. On the one hand, the isolation performance of both systems in terms of peak and RMS equipment acceleration $\ddot{x}_{ae}$ is the same since the same optimization criterion (Eq. (6.51)) has been adopted. On the other hand, the nonlinear isolation system undergoes smaller values of the relative displacement Δ between the equipment and the attachment floor. This is apparent by indices IL_2 and JL_2, which represent the ratios of the RMS and the peak displacement Δ, calculated between the nonlinear and the linear isolation systems. The result is an important point in implementing an isolation system since, in addition to the acceleration requirement, the equipment displacement should be limited as well for the sake of safety and functionality. Reductions of Δ amount to 10% – 20% in terms of peak values and to 30% – 40% in terms of RMS values. In the case of near-fault ground motions (Kobe and Northridge accelerograms), the nonlinear isolation system appears to be less effective to reduce the peak relative displacement because of the impulsive character of the excitation.

In conclusion, it is worth noting that the optimal design period T_0 for the linear isolation system ($T_0 = 3.65$ s) is more than three times greater than the one for the nonlinear system ($T_0 = 1.00$ s). This means that a nonlinear system is able to achieve the same isolation performance as a linear system, yet having a much higher initial stiffness. Hence, the nonlinear isolation system outperforms the linear one also in static conditions, since it could benefit from higher initial stiffness to limit its static displacement as well.

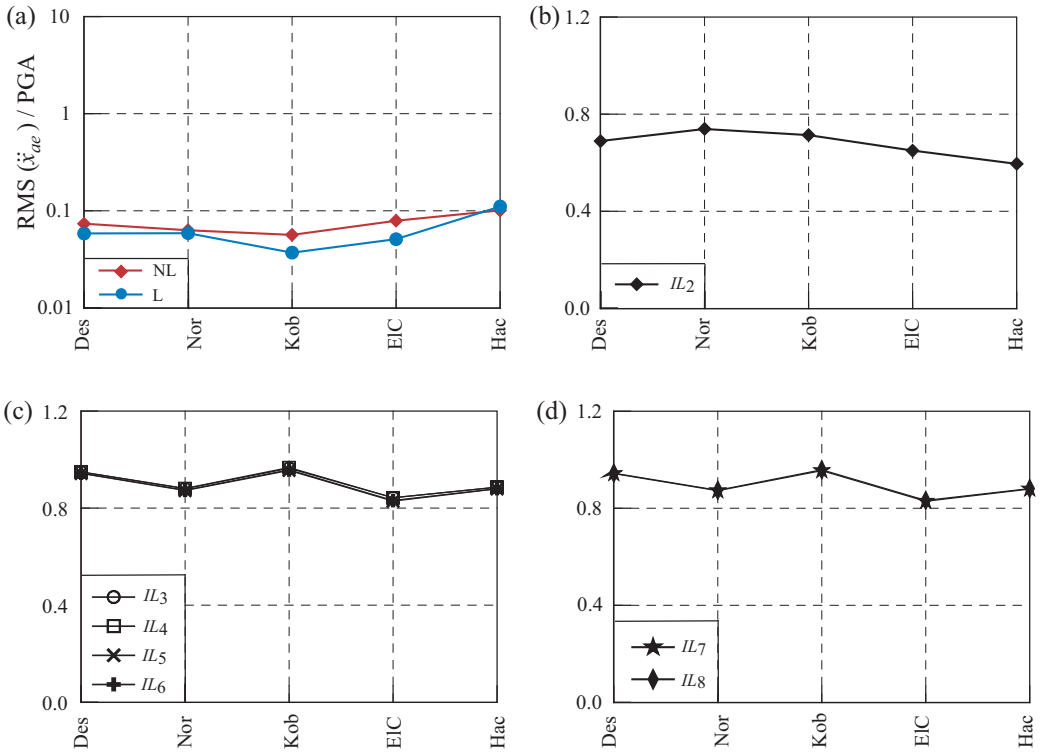

Figure 6.30. Nonlinear hysteretic isolation (NL) *vs* linear isolation (L): performance indices in terms of RMS responses.

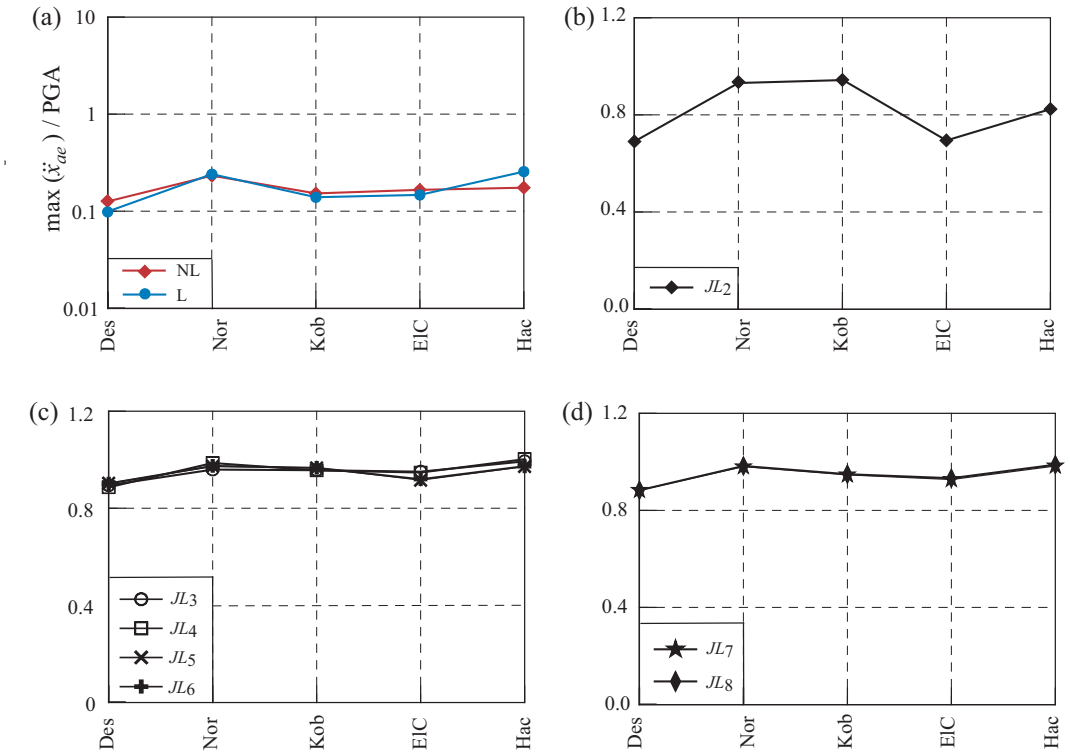

Figure 6.31. Nonlinear hysteretic isolation (NL) *vs* linear isolation (L): performance indices in terms of peak responses.

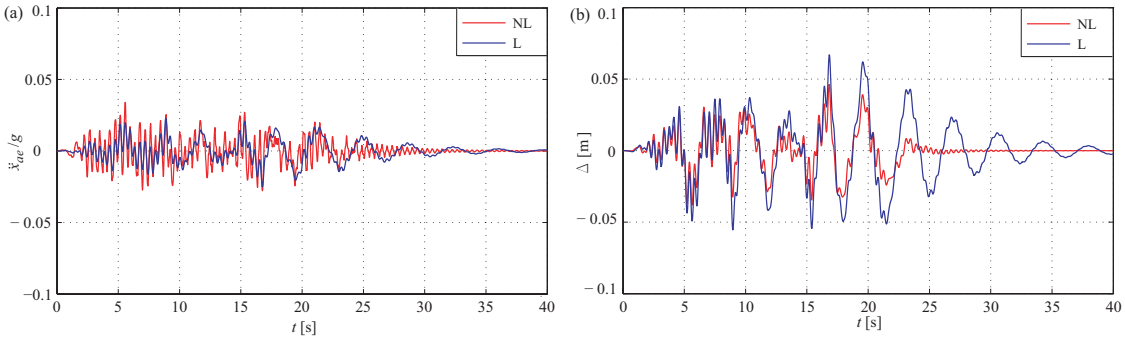

Figure 6.32. Responses of the isolated equipment due to the design accelerogram, PGA $= 0.273\ g$, nonlinear hysteretic isolation (NL) *vs* linear isolation (L). (a) Absolute acceleration $\ddot{x}_e$. (b) Relative displacement Δ.

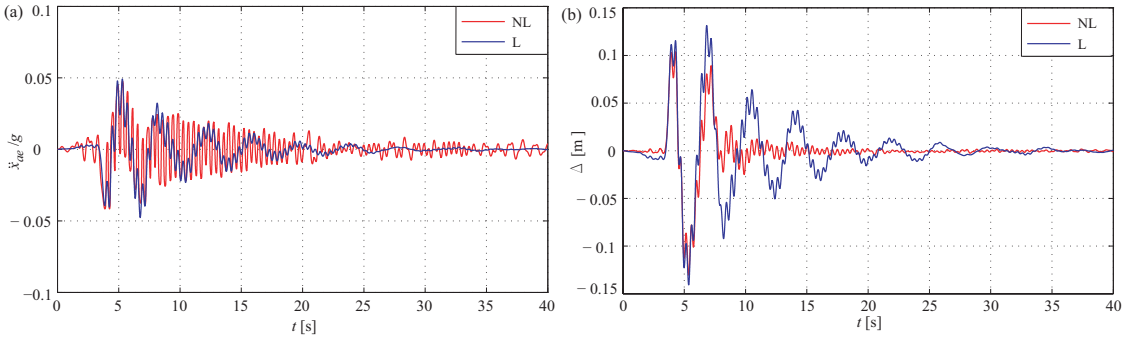

Figure 6.33. Responses of the isolated equipment due to Northridge accelerogram, PGA $= 0.205\ g$, nonlinear hysteretic isolation (NL) *vs* linear isolation (L). (a) Absolute acceleration $\ddot{x}_e$. (b) Relative displacement Δ.

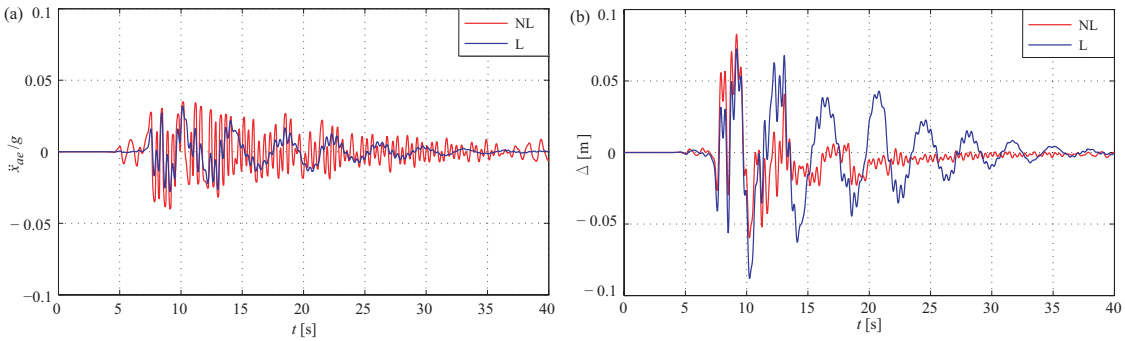

Figure 6.34. Responses of the isolated equipment due to the accelerogram, PGA $= 0.230\ g$, nonlinear hysteretic isolation (NL) *vs* linear isolation (L). (a) Absolute acceleration $\ddot{x}_e$. (b) Relative displacement Δ.

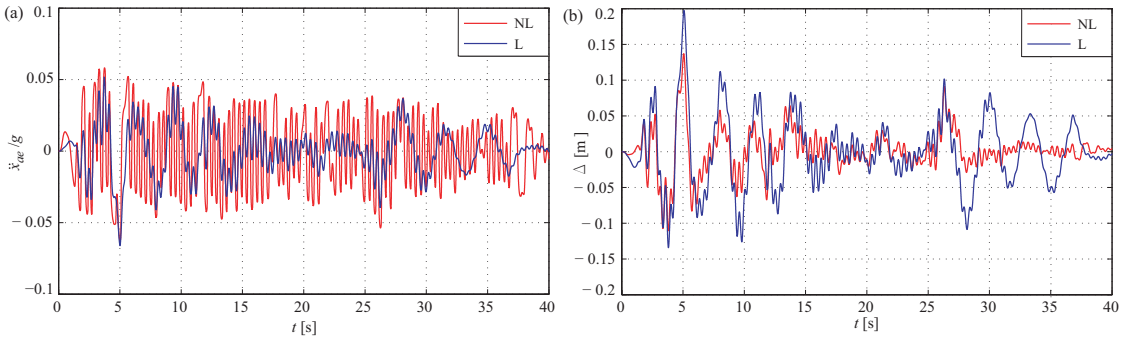

Figure 6.35. Responses of the isolated equipment due to El Centro accelerogram, PGA = 0.352 g, nonlinear hysteretic isolation (NL) *vs* linear isolation (L). (a) Absolute acceleration $\ddot{x}_e$. (b) Relative displacement Δ.

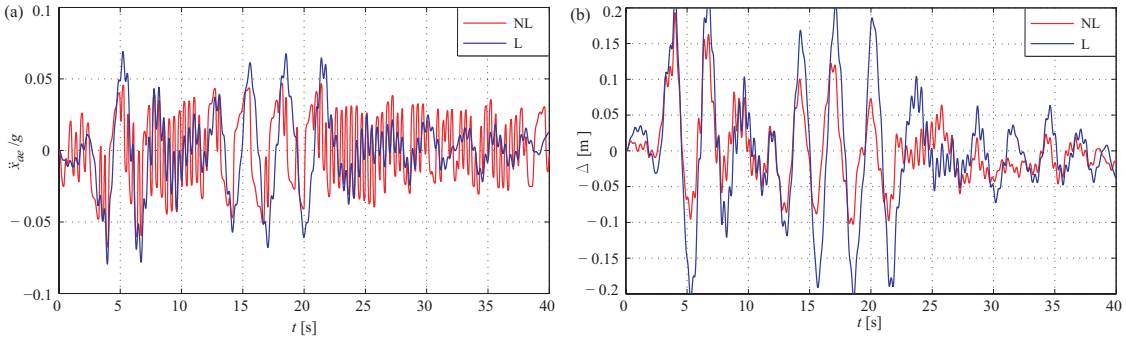

Figure 6.36. Responses of the isolated equipment due to Hachinohe accelerogram, PGA = 0.273 g, nonlinear hysteretic isolation (NL) *vs* linear isolation (L). (a) Absolute acceleration $\ddot{x}_e$. (b) Relative displacement Δ.

Part III

Non-conventional Tuned Mass Damper (TMD) for the seismic protection of equipment

Chapter 7

Dynamic response and optimal design of structures with large mass ratio TMD

7.1 Preliminaries

In this chapter[1], the dynamic behaviour of a non-conventional Tuned Mass Damper (TMD) with large mass ratio is investigated and an optimal design methodology is formulated for seismic applications. Aiming at the seismic protection of equipment, this technology is set in competition with the isolation systems proposed in the previous chapters, though some analogies can be established, as explained hereafter.

The study is first motivated by the results obtained in Chapters 4 and 6 for a system consisting in a supporting structure housing a single equipment. By comparing an uncontrolled configuration, where the equipment is rigidly fixed to the structure, and a controlled configuration, where the equipment is isolated from the structure, reductions of both the equipment response and the structural response are achieved. In other terms, this means that reducing the coupling between the equipment and its supporting structure may benefit not only the equipment to be protected, but also the structure itself.

These results are of particular significance when tackling the different problem of a supporting structure housing a series of equipment. In such a case, an effective protection strategy is proposed in the present Chapter: a mass present on the structure,

[1]Some of the results in this chapter have been published in the following papers:

- ♢ De Angelis, M., Perno, S., Reggio, A. Dynamic response and optimal design of structures with large mass ratio TMD. *Earthquake Engineering and Structural Dynamics*, 41 (1), 41-60, 2012.
- ♢ Reggio, A., De Angelis, M., Perno, S. Controllo della risposta dinamica di struttura dotate di TMD ad elevato rapporto di massa: analisi numeriche e sperimentali. *Proceedings of XIX Congresso AIMETA – Associazione Italiana di Meccanica Teorica e Applicata*, Ancona, Italy, September 14-17, 2009.

an equipment in particular, is supposed to be converted into a TMD for the seismic protection of the supporting structure and of the whole equipment anchored to it. Such a TMD configuration is to be said *non-conventional* because the tuned mass is already a part of the system and keeps maintaining its own functions (structural, architectural, electrical, mechanical, ...) beyond the mere control function. Aiming at a better control performance, and since no additional weight is introduced to realize the TMD, a larger tuned mass can be chosen as compared to a conventional TMD.

Like for the equipment isolation systems previously discussed, the implementation of a non-conventional TMD is based on the decoupling between a mass and its supporting structure. As a consequence of this analogy, the two technologies can be studied by means of the same structural models described in Chapter 3. Besides that, however, the design criteria are essentially different: on the one hand, in the case of an equipment isolation system, the objective is pursued of reducing the absolute acceleration transmitted to the isolated equipment; on the other hand, in the case of a non-conventional TMD, the objective is pursued of minimizing the dynamic response of the supporting structure and, then, of the whole equipment the structure houses.

7.2 Optimal design of TMD for seismic applications

The optimal design methodology here proposed is specifically developed to implement High-Damping Rubber Bearings (HDRB) to connect the device mass to the main structure, taking advantage of combining stiffness and noticeable damping characteristics. A further objective is to exploit the influence of the mass ratio on the TMD performance.

7.2.1 Equations of motion

Consider the system represented in Fig. 3.3 on page 52 as a lumped mass model: it can be regarded as a N-DOF proportionally damped structure equipped with a TMD, connected to the ith DOF of the structure. The connection between the device mass and the structure is supposed to be implemented by means of HDRB and modelled according to the Kelvin-Voigt model, that the parallel of a linear spring and a linear viscous damper. The equations of motion of such a system subjected to the ground acceleration $\ddot{x}_g$ are given as

$$\begin{aligned} &\mathbf{M}\ddot{\mathbf{x}} + \mathbf{C}\dot{\mathbf{x}} + \mathbf{K}\mathbf{x} = -\mathbf{M}\mathbf{R}\,\ddot{x}_g + \mathbf{B}_i\,F \\ &M_e\ddot{x}_e = -M_e\ddot{x}_g - F \\ &F = k\,(x_e - x_i) + c\,(\dot{x}_e - \dot{x}_i) \end{aligned} \tag{7.1}$$

where $\mathbf{M}$, $\mathbf{C}$ and $\mathbf{K}$ are the $(N \times N)$ mass, damping and stiffness matrices of the structure; M_e, c and k are the TMD's mass, damping and stiffness coefficients; $\mathbf{x}(t)$ is

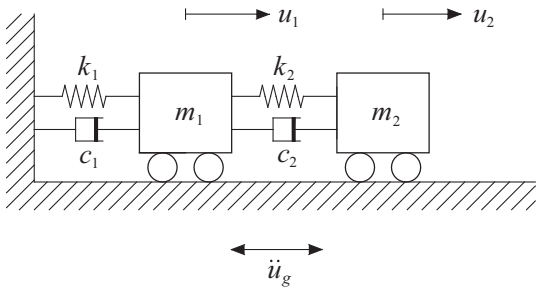

Figure 7.1. Structural model of a SDOF structure – TMD system.

the $(N \times 1)$ displacement vector of the structure with respect to ground; $x_e(t)$ denotes the TMD displacement with respect to ground; $\boldsymbol{R}$ is a $(N \times 1)$ influence vector, whose elements are all unitary in this case; F is the force applied by the TMD on the ith degree of freedom of the structure and $\mathbf{B}_i$ is the corresponding $(N \times 1)$ allocation vector.

Assume that the response vector can be approximated as $\mathbf{x}(t) \approx \boldsymbol{\phi}\, x_i(t)$, where $x_i(t)$ is the structural displacement at the TMD location (ith degree-of-freedom) and $\boldsymbol{\phi}$ is a proper shape vector normalized so that its ith element is unity ($\phi_i = 1$). A generalized single-degree-of-freedom (SDOF) structure – TMD system can be obtained under this assumption (Fig. 7.1). Let us define m_1, k_1, c_1 and m_2, k_2, c_2 as mass, stiffness and damping coefficients of the SDOF structure and the TMD, respectively, while $u_1(t)$ and $u_2(t)$ are the displacements relative to ground. The equations of motion for such a system can be written as

$$\begin{aligned} &\ddot{u}_1 + 2\zeta_1\omega_1\dot{u}_1 + \omega_1^2 u_1 = -\ddot{u}_g + \frac{f}{m_1} \\ &\mu\ddot{u}_2 = -\mu\ddot{u}_g - \frac{f}{m_1} \\ &\frac{f}{m_1} = \mu\alpha^2\omega_1^2\,(u_2 - u_1) + 2\mu\zeta_2\alpha\omega_1\,(\dot{u}_2 - \dot{u}_1) \end{aligned} \tag{7.2}$$

where the following parameters have been introduced: $\omega_1 = \sqrt{k_1/m_1}$ and $\zeta_1 = c_1/\left(2\sqrt{k_1\, m_1}\right)$ are the uncoupled natural frequency and damping ratio of the SDOF structure; $\zeta_2 = c_2/\left(2\sqrt{k_2\, m_2}\right)$ is the uncoupled damping ratio of TMD; $\mu = m_2/m_1$ and $\alpha = \omega_2/\omega_1$ are the mass ratio and the frequency ratio of the SDOF structure – TMD system, denoting with $\omega_2 = \sqrt{k_2/m_2}$ the TMD natural frequency. Response quantities and properties of the generalized SDOF structure – TMD system are related to those of the N-DOF structure – TMD system as shown in Tab. 7.1.

It thus becomes apparent the analogy between the models here adopted to study the TMD systems and the models introduced in Chapters 3, 4 and 6 to study the equipment isolation systems.

N-DOF structure – TMD system	Generalized SDOF structure – TMD system
x_i	u_1
$\boldsymbol{\phi}^\top \mathbf{M} \boldsymbol{\phi}$	m_1
$\boldsymbol{\phi}^\top \mathbf{C} \boldsymbol{\phi}$	c_1
$\boldsymbol{\phi}^\top \mathbf{K} \boldsymbol{\phi}$	k_1
x_e	u_2
m	m_2
c	c_2
k	k_2
$\frac{\boldsymbol{\phi}^\top \mathbf{M} \boldsymbol{R}}{\boldsymbol{\phi}^\top \mathbf{M} \boldsymbol{\phi}}\ \ddot{x}_g$	$\ddot{u}_g$

Table 7.1. Response quantities and properties of the generalized SDOF structure – TMD system.

7.2.2 Seismic excitation model and system response

In order to consider the probabilistic nature of earthquake, ground acceleration $\ddot{u}_g$ is modelled as a Gaussian random process having zero mean $\mu_{\ddot{u}_g}$ and white noise power spectral density $S_{\ddot{u}_g}(\omega) = S_{\mathrm{W}} = \text{const}$. This choice seems to be adequate to a design phase, although it neglects the dependency on the excitation frequency content.

Being the input process stationary with zero mean, such is assumed to be the system response and the following non-dimensional variables are introduced

$$U_1 = \frac{\sigma_{u_1\,\mathrm{TMD}}}{\sigma_{u_1\,\mathrm{RC}}} \qquad U_{21} = \frac{\sigma_{u_{21}\,\mathrm{TMD}}}{\sigma_{u_1\,\mathrm{RC}}} \qquad A_1 = \frac{\sigma_{a_1\,\mathrm{TMD}}}{\sigma_{a_1\,\mathrm{RC}}} \qquad A_2 = \frac{\sigma_{a_2\,\mathrm{TMD}}}{\sigma_{a_2\,\mathrm{RC}}} \tag{7.3}$$

In Eqs. (7.1), standard deviation $\sigma_\cdot$ coincides with the root-mean-square (rms) $\sqrt{\mathsf{E}\left[(\cdot)^2\right]}$, the symbol $\mathsf{E}[\,\cdot\,]$ denoting the expected value operator. Non-dimensional variables represent thus the rms ratios of the system response between the controlled and the uncontrolled configurations: subscript TMD indicates the controlled configuration, where the device mass is connected to the main structure through a flexible link; subscript RC indicates the uncontrolled configuration, where the main structure is not provided with the installation of TMD and the device mass is rigidly connected to it. Values of (7.3) below unity indicate, therefore, that the system response is reduced due to the presence of the TMD: rms ratio U_1 refers to the displacement u_1 of the main structure; U_{21} refers to the TMD stroke $u_{21} = u_2 - u_1$; A_1 and A_2 refer to the absolute accelerations $a_1 = \ddot{u}_1 + \ddot{u}_g$ and $a_2 = \ddot{u}_2 + \ddot{u}_g$ of the main structure and the TMD, respectively.

7.2.3 Optimization

In the present study, a non-conventional TMD with a large mass ratio is designed for the protection of a damped main structure subject to earthquake excitation. The design example presented herein refers to an experimental model later tested on shaking table, whose description is reported in Sec. 7.3.1. It consists of a two-story steel frame equipped with a large mass ratio TMD on the second floor. A preliminary finite element model of the frame is employed to evaluate its dynamic behavior. Considering that the frame response is dominated by the first mode of vibration, a generalized SDOF structure – TMD system is introduced for design purposes. A mass ratio equal to $\mu = 1.049$ is set out to realize a non-conventional TMD while the dynamic properties of the generalized SDOF structure are determined as $\omega_1 = 33.61$ rad/s ($f_1 = 5.35$ Hz) and $\zeta_1 = 0.02$. On the basis of the first-mode assumption, these values correspond to the first modal frequency and damping ratio of the frame.

The structural implementation of the proposed large mass ratio TMD involve high-damping rubber bearings (HDRB) to connect the device mass to the frame. This kind of bearings takes advantage of achieving stiffness and noticeable damping characteristics in the same device. Since the high-damping rubber compound is known to possess elasticity, plasticity and viscosity [155], HDRB show a highly nonlinear behavior combining both hysteresis and rate-dependence. Nevertheless, for the sake of simplicity, a Kelvin-Voigt linear visco-elastic model was adopted in the design phase [74]. For a target shear strain of $100\% - 150\%$, the equivalent damping ratio of HDRB is experimentally found to range from 0.10 to 0.15 [92]. Based on this finding, the damping ratio in the first complex mode of the SDOF – TMD system was assumed to be constant and equal to $\eta_1 = 0.12$. This is equivalent to say that only one design parameter, the frequency ratio α, was varied to find the optimal value, while the damping ratio ζ_2 resulted from the complex modal analysis of the system complying with the required value of η_1.

In Fig. 7.2, the rms response ratios of the generalized SDOF structure – TMD system are shown *versus* the design parameter α. Aiming at increasing structural integrity and reducing internal loads in structural members, an optimization problem was defined which consists in minimizing the rms ratio U_1 of the main structure displacement with respect to α. The equation

$$\frac{\partial U_1(\alpha)}{\partial \alpha} = 0 \tag{7.4}$$

is solved through a numerical search algorithm and the optimal value $\alpha_{\text{opt}} = 0.420$ is selected. The damping ratio $\zeta_2 = 0.163$ is consequently obtained by requiring $\eta_1 = 0.12$. As highlighted by the curves for U_1 and A_1, these parameters lead to significant reductions of the main structure response in terms of both displacement and absolute acceleration. Meanwhile, it should be considered that a non-conventional TMD is a portion of the structure itself, turned to a new role, hence the device is

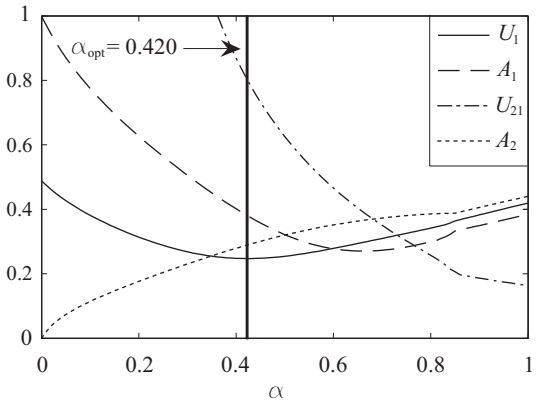

Figure 7.2. Optimal design of a large mass ratio TMD for seismic applications: rms response ratios *versus* frequency ratio α. It is assumed: $\mu = 1.049$, $\zeta_1 = 0.02$, $\eta_1 = 0.12$. It is obtained: $\alpha_{\text{opt}} = 0.420$, $\zeta_2 = 0.1630$.

feasible only if the control function is compatible with any other function the mass might already have. In other words, the dynamic response of the TMD must be limited in practice, avoiding excessive stroke and acceleration. The curve for U_{21} confirms that the TMD stroke is within an allowable range, while A_2 indicates that the device acceleration is even reduced as compared with the uncontrolled configuration.

7.2.4 Comparison with classic design formulae

The design method proposed herein is specifically developed to implement HDRB in a large mass ratio TMD for seismic applications. The optimization problem is tackled by considering the damping ratio ζ_2 as a fixed parameter and selecting the frequency ratio α according to an optimization criterion: a simplification is then introduced as compared with classic, non-specific design formulae for TMD [118] since only one design parameter had to be found. In order to appraise the novelty and effectiveness of the proposed method, it is compared with that developed and successfully applied by Sadek *et al.* [112] to the so-called "mega-substructure configuration", a large substructure used as a TMD in tall buildings. The latter consists in selecting the TMD parameters α and ζ_2 that result in approximately equal and large damping ratios $\eta_1 \cong \eta_2$ in the first two complex modes of vibration.

The comparison is carried out for two generalized SDOF – TMD systems with $\zeta_1 = 0.02$ and different mass ratios: a small one, $\mu = 0.020$, typical of a conventional TMD, and a large one, $\mu = 1.049$, assumed for a non-conventional TMD in the design example presented above. The design parameters α and ζ_2 for the two systems are given in Tab. 7.2 along with the frequencies (β_1, β_2) and damping ratios (η_1, η_2) in the complex modes of vibration. Design parameters are independent of ω_1 in both methods, while modal frequencies β_i ($i = 1, 2$) are normalized to the natural frequency of the system in the uncontrolled configuration (RC). Tab. 7.2 lists also the rms response ratios (U_1, U_{21}, A_1, A_2) of the system under a white noise ground acceleration.

μ	Method	Optimal design		Modal properties				System response			
		α	ζ_2	β_1	β_2	η_1	η_2	U_1	U_{21}	A_1	A_2
0.020	this study	0.930	0.1525	0.93	1.02	0.1200	0.0539	0.67	2.01	0.68	1.86
	Sadek	0.978	0.1596	1.00	1.00	0.0892	0.0920	0.68	1.90	0.68	1.96
1.049	this study	0.420	0.1630	0.55	1.57	0.1200	0.1044	0.25	0.80	0.38	0.31
	Sadek	0.480	0.7253	0.99	0.99	0.5226	0.5370	0.30	0.40	0.33	0.33

Table 7.2. Optimal design of TMD for seismic application using the method proposed in the present study and the method by Sadek *et al.* [112]. It is assumed $\zeta_1 = 0.02$.

Broadly speaking, the largest mass ratio leads to a more effective device, since U_1 indicates greater reductions of the main structure displacement, and this is advantageously achieved through a smaller TMD stroke U_{21}. As shown in the table, the method by Sadek *et al.* involves approximately equal modal damping ratios ($\eta_1 \cong \eta_2$) and equal modal frequencies ($\beta_1 \cong \beta_2$), whereas the method proposed in this study complies with the requirement $\eta_1 = 0.12$. In the case of a small mass ratio, there are no appreciable differences between the two methods; in the case of a large mass ratio, conversely, significant differences emerge in both the optimal design parameters and modal properties. The method by Sadek *et al.* results in much higher damping parameter (ζ_2: 0.7253 *vs* 0.1630) and modal damping ratios (η_1: 0.5226 *vs* 0.1200; η_2: 0.5370 *vs* 0.1044). As stated before, similar values are not feasible with HDRB, hence the need to formulate a HDRB-oriented design method as proposed in the present study. This method produces greater reductions in the main structure displacement, as shown by U_1, despite the cost of a larger TMD stroke U_{21}.

In Fig. 7.3, the frequency response function $H_{u_1\ddot{u}_g}(\beta)$ of the main structure displacement with respect to ground acceleration is plotted in the uncontrolled (RC) and the optimally controlled (TMD) configurations for the two systems and the two design methods. In the (RC) configuration, the frequency response function is given by

$$H_{u_1\ddot{u}_g}(\beta) = -\frac{1}{1-\beta^2+\dfrac{2i\beta\zeta_1}{\sqrt{1+\mu}}} \tag{7.5}$$

where $i = \sqrt{-1}$ and β is the ratio between the input frequency and the natural frequency of the system in the (RC) configuration. In the (TMD) configuration, the frequency response function takes the form

$$H_{u_1\ddot{u}_g}(\beta) = -\frac{C_0(\beta)}{1+\mu-\beta^2 C_0(\beta)+2i\beta\zeta_1\sqrt{1+\mu}} \tag{7.6}$$

where

$$C_0(\beta) = 1+\mu\,\frac{\alpha^2(1+\mu)+2i\zeta_2\beta\alpha\sqrt{1+\mu}}{\alpha^2(1+\mu)-\beta^2+2i\zeta_2\beta\alpha\sqrt{1+\mu}} \tag{7.7}$$

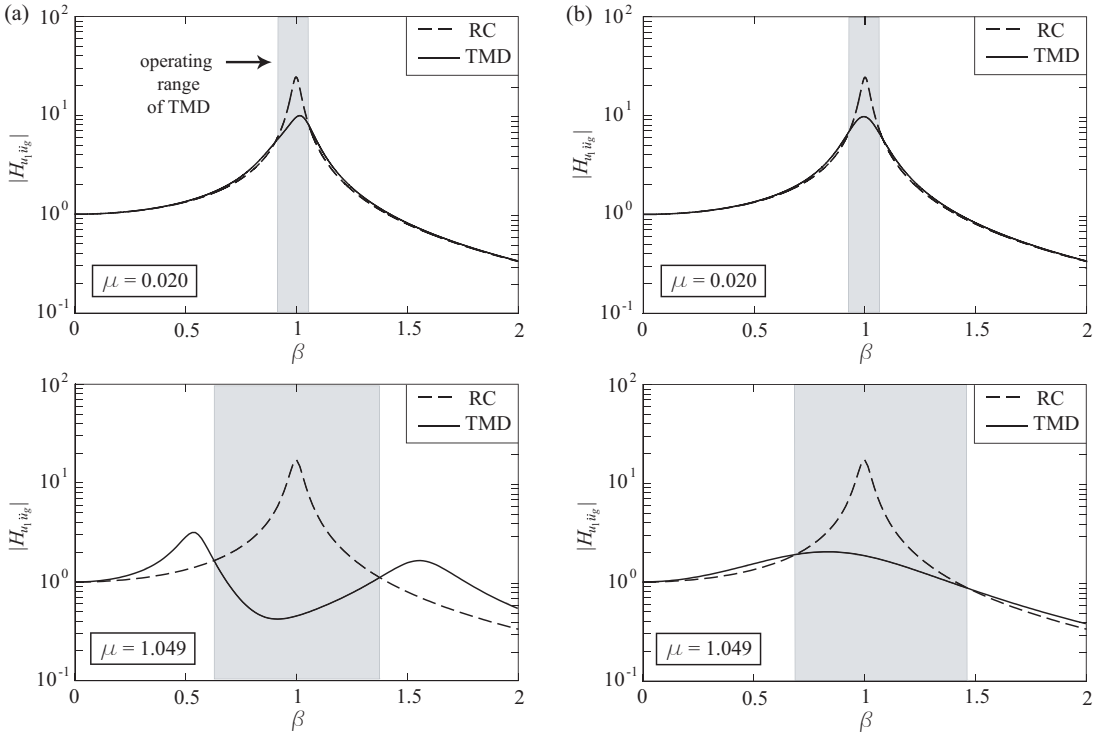

Figure 7.3. Frequency response function of the main structure displacement u_1 with respect to ground acceleration $\ddot{u}_g$ in the uncontrolled (RC) and optimally controlled (TMD) configurations. Optimal design of TMD using: (a) the method proposed in the present study; (b) the method by Sadek *et al.* [112]. Two mass ratios are considered: $\mu = 0.020$ and $\mu = 1.049$.

Frequency response curves in (RC) and (TMD) configurations intersect at two points, which identify the bandwidth controlled by the TMD (*operating range*): between these points, the amplitude of the frequency response function is reduced due to the presence of the device, elsewhere it is increased. Comparing the plots, it is clearly indicated that a large mass ratio TMD leads to greater reductions of the structural displacement response over a much broader frequency range. This result has a strong impact on the seismic effectiveness of TMD, which is generally recognized to be highly dependent on the earthquake frequency content. The structural response is significantly reduced only if the major frequency content of the excitation is included within the operating range, as in the presence of a narrow-band earthquake. For broad-band earthquakes, the TMD may be rather ineffective because of higher modes whose contribution is not reduced or even amplified by the device. As the mass ratio becomes larger, however, the broadening of the operating range makes the seismic effectiveness of TMD less frequency-dependent. In the case of a large mass ratio, differences between the two design methods emerge again: although being equal the operating range of TMD, the curve by the method proposed herein has a deeper anti-resonance region, leading to greater reductions of the main structure displacement, as confirmed by Tab. 7.2.

7.3 Shaking table tests

Aiming at assessing the dynamic behaviour and the seismic effectiveness of the proposed large mass ratio TMD, the present study comprises shaking table tests on a reduced scale model, carried out under a wide selection of accelerograms, both artificial and natural.

7.3.1 Experimental model

Shaking table tests were performed on the 1:5 scale model illustrated in Figs. 7.4 and 7.5. The model is composed of a two-story steel frame and a rigid mass located on the second floor: the former represents the main structure to be protected, the latter has the role of TMD.

The steel frame consists of L cross-section beams and columns and two square plates, one for each floor. Floor dimensions are 0.60 m × 0.60 m and total height is 2.40 m, with an inter-story height of 1.20 m (Fig. 7.5 (a)). Two cross bracings are arranged in the yz-plane so that the frame motion is in the x-direction only, the same as the one of base excitation, avoiding out of plane displacements (Fig. 7.5 (b)). Total floor masses are $M_{\mathrm{I}} = 90$ kg and $M_{\mathrm{II}} = 97$ kg, where I and II indicate the first and the second floor, respectively. A rectangular steel plate weighing 134 kg forms the TMD mass M_{III}. The model was tested in three different configurations:

- (BF) bare frame without mass M_{III};
- (RC) frame with mass M_{III} rigidly connected to the second floor;
- (TMD) frame with mass M_{III} converted into TMD.

In the uncontrolled configuration (RC), mass M_{III} is connected to the second floor of the frame by means of four steel beams with HEA120 cross-section, bolted to each other to realize a rigid connection (Fig. 7.4 (b) and (c)).

In the controlled configuration (TMD), mass M_{III} is disconnected from the second floor of the frame and converted into a large mass ratio TMD. The device is implemented by interposing between the mass and the frame three circular HDRB (Fig. 7.4 (d) and (e)), which realize the optimal TMD parameters designed in Sec. 7.2.3.

The bearings, whose dimensions are shown in Fig. 7.6 (a) and (b), consist of 27 2mm-thick rubber layers and 26 1mm-thick steel shims. Total rubber thickness is 54 mm, while the height of the bearing – excluding the end plates – is 80 mm. Total diameter is 58 mm, including 53 mm of shim diameter and 5 mm of cover. Oversize end plates permit the bearings to be bolted to the beams. The three bearings are placed symmetrically to the x-direction of base excitation (Fig. 7.6 (c)). Typical force – displacement loops experimentally obtained for the HDRB system are shown in Fig. 7.6 (d), while Fig. 7.6 (e) illustrates the effective horizontal stiffness k_H of the HDRB system *versus* the shear strain γ.

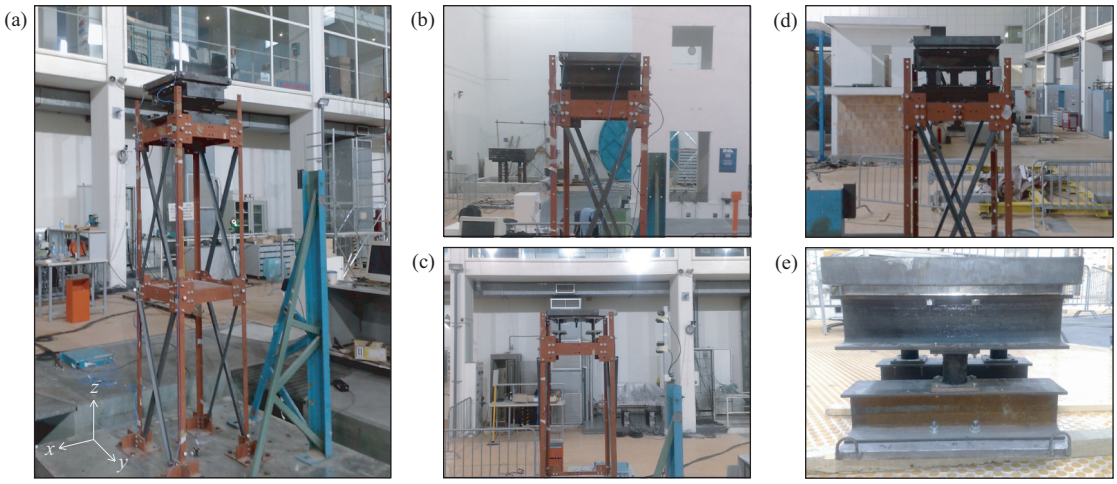

Figure 7.4. Experimental model for shaking table tests. (a) General view of the model. Note the auxiliary metallic frame supporting the laser displacement transducers. (b)and (c) Uncontrolled configuration: details of the rigid connection between the mass and the frame, views in the yz- and the xz-plane. (d) and (e) Controlled configuration: details of the TMD device, views in the yz-plane.

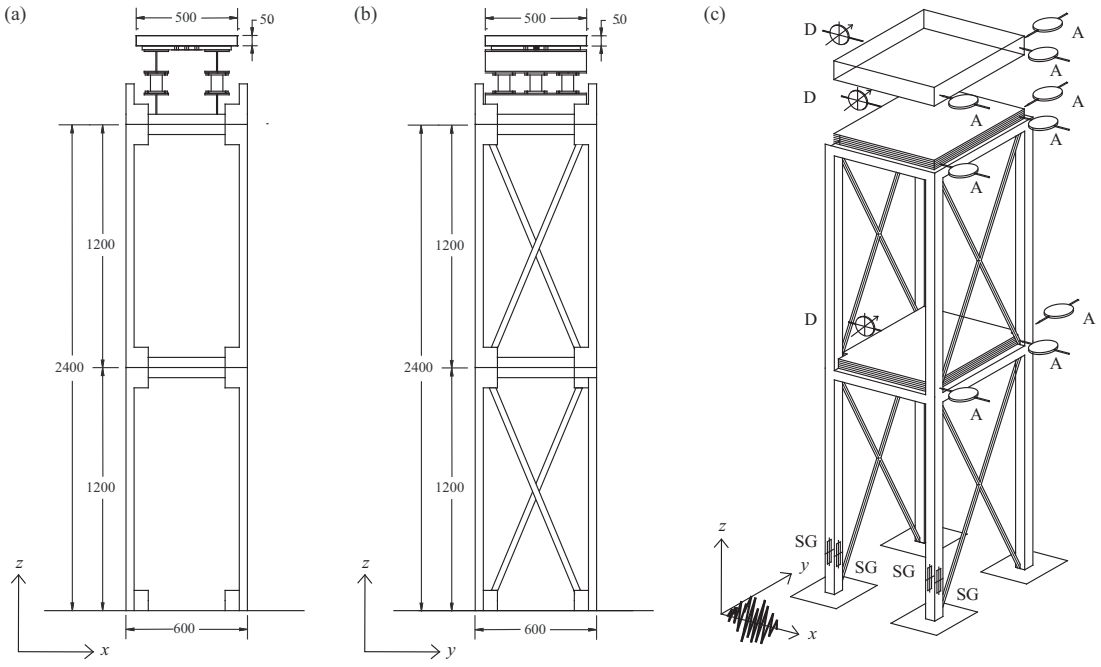

Figure 7.5. Experimental model for shaking table tests, controlled configuration (TMD). (a) View in the xz-plane. (b) View in the yz-plane. (c) Arrangement of measurement sensors. Legend: A = piezoelectric accelerometer; D = laser displacement transducer; SG = strain gauge.

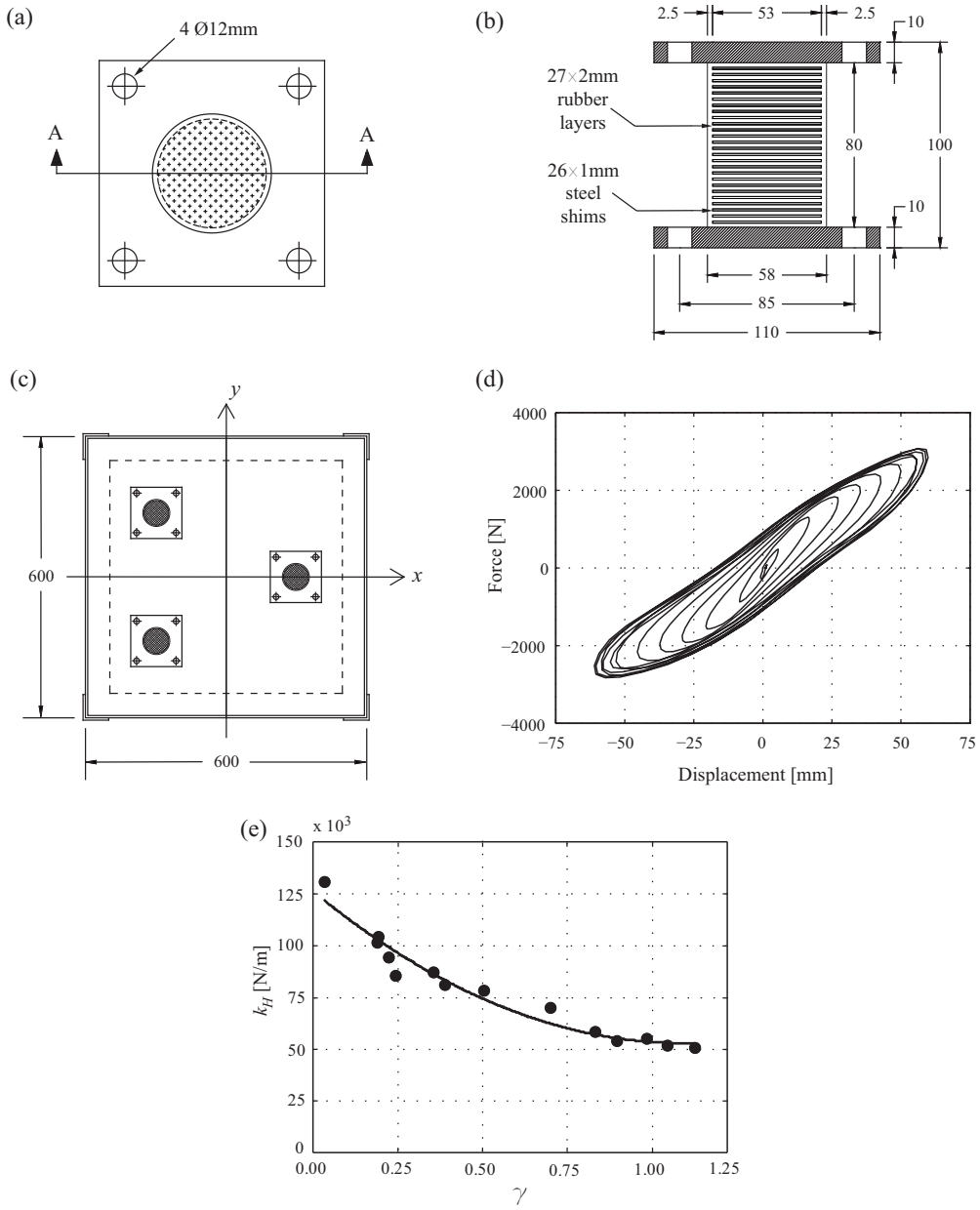

Figure 7.6. HDRB system. (a) Plane view of the circular bearing. (b) Section A-A of the circular bearing. (c) In-plane arrangement of the HDBR system. (d) Experimental force-displacement cycles of the HDRB system. (e) Horizontal stiffness k_H of the HDRB system *vs* shear strain γ.

7.3.2 Test setup

Tests were carried out on a six-degree-of-freedom shaking table in the MAT-QUAL Laboratory of ENEA (Italian National Agency for New Technologies, Energy and Environment), "Casaccia" Research Center in Rome, Italy. The 2.0 m × 2.0 m shaking table, manufactured by the MTS Corporation (USA), has the following characteristics: operating frequency range $0 - 100$ Hz; maximum acceleration $\pm 5g$, where g is the acceleration due to gravity; maximum velocity ± 1 m/s; maximum displacement ± 0.30 m; maximum tested specimen mass of 1 ton when its center of gravity is 1 m high.

Shaking table tests consisted of both dynamic identification tests and seismic tests. Dynamic identification tests made use of random white noise (constant power spectral density between 1 Hz and 20 Hz) and sine sweep accelerograms (variable frequency ranging from 1 Hz to 20 Hz at a rate of 1Hz/s). Seismic tests were performed under a wide selection of ground acceleration time histories, both natural and artificial, so that the influence of input duration and frequency content on the effectiveness of the proposed large mass ratio TMD could be assessed. In detail, time histories were an artificial accelerogram, generated to match the elastic response spectra given by the European Standard EN 1998-1:2005 (Eurocode 8) for 5% viscous damping and C type soil [30], and four natural accelerograms, recorded during historical earthquakes and selected from the database of the Pacific Earthquake Engineering Research Center [100]. Earthquake records are listed in Tab. 7.3. Among them, records from Northridge (Sylmar) and Kobe (KJMA) earthquakes are characterized by long-period pulse-like waveforms, so they are typically classified as near-fault ground motions [15]. Records from Imperial Valley (El Centro) and Tokachi-oki (Hachinohe) earthquakes exhibit instead fewer long-period characteristics, so they are used to represent far-field ground motions.

The time scale of seismic inputs was compressed in order to achieve the equivalence of the acceleration response between the reduced-scale model and the corresponding full-scale system. Considering the geometric scaling factor $\lambda_G = 0.2$ of the model, time scaling factor is equal to $\lambda_T = 0.447$. Seismic tests were carried out at different levels of peak ground acceleration (PGA) for each accelerogram, never exceeding the elastic limit of the frame as well as the design shear strain of the HDRB, set as $\gamma = 1.00$ in the present study.

Earthquake	Date	Station name	Component
Imperial Valley	1940/05/19	El Centro	NS
Tokachi-oki	1968/05/16	Hachinohe	NS
Northridge	1994/01/17	Sylmar	NS
Kobe	1995/01/16	KJMA	NS

Table 7.3. Earthquake records used for the seismic tests.

The model was equipped with the following measurement instrumentation (Fig. 7.5 (c)):

- n.11 Piezotronic PCB piezoelectric accelerometers, two on the shaking table, three on each floor and three on TMD mass;

- n.3 optoNCDT 1607 laser displacement transducers, one on each floor and one on TMD mass;

- n.4 strain gauges, to measure strains at the base of two columns of the model.

On each floor and on the mass, accelerometers were arranged as to measure accelerations in both the x- and the y-direction and to detect any torsional motion that might occur. Laser transducers were used to measure the displacements relative to the shaking table in the x-direction. For doing this, an auxiliary metallic frame was installed on the shaking table and it was employed as a benchmark for displacement measures (Fig. 7.4(a)). The auxiliary frame was verified to be rigid enough, having unitary transmissibility with respect to base acceleration in the frequency range of interest. The displacement responses of the second floor and the mass were further processed to obtain the TMD stroke by difference.

Output signals were acquired with sampling frequency of 200 Hz by means of a MTS 469D unit.

7.4 Analysis of results

7.4.1 Identification of dynamic properties

Previous to the seismic tests, dynamic properties and frequency response functions of the experimental model were identified [71] in all the tested configurations (BF, RC, TMD) to verify the assumptions made in the design phase.

Identified modal frequencies and damping ratios in the various tested configurations are listed in Tab. 7.4. In the (BF) configuration, the first natural frequency, 5.06 Hz, results to be close to the value 5.35 Hz assumed in the design phase. In the (TMD) configuration, nonlinearity in the lateral behavior of HDRB makes the results depend on the excitation level. As shown in Fig. 7.6 (e), HDRB show a nonlinear softening behavior up to $\gamma = 0.80$ since k_H decreases with increasing shear strain. Around the design shear strain $\gamma = 1.00$, k_H is constant and HDRB can be modeled as linear with a sufficient accuracy. Natural frequencies and damping ratios in the (TMD) configuration are then shown with increasing PGA and γ. As expected, the model exhibit decreasing frequencies due to the HDRB softening behavior. Damping ratios, considerably higher than in (BF) and (RC) configurations, are almost constant instead. In particular, the first modal damping ratio, ranging from 0.1143 to 0.1173, is comparable with the value 0.12 assumed in the design phase.

Test configuration	PGA [g]	γ	I mode		II mode		III mode	
			f [Hz]	η	f [Hz]	η	f [Hz]	η
BF	0.20	-	5.06	0.0200	16.72	0.0061	-	-
RC	0.20	-	3.51	0.0200	15.61	0.0045	-	-
TMD	0.61	0.16	2.50	0.1173	8.18	0.0971	16.48	0.0184
	0.86	0.26	2.40	0.1160	7.71	0.1159	16.25	0.0196
	1.08	0.35	2.34	0.1143	7.41	0.1085	16.14	0.0208
	1.32	0.45	2.29	0.1163	7.16	0.0823	16.02	0.0198

Table 7.4. Identified modal frequencies and damping ratios for BF, RC and TMD configurations. For the TMD configuration, modal properties are identified with increasing PGA and HDRB shear strain γ.

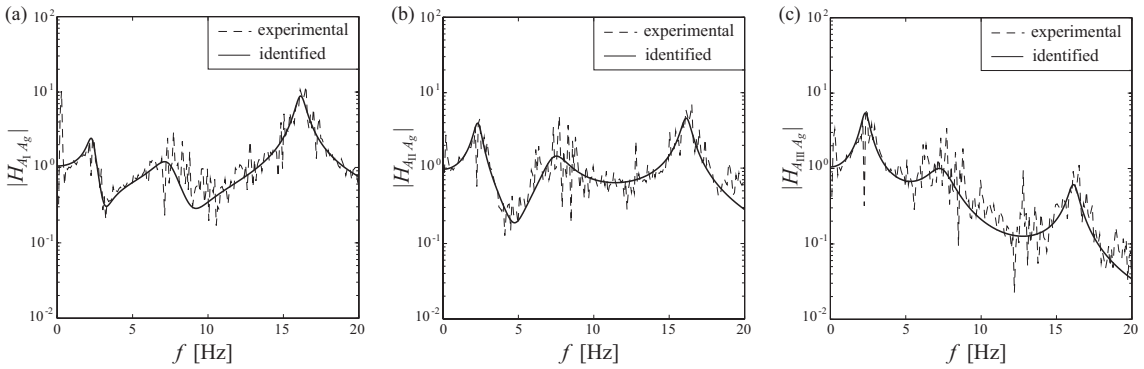

Figure 7.7. Experimental and identified frequency response functions of the model in the controlled configuration (TMD). (a) Absolute acceleration of the first floor A_I. (b) Absolute acceleration of the second floor A_{II}. (c) Absolute acceleration of the TMD A_{III}.

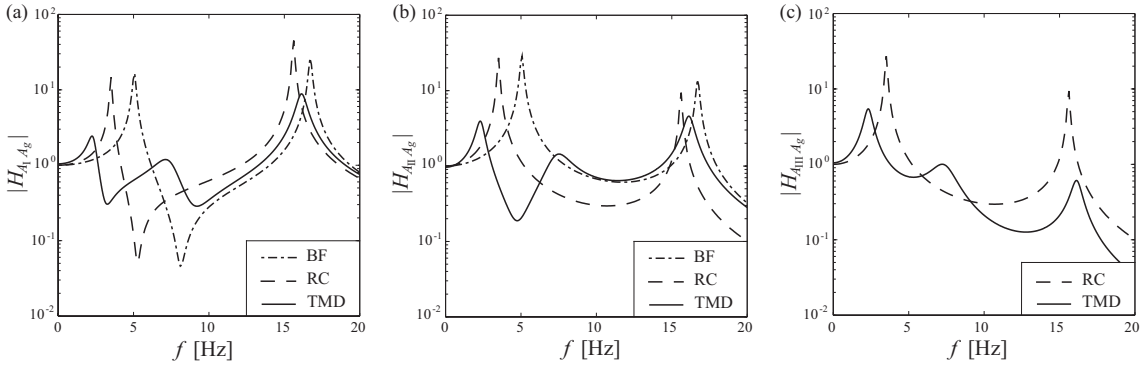

Figure 7.8. Identified frequency response functions of the model in (BF), (RC) and (TMD) configurations. (a) Absolute acceleration of the first floor A_I. (b) Absolute acceleration of the second floor A_{II}. (c) Absolute acceleration of the TMD A_{III}.

Shown in Fig. 7.7 is a comparison between experimental and identified frequency response functions in the (TMD) configuration. Functions refer to floor absolute accelerations A_k (k = I, II) and TMD absolute acceleration A_{III} with respect to ground acceleration A_g. A very good agreement of the curves indicates the accuracy of the identification results.

In Fig. 7.8, the dynamic properties of the model are highlighted by comparing the identified frequency response functions in all the tested configurations. In the uncontrolled configuration (RC), significant amplifications can be seen for both the first and the second mode. These values are greatly reduced in the controlled configuration (TMD) thanks to an increase in the modal damping ratios, as indicated above. The bandwidth controlled by the TMD around the first peak varies depending on the response quantity, but it is quite broad in any case. It is noteworthy that the TMD decreases the response of the second mode as well, with a beneficial effect on the overall structural response.

7.4.2 Evaluation of seismic effectiveness

In order to asses the seismic effectiveness of the proposed large mass ratio TMD, a series of seismic tests was performed on the experimental model in the controlled (TMD) and the uncontrolled (RC) configurations. Seismic effectiveness is evaluated in terms of both rms and peak response by means of performance indices. Once chosen a response quantity of interest, the performance index is defined as the ratio of the response value between the controlled and the uncontrolled configurations.

With regard to the frame, relevant response quantities are floor absolute accelerations A_k (k = I, II) as well as base shear T_b and bending moment M_b, representative of the overall internal loads in the structural members. Base shear T_b is computed by summing the inertial forces acting on each mass; base bending moment M_b is computed by summing the moments of the inertial forces about the base of the frame. Performance indices are expressed in terms of rms responses as

$$I_1 = \frac{\text{rms}\left(T_{b\,\text{TMD}}\right)}{\text{rms}\left(T_{b\,\text{RC}}\right)} \qquad I_2 = \frac{\text{rms}\left(M_{b\,\text{TMD}}\right)}{\text{rms}\left(M_{b\,\text{RC}}\right)} \qquad I_{3,4} = \frac{\text{rms}\left(A_{k\,\text{TMD}}\right)}{\text{rms}\left(A_{k\,\text{RC}}\right)} \quad k = \text{I, II} \tag{7.8}$$

Note that for indices I_1 – I_4, a value smaller than one implies the TMD effectiveness in reducing the structural response.

With regard to the TMD, relevant response quantities are the displacement Δ of the mass relative to the second floor, *i.e.* the TMD stroke, and the mass absolute acceleration A_{III}. Performance indices are expressed in terms of rms responses as

$$I_5 = \frac{\text{rms}\left(\Delta_{\text{TMD}}\right)}{\text{rms}\left(D_{\text{III}\,\text{RC}}\right)} \qquad I_6 = \frac{\text{rms}\left(A_{\text{III}\,\text{TMD}}\right)}{\text{rms}\left(A_{\text{III}\,\text{RC}}\right)} \tag{7.9}$$

Index I_5 represents the TMD stroke divided by the displacement D_{III} of the mass with respect to the shaking table in the uncontrolled configuration. Similarly to $I_1 - I_6$, performance indices $J_1 - J_6$ are defined in terms of peak responses as well.

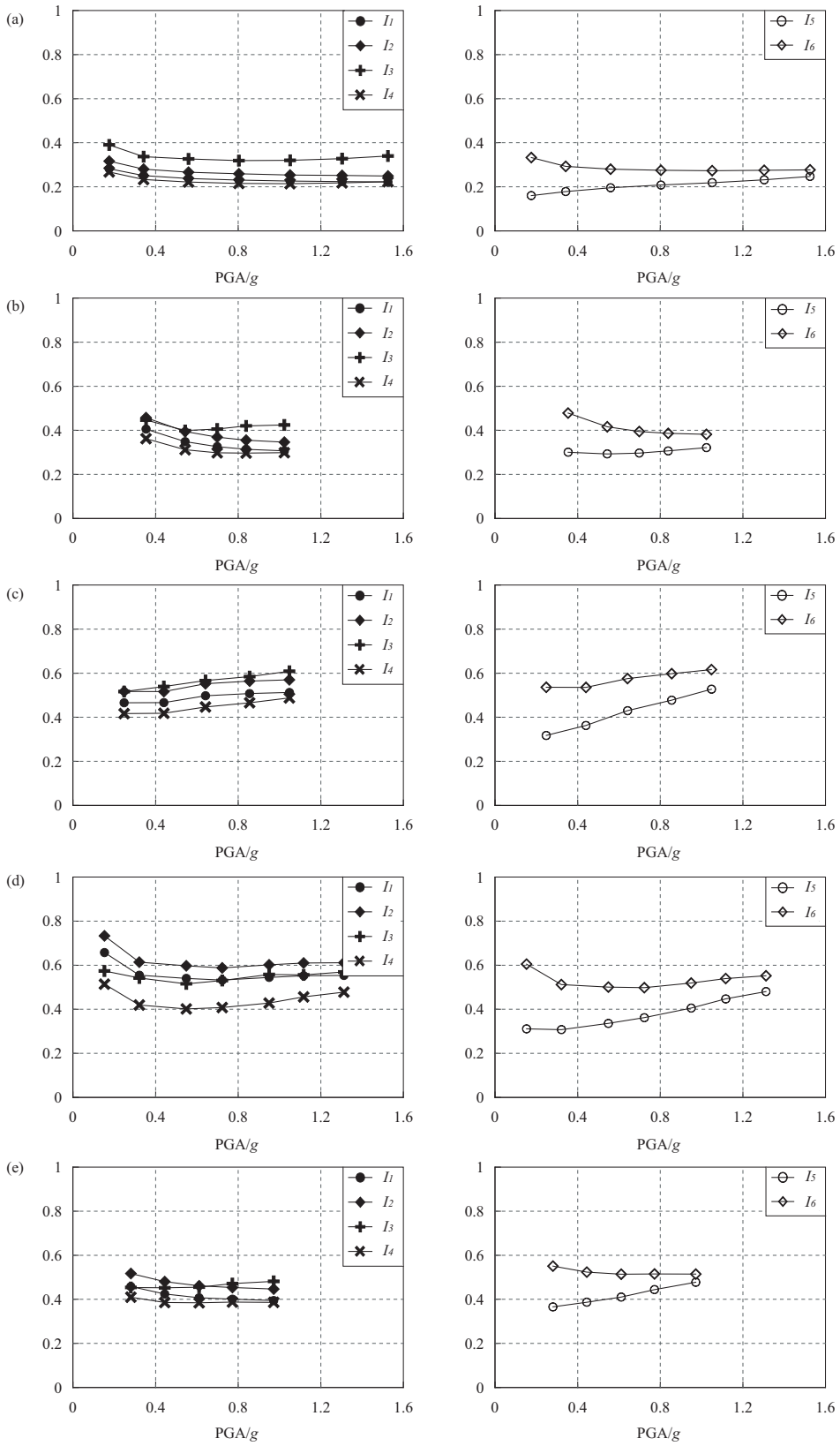

Figure 7.9. Performance indices $I_1 - I_6$ in terms of rms responses. For a given accelerogram, indices are shown *vs* PGA level: (a) Eurocode 8 spectrum-compatible. (b) El Centro. (c) Hachinohe. (d) Northridge. (e) Kobe.

Accelerogram	PGA [g]	γ	J_1	J_2	J_3	J_4	J_5	J_6
EC8	0.18	0.03	0.371	0.407	0.670	0.374	0.208	0.396
	0.34	0.12	0.290	0.323	0.562	0.345	0.256	0.377
	0.56	0.19	0.286	0.313	0.550	0.345	0.247	0.332
	0.80	0.25	0.266	0.234	0.520	0.302	0.236	0.308
	1.05	0.37	0.275	0.289	0.460	0.328	0.268	0.335
	1.30	0.50	0.282	0.296	0.473	0.348	0.294	0.349
	1.52	0.63	0.281	0.299	0.471	0.358	0.315	0.359
El Centro	0.18	0.04	0.589	0.637	0.649	0.674	0.477	0.700
	0.35	0.12	0.463	0.540	0.680	0.531	0.391	0.614
	0.54	0.23	0.429	0.492	0.633	0.502	0.438	0.618
	0.70	0.33	0.417	0.483	0.640	0.538	0.453	0.578
	0.84	0.45	0.433	0.470	0.657	0.565	0.471	0.555
	1.02	0.56	0.442	0.463	0.681	0.615	0.479	0.537
Hachinohe	0.12	0.03	0.737	0.826	0.648	0.743	0.401	0.772
	0.25	0.12	0.625	0.681	0.525	0.575	0.490	0.719
	0.44	0.21	0.594	0.636	0.531	0.605	0.497	0.648
	0.64	0.30	0.624	0.668	0.591	0.682	0.506	0.616
	0.85	0.41	0.620	0.669	0.648	0.740	0.542	0.624
	1.05	0.56	0.625	0.667	0.722	0.737	0.605	0.650
Northridge	0.15	0.04	0.745	0.845	0.933	0.781	0.583	0.812
	0.33	0.12	0.595	0.669	1.016	0.638	0.577	0.742
	0.55	0.21	0.575	0.651	0.983	0.699	0.609	0.727
	0.72	0.31	0.561	0.612	1.034	0.650	0.642	0.718
	0.95	0.43	0.572	0.652	1.175	0.698	0.706	0.766
	1.12	0.57	0.615	0.701	1.251	0.870	0.783	0.834
	1.31	0.72	0.639	0.719	1.192	0.979	0.844	0.895
Kobe	0.18	0.05	0.707	0.806	0.695	0.730	0.516	0.764
	0.28	0.16	0.588	0.651	0.614	0.582	0.487	0.696
	0.44	0.30	0.566	0.648	0.681	0.664	0.550	0.728
	0.61	0.47	0.619	0.645	0.683	0.725	0.606	0.729
	0.77	0.66	0.624	0.650	0.709	0.699	0.656	0.734
	0.97	0.88	0.610	0.645	0.661	0.676	0.703	0.727

Table 7.5. Performance indices $J_1 - J_6$ in terms of peak responses. For a given accelerogram, indices are shown *versus* PGA level and HDRB shear strain γ.

Performance indices $I_1 - I_6$ and $J_1 - J_6$ due to the seismic tests are shown in Fig. 7.9 and Tab. 7.5, respectively. For a given accelerogram, indices are reported *versus* PGA level and HDRB shear strain γ. A comparative analysis of the results highlights the following remarks.

Generally speaking, seismic tests prove the effectiveness of the proposed large mass ratio TMD in reducing the structural response compared with the RC configuration. Performance indices indicate considerable percentage reductions of internal loads and floor accelerations. Base shear and bending moment are suppressed down to $40\% - 70\%$ in terms of both rms and peak values. As regards floor accelerations, a better control performance is recognizable at the location of the TMD and for rms responses: reductions amount to $60\% - 75\%$ for the second floor and $40\% - 60\%$ for the first floor.

For a given accelerogram, performance indices remain almost constant with increasing PGA, confirming that the proposed TMD is robust against the deviations in design parameters which result from the HDRB nonlinear behavior. Similar deviations may also result either from uncertainties about structural properties in the design phase or from nonlinearities in the structural behavior, *e.g.* under a strong earthquake, when the structure experiences inelastic deformations leading to a decrease in natural frequencies and to an increase in damping. In such cases, both the frequency ratio α and the damping ratio ζ_2 undergo an offset from their optimal values, which may significantly prejudice the TMD performance. Authors often indicate the lack of robustness against off-optimum deviations as an inherent limitation to the seismic effectiveness of the TMD. A non-conventional TMD with large mass ratio is found to be significantly more robust, however.

The TMD performance slightly depends on the excitation frequency content and some differences can be noticed comparing different seismic inputs. The best results are attained under the Eurocode 8 spectrum-compatible accelerogram: internal loads and floor accelerations are reduced by $60\% - 75\%$ in terms of both rms and peak values, regardless of the PGA level. The artificial accelerogram is a broad-band excitation whose frequency content can be properly represented by a random white noise in the frequency range of interest for the experimental model. This agreement with the input adopted in the design phase causes the outstanding TMD performance. Aiming at thoroughly comparing these experimental results with the design results obtained in Sec. 7.2, we identify the frequency ratio α realized by the experimental model. Being $\gamma = 0.63$ the maximum shear strain and $k_H = 65055$ N/m the corresponding effective stiffness of the HDRB system, the frequency ratio was $\alpha = 0.693$, that is an offset from the optimal design value $\alpha_{\text{opt}} = 0.420$. This deviation or *detuning* effect, although considerable, affects only marginally the TMD performance thanks to the increased robustness due to the large mass ratio.

Results similar to those for Eurocode 8 accelerogram are expected for far-field ground motions, like El Centro and Hachinohe, which are typically broad-band excitations. As a matter of fact, expectations are confirmed for the El Centro accelerogram,

whereas some differences are found for the Hachinohe accelerogram. First of all, reductions in rms and peak structural responses are smaller, with values ranging from 30% to 50%. Secondly, performance indices exhibit a slight upward trend with increasing PGA, hence the TMD effectiveness decays as the PGA increases from $0.1g$ to $1.0g$. This is mainly due to the different frequency content of the seismic excitations. As observed in Sec. 7.2.4, the TMD effectiveness depends on the input frequency bandwidth, even if a large mass ratio opposes this limitation broadening the operating range of the device. The dominant frequency of the Hachinoe accelerogram, that is the frequency corresponding to the peak of its Fourier spectrum, is not included in the operating range of the proposed TMD and this significantly deteriorates the device effectiveness. In addition, as the PGA increases, off-optimum parameters still further limit the TMD performance.

In the case of near-fault ground motions, like Northridge and Kobe, the TMD seismic effectiveness is limited not so much by the frequency content, which is typically narrow-band, as by the impulsive character of the seismic excitation. For this reason, performance indices in Fig. 7.9 and Tab. 7.5 show that the proposed TMD is able to suppress rms responses, but it is less effective to reduce peak responses. In the case of Northrige accelerogram, for instance, rms values are reduced by $40\% - 55\%$ for base shear and bending moment and $45\% - 60\%$ for floor accelerations. In terms of peak values, however, reductions decrease down to 30% for internal loads, while the first floor peak acceleration results to be even amplified compared with the uncontrolled configuration ($J_3 > 1$). As pointed out by investigators, it must be considered that the TMD passively responds to the structural motion and reduces the structural response by vibrating out-of-phase with it. As a result, the TMD may not be fully effective when impulsive earthquake excitations reach their maximum values, that is during the very first cycles of oscillation. A deeper insight of this comes from a careful analysis of time history responses.

Figs. 7.10 – 7.14 illustrate the time history responses of floor absolute accelerations A_{I} and A_{II}, base shear T_b and base bending moment M_b under the selected accelerograms. As it can be seen, the proposed TMD does not need a significant time delay to activate in the presence of both far-field and near-fault ground motions, but some differences exist. Responses due to far-field accelerograms (Figs. 7.11 – 7.12) slowly build up to their maximum, which occurs few seconds after the beginning of the excitation, when the TMD is already fully effective. Even though uncontrolled and controlled responses are comparable during the very first cycles of oscillation, this affects neither the rms nor the peak performance indices. Responses due to near-fault accelerograms (Figs. 7.13 – 7.14) exhibit a low-frequency oscillation behavior, owing to the long-period pulses of the input, and reach their maximum at the very beginning of the excitation, when the TMD is not fully effective yet. In this case, the first peaks of the structural responses are slightly reduced and performance indices $J_1 - J_6$ suffer from this.

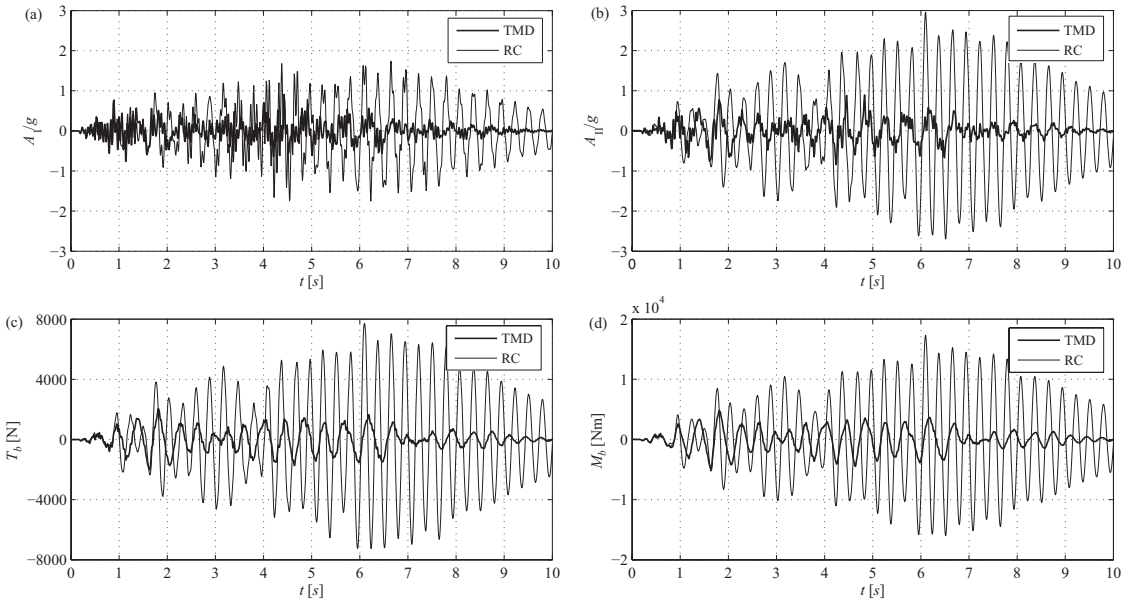

Figure 7.10. Time history responses due to Eurocode 8 spectrum-compatible accelerogram, time scaling factor $\lambda_T = 0.447$, PGA $= 0.8g$. (a) First floor absolute acceleration A_{I}. (b) Second floor absolute acceleration A_{II}. (c) Base shear T_b. (d) Base bending moment M_b.

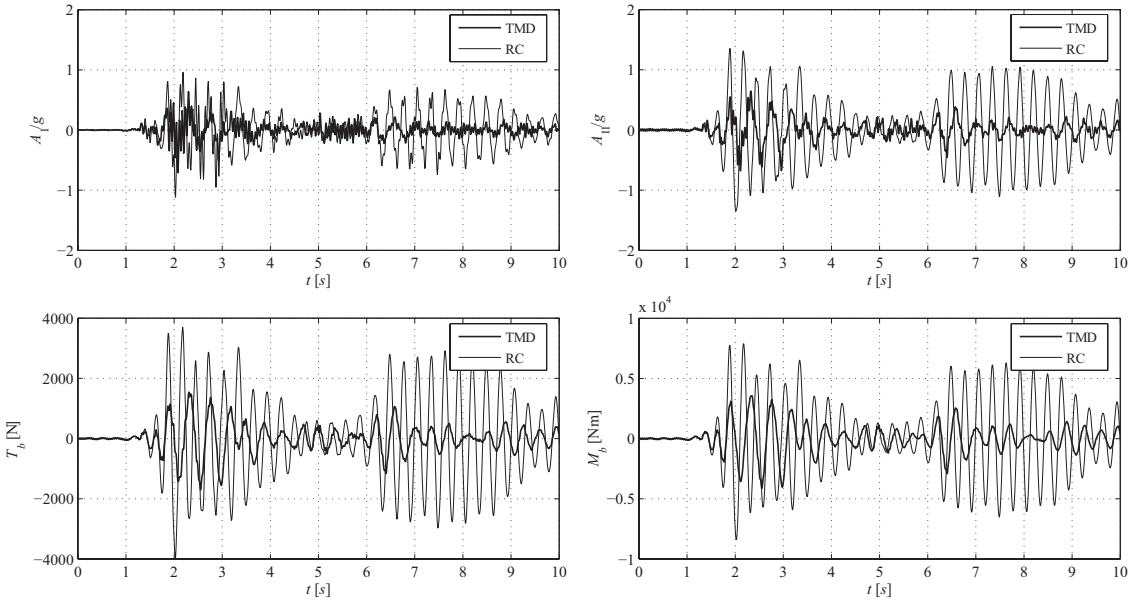

Figure 7.11. Time history responses due to El Centro accelerogram, time scaling factor $\lambda_T = 0.447$, PGA $= 0.5g$. (a) First floor absolute acceleration A_{I}. (b) Second floor absolute acceleration A_{II}. (c) Base shear T_b. (d) Base bending moment M_b.

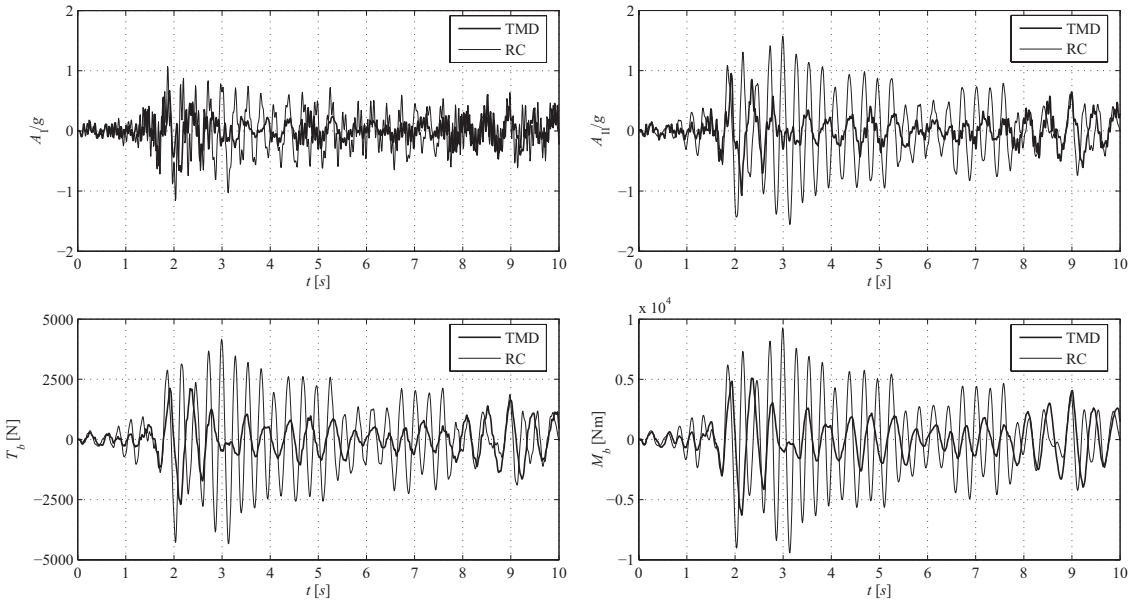

Figure 7.12. Time history responses due to Hachinohe accelerogram, time scaling factor $\lambda_T = 0.447$, PGA $= 0.6g$. (a) First floor absolute acceleration A_{I}. (b) Second floor absolute acceleration A_{II}. (c) Base shear T_b. (d) Base bending moment M_b.

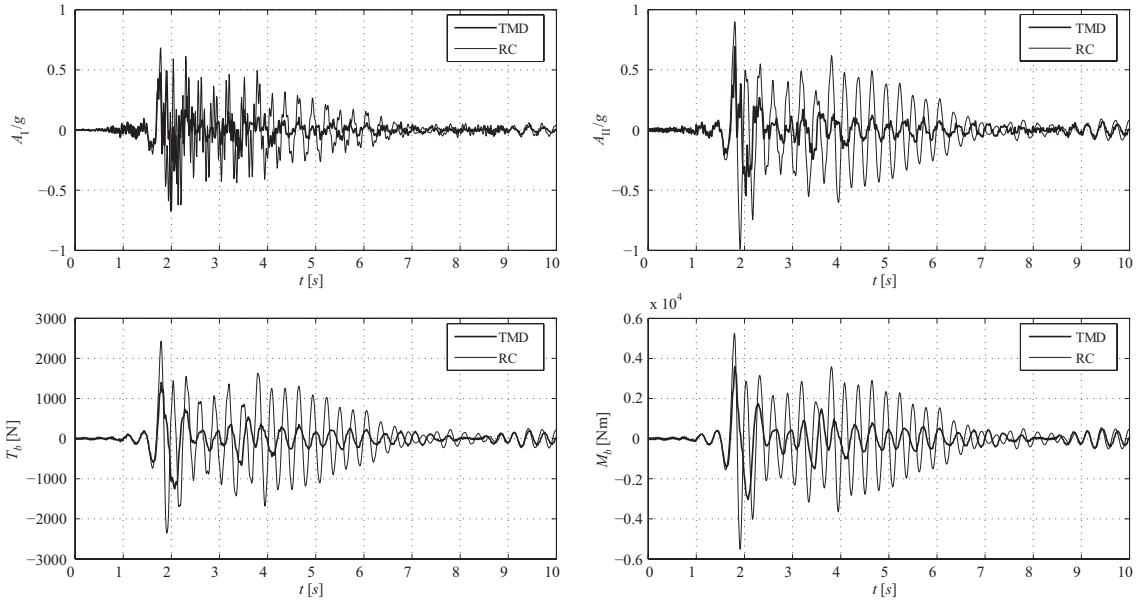

Figure 7.13. Time history responses due to Northridge accelerogram, time scaling factor $\lambda_T = 0.447$, PGA $= 0.5g$. (a) First floor absolute acceleration A_{I}. (b) Second floor absolute acceleration A_{II}. (c) Base shear T_b. (d) Base bending moment M_b.

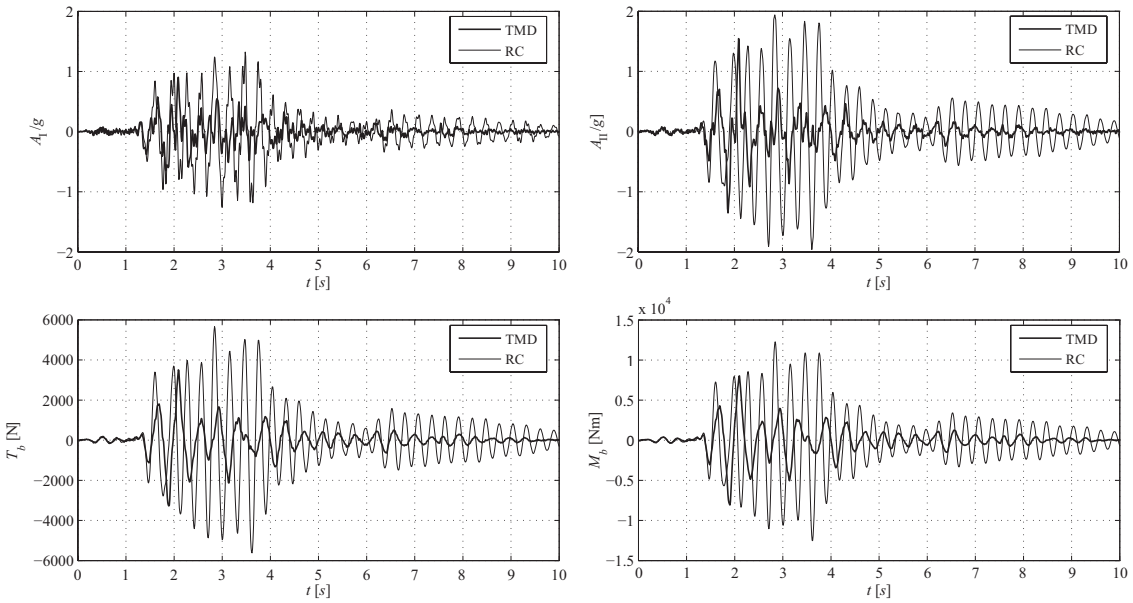

Figure 7.14. Time history responses due to Kobe accelerogram, time scaling factor $\lambda_T = 0.447$, PGA $= 0.6g$. (a) First floor absolute acceleration A_{I}. (b) Second floor absolute acceleration A_{II}. (c) Base shear T_b. (d) Base bending moment M_b.

Concluding remarks refer to the dynamic response of the device mass. In the controlled configuration, the TMD stroke Δ tends to increase with increasing PGA, though the HDRB shear strain never exceeds the design value $\gamma = 1.00$. Meanwhile, its absolute acceleration A_{III} is considerably reduced as compared with the uncontrolled configuration, in terms of both rms ($I_6 < 1$) and peak values ($J_6 < 1$). These results confirm the feasibility of the proposed large mass ratio TMD and its compatibility with any other function (structural or architectural) the device mass might already have.

Conclusions

Summary

The primary objective of the present thesis has been to assess the feasibility and the effectiveness of innovative technologies for the seismic protection of equipment in critical facilities. A preliminary study of current Literature and international seismic codes has led to identify a number of shortcomings and emerging research needs in the field. Although some detailed vulnerability studies already exist, significant theoretical and technical issues associated with the seismic design of equipment result not to be sufficiently investigated. Among the others, the following problems deserve particular attention: how to protect equipment and, especially, how to insure its continuing functioning in the presence of the enhanced performance objectives and the increased seismic hazard level posed to critical facilities; how to deal with the seismic analysis and verification/design of heavy equipment, at the moment excluded from the provisions of international codes; how to treat the dynamic interaction between the equipment and its supporting structure when it is expected to be significant, owing either to the large mass of the equipment or to tuning phenomena.

Once having identified current inadequacies with equipment in critical facilities and the relevant scientific interest of the topic, the study has been focused on the survey of two innovative protection strategies, believed to have the potential for a wide application:

i. equipment and raised floor isolation systems;

ii. non-conventional Tuned Mass Damper (TMD) with large mass ratio.

For the sake of implementation in real applications, two kinds of passive devices have been proposed and studied:

i. High-Damping Rubber Bearings (HDRB), whose mechanical behaviour has been described by means of a linear Kelvin-Voigt visco-elastic model;

ii. a novel isolator showing nonlinear hysteretic behaviour, composed of a rolling pendulum plus hysteretic elements to provide supplemental energy dissipation.

A case study has then been considered, referring to a frame supporting structure housing a block-type equipment, and two reduced-order generalized models have been derived for design purposes: a single-degree-of-freedom model, suited for a decoupled dynamic analysis in which the equipment is assumed to be in cascade with the supporting structure, *i.e.* receiving the input from the structure but not modifying this input; a two-degree-of-freedom model, suited for a coupled dynamic analysis in which the supporting structure and the equipment are considered as coupled parts of a combined primary-secondary system and analyzed together.

The proposed technologies have been extensively investigated in the light of numerical simulations and experimental campaigns of shaking table tests. The main results obtained are here summarized and discussed.

Passive isolation system with linear visco-elastic behaviour

A passive isolation system composed of HDRB has been proposed and implemented in a 1:5 scale model. The model consisted of a two-storey steel frame, having the role of a supporting structure, and a large mass, representing a block-type equipment, isolated from the second floor. The problem of the optimal design of the isolation system has been set and solved. Ground acceleration has been modelled as a Gaussian random process with white noise spectral density. A numerical searching technique has been used to determine the optimal stiffness and damping properties of the isolation system, in order to provide a high control performance in terms of both absolute acceleration and relative displacement of the isolated equipment. Distinctive of the methodology is the consideration of the dynamic interaction between the isolated equipment and the supporting structure and of the peculiar damping properties of HDRB in the context of a non-proportionally damped system. Extensive shaking table tests have been performed on the physical model with the purposes of both dynamic identification and seismic effectiveness assessment.

The analysis of the experimental results has led to the following conclusions. First, dynamic identification tests have shown that HDRB present a nonlinear softening behaviour, *i.e.* decreasing effective horizontal stiffness with increasing shear strain, up to a strain value of $70\% - 80\%$. Afterwards, around the design shear strain level assumed as 100%, the effective stiffness becomes constant. Hence, it has been confirmed that, in the design range, the HDRB system can be modelled as linear with a satisfactory accuracy. Second, seismic tests have proved that the proposed isolation system effectively suppresses the equipment absolute acceleration down to $50\% - 80\%$ under a wide selection of seismic excitations, in terms of both root-mean-square (RMS) and peak values. Furthermore, the performance obtained under far-field and near-fault ground motions is substantially comparable. Only in one case (Northridge earthquake), the presence of a long-period pulse at the beginning of the input time history causes the isolation performance to significantly decay.

Eventually, to ensure strength and serviceability, also the response of the suppor-

ting structure has been monitored. It has been obtained that reducing the coupling between the equipment and the structure, compared to a rigid connection, advantageously reduces the dynamic response of the structure as well. Floor displacements and the actions at the base of the frame (shear and moment) were suppressed down by $60\% - 70\%$ in terms of both RMS and peak values, indicating considerable reductions of overall internal loads in structural members.

Passive isolation system with nonlinear hysteretic behaviour

A novel class of bearings with nonlinear hysteretic behaviour, referred to as High Damping Rolling Pendulum (HDRP) isolators, has been proposed and studied. Characteristic of the new isolators is to be of a rolling-base type and to incorporate hysteretic elements to provide damping. However, the study has been addressed to exploit, rather than a specific implementation, the mechanical properties distinctive of the new class, which can be summarized as follows: (i) the decoupling between an elastic restoring force, to provide a re-centering mechanism, and a hysteretic restoring force, to provide rate-independent damping; (ii) a nonlinear geometric stiffness suitable to achieve multiple performance objectives throughout the course of motion; (iii) a high energy dissipation capability to limit the horizontal displacements induced by severe earthquake.

The study has first dealt with the problem of formulating a constitutive relationship for the isolation system, which is characterized by both physical and geometrical nonlinearities. An integrable hysteresis model, derived from the mathematical Duhem operator, has been adopted owing to its versatility and analytical tractability. The constitutive relationship, describing from a macroscopic viewpoint the restoring force *versus* displacement relation, can be represented by a rheological model composed by a nonlinear spring, a hysteretic element and a linear viscous damper arranged in parallel. Five parameters control the model and, then, the mechanical properties of the isolation system. The total restoring force shows a peculiar behaviour that is called *soft-hardening*, *i.e.* for small displacement amplitudes, the model exhibits softening behaviour, which gradually changes into hardening behaviour for increasing displecement amplitudes.

The developed model has then been used for the optimal design of an isolation system for the seismic protection of equipment. An Operational performance objective has been considered and a set of seven artificial accelerograms matching the response spectrum given by the Italian code has been assumed in the design. Aiming at preserving the serviceability of the isolated equipment by preventing excessive inertial loads, an optimization criterion has been defined which consists in reducing the peak equipment absolute acceleration to a threshold value allowable for full operation, set as 20% of the Peak Ground Acceleration (PGA). A further design criterion, needed to obtain a unique optimal solution, has been defined by requiring the maximization of an energy performance index equal to the ratio of the irrecoverable energy dissi-

pated through hysteresis in the isolation system to the input energy transmitted to the equipment. The proposed idea is that the more is dissipated of the input energy transmitted by the earthquake, the more effective and economic is the isolation system performance. The methodology has been proved to account in a synthetic way for both the response quantities of the equipment, absolute acceleration and relative displacement. Furthermore, a ductility demand corresponding nearly to 10 has been obtained for the isolation system, indicating a full exploitation of its energy dissipation capability.

The seismic effectiveness of the equipment isolation system has been assessed for different frequency contents of natural earthquakes by means of numerical simulations. As an example of a real application, a full scale model of a steel frame structure has been considered, supposing a block-type equipment isolated on the first floor. A mass ratio of 0.2713 has been assumed and a coupled approach has been adopted in the design of an isolation system with nonlinear hysteretic behaviour. As a result, a significant control of the equipment acceleration response has been obtained. The peak absolute acceleration was limited to the design value (20% of PGA) not only under the design input, but also under the natural accelerograms, without substantial differences depending on the different frequency content. This was equivalent to have reductions of 95%, in terms of both peak and RMS acceleration values, as compared to uncontrolled configuration with fixed-base equipment. Meanwhile, the equipment displacement relative to the attachment floor resulted to be limited as well, with peak values not greater than 20 cm, for Hachinohe and El Centro accelerograms, and 10 cm, for the other inputs.

In addition to the acceleration requirement, limiting the displacements across the isolation system is indeed a crucial point for the safety and functionality of equipment in critical facilities. In this regard, the optimal nonlinear hysteretic isolation has also been compared with an optimal isolation system with linear visco-elastic behaviour. Being equal the isolation performance, as required in the design phase, the nonlinear system outperforms the linear one in further limiting the equipment relative displacement. Reductions amount to 10%–20% in terms of peak values and to 30%–40% in terms of RMS values.

Aiming at an exhaustive evaluation of the nonlinear isolation system, the response of the supporting structure has been considered. The structural response was advantageously reduced in the controlled as compared to the uncontrolled configuration, with reductions of floor displacements, base shear and base moments amounting to $50\% - 60\%$, in terms of both peak and RMS values, for three (Kobe, El Centro, Hachinohe) out of five accelerograms. Smaller values have been found for the design input and Northridge accelerogram: in the former case, the displacements across the isolation system are very moderate, less than 5 cm, hence the hysteretic energy dissipation capability of the isolation system is not fully exploited; in the latter case, the worse performance is due to the impulsive character of the seismic excitation.

Non-conventional TMD with large mass ratio

The dynamic behaviour of a non-conventional Tuned Mass Damper (TMD) with large mass ratio has been investigated and an optimal design methodology has been formulated for seismic applications. Compared with conventional TMD, the device mass has been increased up to be comparable with the mass of the structure to be protected, aiming at a better control performance. In order to avoid the introduction of an excessive additional weight, a mass already present on the structure has been converted into a tuned mass, retaining its own function beyond the mere control function.

The study has been motivated first by the results previously obtained for the equipment isolation systems. By comparing an uncontrolled configuration, where the equipment is rigidly fixed to the structure, and a controlled configuration, where the equipment is isolated from the structure, reductions of both the equipment response and the structural response have been achieved. In other terms, this means that reducing the coupling between the equipment and its supporting structure may benefit not only the equipment to be protected, but also the structure itself. Like for the equipment isolation systems, the implementation of a non-conventional TMD is based indeed on the decoupling between a mass and its supporting structure. As a consequence of this analogy, the two technologies have been studied by means of the same structural models, while essentially different design criteria have been adopted.

Aiming at increasing structural integrity and reducing internal loads in structural members, on optimization problem has been defined which consists in minimizing the root-mean-square displacement response of the structure in order to find the optimal design parameter, the frequency ratio of the TMD. The damping ratio of the TMD has been obtained subsequently by requiring the damping ratio in the first complex mode of the combined system to be constant and equal to a set value. This assumption has been due to the use of HDRB in a non-proportionally damped system and has been confirmed by the results of the dynamic identification tests. The methodology has been compared also to classic design formulae to appraise its novelty.

The dynamic behaviour and the seismic effectiveness of the proposed device have been assessed by means of shaking table tests, performed on a 1:5 scale model of a steel frame structure equipped with a non-conventional TMD. The following conclusions have been drawn. (i) A non-conventional TMD with a large mass ratio (*e.g.* $\mu = 1.049$) outperforms a conventional TMD with a small mass ratio (*e.g.* $\mu = 0.020$) leading to greater reductions of the structural response. (ii) A non-conventional TMD with a large mass ratio has been found to be more robust against off-optimum deviations resulting from uncertainties in structural properties or nonlinearities in the structural behavior. (iii) As the mass ratio becomes larger, the TMD performance has been found to be less frequency dependent with a beneficial impact on the seismic effectiveness, mainly in the presence of broad-band earthquake excitations. (iv) Shaking table tests have proved the effectiveness of the proposed large mass ratio TMD in reducing both

the RMS and the peak structural response under earthquake excitations, as well as its robustness against detuning effects. Base shear and bending moment have been suppressed down to $40\% - 70\%$, while floor absolute accelerations have been reduced by $40\% - 60\%$. Results obtained under far-field ground motions was better than those achieved under near-fault ground motions because of the impulsive character of the latter. Furthermore, although a considerable detuning effect concerned the experimental model, the TMD performance was only marginally affected thanks to the increased robustness due to the large mass ratio.

Besides the specific results discussed above, the present thesis has aimed, as a broad objective, to point out some fundamental considerations about the nonstructural seismic design. An apparent conclusion of the research work is that, whenever the operational continuity is required as the primary performance objective of a construction, an effective design of mitigation strategies cannot leave aside the coordination of both structural and nonstructural requirements. This means to integrate the structural design with the design of engineering systems (mechanical, electrical, ...) as different, yet complementary moments of a single, comprehensive process. This process should involve various expertises and professional figures, including structural engineers and service engineers. Each figure has responsibilities for the design of a particular system, with respect to regulatory requirements, client demands and contractual negotiations, but no one of them can have the overall responsibility for the whole design process. Hence, an effort for coordination is strongly needed to achieve the necessary safety levels, particularly in complex and essential constructions as critical facilities.

Future research

The most promising development of the present research lies in the investigation of the so-called *passive adaptive* behaviour inherent in nonlinear hysteretic isolation systems. The aim is to realize a multi-objective performance-based seismic design: by exploiting the adaptive behaviour, *i.e.* several regimes throughout the course of motion, the idea is to separately optimize the isolation system parameters for multiple performance levels at increasing intensities of ground shaking. The proposed class of nonlinear hysteretic isolators shows indeed a soft-hardening stiffness behaviour that is well-suited to a multi-objective performance-based seismic design. Two performance levels (Operational and Life Safe) can be selected and the nonlinear stiffness, particularly the hardening parameter $k_{nl} > 0$, can be designed to obtain an isolation system that: (i) is very stiff with low damping at low level shaking, so to limit the static displacements; (ii) softens with increasing damping in the Operational level, so to reduce the equipment acceleration response for continuing functioning; (c) stiffens at and beyond the Life Safety level, so to limit the displacements under severe earthquakes for the safety of the isolated equipment.

From a more general viewpoint, it is believed that the area of the present research has a strong potential for further theoretical and technical investigations. The broad objective should be the development of comprehensive technologies for the seismic risk mitigation and the permanent health monitoring in critical facilities. To this end, an almost unexplored space is left to the fundamental topic of establishing testing and certification protocols oriented to equipment in critical facilities.

In the end, the results of such developments should aim at improving the framework given by international codes as to the seismic design of nonstructural components and equipment. For the sake of harmonization and coordination between different engineering fields, two grades of seismic design should be recognized, depending on the professional expertise of the designers. Prescriptive simplified methodologies, specifying conservative requirements like the equivalent static lateral force method, should be addressed to designers that have no relevant skills in the field of structural engineering (*i.e.* service engineers). A professional structural engineer should rather be involved in non-ordinary cases, when simplified methodologies result to be inaccurate. Because of his specialist skills, the structural engineer should be allowed to specify performance-based seismic design criteria, according to his professional judgement, and to perform seismic analysis other than those directly prescribed by the codes.

Bibliography

[1] Alhan, C., Gavin, H.P. A parametric study of linear and non-linear passively damped seismic isolation systems for buildings. *Engineering Structures*, 26:485–497, 2004.

[2] Alhan, C., Gavin, H.P. Reliability of base isolation for the protection of critical equipment from earthquake hazards. *Engineering Structures*, 27:1435–1449, 2005.

[3] Aref, A., Bruneau, M., Constantinou, M., Filiatrault A. *et al. Research Progress and Accomplishments 2003-2004*, chapter Seismic response modification of structural and nonstructural systems and components in acute care facilities, pages 95–120. MCEER Publications, New York, 2004.

[4] Bhatti, M.A., Ciampi, V., Kelly, J.M., Pister, K.S. An earthquake isolation system for steam generators in nuclear power plants. *Nuclear Engineering and Design*, 73:229–252, 1982.

[5] Bouc, R. Forced vibration of mechanical systems with hysteresis. In *Proceeding of the 4th International Conference on Nonlinear Oscillations*, page 315, Prague, Czechoslovakia, 1967.

[6] Bouc, R. Modèle mathématique d'hystérésis. *Acustica*, 24:16–25, 1971.

[7] Bursi, O.S., Dusatti, T., Pucinotti, R. A reconnaissance report. The April 6, 2009 L'Aquila Earthquake. Italy. www.reluis.it, 2009.

[8] Capecchi, D., De Felice, G. Hysteretic systems with internal variables. *Journal of Engineering Mechanics*, 127:891–898, 2001.

[9] Carrella, A., Brennan, M.J., Kovacic, I., Waters, T.P. On the force transmissibility of a vibration isolator with quasi-zero-stiffness. *Journal of Sound and Vibration*, 322:707–717, 2009.

[10] Carrella, A., Brennan, M.J., Waters, T.P. Static analysis of a passive vibration isolator with quasi-zero-stiffness characteristics. *Journal of Sound and Vibration*, 301:678–689, 2007.

[11] Chen, G., Soong, T.T. State of the art review: seismic response of secondary systems. *Engineering Structures*, 10(4):218–228, 1988.

[12] Chey, M. H., Chase, J. G., Mander, J. B., Carr, A. J. Semi-active tuned mass damper building system: application. *Earthquake Engineering and Structural Dynamics*, 39:69–89, 2010.

[13] Chey, M.H., Chase, J.G., Mander, J.B., Carr, A.J. Semi-active tuned mass damper building systems: design. *Earthquake Engineering and Structural Dynamics*, 39:119–139, 2010.

[14] Chopra A. K. *Dynamics of structures – Theory and applications to earthquake engineering.* Prentice Hall, Upper Saddle River, N.J., 1995.

[15] Chopra, A.K., Chintanapakdee, C. Comparing response of SDOF systems to near-fault and far-fault earthquake motions in the context of spectral regions. *Earthquake Engineering and Structural Dynamics*, 30:1769–1789, 2001.

[16] Christopoulos, C., Filiatrault, A. *Principles of passive supplemental damping and seismic isolation.* IUSS Press, 2006.

[17] Chung, L.L., Yang, C.Y., Chen. H.M., Lu, L.Y. Dynamic behaviour of nonlinear rolling isolation system. *Structural Control and Health Monitoring*, 16:32–54, 2009.

[18] Computers & Structures Inc., University Avenue, Berkeley, CA. *SAP2000 Release 10 Documentation*, 2007.

[19] Consiglio Superiore dei Lavori Pubblici. Circ. 617/2009. *Istruzioni per l'applicazione delle Nuove NormeTecniche per le Costruzioni di cui al D.M. 14/01/2008*, 2009.

[20] Corless, R.M., Gonnet, G.H., Hare, D.E.G., Jeffrey, D.J. Knuth, D.E. On the Lambert W function. *Advances in Computational Mathematics*, 5:329–359, 1996.

[21] Crandall, S.H., Mark, W.D. *Random vibration in mechanical systems.* Academic, New York, 1963.

[22] De Angelis, M., Perno, S., Reggio, A. Dynamic response and optimal design of structures with large mass ratio tmd. *Earthquake Engineering and Structural Dynamics*, DOI: 10.1002/eqe.1117, 2011.

[23] De Angelis, M., Perno, S., Reggio, A., De Canio, G., Ranieri, N. Prove sperimentali su tavola vibrante di un telaio in scala 1:5 dotato di isolamento di piano. In *Proceedings of the XIII Convegno ANIDIS - Associazione Nazionale Italiana di Ingegneria Sismica*, 2009.

[24] De Angelis, M., Perno, S., Reggio, A., De Canio, G., Ranieri, N. Shaking table tests on a passive equipment isolation system for earthquake protection. In *Proceedings of 2009 ASME Pressure Vessels and Piping Division Conference*, Prague, Czech Republic, July 26-30 2009.

[25] Den Hartog J. P. *Mechanical vibration.* Mc-Graw Hill Inc., New York, NY, 4th edition, 1956.

[26] Der Kiureghian, A., Sackman, J.L., Nour-Omid, B. Dynamic analysis of light equipment in structures: response to stochastic input. *Journal of the Engineering Mechanics Division, ASCE*, 109:90–110, 1983.

[27] Dipartimento della Protezione Civile. *Linee guida per la riduzione della vulnerabilità di elementi non strutturali, arredi e impianti.*, June 2009.

[28] Duhem, P. Die dauernden Aenderungen und die Thermodynamik. *I. Z. Phys. Chem.*, 22:543–589, 1897.

[29] ENEA. Apparato per la protezione dai terremoti di statue, opere d'arte e strutture delicate mediante dispositivi di isolamento sismico. Patent no. ITRM2006A000141, Italy, 2010.

[30] European Committee for Standardization (CEN). *Eurocode 8: Design of structures for earthquake resistance – Part. 1: General rules, seismic actions and rules for buildings*, EN 1998-1. Brussels, 2004.

[31] Falsone, G., Muscolino, G., Ricciardi, G. Combined dynamic response of primary and multiply connected cascaded secondary subsystems. *Earthquake Engineering and Structural Dynamics*, 20:749–767, 1991.

[32] Falsone, G., Muscolino, G., Ricciardi, G. Stochastic response of combined primary-secondary structures under seismic input. *Earthquake Engineering and Structural Dynamics*, 21:927–943, 1992.

[33] Fan, Y.C., Loh, C.H., Yang, J.N., Lin, P.Y. Experimental performance evaluation of an equipment isolation using MR dampers. *Earthquake Engineering and Structural Dynamics*, 38:285–305, 2009.

[34] Federal Emergency Management Agency (FEMA). *NEHRP Recommended Provisions for the Development of Seismic Regulations for New Buildings*, prepared by the Building Seismic Safety Council. Report No. FEMA 222A. Washington, DC, 1994.

[35] Federal Emergency Management Agency (FEMA). *Reducing the Risks of Nonstructural Earthquake Damage.* Report No. FEMA 74. Washington, DC, 1994.

[36] Federal Emergency Management Agency (FEMA). *NEHRP Commentary on the Guidelines for the Seismic Rehabilitation of Buildings*, prepared by the Building Seismic Safety Council. Report No. FEMA 274. Washington, DC, 1997.

[37] Federal Emergency Management Agency (FEMA). *NEHRP Guidelines for the Seismic Rehabilitation of Buildings*, prepared by the Building Seismic Safety Council. Report No. FEMA 273. Washington, DC, 1997.

[38] Federal Emergency Management Agency (FEMA). *Prestandard and Commentary for the seismic rehabilitation of buildings*. Report No. FEMA 356. Washington, DC, 2000.

[39] Federal Emergency Management Agency (FEMA). *NEHRP Recommended Provisions and Commentary for Seismic Regulations for New Buildings and Other Structures*, Part 1: Provisions and Part 2: Commentary, prepared by the Building Seismic Safety Council. Report no. FEMA 450. Washington, DC, 2003.

[40] Federal Emergency Management Agency (FEMA). *NEHRP Next Generation Performance-Based Seismic Design Guidelines*, prepared by the Applied Technology Council. Report no. FEMA 445. Washington, DC, 2006.

[41] Federal Emergency Management Agency (FEMA). *Interim Testing Protocols for Determining the Seismic Performance Characteristics of Structural and Nonstructural Components*. Report No. FEMA 461. Washington, DC, 2007.

[42] Federal Emergency Management Agency (FEMA). *NEHRP Recommended Seismic Provisions for New Buildings and Other Structures*, prepared by the Building Seismic Safety Council. Report No. FEMA-P 750. Washington, DC, 2009.

[43] Feng, M.Q., Mita, A. Vibration control of tall buildings using mega subconfiguration. *Journal of Engineering Mechanics,ASCE*, 121:1082–1088, 1995.

[44] Fenz, D.M., Constantinou, M.C. Spherical sliding isolation bearings with adaptive behavior: Experimental verification. *Earthquake Engineering and Structural Dynamics*, 37:185–205, 2008.

[45] Fenz, D.M., Constantinou, M.C. Spherical sliding isolation bearings with adaptive behavior: Theory. *Earthquake Engineering and Structural Dynamics*, 37:163–183, 2008.

[46] Filiatrault, A., Christopoulos, C., Stearns, C. Guidelines, specifications and seismic performance characterization of nonstructural building components and equipment. PEER Report 2002/05, Pacific Earthquake Engineering Research Center, University of California at Berkely, September 2001.

[47] Frahm, H. *Device for damping vibrations of bodies*. US Patent 989958, 1909.

[48] Gavin, H.P., Zaicenco, A. Performance and reliability of semi-active equipment isolation. *Journal of Sound and Vibration*, 306:74–90, 2007.

[49] Guerreiro, L. Azevedo, J. Muhr, H. Seismic tests and numerical modeling of a rolling ball isolation system. *Journal of Earthquake Engineering*, 11:49–66, 2007.

[50] Gupta, A.K. *Response spectrum method in seismic analysis and design of structures.* Blackwell Scientific Publications, Inc., Cambridge (MA), USA, 1990.

[51] Hall, J.F. Discussion of "the role of damping in seismic isolation". *Earthquake Engineering and Structural Dynamics*, 28:1717–1720, 1999.

[52] Hamidi, M., El Naggar, M.H. On the performance of SCF in seismic isolation of the interior equipment. *Earthquake Engineering and Structural Dynamics*, 36:1581–1604, 2007.

[53] Hoang N., Fujino Y. Optimal tuned mass damper for seismic applications and practical design formulas. *Engineering Structures*, 30:707–715, 2008.

[54] Holmes, D. Listing of installations. *Engineering Structures*, 17:676–678, 1995.

[55] Housner, G.W., Bergman, L.A., Caughey, T.K., Claus, R.O., Masri, S.F., Skelton, R.E., Soong, T.T., Spencer, B.F., Jao, J.T.P. Structural control: Past, present and future. *Journal of Engineering Mechanics, ASCE*, 123:897–971, 1997.

[56] Huang, Y.N., Whittaker, A.S., Constantinou, M.C., Malushte, S. Seismic demands on secondary systems in base-isolated nuclear power plants. *Earthquake Engineering and Structural Dynamics*, 36:1741,1761, 2007.

[57] Hwang, J.S., Huang, Y.N., Hung, Y.H., Huang, J.C. Applicability of seismic protective systems to structures with vibration-sensitive equipment. *Journal of Structural Engineering, ASCE*, 130:1676–1684, 2004.

[58] Ibrahim, R.A. Recent advances in nonlinear passive vibration isolators. *Journal of Sound and Vibration*, 314:371–452, 2008.

[59] Igusa, T., Der Kiureghian, A. Dynamic analysis of multiple tuned and arbitrarily supported secondary systems. UCB/EERC Report 83/07, Earthquake Engineering Research Center, University of California at Berkeley, 1983.

[60] Inaudi A.J., Kelly J.M. Hybrid isolation systems for equipment protection. *Earthquake Engineering and Structural Dynamics*, 22:297–313, 1993.

[61] Inaudi, J.A., Kelly, J.M. Minimum variance control of base-isolated floors. *Journal of Structural Engineering ASCE*, 119(2):438–453, 1993.

[62] International Code Council (ICC). *International Building Code*, 2009. Whittier, CA, 2009.

[63] International Conference of Building Officials (ICBO). *Uniform Building Code*, 1997. Whittier, CA, 1997.

[64] Ismail, M., Rodellar, J., Ikouhane, F. An innovative isolation bearing for motion-sensitive equipment . *Jounal of Sound and Vibration*, 326:503–521, 2009.

[65] Ismail, M., Rodellar, J., Ikouhane, F. Performance of structure-equipment systems with a novel roll-n-cage isolation bearing. *Computers and Structures*, 87:1631–1646, 2009.

[66] Iwan, W.D. The earthquake design and analysis of equipment isolation systems. *Earthquake Engineering and Structural Dynamics*, 6:523–534, 1978.

[67] Jangid, R.S. Stochastic seismic response of structure isolated by rolling rods. *Engineering Structures*, 22:937–946, 2000.

[68] Jangid, R.S., Kelly, J.M. Base isolation for near-fault motions. *Earthquake Engineering and Structural Dynamics*, 30:691–707, 2001.

[69] Jangid, R.S., Lonhe, Y.B. Effectiveness of elliptical rolling rods for base isolation. *Journal of Structural Engineering, ASCE*, 124:469–472, 1998.

[70] Johnson, G.S. . *Earthquake Engineering Handbook.* Chapter 20 – Equipment and Systems. Scawthorn, C., Ed. CRC Press LLC, Boca Raton, Florida, 2002.

[71] Juang JN, Cooper JE, Wright JR. An Eigensystem Realization Algorithm using Data Correlations (ERA/DC) for modal parameter identification. *Control Theory and Advanced Technology*, 4(1):5–14, 1988.

[72] Juhn, G., Manolis, G.D., Costantinou, M.C., Reinhorn A.M. Experimental study of secondary systems in base isolated structures. *Journal of Structural Engineering, ASCE*, 118:2204–2221, 1992.

[73] Kaynia, A.M., Veneziano, D. Seismic effectiveness of tuned mass dampers. *Journal of Structural Engineering, ASCE*, 107:1465–1484, 1981.

[74] Kelly, J.M. *Earthquake Resistant Design with Rubber.* Springer Verlag, London, U.K., 1993.

[75] Kelly, J.M. The role of damping in seismic isolation. *Earthquake Engineering and Structural Dynamics*, 28:3–20, 1999.

[76] Kovacic, I., Brennan, M.J., Waters, T.P. A study on nonlinear vibration isolator with a quasi-zero-stiffness characteristic. *Journal of Sound and Vibration*, 315:700–711, 2008.

[77] Lai, M.L., Soong, T.T. Seismic design considerations for secondary structural systems. *Jounal of Structural Engineering ASCE*, 117(2):459–472, 1991.

[78] Lambrou, V., Constantinou, M.C. Study of seismic isolation systems for computer floors. Technical Report NCEER 94-0020, National Center for Earthquake Engineering Research, State University of New York at Buffalo, July 1994.

[79] Lin, C.C., Wang, J.F., Ueng, J.M. Vibration control identification of seismically excited MDOF structure-PTMD systems. *Journal of Sound and Vibration*, 240(1):87–115, 2001.

[80] Lin, T.W., Chern, C.C.,Hone, C.C. Experimental study of base isolation by free rolling rods. *Earthquake Engineering and Structural Dynamics*, 24:1645–1650, 1995.

[81] Lin, T.W., Hone, C.C. Base isolation by free rolling rods under basement. *Earthquake Engineering and Structural Dynamics*, 22:261–273, 1993.

[82] Lin, Y.K. *Probabilistic Theory of Structural Dynamics*. Mc-Graw Hill Inc., 1967. Reprint: Krieger Publishing Company 1976 – 1986.

[83] Lopez Garcia D., Soong T.T. Sliding fragility of block-type non-structural components. part 1: Unrestrained components. *Earthquake Engineering and Structural Dynamics*, 32:111–129, 2003.

[84] Lopez Garcia D., Soong T.T. Sliding fragility of block-type non-structural components. part 2: Restrained components. *Earthquake Engineering and Structural Dynamics*, 32:131–149, 2003.

[85] Lu, L.Y., Lin, G.L. Predictive control of smart isolation system for precision equipment subjected to near-fault earthquakes. *Engineering Structures*, 30:3045–3064, 2008.

[86] Lu,L.Y., Lee, T.Y., Y, S.W. Theory and experimental study for sliding isolators with variable curvature. *Earthquake Engineering and Structural Dynamics*, DOI: 10.1002/eqe.1106, 2011.

[87] Makris, N., Chang, S.P. E!ect of viscous, viscoplastic and friction damping on the response of seismic isolated structures. *Earthquake Engineering and Structural Dynamics*, 29:85–107, 2000.

[88] Matta, E., De Stefano, A. Robust design of mass-uncertain rolling-pendulum TMDs for seismic protection of buildings. *Mechanical Systems and Signal Processing*, 23:127–147, 2009.

[89] Medina, R.A., Sankaranarayanan, R., Kingston, K.M. Floor response spectra for light components mounted on regular moment-resisting frame structures. *Engineering Structures*, 28:1927, 1940, 2006.

[90] Ministero delle Infrastrutture e dei Trasporti. *Nuove Norme tecniche per le Costruzioni*, D.M. 14.01.2008. Rome, 2008.

[91] Muscolino G. *Dinamica delle Strutture*. McGraw-Hill, Milano, 2002.

[92] Naeim, F., Kelly, J.M. *Design of Seismic Isolated Structures: from Theory to Practice*. John Wiley and Sons, Inc., New York, 1999.

[93] Nayfeh, A.H., Balachandran, B. *Applied nonlinear dynamics. Analytical, computational and experimental methods.* Wiley Series in nonlinear science. Wiley, New York, 1995.

[94] Ni, Y.Q., Ko, J.M., Wong,C.W. Identification of nonlinear hysteretic isolators from periodic vibration tests. *Journal of Sound and Vibration*, 217:737–756, 1998.

[95] Ni, Y.Q., Ko, J.M., Wong,C.W. Nonparametric identification of nonlinear hysteretic system. *Journal of Engineering Mechanics, ASCE*, 125:205–215, 1999.

[96] Ni, Y.Q., Ko, J.M., Wong,C.W., Zhan, S. Modelling and identification of a wire-cable vibration isolator via a cyclic loading test. Part 1: experiments and model development. *Journal of Systems and Control Engineering*, 213:163–171, 1999.

[97] Ni, Y.Q., Ko, J.M., Wong,C.W., Zhan, S. Modelling and identification of a wire-cable vibration isolator via a cyclic loading test. Part 2: identification and response. *Journal of Systems and Control Engineering*, 213:173–182, 1999.

[98] Ni, Y.Q., Ying, Z.G., Ko, J.M., Zhu, W.Q. Random response of integrable Duhem hysteretic systems under non-white excitation. *International Journal of Nonlinear Mechanics*, 37:1407–1419, 2002.

[99] Ormondroyd, J., Den Hartog, J.P. The theory of dynamic vibration absorber. *Transactions of the American Society of Mechanical Engineers, Journal of Applied Mechanics*, 13:A–284, 1946.

[100] Pacific Earthquake Engineering Research Center (PEER). Strong ground motion database, 2009. http://peer.berkeley.edu/ [10 June 2010].

[101] Parise, G., De Angelis, M., Reggio, A. A Darwinian evolution of electrical power systems design for preventing seismic risks in sensitive buildings. In *Proceedings of 2011 I&CPS (Industrial & Commercial Power Systems) – IEEE Technical Conference*, Orange County, CA (USA), May 1-5, 2011 2011.

[102] Pinkaew, T., Lukkunaprasit, P., Chatupote, P. Seismic effectiveness of tuned mass dampers for damage reduction of structures. *Engineering Structures*, 25:39–46, 2003.

[103] Rana, R., Soong, T. T. Parametric study and simplified design of tuned mass dampers. *Engineering Structures*, 20(3):193–204, 1998.

[104] Ravindra, B., Mallik, A.K. Performance of nonlinear vibration isolators under harmonic excitation. *Journal of Sound and Vibration*, 170:325–337, 1994.

[105] Reggio, A., De Angelis, M. Feasibility of a passive isolation system with nonlinear hysteretic behaviour for the seismic protection of critical equipment. In *Proceedings of the XIV Convegno ANIDIS Associazione Nazionale Italiana di Ingegneria Sismica*, Bari, Italy, September, 18-22 2011.

[106] Reggio, A., De Angelis, M. A passive isolation system with nonlinear hysteretic behaviour: modelling and numerical investigations. In *Proceedings of the XIX Congresso AIMETA Associazione Italiana di Meccanica Teorica e Applicata*, Bologna, Italy, September, 12-15 2011.

[107] Reggio, A., De Angelis, M., Perno, S. Controllo della risposta dinamica di strutture dotate di TMD ad elevato rapporto di massa: analisi numeriche e sperimentali. In *Proceedings of the XIX Congresso AIMETA Associazione Italiana di Meccanica Teorica e Applicata*, Ancona, Italy, September 14-17 2009.

[108] Reitherman, B. (Coordinator). 1994 Northridge Earthquake: Reconnaissance Report. Nonstructural Damage. *Earthquake Spectra*, 11(Issue S2):453–514, 1995.

[109] Rivin, E.I. *Passive Vibration Isolation.* ASME Press, 2001.

[110] Sackman, J.L., Der Kiureghian, A., Nour-Omid, B. Dynamic analysis of light equipment in structures: modal properties of the combined system. *Journal of the Engineering Mechanics Division, ASCE*, 109:73–89, 1983.

[111] Sackman, J.L., Kelly, J.M. Seismic analysis of internal equipment and components in structures. *Journal of Engineering Structures*, 1(4):179–190, 1979.

[112] Sadek, F., Mohraz, B., Taylor, A.W., Chung, R.M. A method of estimating the parameters of tuned mass dampers for seismic applications. *Earthquake Engineering and Structural Dynamics*, 26:617–635, 1997.

[113] Scawthorn, C., Ed. The Marmara, Turkey Earthquake of August 17, 1999: Reconnaissance Report. MCEER Reconnaissance Report 019.0001, Multidisciplinary Center for Earthquake Engineering Research, University at Buffalo, State University of New York, 2000.

[114] Shaska, K., Ibrahim, R.A., Gibson, R.F. Influence of the excitation amplitude on the characteristics of nonlinear butyl rubber isolators. *Nonlinear Dynamics*, 47:83 – 104, 2007.

[115] Singh, M.P., Moreschi, L.M., Suarez, L.E., Matheu, E.E. Seismic Design Forces. I: Rigid Nonstructural Components. *Jounal of Structural Engineering, ASCE*, 132(10):1524–1532, 2006.

[116] Singh, M.P., Moreschi, L.M., Suarez, L.E., Matheu, E.E. Seismic Design Forces. II: Flexible Nonstructural Components. *Jounal of Structural Engineering, ASCE*, 132(10):1533–1542, 2006.

[117] Sladek, J.R., Klingner, R.E. Effect of tuned mass dampers on seismic response. *Journal od Structural Engineering, ASCE*, 109:2004–2009, 1983.

[118] Soong, T. T., Dargush, G. F. *Passive energy dissipation systems in structural engineering*. John Wiley and sons, New York, 1997.

[119] Soong, T.T. Seismic behavior of nonstructural elements - State-of-the-art report. In Duma, G., editor, *Proceedings of the 10th European Conference on Earthquake Engineering*, Rotterdam, 1995.

[120] Soong, T.T., Chen, G., Wu, Z., Zhang, R.H., Grigoriou, M. Assessment of the 1991 provisions for nonstructural components and recommended revisions. Technical Report NCEER 93-0003, National Center for Earthquake Engineering Research, State University of New York at Buffalo, March 1993.

[121] Soong, T.T., Grigoriu, M. *Random vibrations of mechanical and structural systems*. Prentice-Hall inc., New Jersey, 1996.

[122] Soong, T.T., Spencer, B.F. Supplemental energy dissipation: state-of-the-art and state-of-the-practice. *Engineering Structures*, 24:243–259, 2002.

[123] Soong, T.T., Yao, G.C., Lin, C.C. Near-fault seismic vulnerability of nonstructural components and retrofit strategies. *Earthquake Engineering and Engineering Seismology*, 2(2):67–76, 2000.

[124] Soto-Brito, R., Ruiz, S.E. Influence of ground motion intensity on the effectiveness of tuned mass dampers. *Earthquake Engineering and Structural Dynamics*, 28:1255–1271, 1999.

[125] Spencer, B.F., Nagarajaiah, S. . State of the art of structural control. *Journal of Structural Engineering, ASCE*, 7:845–856, 2003.

[126] Standards New Zealand. Seismic performance of engineering systems in buildings. NZS 4219:2009., 2009.

[127] Structural Engineers Association of California. SEAOC Vision 2000. Performance-based Seismic Engineering of Buildings, 1995.

[128] Suarez, L.E., Singh, M.P. Eigenproperties of non-classically damped structure and equipment systems by a perturbation approach. *Journal of Earthquake Engineering and Structural Dynamics*, 15:565–583, 1987.

[129] Suarez, S.L., Singh, M.P. Floor response spectra with structure – equipment interaction effects by a mode synthesis approach. *Jounal of Earthquake Engineering and Structural Dynamics*, 15:141–158, 1987.

[130] Taghavi S., Miranda E. Response assessment of nonstructural building elements. PEER Report 2003-05, Pacific Earthquake Engineering Research Center, University of California at Berkeley, September 2003.

[131] Tajirian F.F., Kelly J.M., Aiken I.D. Seismic isolation for advanced nuclear power stations. *Earthquake Spectra*, 6 (2):371–401, 1990.

[132] The MathWorks, Inc. *MATLAB Version R2009b Documentation*, 2009.

[133] Tiang, Z., Qian, J., Zhang L. Slide roof systems for dynamic response reduction. *Earthquake Engineering and Structural Dynamics*, 37:647–658, 2008.

[134] Tsai, C.S., Chiang, T.C., Chen, B.J., Lin, S.B. An advanced analytical model for high damping rubber bearings. *Earthquake Engineering and Structural Dynamics*, 32:1373–1387, 2003.

[135] Tsai H., Hsueh S. . Mechanical properties of isolation bearings identified by a viscoelastic model. *International Journal of Solids and Structures*, 38:53–74, 2001.

[136] Uang, C.M., Bertero, V.V. Use of energy as a design criterion in earthquake-resistant design. Report No. UCB/EERC 88-18, Earthquake Engineering Research Center, University of California at Berkeley, November 1988.

[137] U.S. Nuclear Regulatory Commission. Development of floor design response spectra for seismic design of floor-supported equipment or components. regulatory guide 1.122, 1978.

[138] Valanis, K. C. A Theory of viscoplasticity without a yield surface. Part I: general theory. *Arch. Mech.*, 23:517–533, 1971.

[139] Vanmarcke, E.H.,Gasparini, D. A. *SIMQKE: A program for artificial motion generation*. MIT civil engineering research report R76-4. Technical report, Dept. of Civil Engineering, Massachusetts Institute of Technology., 1976.

[140] Vestroni, F., Noori, M. Hysteresis in mechanical systems - modeling and dynamic response. *International Journal of Nonlinear Mechanics*, 37:1261–1262, 2002. Special Issue.

[141] Villaverde, R. Seismic design of secondary structures: state of the art. *Journal of Structural Engineering, ASCE*, 123(8):1011–1019, 1997.

[142] Villaverde, R. Implementation study of aseismic roof isolation system in 13-story building. *Journal of Seismology and Earthquake Engineering*, 2:17–27, 2000.

[143] Villaverde, R. *Earthquake engineering: from engineering seismology to performance-based engineering.* Chapter 19 – Seismic analysis and design of nonstructural elements. Bozorgnia, Y., Bertero, V., Eds. CRC Press LLC, Boca Raton, Florida, 2004.

[144] Villaverde, R. Simple method to estimate the seismic nonlinear response of nonstructrural components in buildings. *Engineering Structures*, 28:1209–1221, 2006.

[145] Villaverde, R., Aguirre, M., Hamilton, C. Aseismic roof isolation system built with steel oval elements. *Earthquake Spectra*, 21 (1):225–241, 2005.

[146] Visintin, A. *Differential models of hysteresis.* Springer-Verlag, Germany, 1994.

[147] Warburton, G.B. Optimum absorber parameters for various combinations of response and excitation parameters. *Earthquake Engineering and Structural Dynamics*, 10:381–401, 1982.

[148] Warburton, G.B., Ayorinde, E.O. Minimizing structural vibrations with absorber. *Earthquake Engineering and Structural Dynamics*, 8:219–236, 1980.

[149] Warburton, G.B., Ayorinde, E.O. Optimum absorber parameters for simple systems. *Earthquake Engineering and Structural Dynamics*, 8:197–217, 1980.

[150] Wen Y. K. Method for random vibration of hysteretic system. *Journal of Engineering Mechanics, ASCE*, 120:2299–2325, 1976.

[151] Wirshing, P.H., Campbell, G.W. Minimal structural response under random excitation using the vibration absorber. *Earthquake Engineering and Structural Dynamics*, 2:303–312, 1974.

[152] Xu, Y.L., Li, B. Hybrid platform for high-tech equipment protection against earthquake and microvibration. *Earthquake Engineering and Structural Dynamics*, 35:943–967, 2006.

[153] Xu, Y.L., Yu, Z.F., Zhan, S. Experimental study of a hybrid platform for high-tech equipment protection against earthquake and microvibration. *Earthquake Engineering and Structural Dynamics*, 37:747–767, 2008.

[154] Yang, J.N., Agrawal, A.K. Protective systems for high-technology facilities against microvibration and earthquake. *Structural Engineering and Mechanics*, 10:561–575, 2000.

[155] Yoshida, J., Abe, M., Fujino, Y. Constitutive model of high-damping rubber materials. *Journal of Engineering Mechanics, ASCE*, 130:129–141, 2004.

[156] Zhou, Q., Lu, X., Wang, Q., Feng, D., Yao, Q. Dynamic analysis on structures base-isolated by a ball system with restoring properties. *Earthquake Engineering and Structural Dynamics*, 27:773–791, 1998.

[157] Ziyaeifar, M., Noguchi, T. Partial mass isolation in tall buildings. *Earthquake Engineering and Structural Dynamics*, 27:49–65, 1998.

Publications from the present thesis

Some of the results discussed in the present thesis have been published in international scientific journals in the following papers:

1. De Angelis, M., Perno, S., Reggio, A., Dynamic response and optimal design of structures with large mass ratio TMD. *Earthquake Engineering and Structural Dynamics*, 41 (1), 41-60, 2012.

2. Reggio, A., De Angelis, M. Optimal design of an equipment isolation system with nonlinear hysteretic behaviour. *Earthquake Engineering and Structural Dynamics*, 42 (13), 1907-1930, 2013.

3. Reggio, A., De Angelis, M. Combined primary-secondary system approach to the design of an equipment isolation system with High-Damping Rubber Bearings. *Journal of Sound and Vibration*, 333 (9), 2386-2403, 2014.

4. Parise, G., Reggio, A., De Angelis, M. Criteria for the Definition of the Equipment Seismic Levels (ESL): Comparisons between USA and European Codes. *IEEE Transactions on Industry Applications*, DOI: 10.1109/TIA.2013.2289947, 2014.